

Characterization of Fire Properties for Coupled Pyrolysis and Combustion Simulation and Their Optimised Use

Ariza Sharikin Abu Bakar

A thesis submitted in fulfilment of the requirement
for the degree of Doctor of Philosophy



Centre for Environmental Safety and Risk Engineering
(CESARE)
College of Engineering and Science
Victoria University

August 2015

ABSTRACT

Performance-based fire safety system design enables fire safety engineers to assess the performance of buildings and components by taking into account various scenarios of real fires and their severity. This approach offers more flexibility to the fire safety engineer to adopt new design concepts such as aesthetic values, material and energy efficiencies, while complying with regulatory building codes. For such an approach, the testing of fire safety systems either experimentally or numerically is essential and since experimental studies are vastly expensive, fire models are usually used.

State-of-the-art Computational Fluid Dynamics (CFD) based fire models typically include pyrolysis and combustion sub-models for predicting fire growth and spread in addition to background mass, momentum and energy balance sub-models. Separately, the phenomena of pyrolysis and combustion of materials are quite complex and during a fire both phenomena occur simultaneously thus compounding the complexity. Simulating these phenomena relies primarily on the prescribed fire properties of combustible materials and any error in providing the input fire properties data may affect the prediction of the fire behaviour. This study has been conducted to characterize the fire properties for coupled pyrolysis and combustion simulation.

The overarching objective is to find, given an unknown or novel material, how would a user go about quantifying the representative fire properties and use them optimally? A range of experimental techniques and where necessary, data post-processing methods have been established, developed, selected and implemented to determine critical fire properties. Two bench-scale instruments, the cone calorimeter and hot disk analyser, as well as two milligram-scale instruments, a thermogravimetric analyser and differential scanning calorimeter, have been used for this purpose.

Fire properties of four representative materials including a non-charring polymer (poly (methyl methacrylate, PMMA) and charring materials (pine, cotton and wool) were selected and characterized for the coupled simulations. It was observed that the values of the kinetic triplet (i.e. activation energy, pre-exponential factor, reaction order) and heat of reaction (*HoR*) vary with the heating rate. This variation with heating rate is not widely reported or quantified to any extent in the literature and this has therefore been a focus in this study. The physical and chemical properties of the tested materials may have influence on this variation. As a non-charring polymer, PMMA physically

undergoes glass transition and melting when exposed to heat. For charring materials, the char development process takes place when the material is exposed to higher temperature. The variation of *HoR* with heating rates can be explained by the likelihood that a sample has less residence time for undergoing volatilisation process in particular temperature at higher heating rates. As a result, the volatiles are formed when the sample has reached higher temperature and therefore more heat flow is needed to assist this process at higher heating rates.

Similarly combustion parameters are also found to vary with the incident radiation flux. However the variation is relatively minimal except for the effective heat of combustion (EHoC) in pine and wool. It is likely that the presence of high moisture content in pine and wool has a significant effect to the EHoC variation with the incident radiation flux. Since these are charring materials, a likely variation in char development with respect to incident radiation flux may also have some influence, particularly in the case for thick and denser samples. Additionally, moisture evaporation and char development may not be uniform through the depth of the sample during the fire test. As expected, thermal conductivity and specific heat of charring materials were found to vary with temperature. However, unlike some other reported data, these two parameters did not vary with temperature for PMMA. The variations in these parameters in charring materials may be influenced by the physical and chemical nature of the charring materials at different temperatures.

Characterized fire properties have been used in the coupled pyrolysis and combustion modelling using the open-source software Fire Dynamics Simulator (FDS) version 6, a widely used CFD-based fire modelling program. It is important to note that due to enormous computational requirements, fire safety engineers typically avoid modelling pyrolysis component in their overall modelling of fire scenarios. In this study modelling is limited to cone calorimeter fire experiment simulations at 30 and 50 kW/m² irradiance for two relatively “pure” materials (pine and PMMA). These fire experiments were considered to provide a benchmark for coupled pyrolysis and combustion modelling. In the modelling process, almost all input fire properties used were obtained experimentally with only the emissivity and absorption coefficients obtained from literature values. A sensitivity study was conducted by varying a series of parameters in tandem, namely thermo-physical properties and yield of char; and chemical kinetics and *HoR*. The FDS results are uniquely found to be converged as the spatial resolution

increases to the order of mm. Sensitivity analysis and comparison of HRR output from FDS simulations show that experimental HRR profile can be reasonably predicted if appropriate input parameters are used. This has verified the accuracy of experimental and post-processing techniques as well as FDS model itself. In addition, a discussion of new approaches in relation to the optimized use of variable fire properties with respect to heating rate, irradiance and temperature is presented for future studies: (i) genetic algorithm based optimisation method and (ii) a little known alternative method whose expanded version is proposed in this study.

ACKNOWLEDGEMENT

Alhamdulillah.

There is an endless list of those whom I am greatly indebted. Foremost, I would like to express my sincere gratitude to Associate Professor Khalid Moinuddin for his outstanding support, patience, motivation, enthusiasm and immense knowledge. Thank you for having faith in me. I would also like to extend my appreciation to my associate supervisor, Dr Marlene Cran who has given a continuous support, sharing knowledge and experience theoretically and technically. Your sincerity has always inspired me.

I acknowledge Dr Anna Matala of VTT Technical Research Centre and Dr Simo Hostikka of Aalto University Finland on our invaluable discussion and also access to Dr Matala's experimental data for my further investigation in some part of my study. I would like thank to Dr Yun Jiang of Xtralis for stimulus discussion throughout this process. My acknowledgement also goes to Dr Long Shi and Dr Duncan Sutherland of CESARE for their knowledge and support.

My special thanks are also extended to those who, along the way, have helped me in completing my doctoral study. I would like to express my gratitude to these people at CESARE for their technical support: Dr Maurice Guerrieri, Mr Lyndon Macindoe, Joe Sam Abraham, Harry James, Rahul Wadhvani and former staff, Mr Michael Culton. Also thank Ms Debra Fitzpatrick and Ms Maria Penagandara and former staff Ms Helen Demczuk for their administrative support. To my PhD colleagues, I enjoyed and cherished our discussions and laugh also the assistance that I received throughout these years.

I acknowledge a financial support from Omnii Pty Ltd, Xtralis and Scientific Fire Services for this project. I would also like to acknowledge the Universiti Sains Malaysia and Ministry of Higher Education Malaysia for the scholarship during my study.

Special thanks to my family. Words cannot express how grateful I am to my mother and my mother-in-law for the sacrifices and prayers that you both have made on my behalf.

Last but not least, I would like to express appreciation to my beloved husband, Zainal Fitri Ahmad. Thank you for the endless support and understanding, taking care of our baby when I was a thousand miles away from home, finishing my thesis write-up. Without you, I could not have come this far. To my daughter Zara Adelia, thank you for lending me your precious three months, only God knows how much I miss you during this separation.

I dedicate this thesis to the memory of my father, Abu Bakar Mat Lazim.

DECLARATION BY AUTHOR

I, Ariza Sharikin Abu Bakar, declare that the PhD thesis entitled “Characterization of Fire Properties for Coupled Pyrolysis and Combustion Simulation and Their Optimised Use” is no more than 100,000 words in length including quotes and exclusive of tables, figures, appendices, bibliography, references and footnotes. This thesis contains no material that has been submitted previously, in whole or in part, for the award of any other academic degree or diploma. Except where otherwise indicated, this thesis is my own work.

Signature



Date: 31/08/2015

NOMENCLATURE

A	pre-exponential factor (1/s)
A'	area under the peak (m ²)
C	inflection line
D_i	diffusion coefficient (m ² /s)
C_p	specific heat capacity (J/kg.K)
$C_{p,max}$	specific heat capacity at peak value (J/kg.K)
DTG	derivative of TG curve
dY/dT	conversion rate
dT/dt	heating rate (K/min)
E	activation energy (kJ/mol)
E_{HoC}	effective heat of combustion (MJ/kg)
g	gravity (N/kg)
HoR	effective heat of gasification/reaction (kJ/kg)
HRR	heat release rate (kW)
HRR_{PUA}	heat release rate per unit area (kW/m ²)
H_{max}	peak conversion rate
K	calibration coefficient
k	reaction rate constant (1/s)
L	length (mm)
MC	moisture content (%)
MLR	mass loss rate (m ² /kg)
m	slope
m_0	initial mass (mg)
m_i	mass of the sample (mg)
m''	mass flux per unit area (kg/m ²)
\dot{m}''	mass loss rate per unit area (kg/m ² .s)
n'	number of approximations
n	reaction order
$P1$	evaporation
$P2$	first peak of cotton pyrolysis
$P3$	second peak of cotton pyrolysis
Pr	Prandtl number (ν/α) (-)

\bar{p}_0	background pressure (Pa)
Re	Reynolds number (ux/ν) (-)
SEA	specific extinction area (m^2/kg)
T	temperature ($^{\circ}C$)
T_s	start temperature ($^{\circ}C$)
T_e	end temperature ($^{\circ}C$)
T_{max}	temperature at peak conversion rate ($^{\circ}C$)
TG	Thermogravimetric
τ_{turb}	filtered turbulence
\bar{u}_i	filtered velocity (m/s)
W	width (mm)
\dot{w}''	mass production rate of a species
w	mass at particular temperature (mg)
w_i	initial sample mass (mg)
w_f	final sample mass (mg)
w_{fc}	final sample mass (mg)
w_{ic}	initial sample mass (mg)
Y	mass fraction of conversion
$f(Y)$	reaction model
$Y(0)$	initial mass fraction
Y_{max}	sample mass fraction of conversion at peak conversion rate

Greek symbols

ρ	Density (kg/m^3)
κ	absorption coefficient ($1/m$)
ε	emissivity
λ	thermal conductivity ($W/m.K^{-1}$)
\emptyset	combustion efficiency
$\Delta H_{c,eff}$	effective heat of combustion (MJ/kg)

ΔH_c	theoretical heat of combustion (MJ/kg)
τ_{lag}	tau lag
μL	microlitre
β	heating Rate (K/min)
ϕ	phi (constant)
$\Delta H_{convent}$	normalised <i>HoR</i> (kJ/kg)
$\Delta H_{enhanced}$	enhanced <i>HoR</i> (kJ/kg)
A_T	area under the curve
ΔE	heat flow (mW)
ΔH_{DSC}	heat of reaction in DSC (kJ/kg)
$\Delta H_{r,\alpha\beta}$	heat of reaction in FDS (kJ/kg)

Subscripts/ Superscripts

CO_2	carbon dioxide
H_2O	water
N_2	nitrogen
O_2	oxygen
i	initial sample mass
f	final sample mass
H_c	heat of combustion
eff	efficiency
T_1	lower peak integration temperature
T_2	upper peak integration temperature
M_{tot}	total mass of the sample
Y_i	yield of gaseous products
X_i	mass fraction of the mass loss
v_s	yield of solid residue
n_s	yield of solid residue
R^2	correlation coefficient

Abbreviations

ANN	Artificial Neural Network
AS	Australian Standards
ASTM	American Society for Testing and Materials
CFD	Computational Fluid Dynamics
CO	Carbon Monoxide
DNS	Direct Numerical Simulation
DSC	Differential Scanning Calorimetry
FDS	Fire Dynamics Simulator
FEM	Finite Element Modelling
FTIR	Fourier-transform infrared
FTT	Fire Testing Technology
GA	Genetic Algorithm
HDA	Hot Disk Analyser
ISO	International Organization for Standardization
LES	Large Eddy Simulation
MLR	Mass Loss Rate
NIST	National Institute of Standards and Technology
NZS	New Zealand Standard
OFW	Ozawa-Flynn-Wall
PE	Perkin Elmer
PMMA	Poly(methyl methacrylate)
3D	Three-Dimensional
TC	Thermal Constant
TGA	Thermogravimetric Analyser
TPS	Transient Plane Source

Table of Contents

Abstract	i
Acknowledgement	iv
Declaration By Author.....	vi
Nomenclature	vii
CHAPTER 1 BACKGROUND THEORY AND SCOPE	1
1.1 Introduction.....	1
1.1.1 Pyrolysis Parameters	5
1.1.2 Thermal Properties	6
1.1.3 Combustion Parameters	7
1.1.4 Physical Properties	8
1.2 Selection of Materials	8
1.2.1 Poly (methyl methacrylate).....	8
1.2.2 Pine.....	9
1.2.3 Fabrics (Cotton and Wool)	9
1.3 Overview of Previous Studies.....	10
1.3.1 Cone Calorimeter	10
1.3.2 Thermal Analysis (TGA and DSC)	12
1.3.3 Hot Disk Thermal Constant Analyser (HDA)	14
1.3.4 Coupled Pyrolysis and Combustion Simulation.....	15
1.4 Research Gaps.....	15
1.5 Research Aims	17
1.6 Research Methods	17
1.7 Thesis Outline.....	18
CHAPTER 2 EXPERIMENTAL TECHNIQUES	19
2.1 Cone Calorimeter	19
2.1.1 Calibration.....	21

2.1.2	Operating Procedure.....	23
2.2	Hot Disk Thermal Constant Analyser.....	24
2.2.1	Calibration.....	26
2.2.2	Probing Depth.....	26
2.2.3	Operating Procedure.....	28
2.3	Thermogravimetric Analyser.....	29
2.3.1	TGA Components	30
2.3.2	TGA Calibration	31
2.3.3	Operating Procedure.....	31
2.4	Differential Scanning Calorimeter	33
2.4.1	Calibration.....	34
2.4.2	Operating Procedure.....	34
2.5	Summary	35
CHAPTER 3 DATA POST-PROCESSING TECHNIQUES.....		36
3.1	Introduction.....	36
3.2	Data Reduction Method for Kinetics Parameter.....	36
3.2.1	Seungdo and Park Method	38
3.2.2	Ozawa-Flynn-Wall (OFW) Method.....	39
3.2.3	Coates Redfern Method.....	40
3.2.4	The Inflection Point Method	41
3.3	Data Reduction Method for Heat of Reaction	43
3.3.1	Test Method ASTM E 2160.....	43
3.3.2	Hoffman and Pan Method	43
3.3.3	Rath et al. Method.....	45
3.3.4	Hoffman and Pan Derivative Method	45
3.3.5	New Data Reduction Method using Normalised Values.....	48
3.4	Summary	49

CHAPTER 4 CHARACTERIZATION OF PYROLYSIS PARAMETERS	51
4.1 Introduction.....	51
4.1.1 Thermal Lag Calibration.....	51
4.1.2 Changes in Decomposition with Temperature	53
4.2 Pyrolysis Parameters of Pine and PMMA.....	54
4.2.1 Kinetic Parameters of Pine.....	56
4.2.2 <i>HoR</i> of Pine.....	59
4.2.3 Kinetic Parameters of PMMA.....	59
4.2.4 Alternative Kinetic Parameters for Pine and PMMA.....	63
4.2.5 <i>HoR</i> of PMMA.....	65
4.3 Pyrolysis Parameters of Fabrics.....	65
4.3.1 Kinetic Parameters of Cotton	66
4.3.2 <i>HoR</i> of Cotton	75
4.3.3 Kinetic Parameters of Wool.....	77
4.3.4 <i>HoR</i> of Wool.....	81
4.3.5 Heating Rate Effects	83
4.4 Summary	84
CHAPTER 5 COMBUSTION MODEL PARAMETERIZATION	85
5.1 Introduction.....	85
5.2 PMMA Combustion Parameters	86
5.2.1 Heat Release Rate.....	86
5.2.2 Mass Loss Rate	88
5.2.3 Specific Extinction Area	89
5.2.4 CO and CO ₂ Yield.....	90
5.2.5 Correlation of Parameters	92
5.3 Pine Combustion Parameters.....	94
5.3.1 Heat Release Rate.....	94

5.3.2	Mass Loss Rate	95
5.3.3	Specific Extinction Area	96
5.3.4	CO and CO ₂ Yield.....	97
5.3.5	Char residue	99
5.3.6	Correlation of Parameters	100
5.4	Cotton Combustion Parameters	102
5.4.1	Heat Release Rate.....	102
5.4.2	CO and CO ₂ Yield.....	103
5.4.3	Correlation of Parameters	103
5.5	Wool Combustion Parameters.....	106
5.5.1	Heat Release Rate.....	106
5.5.2	Specific Extinction Area	106
5.5.3	CO and CO ₂ Yield.....	107
5.5.4	Correlation of Parameters	110
5.6	Summary	110
CHAPTER 6 CHARACTERIZATION OF THERMO-PHYSICAL PARAMETERS		112
6.1	Introduction.....	112
6.2	Thermal Conductivity.....	113
6.2.1	PMMA	113
6.2.2	Pine.....	114
6.2.3	Pine Char	115
6.2.4	Cotton	117
6.2.5	Wool.....	118
6.3	Specific Heat Capacity	119
6.3.1	PMMA	119
6.3.2	Pine.....	120
6.3.3	Pine Char.....	121

6.3.4	Cotton	122
6.3.5	Wool.....	123
6.4	Moisture Affected Region of Charring Materials	124
6.5	Summary	126
CHAPTER 7 NUMERICAL SIMULATION AND OPTIMISED METHODS.....		127
7.1	Introduction.....	127
7.2	Governing Equations of FDS.....	127
7.2.1	Hydrodynamic Model	127
7.2.2	Heat Transfer Model	130
7.2.3	Pyrolysis Model.....	132
7.2.4	Mixture Controlled Combustion Model	133
7.3	Numerical Simulation.....	134
7.3.1	TGA simulation	134
7.3.2	Cone Calorimeter Simulation	137
7.4	Optimised Use of Input Parameters.....	152
7.4.1	RAMP Function.....	153
7.4.2	Tabular Function	155
7.4.3	Systematic Approach	157
7.5	Summary	158
CHAPTER 8 SUMMARY AND CONCLUSIONS.....		159
8.1	Introduction.....	159
8.2	Experimental Techniques	159
8.3	Data Post-Processing.....	160
8.4	Characterization of Fire Properties	161
8.4.1	Effect of Heating Rate on Pyrolysis Parameters	161
8.4.2	Effects of Irradiance on Combustion Parameters.....	162
8.4.3	Effects of Temperature on Thermal Properties	164

8.5	Fire Simulation Using Post-Processed Data as Input Variables	165
8.6	Future Optimised Data Use	166
8.7	Recommendations for Future Studies	167
8.7.1	FDS Simulation of Fabric Fire	167
8.7.2	Development of an Optimisation Tool	167
8.7.3	Optimization Study.....	168
8.7.4	Other Studies.....	169
	REFERENCES	170
	APPENDIX A - ADDITIONAL TGA DATA.....	192
	APPENDIX B – CONE CALORIMETER DATA.....	195
	APPENDIX C– DETAILS OF TGA SIMULATION USING FDS.....	197
	C.1 FDS input file for TGA simulation of Pine at 20 K/min	197
	C.2 FDS input file for TGA simulation of PMMA at 20 K/min	198
	C.3 Visualisation of the domain	199
	Figure C.1: Visualisation of typical domain: blue represents the sample and red represents radiative heating from surrounding.	200
	APPENDIX D– DETAILS OF CONE CALORIMETER SIMULATION USING FDS FOR GRID SENSITIVITY	201
	D.1 FDS input file for Cone Calorimeter simulation of Pine for grid sensitivity	201
	D.2 FDS input file for Cone Calorimeter simulation of PMMA for grid sensitivity ..	203
	D.3 Visualisation of the domain	205
	Figure D.1: Visualisation of typical domain: black represents the sample and red represents the steel casing.....	206
	APPENDIX E– REPRESENTATIVE FULL INPUT FILES FOR CONE CALORIMETER SIMULATION USING FDS WITH IN-HOUSE INPUT DATA	207
	E.1 FDS input file for Cone Calorimeter simulation of Pine with in-house input data	207

E.2 FDS input file for Cone Calorimeter simulation of PMMA with in-house input data
.....209

List of Figures

Figure 2.1: Schematic drawing of the cone calorimeter	20
Figure 2.2: Burning test sample material in the cone calorimeter	22
Figure 2.3: Sample material preparation for the cone calorimeter test	23
Figure 2.4: Hot disk thermal constant analyser.....	25
Figure 2.5: Kapton sensors used in the thermal properties measurement.....	25
Figure 2.6: Calibration is performed using stainless steel.....	26
Figure 2.7: Limit of the probing depth	27
Figure 2.8: Images of various pine char specimens	28
Figure 2.9: Sample materials placed in the oven prior to measurement	29
Figure 2.10: Thermogravimetric analysers	30
Figure 2.11: Preparation of sample materials for TGA and DSC measurements	32
Figure 2.12: Mettler Toledo DSC and its sample furnace	33
Figure 2.13: Schematic diagram of DSC (Mettler-Toledo 2011)	34
Figure 3.1: MLR curve versus temperature profile.....	37
Figure 3.2: Plot to determine inflection point equation for pine	42
Figure 3.3: Determination of pine <i>HoR</i> by TGA and DSC data.....	47
Figure 3.4: Example of a reaction path for the charring material	48
Figure 3.5: <i>HoR</i> of wool vs. heating rate by normalised and gross method.....	49
Figure 3.6: Flow process for characterizing fire properties of building materials	50
Figure 4.1: First derivative of TGA curve for pine using Mettler TGA.....	52
Figure 4.2: Heat flow curve for pine using Mettler DSC.....	52
Figure 4.3: DTG vs temperature for pine using Perkin Elmer TGA	52
Figure 4.4: Perkin Elmer DTG data showing moisture release from pine	53
Figure 4.5: TGA thermograms of PMMA at various heating rates	55
Figure 4.6: DTG plot of PMMA at various heating rates	55
Figure 4.7: DSC thermograms of PMMA at various heating rates	55
Figure 4.8: Kinetic parameters and <i>HoR</i> for pine.....	57
Figure 4.9: Kinetic parameters and <i>HoR</i> for PMMA.....	58
Figure 4.10: Reference temperature, reaction rate and pyrolysis range for PMMA ..	62
Figure 4.11: Reaction rate, reference temperature and pyrolysis range of pine	63
Figure 4.12: TGA thermograms of pine at various heating rates	65
Figure 4.13: TG of cotton obtained using Mettler TGA	67

Figure 4.14: DTG of cotton obtained using Mettler TGA.....	67
Figure 4.15: DSC heat flow of cotton obtained using Mettler DSC	67
Figure 4.16: TG of cotton obtained using Perkin Elmer TGA.....	68
Figure 4.17: Kinetic parameters and <i>HoR</i> of Cotton 1 (P2)	69
Figure 4.18: Kinetic parameters and <i>HoR</i> of Cotton 2 (P3)	70
Figure 4.19: Kinetic parameters and <i>HoR</i> of Cotton ('single effective' method).....	71
Figure 4.20: Kinetic parameters for Cotton 1	72
Figure 4.21: Kinetic parameters for Cotton 2	73
Figure 4.22: Kinetic parameters for Cotton 'single effective'	74
Figure 4.23: DSC/TGA temperature matched heat flow/mass for cotton (20 K/min)	76
Figure 4.24: TG of wool obtained using Perkin Elmer TGA	78
Figure 4.25: DTG of wool obtained using Perkin Elmer TGA.....	78
Figure 4.26: DSC heat flow of wool obtained using Mettler DSC.....	78
Figure 4.27: Kinetic parameters and <i>HoR</i> for wool	80
Figure 4.28: Kinetic parameters for wool and moisture	81
Figure 4.29: DSC/TGA temperature matched heat flow/mass for wool (20 K/min) ...	82
Figure 5.1: Average HRR for PMMA at various heat fluxes.....	87
Figure 5.2: Average MLR of PMMA at various heat fluxes	89
Figure 5.3: Comparison of SEA of PMMA at various heat fluxes.....	90
Figure 5.4: CO yield of PMMA at various heat fluxes.....	91
Figure 5.5: CO ₂ yield of PMMA at various heat fluxes	91
Figure 5.6: Variation of combustion parameters of PMMA with respect to heat flux .	93
Figure 5.7: Average HRR of pine at various heat fluxes	94
Figure 5.8: Average MLR of pine at various heat fluxes	96
Figure 5.9: Comparison of SEA of pine at various heat fluxes.....	97
Figure 5.10: CO yield of pine at various heat fluxes	98
Figure 5.11: CO ₂ yield of pine at various heat fluxes.....	98
Figure 5.12: Variation of combustion parameters of pine with respect to heat flux ..	101
Figure 5.13: Average HRR of cotton at various heat fluxes	102
Figure 5.14: CO yield of cotton at various heat fluxes	104
Figure 5.15: CO ₂ yield of cotton at various heat fluxes	104
Figure 5.16: Variation of combustion parameters of cotton at various heat fluxes...	105
Figure 5.17: Average HRR of wool at various heat fluxes.....	106
Figure 5.18: Average SEA of wool at various heat fluxes	107

Figure 5.19: CO yield of wool at various heat fluxes.....	108
Figure 5.20: CO ₂ yield of wool at various heat fluxes	108
Figure 5.21: Variation of combustion parameters of wool with respect to heat flux .	109
Figure 6.1: Thermal conductivity as function of temperature for PMMA	113
Figure 6.2: Thermal conductivity of pine as function of temperature	115
Figure 6.3: Thermal conductivity as function of temperature for pine char.	116
Figure 6.4: Thermal conductivity as function of temperature for cotton	117
Figure 6.5: Thermal conductivity as function of temperature for wool.....	119
Figure 6.6: Specific heat as function of temperature for PMMA.....	120
Figure 6.7: Specific heat as function of temperature for pine.....	121
Figure 6.8: Specific heat as function of temperature for pine char.....	122
Figure 6.9: Specific heat as function of temperature for cotton.....	123
Figure 6.10: Specific heat as function of temperature for wool	124
Figure 7.1: Simulation of pine DTG curve using experimental kinetic data	135
Figure 7.2: Simulation of pine and PMMA DTG curves using experimental kinetic data at 20 K/min heating rate.....	136
Figure 7.3: Grid convergence tests for PMMA and pine	139
Figure 7.4: Fire simulation sensitivity to pine char properties (50 kW/m ² irradiance)	142
Figure 7.5: Variation of emissivity, absorption coefficient and char fraction (irradiance 50 kW/m ²)	145
Figure 7.6: Experimental and simulation results obtained using kinetic triplets and HoR at various heating rates for pine	147
Figure 7.7: Experimental and simulation results for PMMA at various heating rates	148
Figure 7.8: Modelled flaming combustion of PMMA slab using FDS	150
Figure 7.9: Modelled flaming combustion of Pine slab using FDS	151
Figure 7.10: Specific heat-temperature profile from (Kousksou et al. 2011)	157
Figure 7.11: Optimisation tool linked to the CFD-based fire model to assess appropriate fire condition	157
Figure 8.1: Proposed method for future studies.....	168

List of Tables

Table 1.1: Summary of flammability studies using cone calorimetry.....	10
Table 1.2: Summary of heating rates used in TGA studies.....	12
Table 1.3: Summary of heating rates used in <i>HoR</i> studies by DSC	14
Table 1.4: Summary of temperature ranges in HDA studies.....	14
Table 2.1: Cone calorimeter component overview.....	20
Table 4.1: Summary of kinetic parameters and <i>HoR</i> trends	61
Table 4.2: Summary of kinetic parameters for moisture in virgin pine	62
Table 4.3: Yield of solid residue and initial mass fraction of pine and PMMA	64
Table 4.4: Summary of all kinetic parameters and <i>HoR</i> trends of cotton.....	76
Table 4.5: Summary of kinetic parameters for moisture in wool	79
Table 4.6: Summary of all kinetic parameters and <i>HoR</i> trends of wool and moisture	83
Table 4.7: Yield of solid residue and initial mass fraction for fabrics.....	83
Table 5.1: Chemical composition of studied materials.....	85
Table 6.1: Properties of the tested materials	112
Table 6.2: Summary of the trend for all materials	126
Table 7.1: Experimental combustion parameters	138
Table 7.2: Specified thermo-physical properties.....	140
Table 7.3: Specified thermo-physical properties.....	141
Table 7.4: Physical properties for sensitivity analysis.....	143
Table 8.1: Summary of kinetic parameters and <i>HoR</i> trends of tested materials	163
Table 8.2: Summary of combustion parameters trends of materials.....	163
Table 8.3: Summary of all thermal properties trends of materials.....	165

CHAPTER 1

BACKGROUND THEORY AND SCOPE

1.1 Introduction

Fire safety engineering is the application of engineering principles based on understanding of fire phenomena to assess the risk of fire in order to protect people and property (Institution of Fire Engineers 2014). Fire safety engineering comprises a number of disciplines including fire science, fire protection systems, human behaviour and occupant management. The principals of fire safety engineering are an integral and vital part in modern building structures from design through to construction and occupation.

Fire is also a complex issue which attracts much public interest and concern. Worldwide, fire related incidents are given major attention by the media, particularly when the fire results in a loss of life. For example, the Australian bushfires known as Black Saturday in 2009 (Black Saturday Bushfires 2015) and Ash Wednesday in 1983 (Commonwealth of Australia , Bureau of Meteorology 2015), bushfires in California (CNN International 2007) and Athens (Founda & Giannakopoulos 2009) and building fires such as the collapse of the World Trade Centre (Edelman et al. 2003) were widely reported. Thus, it is crucial for fire safety engineers and researchers to understand the fundamentals of fire science and also to improve the prediction of fire behaviour. If fire growth and flame and smoke propagation within a building are well predicted, the accurate prediction of fire behaviour can enable the design of appropriate fire safety systems.

Fire safety system design starts at the commencement of the first stages of building design. By regulation, buildings must be designed against fire risk either prescriptively or on a performance basis. The latter enables fire safety engineers to assess the performance of a building and its components by taking into account real fires and their severity. This approach gives more flexibility to fire safety engineers to adopt new design concepts (e.g. aesthetic values, material and energy efficiencies) whilst complying with building codes. For such an approach, for designed building, testing fire safety systems either experimentally or numerically is required to ensure it meets the

acceptable level of safety required by the building code. As experimental studies are vastly expensive, fire models are usually used.

The development of computational fluid dynamics (CFD) based fire models such as the Fire Dynamics Simulator (FDS) is driven by a rapid growth of computing power. Its primary aims are to predict real life fire growth and flame and smoke propagation as well as to provide a tool to study fire dynamics and combustion (McGrattan et al. 2009b, McGrattan & Forney 2006). The FDS is an open source CFD-based model developed by the National Institute of Standards and Technology (NIST).

The FDS is comprised of a number of sub models including: large eddy simulation (LES) turbulence model; evaporation and pyrolysis model; mixture controlled combustion model; finite-volume radiation heat transfer, simple surface convection heat transfer and one-dimensional conduction heat transfer models. It also has a direct numerical simulation (DNS) option. The FDS has a unique ability to simulate the course of a fire through all of the stages of ignition, growth, established burning and decline to extinguishment / burnout. Thus pyrolysis and combustion are two critical sub models of FDS.

Pyrolysis is a process of chemical decomposition of solids and release of gaseous products by heating in the absence of oxygen while combustion is a chemical reaction between decomposed gaseous fuel and oxygen which produces heat and smoke (details in CHAPTER 7).

However, the FDS model still has a number of areas requiring improvement, particularly an appropriate determination of thermo-physical properties and reaction parameters as model inputs, i.e. parameters required to simulate phase change from solid or liquid phase to gas phase. Since FDS version 5 (McGrattan et al. 2009a), a sample material properties database is no longer included as part of the model simulation. Anecdotal evidence suggests that, because of the absence of database since version 5, a large section of users are still using the previous version of this sample data regardless of the relevance to their building materials and combustibles which are modelled in the simulation. This has potentially resulted in inaccurate analyses and estimations of life safety and property protection.

Simulation of real fire scenarios should ideally specify the material properties which are used for that particular building. For example, Moghaddam et al. (2004) conducted a fire behaviour study of combustible wall linings using FDS versions 3 and 4 for ISO 9705 room fire tests. A lining test was conducted to determine the contribution of combustible lining materials to the development of room fires. The absence of representative fire properties related to the lining material led to an inaccurate numerical simulation results.

This year, the latest version of FDS (version 6.0.9) was released (McGrattan et al. 2012). Although the pyrolysis model of solid materials has not been changed from version 5, several changes in input parameters have been made to increase the functionality and readability of the input file where the pyrolysis model is allowed for shrinkage and swelling based on the specified material density (McGrattan et al. 2008). However, evaporation and combustion models have been partially changed from version 5. In addition, four different LES model options are introduced with the Deardoff model (Deardoff 1972) being the new default model whereas constant Smagoronski model (Smagorinsky 1963) was the previous default model.

Jiang (2006) conducted a detailed literature review on decomposition processes (such as pyrolysis) as well as ignition and flame spread processes and required experimental techniques to study these processes. It was reported that the pyrolysis of combustible solids and evaporation of liquid can be represented in fire models by the mass loss rate (MLR). A number of properties are required to obtain the correct MLR (combustible volatile production rate) and then convert it to the heat release rate (HRR) through oxidative reactions within the CFD-based fire model.

The required properties are:

- Pyrolysis parameters:
 - Chemical kinetics:
 - Activation energy (E)
 - Pre-exponential factor (A)
 - Reaction order (n)
 - Effective heat of gasification/reaction (HoR)
 - Char yield
- Combustion parameters:

- Effective heat of combustion (E_{HoC})
- Smoke yield
- Soot yield
- CO yield
- CO₂ yield
- Char residue
- Thermal properties:
 - Thermal conductivity (λ)
 - Specific heat capacity (C_p)
- Physical properties:
 - Density (ρ)
 - Absorption coefficient (κ)
 - Emissivity (ε)

The abovementioned properties can be collectively termed fire properties. Most of these are macroscopic or bulk effective model parameters, rather than microscopic or fundamental properties. As the model output is strongly dependent on these fire properties, characterization of these properties is vital. Traditionally, bench-scale tests were used to obtain the various properties and parameters mentioned above. However, there is not a single bench-scale test method available to measure all of these properties, thus requiring the use of a number of techniques and instrumentation including:

- A cone calorimeter (American Society for Testing and Materials 2004a) to measure combustion parameters;
- A thermogravimetric analyser (TGA) (American Society for Testing and Materials 2007) to measure pyrolysis/combustion kinetics;
- A differential scanning calorimeter (DSC) (American Society for Testing and Materials 2005) to measure the effective heat of reaction and specific heat capacity (usually in conjunction with TGA);
- A hot disk thermal constant analyser (HDA) (American Society for Testing and Materials 2015) to measure density, thermal conductivity and specific heat capacity;

- An infrared thermograph (American Society for Testing and Materials 2014) to measure the emissivity of the material;
- Other innovative experimental techniques. For example, a technique developed by Li et al. (2014) consisting of a radiant heater, heat flux gauge, kaowool slab etc., can measure absorption coefficient.

For the standard techniques, many of the material properties obtained are constant while others vary with respect to temperature, heating rate, radiation flux etc. In fire situations, the temperature of materials (both combustible and non-combustible) and incident radiation constantly change. The FDS handles the change in some thermo-physical property values (i.e. λ and C_p) with respect to material temperature using thermal RAMP and tabular functions (details in CHAPTER 7). In addition, the size of a growing fire changes with time and so the temperature of materials (both combustible and non-combustible), the rate at which the materials are heated, and the incident radiation upon the materials also changes. By accounting for these parameter value variations in CFD based fire models, improvements in fire simulations can be made.

1.1.1 Pyrolysis Parameters

Pyrolysis parameter values describe the solid phase reaction that occurs leading to and during burning of a material. The kinetic parameters are important in characterizing the rate of pyrolysis reactions and are collectively known as the kinetic triplet:

- Pre-exponential factor, A (1/s), also known as a *frequency factor* is the frequency of the collisions between molecules.
- Activation Energy, E (kJ/mol), is the minimum amount of energy required to start a chemical reaction.
- Order of reaction (n), is the index or exponent, to which its concentration term in the chemical reaction rate equation is raised.

Chemical kinetic values can be obtained by means of TGA which is perhaps the most common technique used to investigate the thermal decomposition of materials. It is widely used to obtain a better understanding of pyrolysis (Slopiecka et al. 2012) and

can provide a rapid method to measure the temperature decomposition profile of a material (American Society for Testing and Materials 2007). For charring materials to describe pyrolysis, char yield is needed to be determined from TG analysis which is the amount of solids remaining at the end of the pyrolysis process under an inert atmosphere.

Another important parameter is the effective heat of reaction (*HoR*) or gasification. In the context of pyrolysis, the heat of reaction (*HoR*) can be defined as the latent heat required during the gasification of a solid fuel (Sibulkin 1986). For relatively low (microscopic) heating rates such as those encountered using TGA experiments, a gasification process will occur *via* solid-liquid-gas transformation, particularly in the case of materials that melt such as PMMA.

For higher heating rates, gasification can occur *via* a solid-gas transformation which may require more energy. For some materials undergoing endothermic reactions, heating rates higher than 5 K/min are recommended (Kodur & Harmathy 2002) and are considered to be macroscopic heating rates. In this study, the term of *HoR* is defined as an effective model parameter to account for heat loss during a pyrolysis process for the range of materials tested.

1.1.2 Thermal Properties

Several thermal properties influence the rise in temperature of a material when it is exposed to heat including:

- Thermal conductivity, λ ($W m^{-1} K^{-1}$), where the transfer of heat energy over a mass can result in a temperature gradient. In porous materials, heat transfer can occur through all its forms; conduction, radiation and convection while for non-porous solids it is solely through conduction. This property can be obtained *via* various techniques (Assael & Gialou 2003, Gupta, Yang & Roy 2003, Baxter 1946, Hankalin, Ahonen & Raiko 2009, Hu, Yu & Wei 2007). In this study, the measurement of the thermal conductivity is conducted by means of a Transient Plane Source (TPS) technique using a Thermal Constant (TC) Analyser TPS 500.
- Specific heat, C_p ($kJ kg^{-1} K^{-1}$), is the amount of heat energy needed to elevate a single unit of mass of a material by a unit of temperature. A single TGA

instrument is able to provide specific heat data in $\text{MJ m}^{-3} \text{K}^{-1}$. It should also be noted that both thermal conductivity and specific heat capacity can be temperature dependant.

- Thermal diffusivity (combination of ρ , λ and C_p).
- Thermal expansion/contraction (i.e. the linear shrinkage of materials due to heating per degree of temperature (Kodur & Harmathy 2002)).

In this research the focus is on the thermal conductivity and specific heat capacity of charring and non-charring combustible materials as these properties are important inputs required in fire simulations (Pau et al. 2014). The theoretical background and the experimental techniques conducted in deriving the thermal properties are presented and discussed in CHAPTER 2.

1.1.3 Combustion Parameters

The flammability of a material (combustion parameters) can be studied by means of a cone calorimeter, one of the more widely used bench-scale techniques in fire studies. These are crucial properties for a CFD-based fire model which can be obtained from the measurement and include:

- Heat release rate, HRR (kW), is the rate of heat that is produced by the fire. It is a critical parameter to characterise the fire.
- Effective heat of combustion, EHoC (kJ/kg) is the amount of heat released when one kg of material is burned during a fire. It is derived by dividing the HRR by material mass loss; both measured in a cone calorimeter test.
- Smoke yield is the volume of smoke produced during combustion.
- Soot yield is the quantification of carbon particulates generated during combustion.
- CO yield is the volume of carbon monoxide generated during combustion.
- CO₂ yield is the volume of carbon dioxide generated during combustion.

- Char residue is the amount of solids remaining at the end of the pyrolysis process under an inert atmosphere with respect to charring materials.

1.1.4 Physical Properties

In addition to the aforementioned properties and parameters, several material physical properties are also used in FDS modelling including:

- Absorption Coefficient, κ (m^{-1}) which represents the depth from the material surface up to which radiation is absorbed, usually expressed as the inverse of that depth. For opaque materials, it is considered that radiation is absorbed at the surface but for translucent material this property is more important.
- Emissivity, ε , based on Kirchhoff's Law, it is the ratio of the radiation emitted by the surface from a blackbody at the same temperature (Bergman, Incropera & Lavine 2011).

1.2 Selection of Materials

The combustible materials selected for investigation in this study can be divided into three (3) groups namely thermoplastic-based, wood-based and fabric. While the first group belongs to the non-charring category of materials, the latter two groups fall in charring category of combustible building materials. Poly (methyl methacrylate) (PMMA), also widely known as acrylic or plexiglass, is the selected thermoplastic-based non-charring material. Among the charring materials, pine, cotton and wool are tested. The selection of these materials was based on their extensive use in the building and construction industries. Among these, PMMA and pine can be considered as relatively “pure” materials representative of non-charring and charring materials respectively and are used for validating the coupled pyrolysis and combustion model after parameterization.

1.2.1 Poly (methyl methacrylate)

Poly (methyl methacrylate) is a synthetic polymer that is widely used in building construction particularly for windows, doors, skylight roof, bath enclosures etc. There are many advantages in using acrylic as a glass substitute in building components or

finishes. Acrylic is much lighter and more transparent than glass, and therefore windows and skylights, for example, give better light transmission and insulation than glass. However this material has a critical disadvantage in that it has a relatively low melting point although this may prove useful in some applications such as in roofing materials for shopping centres etc. where melting creates an escape route for smoke and any hot toxic gases.

1.2.2 Pine

Pine is widely used in buildings due to its versatility in structural and decorative applications. Used in flooring, ceilings, doors, window frames and furniture, applications can range from the basics such as plywood, and panelling to more complex as joinery, cladding, decking, fencing and furniture.

1.2.3 Fabrics (Cotton and Wool)

Fabric based furnishing materials are not only the source of fuel but they also the contributor to the spread of flames (Jiang 2006). The composition of fabric materials is highly variable with 100% cotton or 100% wool fabrics commonly used as curtains and furnishing. These materials enhance the interiors of buildings due to the wide variety of colours and designs. However, fabrics are generally fast to ignite in fires and quickly respond to the heat exposed. Thus, a detailed study of flammability and thermal properties are crucial to understand the combustion behaviour under various conditions where there is currently a limited source of literature data.

Each of these materials was selected to address the need for a comprehensive set of fire properties for parameterization of a coupled pyrolysis and combustion model. Only two properties (absorption coefficient and emissivity) are excluded in this study. Since most combustible building materials absorb radiative heat at the surface and blacken soon after ignition occurs, default values for these are often applicable and acceptable. In the following section, a literature review is presented with a focus on the results of studies where the properties of these materials are studied using equipment such as the cone calorimeter, TGA, DSC and HDA.

1.3 Overview of Previous Studies

Researchers have used a variety of bench scale equipment to characterize the materials investigated in this study and these are discussed in this section.

1.3.1 Cone Calorimeter

The cone calorimeter is widely used to measure the combustion properties of different materials and a summary of several key studies is presented in Table 1.1. In these studies, the focus is primarily the determination of the flammability parameters for a range of material groups including wood, wood based products, polymer and fabrics.

Table 1.1: Summary of flammability studies using cone calorimetry

Material	Authors	Heat Flux (kW/m²)
PMMA	(Rhodes & Quintiere 1996)	0 to 75
PMMA	(Chung & Drysdale 2002)	15 and 20
PMMA	(Zeng, Li & Chow 2002)	10 to 50
PMMA	(Chow et al. 2004)	20
PMMA	(Linteris et al. 2005)	0,5,10,25, 50, and 75
PMMA	(Moghtaderi et al. 1998)	25, 35 and 50
PMMA	(Tsai 2009)	15, 30, and 50
PMMA	(Brescianini et al. 1997)	50
Charring Material	(Yang et al. 2003)	20, 30, 40 and 50
Maple plywood	(Swann, Hartman & Beyler 2008)	6 to 15
Timber	(Delichatsios, Paroz & Bhargava 2003)	20, 25, 30, 40 and 50
Timber (various)	(Jiang 2006)	20, 30, 40, 50 and 75
Plywood	(Delichatsios 2005)	25, 35 and 50
Plywood	(Fateh, Rogaume & Richard 2014)	20,30,40,50,60 and 70
Pine	(Moghtaderi et al. 1997)	14 to 65
Wood based product	(Tsai 2009)	15,30 and 50
Redwood slab	(Hagge, Bryden & Diitenberger 2004)	35 and 50
Woods	(Diitenberger 2012)	35
Wood products	(östman & Tsantaridis 1995)	50

Material	Authors	Heat Flux (kW/m²)
Wood products	(Dietenberger & Grexa 2000)	35
Wood	(Moghtaderi et al. 1998)	25, 35 and 50
Woods	(Grexia et al. 1996)	20,25,30,35,40,50 and 65
Nordic Spruce wood	(Hagen et al. 2009)	30, 40, 50 and 60
Wool	(Flambard et al. 2002)	75
Fabric	(Nazaré, Kandola & Horrocks 2002)	15 to 60
Cotton	(Hshieh & Beeson 1995)	25
Fabric	(Price et al. 2000)	35
Upholstered furniture	(Babrauskas et al. 1997)	35
Upholstered furniture	(Denize 2000)	35
Upholstered furniture	(Coles 2001)	35
Upholstered furniture	(Ho 2007)	25, 35, 50 and 75
Furniture materials	(Chow 2002)	50
Furniture materials	(Jiang 2006)	10 to 75
Furniture materials	(Price et al. 2000)	35

Rhodes and Quintiere (1996) generated ignition and burning rate data for PMMA to establish an experimental procedure in order to predict the ignition and burning of samples. Chung and Drysdale (2002) measured a range of fire properties and data obtained was used to model the upward flame spread of PMMA sheets. Zeng, Li and Chow. (2002) studied the burning behaviour of PMMA at radiation levels ranging from 10 to 50 kW/m² and found that the material would burn steadily under low heat flux or with a thicker sample size.

Denize (2000) adopted a similar approach for upholstered furniture materials, particularly polyurethane foam, propylene and fabric materials. He found that the variation in a materials' cover has a significant effect on the characteristic of combustion. Coles (2001) continued the study carried out by Denize (2000) using 3 types of foams and 14 types of fabrics. He concluded that fabrics demonstrate a strong influence on the small-scale test and the presence of fabric on foam increased the

ignition time. Ho (2007) conducted a cone calorimeter study on charring timber in order to develop a flame spread model.

Jiang (2006) carried out studies using a cone calorimeter and TGA with materials including timber, different types of polyurethane foam and fabrics, to obtain fire properties and enhance the understanding of the decomposition and pyrolysis process. He reported that the major parameters measured were matched with the others' experimental data.

1.3.2 Thermal Analysis (TGA and DSC)

Researchers have conducted numerous kinetic and *HoR* studies on charring and non-charring materials using TGA and DSC. A number of these studies have been carried out to determine kinetic parameters including those of Ozawa (1975, 1970), Lesnikovich and Levchik (1983), Anderson et al. (1997), Jiang (2006) and Hillier, Bezzant and Fletcher (2010). Senecca (2007) carried out five set of TGA tests on biomasses namely pine seed shells, olive husk and wood chips to assess their reactivity for pyrolysis and other chemical properties. Table 1.2 summarises many of these studies for the determination of the kinetic parameters by means of TGA with the various heating rates employed in the test protocols.

Table 1.2: Summary of heating rates used in TGA studies

Material	Authors	Heating Rate (K/min)
PMMA	(Ballistreri, Montaudo & Puglisi 1984)	5, 10, 15 and 20
PMMA	(Kashiwagi, Inaba & Brown 1986)	0.5, 0.7, 1, 2, 3 and 5
PMMA	(Peterson, Vyazovkin & Wight 1999)	0.5 to 20
PMMA	(Lee & Viswanath 2000)	10
PMMA	(Ferriol et al. 2003)	2, 5, 8, 10
PMMA	(Matala 2008)	2,5,10 and 20
PMMA	(Zhang 2004)	10
Pinewood	(Jiang 2006)	5 to 200
Pinewood	(Matala 2008)	2,5,10 and 20
Pine	(Anca-Couce et al. 2012)	2.5 to 10

Material	Authors	Heating Rate (K/min)
Pine	(Su et al. 2012)	20
Poplar wood	(Slopiecka, Bartocci & Fantozzi 2012)	2,5,10 and 15
Cellulose and pine sawdust	(Bilbao, Arauzo & Salvador 1995)	Between 2 and 53
Birch and pine	(Hasalová, Ira & Jahoda 2012)	5,15 and 25
Cellulose	(Suuberg, Milosavljevic & Oja 1996)	1, 6 and 60
Cellulose	(Grønli, Antal & Varhegyi 1999)	5 and 40
Lignin	(Jiang, Nowakowski & Bridgewater 2010)	2 to 200
Cotton	(Chatterjee & Conrad 1966)	3
Cotton	(Shafizadeh et al. 1982)	15
Cotton	(Faroq et al. 1994)	2 to 15
Cotton	(Moltó et al. 2006)	5, 10 and 20
Cotton	(Jiang 2006)	50 to 200
Cotton	(Gaan & Sun 2009)	10 to 40
Cotton	(Forouharshad et al. 2011)	10
Cotton	(Zhu et al. 2004)	10
Cotton and cotton mix	(Muralidhara & Sreenivasan 2010)	10
Wool	(Beck, Gordon & Ingham 1976)	4, 16, 20 and 128
Wool	(Popescu & Augustin 1999)	10, 13, 15, 17 and 20
Wool	(Tian et al. 1998)	10

A summary of studies reporting the DSC analysis of different materials at various heating rates is presented in Table 1.3 and it is clear that in these studies, the maximum heating rate used is 20 K/min. There are also few studies using the same materials that are reported in this research. For example, Rath et al. (2003) studied the heat of pyrolysis of beech and spruce wood, using the DSC from 75 to 500°C, however, these materials were only tested at 10 K/min. In another study, Su et al. (2012) investigated the *HoR* of pine at 20 K/min although this study was conducted only in oxygen

environment where the effects of its concentration were compared. The pyrolysis phenomenon is typically study in an inert atmosphere with a nitrogen purge which is the case in the study presented in this current work. In another study, Zhu et al. (2004) conducted a study on cotton fabric over a temperature range of 80 to 500°C at 10 K/min.

Table 1.3: Summary of heating rates used in *HoR* studies by DSC

Material	Authors	Heating Rate (K/min)
Polymer	(Frederick & Mentzer 1975)	10
Polymer	(Stoliarov & Walters 2008)	5
PMMA	(Peterson, Vyazovkin & Wight 1999)	20
PMMA	(Zhang 2004)	10
Pinewood	(Anca-Couce et al. 2012)	10
Pinewood	(Su et al. 2012)	20
Wood	(Rath 2003)	10
Cotton	(Zhu et al. 2004)	10

1.3.3 Hot Disk Thermal Constant Analyser (HDA)

Thermal conductivities for PMMA have been studied by different researchers (Assael et al. 2005, Jansson 2004) and over various temperature ranges using HDA as shown in Table 1.4. However, these studies are limited to the maximum temperature range of 80°C. Hankalin, Ahonen and Raiko (2009) investigated the thermal properties of pine over various temperature ranges and Fonseca and Barreira (2009) investigated both virgin and charred pine.

Table 1.4: Summary of temperature ranges in HDA studies

Material	Authors	Temperature (°C)
PMMA	(Jansson 2004)	20 to 80
PMMA	(Assael et al. 2005)	34 to 79
Wood	(Suleiman et al. 1999)	20, 100
Wood	(Adl-Zarrabi, Boström & Wickström 2006)	20
Charred wood	(Gupta, Yang & Roy 2003)	36

Pinewood	(Hankalin, Ahonen & Raiko 2009)	36, 64 and 97
Pinewood & Char	(Fonseca & Barreira 2009)	350 and 500

1.3.4 Coupled Pyrolysis and Combustion Simulation

It should be noted that due to the enormous computational requirements, many fire safety engineers and fire researchers avoid modelling a pyrolysis component in their modelling of fire scenarios. Three-dimensional CFD based simulations of bench-scale (cone calorimeter) tests with coupled solid and gas phase reactions have only recently been conducted (Marquis et al. 2013, Riccio et al. 2013, Pau 2013). The lack of similar studies may be due to the impractical computational requirements of modelling reactions at a millimetre scale. Marquis et al. (2013) and Pau (2013) have used version 5 of FDS, whereas others have implemented a user-defined function excluding the fluid momentum equation in the ANSYS commercial Finite Element Modelling (FEM) software (Riccio et al. 2013). All three studies have been carried out with complex materials rather than 'pure' charring and non-charring materials.

Although the present study uses FDS as a sample CFD-based fire model for parameterization and validation, the same methods can be applied to any coupled pyrolysis and combustion model. It should also be noted that there have been some studies that parameterize only FDS's pyrolysis model, (Li, Gong & Stoliarov 2014, Kim, Lautenberger & Dembsey 2009) while the current study is focussed on coupled pyrolysis and combustion models. The study of Pau (2013) is somewhat comparable to the current study, however it focused on the burning behaviour of specific types of complex non-charring materials (i.e. polyurethane foams) and the effects of variations in heating rates and irradiance were not studied.

1.4 Research Gaps

It is evident from the previous studies that although a number of researchers have reported fire properties of selected materials using cone calorimeter, TGA, DSC and HDA, these have been mainly tested in isolation. However, to determine a more complete combustible volatile production rate of a material and their oxidized reaction rate, a full set of fire properties is needed. There are few comprehensive studies that

have reported a full set of fire property data that is required for coupled pyrolysis and combustion modelling. Certainly no such study was carried out for combustible materials commonly used in Australian buildings with the study of Jiang (2006) only including cone calorimeter and TGA measurements.

Furthermore, at different irradiation levels, various property values change (Shi 2014, Jiang 2006) and this is also the case with changes in heating rates (Celina, Gillen & Assink 2005, Celina 2013, Vyazovkin et al. 2011, Missoum, Gupta & Chen 1997, Milosavljevic, Oja & Suuberg 1996). Thus, it is important to understand how properties change with various fire conditions and how they can affect fire simulations. The above discussion demonstrates that there is a need to carry out a study to develop a method to characterize fire properties for unknown, new or novel materials and enable users to optimise the use of these properties for coupled pyrolysis and combustion modelling. It is also important to comprehensively study several charring and non-charring combustible materials commonly used in Australian buildings as sample materials. These are summarised in Section 1.2 with previous isolated or standalone studies using these materials presented in Section 1.3.

In this study, a fire property characterization method will be developed and explored by extensively measuring fire properties of four charring and non-charring materials (except emissivity and absorption coefficient) at various heating rates and radiation fluxes; and proposing the possibility of inclusion of this variation of values as functions of heating rates or radiation fluxes or temperature in CFD based fire models. Although this study uses FDS as a sample CFD-based fire model for parameterization and validation, the methods can be applied to any coupled pyrolysis and combustion model. It should also be noted that there have been studies to parameterize only the FDS's pyrolysis model, (Li, Gong & Stoliarov 2014, Kim, Lautenberger & Dembsey 2009) while this study is focussed on coupled pyrolysis and combustion model.

From section 1.3.4, it is revealed that validation of version 6 of FDS (FDS6) for coupled solid and gas phase reactions has not yet been conducted. As mentioned earlier FDS6 incorporates improved combustion and LES so it is therefore important that any validation study should be conducted with FDS6 and it is much simpler to involve 'pure' materials, rather than complex combustible materials. Characterization of all required fire properties of 'pure' materials and their optimum use will greatly assist such

validation study. In fact, this three-dimensional simulation with coupled solid and gas phase reactions will provide a check of the validity of these fire properties as well as the validation of FDS itself.

1.5 Research Aims

This study is motivated to enable a user to quantify the representative fire properties of unknown or novel materials by developing a comprehensive method of data collection and analysis. Once the methods for determining fire properties is proposed, the derived properties will be used as inputs into a CFD-based fire model to accurately simulate fire growth, established burning and decay to extinguishment or burnout. The primary aim of this research is therefore to characterize the fire properties of a representative set of materials for coupled pyrolysis and combustion simulation and to explore a method for the optimised use of those properties.

These aims will be achieved by the following objectives:

1. To investigate and implement suitable experimental techniques and data post-processing schemes and methods by bench-scale tests at various heat fluxes, heating rate and temperature range for determining complete set of fire properties;
2. To develop relationships between fire properties as a function of heat flux or heating rate or temperature through regression analysis;
3. To conduct coupled pyrolysis and combustion simulations using the fire properties collected by the experimental study as input variables and to optimise the use of those properties in the model;

1.6 Research Methods

The proposed charring and non-charring combustible materials to be considered are common combustible materials used and found in the Australian building construction and consist of wood-based, thermoplastic-based and fabric-based materials. The selected materials are pine, PMMA, cotton and wool with the selection of these materials based on their extensive use in the building and construction industries (see Section 1.2).

1.7 Thesis Outline

The research presented in this thesis was performed over a series of stages and is outlined below:

Chapter(s)	Contents
1	Introduction and literature review of previous studies on fire properties.
2,3	Development of experimental techniques and data post-processing schemes/methods.
2,3	Experimental study combining the use of cone calorimeter, TGA, DSC and HDA to obtain required fire properties. Data reduction for chemical kinetics and heat of reaction.
4, 5, 6	Regression analysis of fire properties obtained from the experimental work to obtain relationship as a function of heat flux or heating rate or temperature.
7	Coupled pyrolysis and combustion simulations using input data of characterized fire properties with a sensitivity study to: <ul style="list-style-type: none">• assess the sensitivity of variation of grid; thermo-physical properties and yield of char; and chemical kinetics and heat of reaction values with respect to heating rates• assess how well CFD-based fire model can predict HRR• assess any need for optimised use of fire properties.
8	<ul style="list-style-type: none">• Proposal for development of optimised use method to include variations of fire properties obtained from the experimental work.• Conclusions and recommendations.

CHAPTER 2

EXPERIMENTAL TECHNIQUES

2.1 Cone Calorimeter

The cone calorimeter is a bench-scale apparatus for measuring the heat release rate (HRR) of materials by the principle of oxygen consumption (Huggett 1980). It also simultaneously measures the mass loss rate (MLR), CO yield, CO₂ yield and soot yield. The effective heat of combustion (EHoC) is calculated using the measured values of HRR and MLR. The HRR in particular has a significant effect that leads to the fire hazard in a closed compartment and greatly influences the fire development (Jiang 2006).

The HRR is typically measured per unit area, \dot{q}'' (kW/m²). The EHoC is derived from the HRR and the mass flux, \dot{m}'' (mass loss rate per unit area):

$$\Delta H_{c, \text{eff}} = \dot{q}'' / \dot{m}'' \quad (2.1)$$

The combustion efficiency (\emptyset) of the tested material can be determined by the following equation:

$$\emptyset = \Delta H_{c, \text{eff}} / \Delta H_c \quad (2.2)$$

where the ΔH_c is the theoretical heat of combustion.

The cone calorimeter is manufactured by Fire Testing Technology (FTT) in the United Kingdom, a company established in 1989. The FTT cone calorimeter complies with standards including ISO 5660 (International Organization for Standardization (ISO) 2002) and ASTM 1354 (American Society for Testing and Materials 2004a). Figure 2.1 shows a schematic diagram of the FTT cone calorimeter. As shown in figure, the cone calorimeter system is comprised of a number of components as outlined in Table 2.2. Complete details of the various components are described elsewhere (Fire Testing Technology 1998).

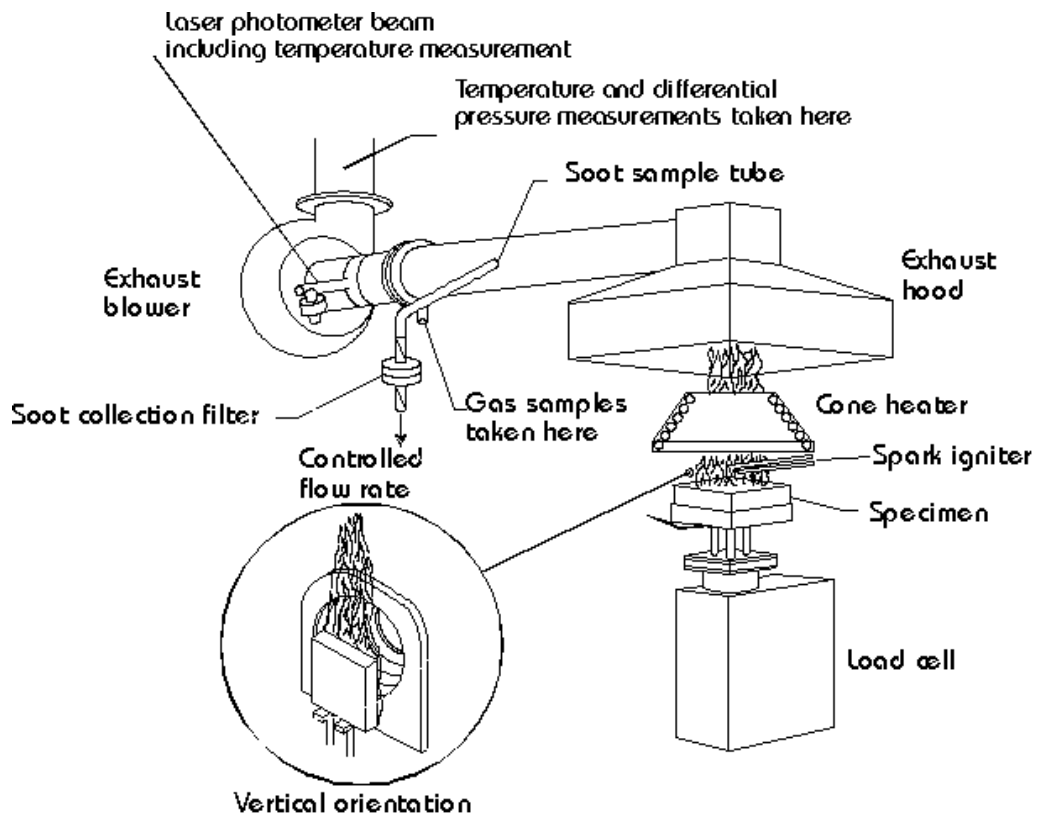


Figure 2.1: Schematic drawing of the cone calorimeter from (Babrauskas & Peacock 1992)

Table 2.1: Cone calorimeter component overview

Component	Purpose
Cone heater	To provide a heat flux at the maximum of 100 kW/m ²
Radiation shield	To protect sample from radiation before starting the test
Specimen holder	To place the specimen for testing
Load cell	To measure the mass loss
Spark igniter	To provide spark ignition for specimen
Heat flux meter	To set the irradiance level of the test
Calibration burner	To calibrate the rate of heat release of the apparatus
Data collection and analysing system	To process and analyse data

2.1.1 Calibration

Calibration of the cone calorimeter is vital to maintain the equipment and to ensure the accuracy of its measurement. Daily, weekly and intermittent calibration routines were performed over the course of this research in accordance with the manufacturers' specifications (Fire Testing Technology 1998).

Daily Calibration Procedure

- Changing the drying and CO₂ removal agent: under normal operation, the gas flow passes through a series of columns to remove moisture and CO₂ in the gas stream passing the cold trap. The outer columns contain Drierite used to remove moisture with a centre column containing Ascarite used to remove CO₂ and changing these absorbing resins in the columns in each of three glass tubes located near the oxygen analyser is part of the daily calibration/maintenance procedures.
- Changing soot filter: a disposable soot filter is changed when needed to prevent the soot from getting into the pump and the analysers.
- Gas analyser calibration: this task is performed mostly during each test to ensure the overall calibration is correct. This task involved zeroing the O₂, CO₂ and CO analysers and then spanning the CO₂ and CO analysers.
- Setting the flow rates for the exhaust and soot sampler: the exhaust fan must be turned to ensure that the fan is functioning. The flow rates need to be checked and the reading should be around 24 L/s or manually adjusted accordingly.

Weekly Calibration Procedure

In addition to the daily calibrations, a more thorough weekly calibration procedure is required as outlined in the User's Guide (Fire Testing Technology 1998).

- Mass calibration of the load cell: to ensure that the sample weight recorded by the instrument is correct.
- Laser calibration for smoke measurement: to ensure that the laser is functioning for the measurement.

- Checking system calibration with PMMA: following a daily calibration, this task is performed by burning the PMMA sample at irradiance level of 50 kW/m². The data is recorded once the test is completed to ensure that measured parameters (see Table 2.1) are within the correct range.

Intermittent Calibration Procedure

At less frequent intervals, additional calibration procedures are also carried out:

- Heater thermocouple calibration (cone irradiance level): to ensure the heat flux measurement of each test is correct. This task was performed at each irradiance level tested in this study. Tabulated data of heat flux vs. temperature for previous calibration is followed as a guide and the temperature set point is constantly adjusted during this test if needed to set the thermocouples at the right temperature.
- Gas burner (methane calibration) check, 5 kW: following a daily calibration, this procedure is performed to ensure that the heat release rate record by the instrument is correct and is performed manually by checking the methane gas calibration burner as shown in Figure 2.2. During this task, the burner should read the heat release rate at 5 kW, or should be adjusted manually over a period of about 4 minutes.



Figure 2.2: Burning test sample material in the cone calorimeter

2.1.2 Operating Procedure

The selected materials in this study were tested in the cone calorimeter at different irradiance levels of 20, 30, 40, 50 and 75 kW/m² with multiple runs performed to obtain average values. For each test, the sample was cut into 100 x 100 mm sections and conditioned for 48 hours at 23°C with 50% relative humidity (RH).

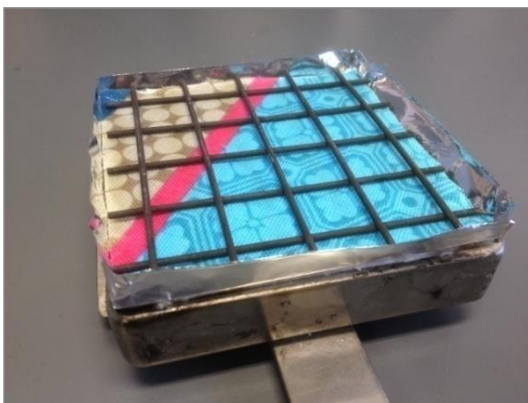
For PMMA and pine, samples were wrapped with aluminium foil around the edge with the shiny part of the foil facing towards the sample. A piece of fibre blanket was placed in the bottom of the sample holder for insulation purpose. The sample was then placed in the sample holder as illustrated in Figure 2.3(a) and (b). For fabrics, the sample was setup as shown in Figure 2.3(c) and (d). An aluminium foil frame was prepared to hold the sample and a wire grid was placed on top of the sample following the guideline [International Organization for Standardization (ISO) 2002]. Since fabrics are very low in mass, this provides better attachment to the backing pad as outlined by Tata et al. (2011).



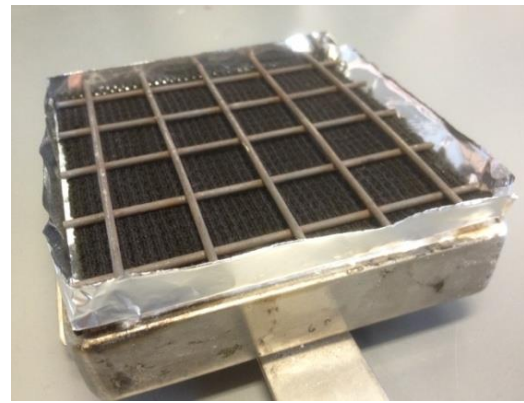
(a) PMMA



(b) Pine



(c) Cotton



(d) Wool

Figure 2.3: Sample material preparation for the cone calorimeter test

Initially, there was a concern relating to the use of wire grids while conducting the test due to the high conductivity of the grid material. However, Tata et al. (2011) reported that the wire grid has little effect on the peak HRR and also time to ignite. They also found that the test conducted without wire grid has resulted in higher standard deviation due to the sample folding and touching the spark igniter.

2.2 Hot Disk Thermal Constant Analyser

A number of techniques and types of equipment are available to measure thermal conductivity and specific heat capacities of materials. In this study, these thermal properties were measured using the Transient Plane Source (TPS) technique which is a non-steady state method that allows fast, accurate measurements of thermal properties. This technique is widely used for its ability to simultaneously measure thermal properties including conductivity, thermal diffusivity and specific heat capacity (Gustafsson 1991).

It is arguable that before non-steady state methods such as TPS, measurements would typically take a significantly longer time to perform resulting in the prioritisation of tests performed over a wider range of elevated temperatures. However, as the technology has progressed with new and faster methods, material properties can be obtained on a greater scale and with more detail.

In this study the measurements were conducted using Hot Disk Thermal Constant Analyser TPS 500 (Thermtest Inc. 2012) as shown in Figure 2.4. The equipment consists of the HDA unit, a sensor and a sample holder. The test can be performed at ambient temperature or at higher temperatures with the aid of a temperature-controlled oven. The range of temperature accessible for the measurement depends on the sensor specification and also the capabilities of the temperature-controlled oven.



Figure 2.4: Hot disk thermal constant analyser

For these experiments, samples are placed on the sample holder and the sensor is sandwiched between two samples. For measurements at high temperatures up to 300°C, a TPS PEEK High Temperature Adapter was used with a different adapter used for measurements at ambient temperatures. Kapton sensors type 5501 with a 6.403 mm radius and type 5465 with a 3.189 mm radius as shown in Figure 2.5 were used in this study. These sensors act as a heat source as well as temperature sensors (Pau 2013) and can be used for temperatures up to 300°C. In these experiments, the sensors were placed on the adapter connected to the HDA and a forced-air oven (TFO-1) was used for high temperature measurements up to 300°C. Details of the installation procedure are discussed in the User's Manual (Thermtest Inc. 2012).



(a) type 5501



(b) type 5465

Figure 2.5: Kapton sensors used in the thermal properties measurement

2.2.1 Calibration

Calibration of the HDA is performed by testing a stainless steel sample using the Kapton sensor type 5501 at room temperature, 75°C and 100°C. The experimental setup shown in Figure 2.6 depicts the covered sensor which is centrally sandwiched between two samples. It is also tightly clamped to minimise the air gap between the sample and sensor to avoid the risk of overheating and potential damage to the sensor as outlined in User's Manual (Thermtest Inc. 2012). In this work, the stainless steel calibration was performed using 1 W of heating power for 10 seconds before performing the sample measurement.

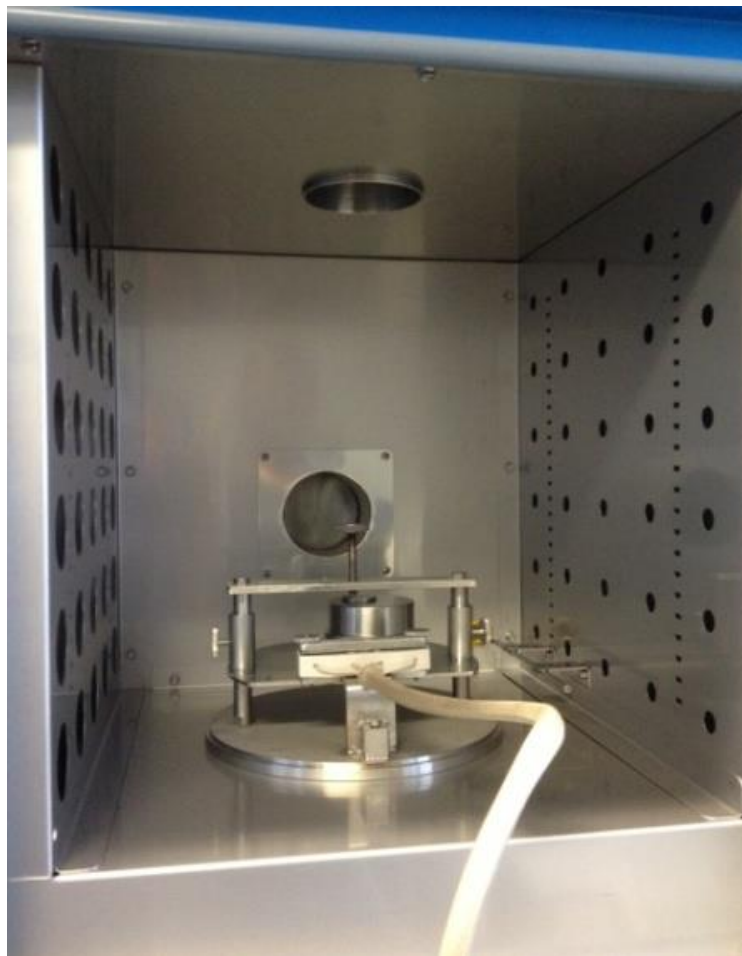


Figure 2.6: Calibration is performed using stainless steel

2.2.2 Probing Depth

For low conducting samples such as pine, pine char, cotton and wool, the heating power was set to 100 mW and was increased to 600 mW for the polymeric materials

such as PMMA. The probing depth is one of the crucial factors in the determination of thermal conductivity and heat capacity by means of HDA. Gustavsson, Karawachi & Gustafsson. (1994) discussed the transient measurements for thin samples using HDA and the dependence of probing depth for accurate measurement. In this study, the probing depth in mm was different for each of the materials as their thickness and dimensions varied.

The instrument works on the assumption that the sample has sufficient depth to allow enough time for the thermal wave or thermal penetration depth over the measurement period. The probing depth should be less than the geometrical boundary of the sample so that the thermal wave should not cross the sample boundary. Furthermore, the total to characteristic time ratio should be in the range of 0.98 to 1.1. Total characteristic time is defined as a relation between diffusivity, time for measurement and radius of sensor (Thermtest Inc. 2012). It was found that a total to characteristic time ratio of 1 gave converged results. Therefore for all samples (as they are thermoplastic and low conducting materials), a measuring time of 160 seconds (suggested characteristic time by HDA manufacturer) per test was used. Figure 2.7 shows the limit of the probing depth, which is less than the smallest distance between the probe and the nearest geometrical boundary. In this study, the probing depth used for measurement for PMMA, pine, charred pine, cotton and wool were 14, 15, 15, 10.5 and 10.4 mm respectively.

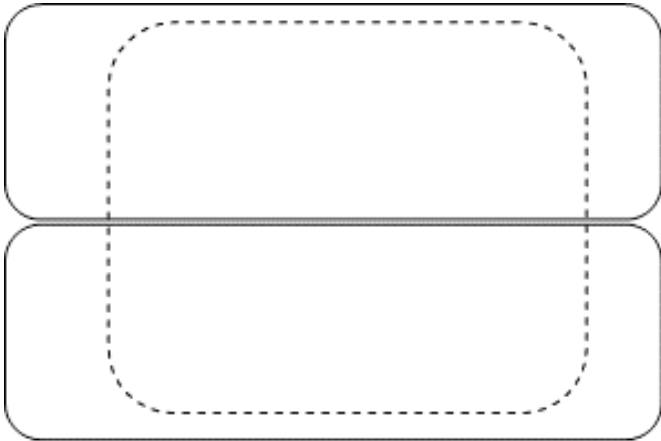


Figure 2.7: Limit of the probing depth

2.2.3 Operating Procedure

Adequate pre-heating of the oven prior to the test was required in order to stabilise the inside temperature. In the programme software, the heating power was set accordingly as explained in Section 2.2.2. The probing depth used is also discussed in Section 2.2.2 and illustrated in Figure 2.7.

The thermal properties of non-charring and charring combustible building materials (PMMA, pine, charred pine, cotton and wool) were measured from ambient temperature up to 225°C. Samples of approximately 100 x 100 mm (L x W) of PMMA and pine sample were tested with the charred pine reduced to approximately 60 x 46mm due to the flaky nature of fully charred pine and difficulties obtaining appropriate samples (see Figure 2.8). In all cases, the thickness of each sample varied between 12 to 34 mm.

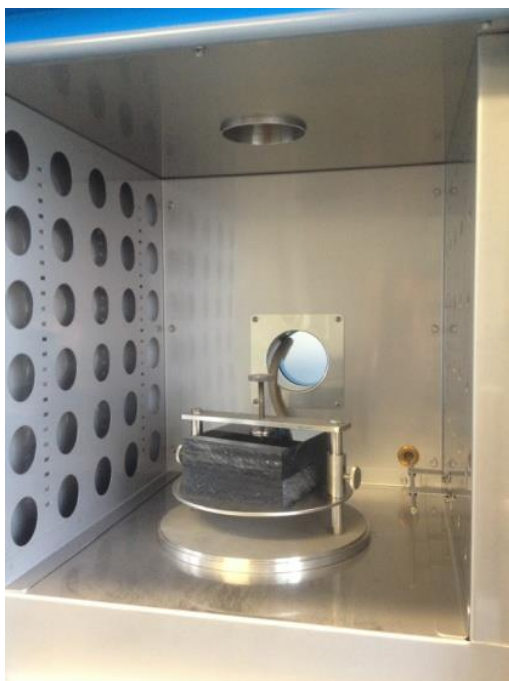


Figure 2.8: Images of various pine char specimens

The specimens were placed on the sample holder and sandwiched over the hot disk sensor as shown in Figure 2.9. A thermocouple was used to measure the temperature of the sample as a secondary measurement to confirm the temperature measured by the sensor. For PMMA and pine, a hole was drilled horizontally into the sample to accommodate the thermocouple. For fabrics, the thermocouple was placed between the layers of fabrics whereas for charred pine, the thermocouple was sandwiched between samples together with the sensor. The test was conducted when the reading

from the thermocouple reached the testing temperature. Samples of PMMA were measured from ambient to 100°C with an appropriate heat flow as discussed with this range selected to avoid melting of the polymer (Smith & Hashemi 2006) which normally occurs beyond the maximum test temperature. Furthermore, the oven is not designed to reach temperatures in the ignition range or melting phase (Thermtest Inc. 2012).

Multiple runs were performed at each of the temperature measurement points for several test samples to obtain an average value. The samples were conditioned in the humidity chamber prior to the test under the same conditions as other tests discussed in this chapter.



(a) PMMA



(b) Pine

Figure 2.9: Sample materials placed in the oven prior to measurement

2.3 Thermogravimetric Analyser

Thermogravimetric analysis is the measurement of the mass change of a material as a function of time or temperature under a controlled environment (Perkin Elmer 1997). The sample is heated in the presence of an inert gas such as nitrogen or in oxidative environments using air or oxygen and the change in mass is measured by a microbalance in the TGA instrument.

In this study, two different TGA instruments were used, one manufactured by Perkin Elmer (more than 15 years old) and the other by Mettler Toledo (current model). These are shown in Figure 2.10. Due to its age, the Perkin Elmer TGA is likely to have a thermal lag. Initially, the measurements were conducted using the Perkin Elmer model. Subsequently, a new TGA was purchased and the measurements were continued using this machine. Data obtained from these two equipment were then analysed and compared. Details of the analyses were discussed in CHAPTER 4.



(a) Perkin Elmer TGA 7



(b) Mettler Toledo TGA 1

Figure 2.10: Thermogravimetric analysers

2.3.1 TGA Components

Generally, TGA instruments consist of a number of main components including a balance, a furnace, a series of thermocouples, and a recorder or PC connection with analysis software.

The balance is designed to measure the sample weight throughout the measurement while the furnace is a device that produces the required temperature range for measurement purpose. The temperature is controlled and monitored with the aid of thermocouples and the reading of the measurement is recorded electronically as the sample is heated.

2.3.2 TGA Calibration

There are three types of calibration required for TGA instruments, namely furnace, temperature (with standards) and weight calibrations. These calibrations are performed on a regular basis or in the event of one or more of the following conditions (depending on the type of instrument used):

- Change of temperature range
- Change of purge gas or purge gas rate
- Replacement of furnace or thermocouple
- Replacement of new hang-down wire
- Relocation of the instrument

Furnace calibration is carried out if a change in temperature range is required between a new minimum and maximum. Temperature calibration is a routine calibration which requires different calibration standards including nickel, alumel and perkalloy and these were used for temperature calibration in this study. Weight calibration was performed using a 100 mg Class M standard. Detail procedure of the calibration is available in the User's Manual (Perkin Elmer 1997, Mettler-Toledo 2012). All sample measurements were carried out and maintained in an inert environment of nitrogen (N₂) gas at a flow rate of 50 mL/min.

2.3.3 Operating Procedure

The mass loss rate (MLR) with respect to temperature is used for determining chemical kinetics, namely activation energy (E), pre-exponential factor (A) and reaction order (n) which can be used as inputs for pyrolysis modelling. The effects of heating rate, sample mass and nitrogen flow on MLR were investigated by Abu-Bakar and Moinuddin (2012) using PMMA (non-charring) and pine (charring) materials. It was reported that the variations in heating rates have resulted in a significant difference in kinetic values whereas sample mass and nitrogen flow variation caused only slight impact. Therefore in this study, materials are tested at different heating levels range from 5 to 200 K/min over the same temperature range between 50°C and 550°C.

For PMMA and pine, samples were cut into small pieces approximately 1 x 1 mm. For fabrics, samples were also cut into small pieces approximately 0.5 x 0.5 mm and all materials were conditioned similar to other tests conducted in this research. The same

samples were also used for DSC measurement and examples of the sample materials are shown in Figure 2.11(a) to (d).

Samples weighing 5 mg were used for TGA experiments performed with the Perkin Elmer instrument as well as DSC tests for the determination of *HoR*. However, the Mettler TGA requires a larger sample mass (i.e. >20 mg) and it was therefore used for deriving kinetic parameters only. Test data from the Mettler TGA were also used to identify any difference in thermal lag between the two sets of instruments. Details of these will be discussed in CHAPTER 4. The nitrogen flow was maintained at 50 mL/min which represents a pyrolysis process in the absence of air. This usually occurs when there is a flaming combustion reaction preventing air reaching the material. The samples were conditioned prior to TGA tests, similar to other measurements.

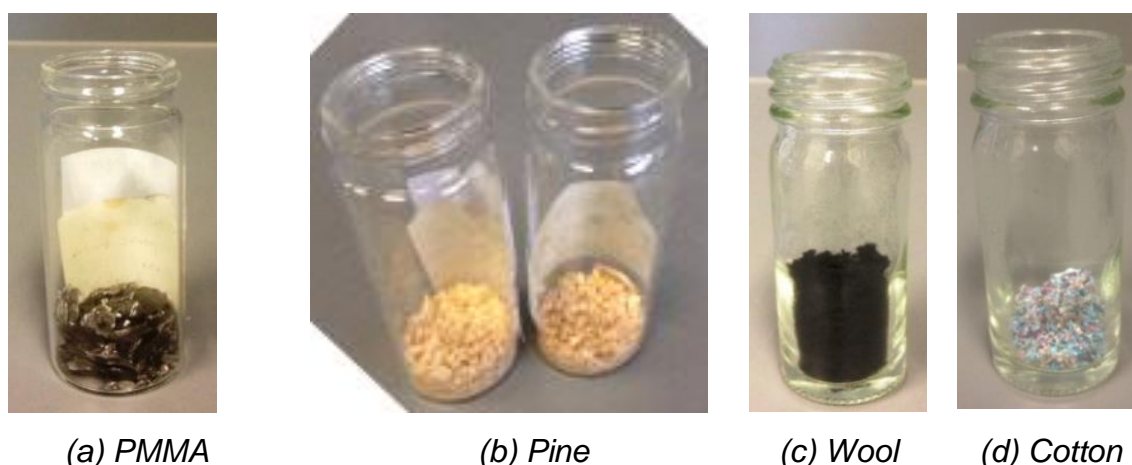


Figure 2.11: Preparation of sample materials for TGA and DSC measurements

Data from the completed measurements were recorded electronically, then collected and analysed. The number of output data points obtained is based on the time interval set by the user. The TG and DTG curves were prepared by plotting the mass fraction of the sample at particular heating rate within the set temperature range. Post-processing of this data was necessary in order to obtain the kinetic parameters and details of this data treatment are discussed later in CHAPTER 3.

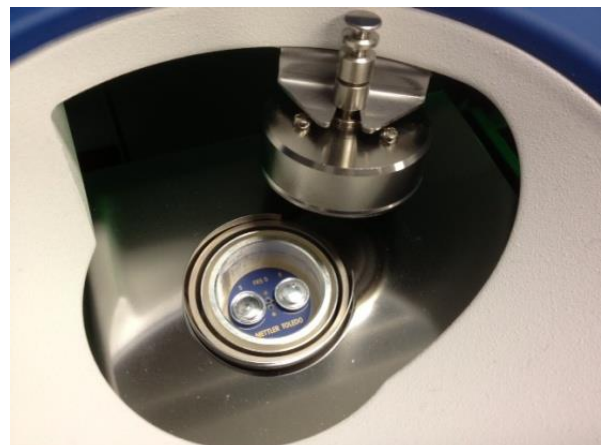
2.4 Differential Scanning Calorimeter

The DSC is a thermal analysis tool that measures the difference in the amount of heat required to increase the temperature of a sample and reference as a function of temperature. A sample of known mass is heated or cooled to track the changes in its heat capacity as heat flow changes. It enables the measurement of a range of thermal parameters including endothermic and exothermic heat flows, peak melting temperatures and peak areas. The DSC is also widely used to study physical transitions and chemical reactions of materials and can be used to determine the specific heat capacity (C_p) of samples. However, in the last 25 years, DSC has been used to quantify the *HoR* for combustible materials (Hoffman & Pan 1990).

Typical instruments consist of a furnace, a furnace lid, sample and reference crucible, sensor disk and thermocouples. The heat flow is measured via thermocouples whereas the furnace temperature is measured via sensors. Figure 2.12(a) shows the DSC equipment used to conduct the tests in this study with Figure 2.12(b) showing the sample (left) and reference (right) crucible used in the tests. Figure 2.13 shows a schematic diagram of the DSC.



(a) Mettler Toledo DSC



(b) Sample and reference crucible

Figure 2.12: Mettler Toledo DSC and its sample furnace

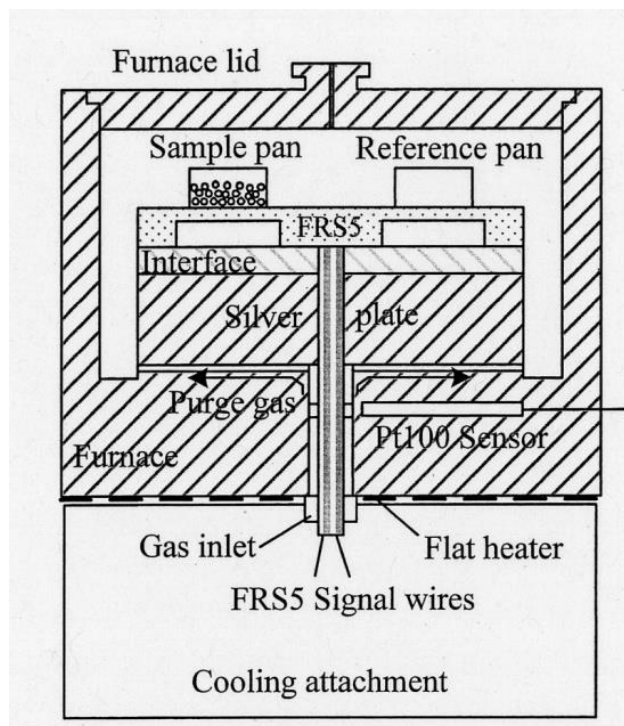


Figure 2.13: Schematic diagram of DSC (Mettler-Toledo 2011)

2.4.1 Calibration

The DSC also requires routine calibration and the frequency depends on the usage of the instrument. Routine calibrations include the heating rate dependence of temperature (τ_{lag}), temperature and heat flow and these calibrations are performed using a particular reference substance provided by the manufacturer. The τ_{lag} is a thermal lag calibration performed to ensure that the reference temperature and sample temperature are in agreement with the program temperature and this is typically performed using an indium calibration standard. The temperature calibration is performed using zinc standard substance and the heat flow calibration is also performed using indium.

2.4.2 Operating Procedure

In this study, the Mettler Toledo DSC1 instrument was used to measure the samples under similar conditions as the TGA tests (i.e. temperature range and heating rate). The sample used in DSC measurement was limited to 5 mg, due to the physical form (size) of the sample and also to avoid overfilling the sample pan with samples sealed in 40 μL aluminium pans prior to testing. Some researchers conducting similar studies use sealed pans without pin-holes in the lids (Kousksou et al. 2011, Fujino & Honda 2007, Lee, Loos & Springer 1982, Frederick & Mentzer 1975) whereas others use pin-holed lids (Shalaev & Steponkus 2000, Milosavljevic, Oja & Suuberg 1996). Rath et al.

(2003) conducted their study on wood using both pin-holed and open pan techniques for comparison.

Initially, a number of techniques were carried out to optimise sample preparation including the use of a sealed pan with and without pin-holes. The initial results suggested that the lid of the non-pin-holed pan had reacted with the gaseous product and the pan at some stage melted and the lid was swollen in a number of tests. To overcome this observation and its possible effect on the sensor/measuring cell of DSC machine, all aluminium lids were pin-holed (both sample pan and reference pan) to release the gaseous products from the pan.

2.5 Summary

Of the experimental techniques utilised in this study, the cone calorimeter and HDA provide a direct post-processed result. However, to obtain the kinetic parameters and *HoR* via TGA and DSC, post-processing of raw data is required. Thus, an investigation into data reduction techniques was required prior to implementation in the latter stages of this study and a range of post-processing techniques are presented in the next chapter.

CHAPTER 3

DATA POST-PROCESSING TECHNIQUES

3.1 Introduction

The data output from the HDA and cone calorimeter do not require any further post-processing or data reduction prior to their input into the modelling software. However, to compute non-isothermal kinetic parameters from TG curves and to determine *HoR* from raw TGA and DSC data, some post-processing is required. In this chapter, a review of available post-processing methods is presented to provide an overview of the techniques as well as their advantages and disadvantages. A discussion of suitable techniques employed in this study is presented followed by a new method derived from the existing approaches.

3.2 Data Reduction Method for Kinetics Parameter

Chemical kinetic data can be obtained by means of TG analysis, the most common technique used in investigating thermal decomposition and understanding pyrolysis phenomena (Slopiecka, Bartocci & Fantozzi 2012). The TGA instrument provides a rapid method for determining the temperature-decomposition profile of a material (American Society for Testing and Materials 2007) under a controlled environment at a specific heating rate. Typically, TGA operating software does not include a post-processing tool to directly obtain chemical kinetic values from the raw data. Therefore, it is essential that an appropriate post-processing scheme is selected and applied. The sample mass is recorded by the TGA as a function of temperature at a specific heating rate or isothermally at a single temperature for a specific time. The mass loss rate (MLR) with respect to temperature i.e., fraction of conversion (Y) versus temperature data is used for determining chemical kinetics and is determined by:

$$Y = \frac{w - w_f}{w_i - w_f} \quad (3.1)$$

where, w is the mass at a particular temperature, w_i is the initial sample mass and w_f is the final sample mass, all measure in mg.

A typical sample TGA profile can be presented in two forms as shown in Figure 3.1 (a) and (b) showing the TG and DTG profiles of pine respectively under 100 K/min heating rate. From these figures, it is evident that the initial mass loss is completed below 160°C which is representative of the moisture removal process from the sample (Reaction 1). The second mass loss occurs between 275-475°C which is the pyrolysis reaction of the tested material (Reaction 2).

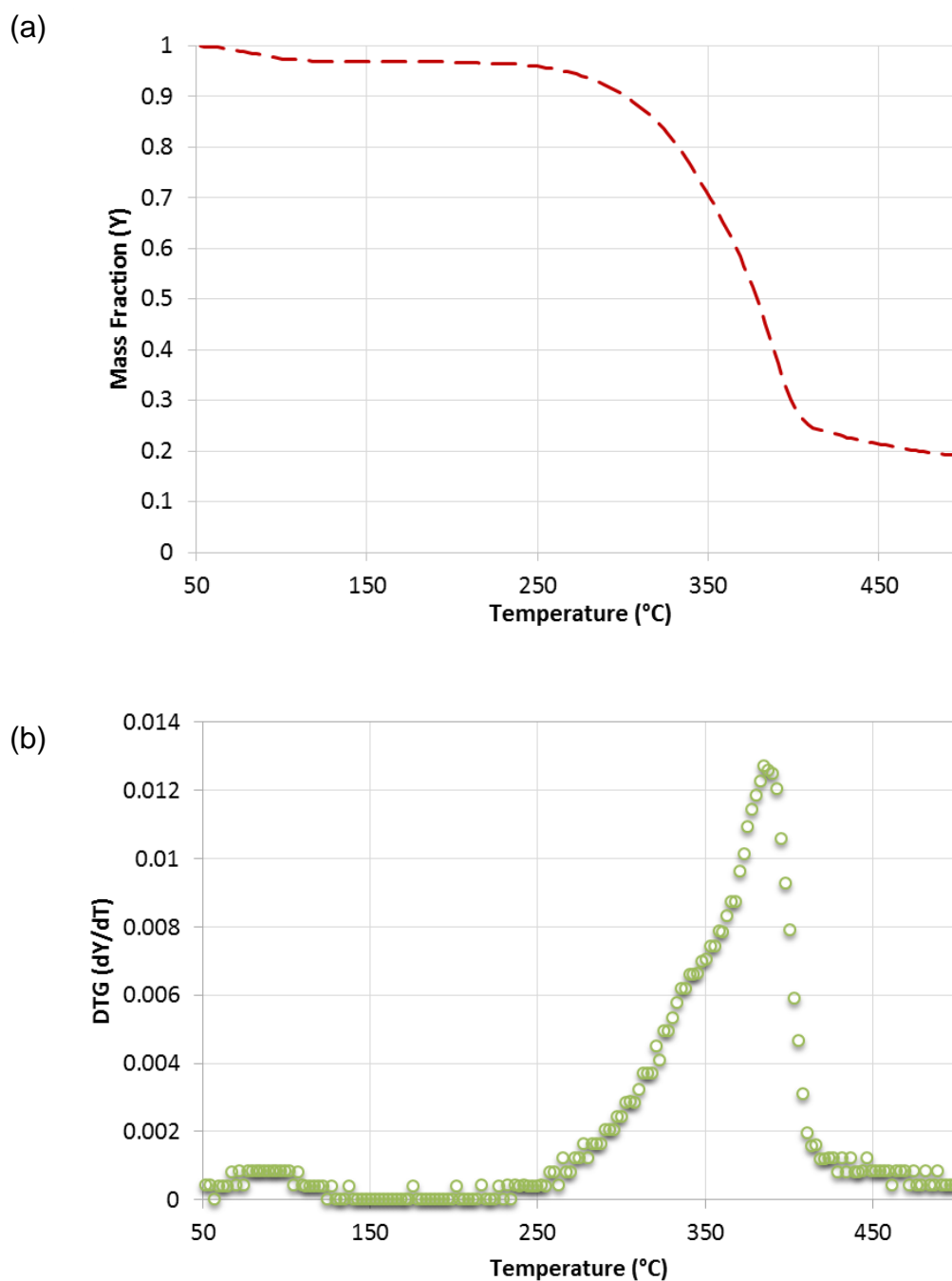


Figure 3.1: MLR curve versus temperature profile for (a) TG and (b) DTG profiles.

Although there are some methods that are used to derive the kinetic parameters of materials, they each have some limitations. Jiang (2006), for example, summarized various methods including those of (i) Seungdo and Park; (ii) Ozawa-Flynn-Wall (OFW); and (iii) Coates Redfern.

The most commonly adopted equation to express the kinetic reactions of a material is the Arrhenius equation based on a one step first order reaction as shown in Equation 3.2.

$$k = Ae^{\frac{-E}{RT}} \quad (3.2)$$

where k is the reaction rate constant (1/s), A is the pre-exponential factor (s^{-1}), E is the activation energy ($\text{kJ}\cdot\text{mol}^{-1}$), R is the universal gas constant ($8.314 \times 10^{-3} \text{ kJ}\cdot\text{mol}^{-1}\cdot\text{K}^{-1}$) and T is the temperature (K).

3.2.1 Seungdo and Park Method

Seungdo and Park (1995) derived the Arrhenius equation based on a variable reaction order (n) as follows:

$$\frac{dY}{dT} = \frac{A}{\beta} e^{-\frac{E}{RT}} (1 - Y)^n \quad (3.3)$$

where β is the heating rate ($^{\circ}\text{C}/\text{min}$), n is the order of reaction and Y is the mass fraction of conversion.

At maximum temperature, differentiating Equation (3.3) with respect to temperature yields to zero:

$$\frac{E}{nRT_{max}^2 (1 - Y_{max})^{n-1}} - \frac{A}{\beta} e^{-\left(\frac{E}{RT_{max}}\right)} = 0 \quad (3.4)$$

where T_{max} is the temperature at peak conversion rate, dY/dT , Y_{max} is the sample mass fraction of conversion at peak conversion rate.

Substituting Equation (3.3) into Equation (3.4) and considering n as unity, the expression for activation energy (E) is obtained:

$$E = \frac{nRT_{max}^2 H_{max}}{1 - Y_{max}} \quad (3.5)$$

where H_{max} is the peak conversion rate:

$$H_{max} = \left(\frac{dY}{dT} \right)_{max} \quad (3.6)$$

Now, the expression for the pre-exponential factor is obtained by substituting Equation (3.5) in Equation (3.4):

$$A = \frac{H_{max} \beta e^{\left(\frac{E}{RT_{max}} \right)}}{(1 - Y_{max})^n} \quad (3.7)$$

3.2.2 Ozawa-Flynn-Wall (OFW) Method

The OFW method (Ozawa 1970) is based on a multiple heating rate technique in which the material is tested at two different heating rates. A special format of the OFW method is discussed based on the observation that Y_{max} will not change with respect to the heating rate for each peak in a DTG curve (Flynn & Wall 1966). So there is no need to compute the activation energy based on the entire set of mass conversion fraction thereby simplifying the method for practical applications.

The following expression is derived from Equation (3.7) for different heating rates:

$$\ln \beta = \ln \left[\frac{A(1 - Y_{max})^n}{H_{max}} \right] - \frac{E}{RT_{max}} \quad (3.8)$$

Applying Equation (3.8) at two different heating rates, the activation energy can be obtained by T_{max} , H_{max} and the values of β from the two tests:

$$E = R \left(\frac{T_{max1} \cdot T_{max2}}{T_{max1} - T_{max2}} \right) \ln \left[\left(\frac{\beta_1}{\beta_2} \right) \left(\frac{H_{max1}}{H_{max2}} \right) \right] \quad (3.9)$$

3.2.3 Coates Redfern Method

To obtain the three kinetic parameters, the Coates Redfern method (Vyazovkin & Wight 1998) uses the following equation:

$$\ln \left(\frac{f(Y)}{T^2} \right) = \ln \left(\frac{AR}{\beta E} \right) - \frac{E}{RT} \quad (3.10)$$

where $f(Y)$ is a function that represents the reaction model. When the Arrhenius equation is assumed, the expression from Equation (3.2) can be applied, i.e. $f(Y) = (1 - Y)^n$.

Therefore equation (3.2) can be rewritten as:

$$\left[\frac{1 - (1 - Y)^{1-n}}{1 - n} \right] \frac{1}{T^2} = \frac{AR}{\beta E} e^{\frac{-E}{RT}} \quad , (n \neq 1) \quad (3.11)$$

$$\frac{-\ln(1 - Y)}{T^2} = \frac{AR}{\beta E} e^{\frac{-E}{RT}} \quad , \quad (n = 1) \quad (3.12)$$

Plots of $\ln[-\ln(1 - Y)/T^2]$ vs. $1/T$ for ($n=1$) or $\ln\left[\frac{1 - (1 - Y)^{1-n}}{(1 - n)T^2}\right]$ vs. $1/T$ (for $n \neq 1$) gives straight lines of slope $-E/R$. The intercept of these straight lines yields the pre-exponential factor (A). The reaction order, n , is determined by optimizing values which give the best fit to the plots.

The Seungdo and Park (1995) method has the advantage of calculating all parameters from a single run of tests whereas the OFW method requires multiple test runs at different heating rates. However, the OFW method has higher accuracy as it does not rely on the assumption of reaction order as unity. From this study, it was observed that these two methods are highly sensitive to the peak values of mass fraction of conversion (Y) and conversion rate (dY/dT) obtained from TGA to determine kinetic parameters. Although the Coates Redfern method is more stable, it requires complex

mathematical computation to process data and to determine the kinetic parameters associated with the material. Furthermore, this method is not well documented in the literature and is therefore the least stable method for data reduction.

3.2.4 The Inflection Point Method

The inflection point method introduced by Vishwanath and Gupta (1996) represents the Arrhenius equation in logarithmic form based on a single kinetic reaction from a DTG curve:

$$\ln\left(\frac{dY}{dT}\right) = n \ln(1 - Y) - \frac{E}{RT} + \ln\left(\frac{A}{\beta}\right) \quad (3.13)$$

At the inflection point, the second derivative (d^2Y/dT^2) = 0 and (dY/dT) is maximum so therefore the equation at the inflection point can be written as:

$$\left(\frac{dY}{dT}\right)_{max} = \frac{(1 - Y_{max})}{n} \times \frac{E}{RT_{max}^2} \quad (3.14)$$

The order of reaction, n , is obtained by rearranging equation (3.14)

$$\text{Reaction Order, } n = \frac{(1 - Y_{max})}{\left(\frac{dY}{dT}\right)_{max}} \times \frac{E}{RT_{max}^2} \quad (3.15)$$

Equation (3.15) is substituted into the logarithmic form of Arrhenius equation (3.13) which is then written as follows:

$$\ln\left(\frac{dY}{dT}\right) = (E/R) \left[\ln \frac{1 - Y}{\phi} - \frac{1}{T} \right] + \ln\left(\frac{A}{\beta}\right) \quad (3.16)$$

where ϕ (phi) is, given by:

$$\phi = \frac{T_{max}^2}{(1 - Y_{max})} \times \left(\frac{dY}{dT} \right)_{max} \quad (3.17)$$

A plot of $\ln(dY/dT)$ vs. $1000 [\ln(1-Y)/\phi - (1/T)]$ gives a linear plot with a slope (m) equal to E/R and intercept (C) A/β . An example of this plot is shown in Figure 3.2.

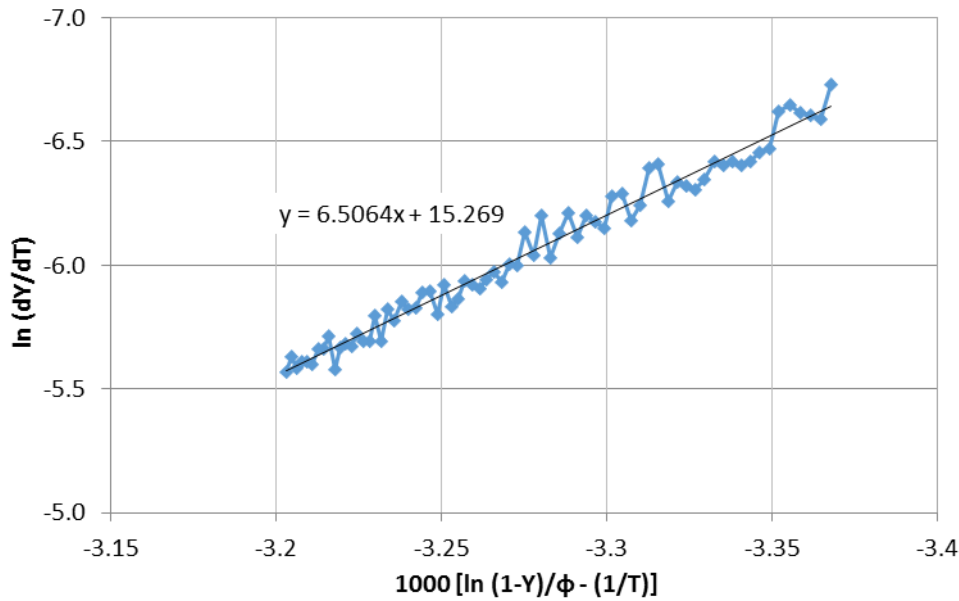


Figure 3.2: Plot to determine inflection point equation for pine

Thus

$$E = R \left(\frac{T_{max1} \cdot T_{max2}}{T_{max1} - T_{max2}} \right) \ln \left[\left(\frac{\beta_1}{\beta_2} \right) \left(\frac{H_{max1}}{H_{max2}} \right) \right] \quad (3.18)$$

$$\text{Pre Exponential Factor, } A = (\beta/60) \times \ln(C) \quad (3.19)$$

where m is the slope and C is the intercept of the inflection line.

The inflection point method proposed by Vishwanath and Gupta (1996) is a robust method which analyses the data points from TGA in their entirety to determine the kinetic parameters of the sample linearly. Most importantly, unlike some other methods described above, this method is not sensitive to peak values of mass fraction and

conversion rates. Thus, this method was utilised to derive the kinetic parameters in this study.

3.3 Data Reduction Method for Heat of Reaction

Although the *HoR* is an important parameter for pyrolysis modelling, very few studies in the literature are available describing its determination. A limited number of methods that have been proposed by various researchers to determine *HoR* by conducting DSC tests and these are discussed below.

3.3.1 Test Method ASTM E 2160

The test method ASTM E 2160 (2004b) describes the procedure to be followed to test a specimen producing exothermic reactions by DSC. A small, known quantity of the specimen is heated at 10 K/min in the temperature region where chemical reaction is known to take place. The specimen is heated until the heat flow returns back to the baseline. The weight loss during the reaction is recorded by reweighing the sample after the specimen has been cooled back to ambient temperatures. A straight line is then drawn connecting the baseline before and after the exothermic reaction and the *HoR* is calculated by integrating the recorded heat flow versus time bounded by the baseline and the heat flow curve. The normalised *HoR* is the calculated by dividing the *HoR* by the initial mass (m_0) of the specimen. However, this method is not valid for endothermic reactions such as pyrolysis and is also not applicable if the thermal curve has not returned to the baseline before the temperature reaches 600°C.

3.3.2 Hoffman and Pan Method

Hoffman and Pan (1990) observed that using the initial sample mass in the calculations can lead to inconsistencies in the results. They suggested that this practice is invalid when testing samples which undergo a phase change or thermal degradation during the experiment and thus compared two methods; one which uses initial mass and another using instantaneous mass which is obtained from TG. Since the DSC does not have the capability to measure mass change during the experiment, the mass change data, as a function of sample temperature needs to be obtained from a TG curve instead. It is essential to maintain the same experimental conditions in both the experiments in order to make relevant correlation between them. The shape of the

sample, difference in cell instrumental errors and thermocouple placements must be taken into consideration to study these effects on the results.

Hoffman and Pan (1990) measured the area under the curve of heat flow vs time or temperature and developed the following two equations to determine heat of reaction:

$$\Delta H_{convent} \times m_0 = KA' \quad (3.20)$$

$$\Delta H_{enhanced} = \sum \frac{KA'_T}{nm_i} \quad (3.21)$$

Here, $\Delta H_{convent}$ corresponds to a normalised *HoR* calculation using the initial mass while $\Delta H_{enhanced}$ takes into account of the mass change throughout the experiment. Furthermore, K is the calibration coefficient and A' is the area under the peak. In Equation 3.21, n' is the number of approximations, m_i is the mass of the sample at that approximation and A'_T is the area under the curve within approximation segment. The calibration constant varies with the instrument used.

Hoffman and Pan (1990) also discussed the method involved in interfacing the mass loss data from TG with heat flow from DSC. Either time or temperature can be used as a parameter to match the data and if time is used as reference, steps must be taken to ensure that the time rates on both instruments are synchronised. If temperature is used as reference point, steps to measure temperature constantly between the two systems should be employed. Their study concluded that the *HoR* value obtained using enhanced equation is higher than that calculated using conventional equations for an experiment involving decomposition (endothermic) while it is lesser for materials that react with volatile gases (exothermic). The *HoR* calculated using the enhanced and conventional equation is observed to be the same for materials that undergo phase transitions.

3.3.3 Rath et al. Method

Similar to the method of Hoffman and Pan (1990), Rath et al. (2003) used combined DSC and TG tests to determine the *HoR* of beech and spruce wood. Samples in both DSC and TG tests were heated at 10 K/min from 348K to 773 K, and the heat flow required to heat the sample was expressed as follows:

$$\Delta E = m_0 C_p \frac{dT}{dt} \quad (3.22)$$

where, C_p is the specific heat of the sample as a function of temperature and dT/dt is the heating rate (β).

The *HoR* (ΔH_{DSC}) of a complete endothermic process is given by:

$$\Delta H_{DSC} = \frac{1}{m_0} \int_{T_1}^{T_2} \Delta E dt \quad (3.23)$$

where, T_1 denotes the lower peak integration temperature from the DTG curve via TGA experiments, and T_2 the upper peak integration temperature. However exothermic and endothermic components are separately calculated and then added together.

It should be noted that unlike Hoffman and Pan (1990), Rath et al. (2003) used the initial sample mass instead of corresponding sample mass. The TGA data is primarily used to identify the temperature range of reaction peak and secondarily to accommodate the charring effect.

3.3.4 Hoffman and Pan Derivative Method

Professor Simo Hostikka of Aalto University, Finland through private communication (Hostikka 2012) suggested following a method similar to Hoffman and Pan (1990) which will be referred to as the “method derivative from Hoffman and Pan (1990)” in this study. In this method, the initial sample masses for both TGA and DSC are required to be the same. Then, thermal analyses are performed at the same heating rates with the TGA as well as DSC. The temperatures of DSC data are matched with TGA and the respective heat flows obtained from DSC test are divided by respective un-subtracted masses obtained from TGA test. The heat flow/mass vs temperature are plotted and the area under the curve where pyrolysis occurs is calculated to determine *HoR*.

The *HoR* required for pyrolysis modelling is represented by:

$$\Delta H_{r,\alpha\beta} = \frac{\Delta H_{DSC} \cdot M_{tot} Y_i}{X_i M_{tot}} = \frac{\Delta H_{DSC} \cdot Y_i}{X_i} \quad (3.24)$$

where $\Delta H_{r,\alpha\beta}$ is the *HoR* in FDS, ΔH_{DSC} is the normalized enthalpy (or *HoR* of DSC), M_{tot} is the total mass of the sample, Y_i is the yield of gaseous products, X_i is the mass fraction of the mass loss (compared to sample mass).

To obtain ΔH_{DSC} , Equation (3.25) should be applied between the temperatures ranges over which the reaction occurs:

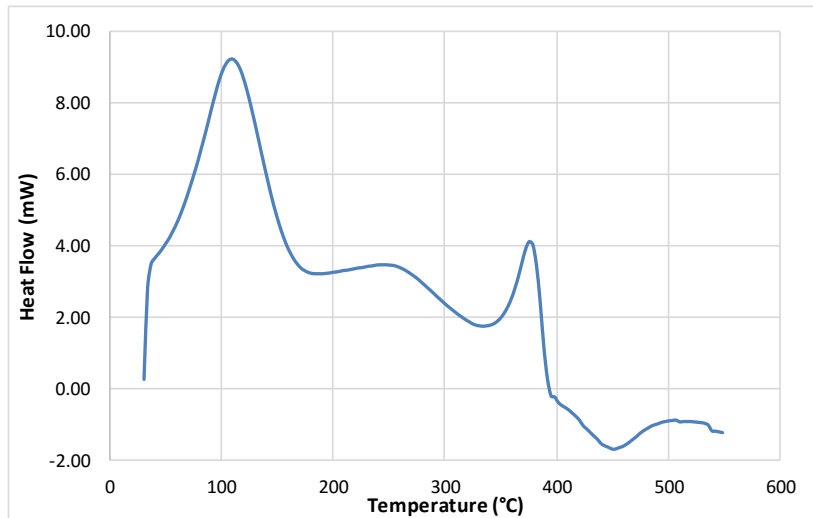
$$\Delta H_{DSC} = \int_{T_1}^{T_2} \frac{\Delta E}{m_i} dT \quad (3.25)$$

where ΔE is the instantaneous heat flow into the sample. This is similar to Equation (3.23), however the calibration constant is considered unity in Equation (3.25).

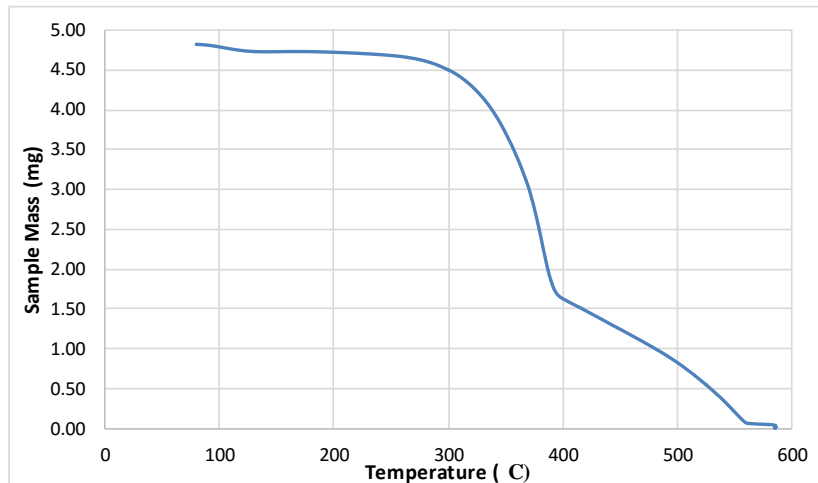
For pine samples, Figure 3.3 shows: (a) the heat flow vs temperature curve, (b) the mass vs temperature curve obtained from the TGA test, and (c) the heat flow/unit mass vs temperature profile derived from the DSC and TGA data by matching temperatures in the two sets of data. Here the first peak represents moisture evaporation and the second peak represents the pyrolysis of the pine.

In order to determine the range at which the reaction occurs, the temperature range at which reaction (peak) occurs on TG curve should be closely observed. In Figure 3.3 (c), the reaction of pine pyrolysis occurs between 325°C to 395°C (shaded) and the shaded area is the ΔH_{DSC} and in this study this is calculated using a MATLAB program developed in-house. Here, ΔH_{DSC} is calculated using:

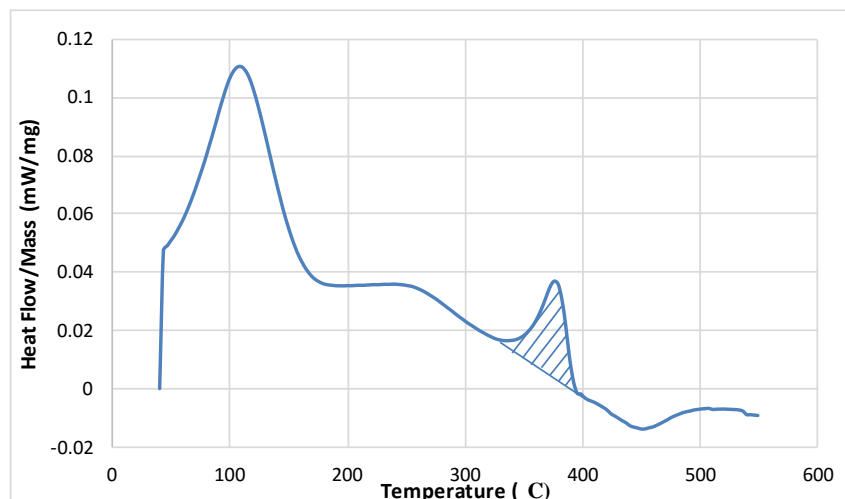
$$\frac{\text{heat flow (kW)}}{\text{instantaneous mass (kg)}} \times \frac{\text{pyrolysis range (°C)}}{\text{heating rate } \left(\frac{\text{°C}}{\text{sec}}\right)} = \frac{\text{kJ}}{\text{kg}} \quad (3.26)$$



(a) Heat flow vs temperature obtained from DSC raw data for pine at 20 K/min.



(b) TG curve obtained from TGA raw data for pine over the same heating rate.



(c) Heat flow/mass plotted with matched temperatures from DSC and TGA.

Figure 3.3: Determination of pine *HoR* by TGA and DSC data

In Equation (3.24), values of Y_i and X_i for non-charring materials are equal to unity. However for charring materials, two reactions normally occur where the first is attributed to the moisture release and the second reaction is a product of fuel gas and char. Thus, the reaction path needs to be estimated as shown in the example presented in Figure 3.4 where $Y_i=0.84$ and $X_i= 0.985 \times 0.84 = 0.827$.

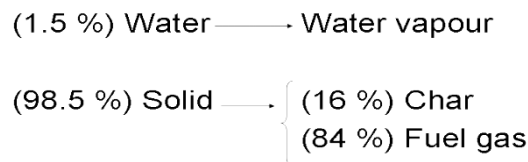


Figure 3.4: Example of a reaction path for the charring material

3.3.5 New Data Reduction Method using Normalised Values

In this study, the potential to use different initial sample masses for TGA and DSC tests to obtain accurate *HoR* values was explored. This part of the investigation was motivated by the possibility that laboratories may have TGA and DSC equipment which require different initial or minimum/maximum sample masses. Indeed, the requirement that the same initial sample mass is used can be challenging, particularly if sample crucibles have different dimensions. In this study, the Mettler Toledo TGA requires a larger minimum sample mass (>20mg) compared to Perkin Elmer TGA and Mettler Toledo DSC (~5mg). Therefore a method is proposed to use weight normalised values rather than gross values.

In this method, the instantaneous heat flow into the sample in the DSC experiment is normalised by its initial mass. Here, a heat flow per unit initial sample mass (mW/mg) vs. T profile is obtained, rather than mW vs. T profile as shown in Figure 3.3(a). Similarly, the instantaneous sample mass in TGA experiments is normalised by its initial mass. A dimensionless mass vs. temperature (°C) profile is obtained rather than mass vs. T profile as shown in Figure 3.3(b). Then, the temperatures of both profiles are matched and at corresponding temperatures, the heat flow per unit initial sample mass (mW/mg) value from DSC is divided by the dimensionless mass from TGA. As a result, a profile of mW/mg vs. T similar to Figure 3.3(c) can be obtained. The ΔH_{DSC} can be obtained from this profile using the same method described in Section 3.3.4.

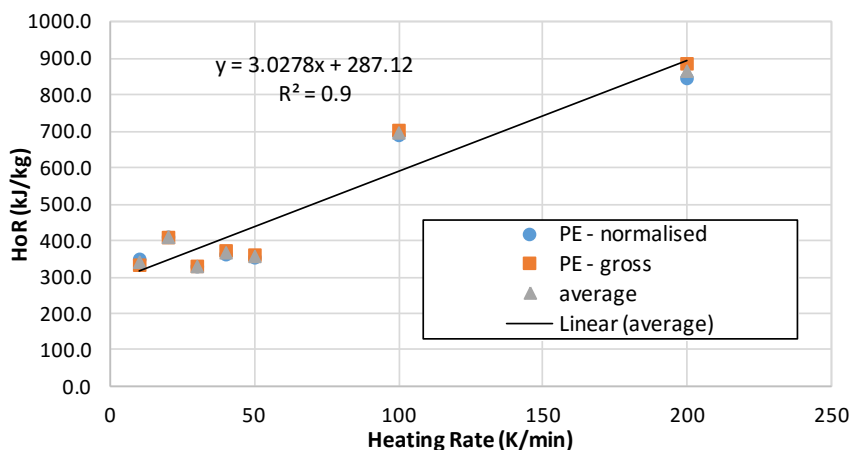


Figure 3.5: *HoR* of wool vs. heating rate by normalised and gross method

The comparison revealed that the *HoR* values are very close and it can be concluded that both types of data can be used for determination of *HoR*. By averaging both types of data, a set of formulae can be derived through a regression analysis to represent the variations of *HoR* values with respect to heating rates. For example, Figure 3.5 shows *HoR* of wool vs. heating rates for both the normalised and gross methods and the average value of both sets. A very strong correlation is observed for the *HoR* between these methods.

This study has revealed that a matched sample mass between TGA and DSC sample is not an essential requirement and a normalised weight profile from TGA and normalised heat profile from DSC can be used to adequately determine the *HoR*.

3.4 Summary

In this chapter, suitable data reduction methods for determining chemical kinetics from the raw TGA data and *HoR* from the raw TGA and DSC were identified. Techniques for obtaining *HoR* were further generalized and finally applied to wool material. The *HoR* of wool was determined using both gross and normalised data from TGA and DSC and the comparison revealed that the *HoR* values are very close and both types of data can be used for determination of *HoR*. In the next chapter the characterization of pyrolysis parameters using the experimental techniques and data reduction methods established in Chapters 2 and 3 is presented. The process of characterising fire properties developed in this study is illustrated in Figure 3.6.

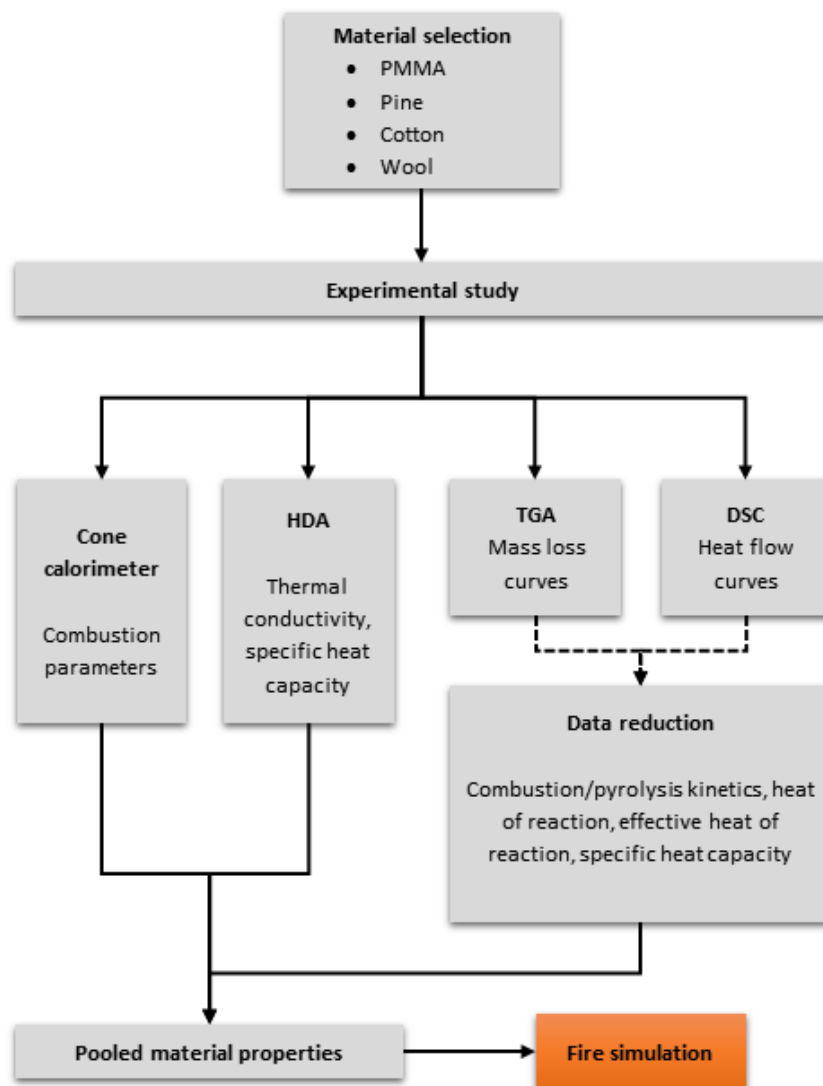


Figure 3.6: Flow process for characterizing fire properties of building materials

CHAPTER 4

CHARACTERIZATION OF PYROLYSIS PARAMETERS

4.1 Introduction

The characterization of pyrolysis parameters determined using mg-scale experiments are discussed in this chapter. Pine, PMMA and fabrics (cotton and wool) were subject to TGA and DSC analysis at various heating rates under specific conditions outlined in the previous chapter. The experimental data was then used in the determination of the material properties of kinetic parameters, namely A , E , n and the HoR .

This chapter is divided into several sections with the results of the experimental studies presented by type of material. The thermal lag calibration and decomposition temperature are first discussed for the two relatively “pure” materials, pine and PMMA, which are representative of charring and non-charring materials respectively. The kinetic parameters and HoR of these two materials are then presented and discussed followed by the results of the more complex fabric materials, cotton and wool.

4.1.1 Thermal Lag Calibration

Figure 4.1 shows the DTG curves for pine obtained using the Mettler TGA at seven heating rates ranging from 5 K/min to 200 K/min. The corresponding heat flow vs. temperature curves at the matching heating rates are presented in Figure 4.2. In both set of curves, virgin pine peaks generally appear at the same temperatures and this is expected to occur as reported in the literature (Le Bras, Wilkie & Bourbigot 2005).

The thermal lags in the Perkin Elmer TGA curves were calibrated so that peaks representing pyrolysis reactions occur at the corresponding temperatures at which DSC peaks occur. The issues of thermal lag are a quite well known problem with older equipment when instrumentation cannot keep up with changing sample temperature.

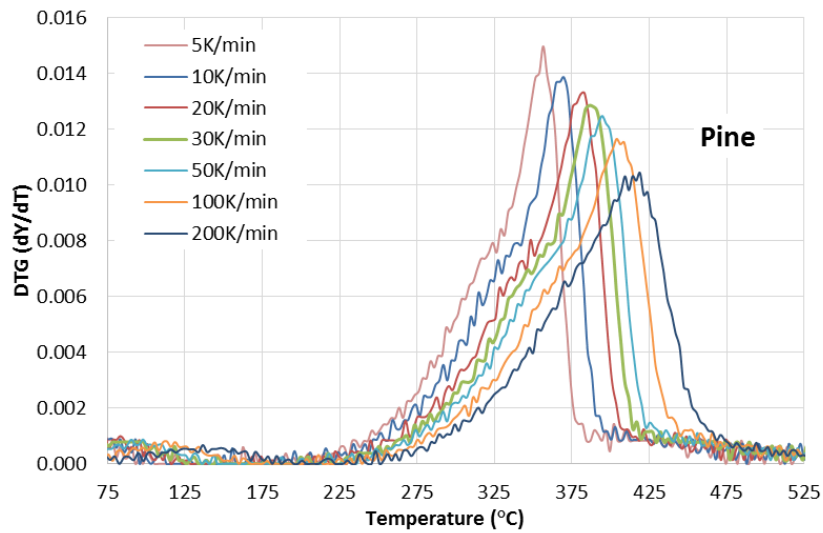


Figure 4.1: First derivative of TGA curve for pine using Mettler TGA.

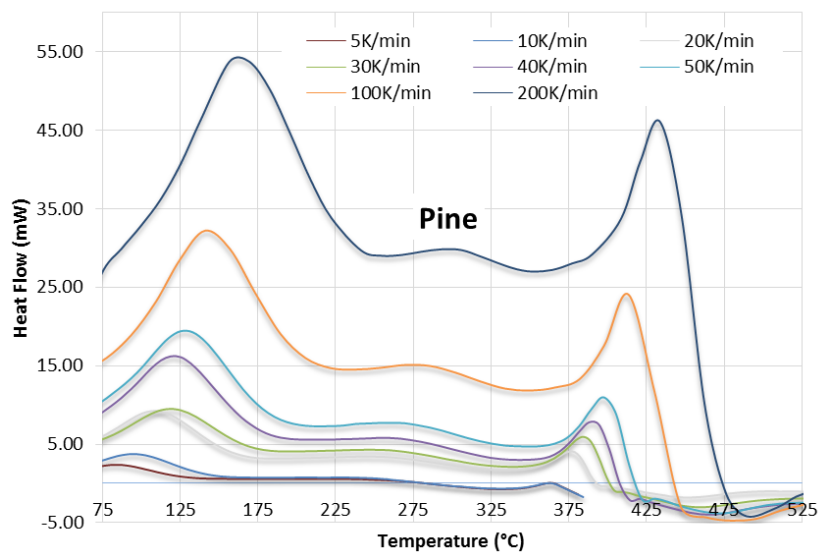


Figure 4.2: Heat flow curve for pine using Mettler DSC.

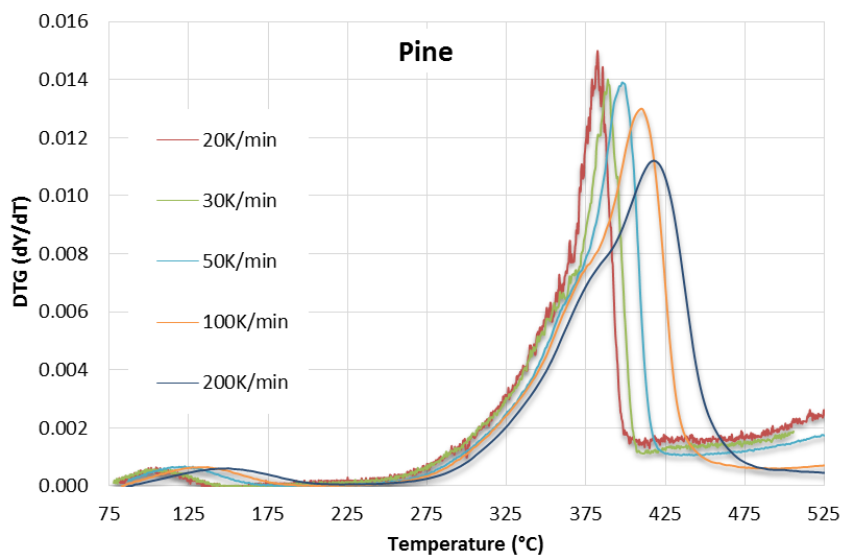


Figure 4.3: DTG vs temperature for pine using Perkin Elmer TGA.

Moisture release peaks are not clearly visible in Figure 4.1, whereas the peaks representing moisture evaporation are present in Figure 4.3 at the corresponding temperatures of the peaks present in Figure 4.2. Therefore the calibrated Perkin Elmer TGA data were used for deriving kinetic parameters for moisture, as well as for calculating *HoR* values. According to Shi and Chew (Shi & Chew 2013) moisture evaporation can be modelled using the Arrhenius relationship with kinetic triplets and *HoR*.

4.1.2 Changes in Decomposition with Temperature

Figure 4.1 and Figure 4.3 show that the DTG peak locations of the virgin fuel are shifted to higher temperatures as the heating rate is increased which is in accordance with various previous studies (Li et al. 2014, Zhang et al. 2013, Kim et al. 2010, Font et al. 2009, Matala 2008, Wang et al. 2008, Mui et al. 2008, Jiang 2006, Kashiwagi, Inaba & Brown 1986) since one of the earlier studies of Kissinger (1956). Moreover, the peak value is gradually reduced as the heating rate is increased and this was also observed by Wang et al. (2008). To more closely observe this phenomenon in the moisture evaporation range, the same data specific to the moisture release is presented in Figure 4.4. A similar pattern of peak shifting towards higher temperatures as the heating rate increases is observed for the moisture release and the peak value also appears to decrease as the heating rate increases.

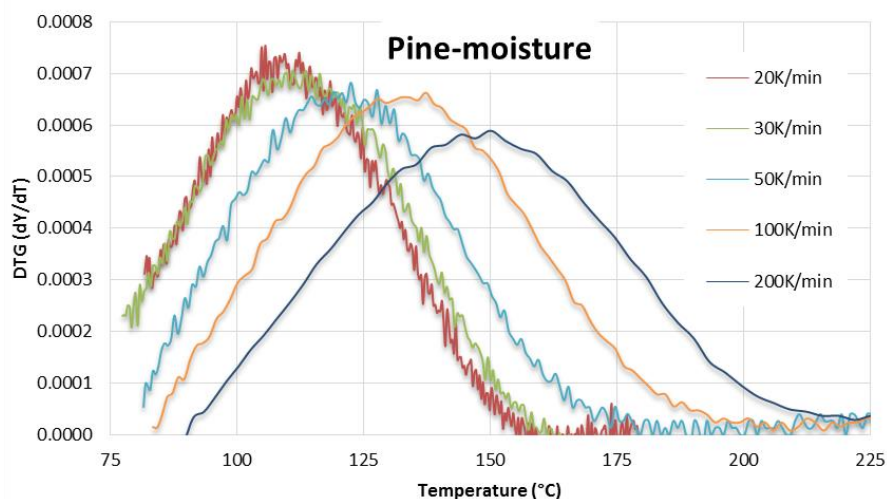


Figure 4.4: Perkin Elmer DTG data showing moisture release from pine

Similar to the TGA data, the DSC data in Figure 4.2 shows that heat flow peak locations for both moisture and fuel release shift towards the higher temperatures as the heating rate increases. However, in terms of the peak values, it is observed that the peak value generally increases as the heating rate is increased, indicating an increase in *HoR* with the increase of heating rate.

To demonstrate heating rate effects on the thermal properties of PMMA, the TG, DTG and DSC heat flow profiles at all heating rates are plotted in Figure 4.5 to Figure 4.7. With the exception of moisture loss, similar trends in peak shifting for these profiles are observed in the PMMA data compared to the pine data. Several researchers have proposed explanations for the observed decomposition shift. Based on their study of cellulose, Missoum et al. (1997) suggested that one reason for such a decomposition shift is the result of decreased residence time of volatiles within the material and which results in the reaction commencing at higher temperature (Quan, Li & Gao 2009). At high heating rates volatiles are more quickly formed and therefore they spend less time within the sample and this can also be applicable to non-charring materials. Milosavljevic (1996) suggested that a “mass transport limitation”, i.e. the restriction of physical transport of the reactants at the gas–solid interface, may also be responsible for the shift in cellulosic materials.

It may be suggested that the samples have less residence time within the vicinity of any specific temperature at the higher heating rates. Therefore, by the time the volatiles are formed, the sample has reached a higher temperature and thus, more heat flow is needed to assist the formation of volatiles quickly at higher heating rates.

4.2 Pyrolysis Parameters of Pine and PMMA

In Figures 4.1 and 4.6, it has been observed that only single pyrolysis reactions take place, though it is known that for various combustible materials, multiple pyrolysis reactions occur. However, for simplicity, most of the pyrolysis models are based on a single “effective” reaction. The inflection point method by Viswanath and Gupta (1996) is capable of determining multiple reaction kinetics as well as single “effective” reaction kinetics.

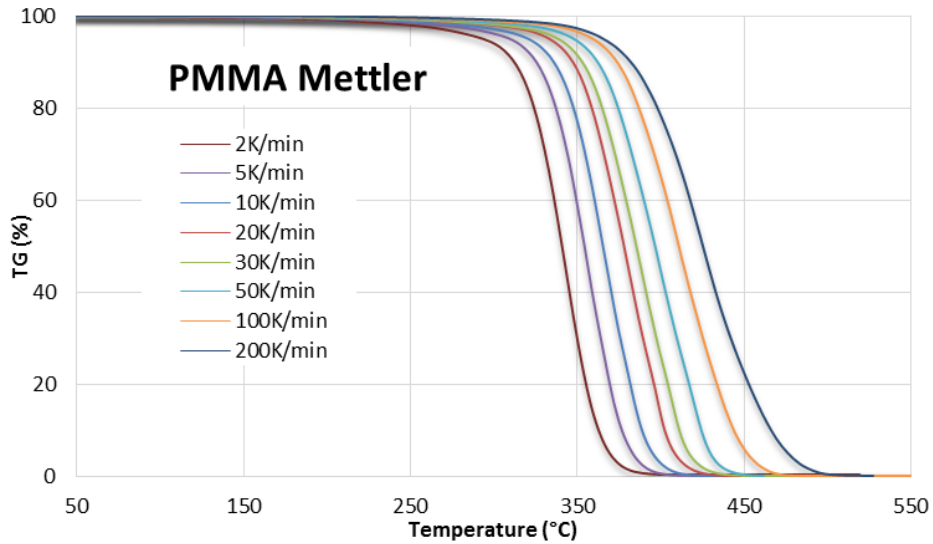


Figure 4.5: TGA thermograms of PMMA at various heating rates

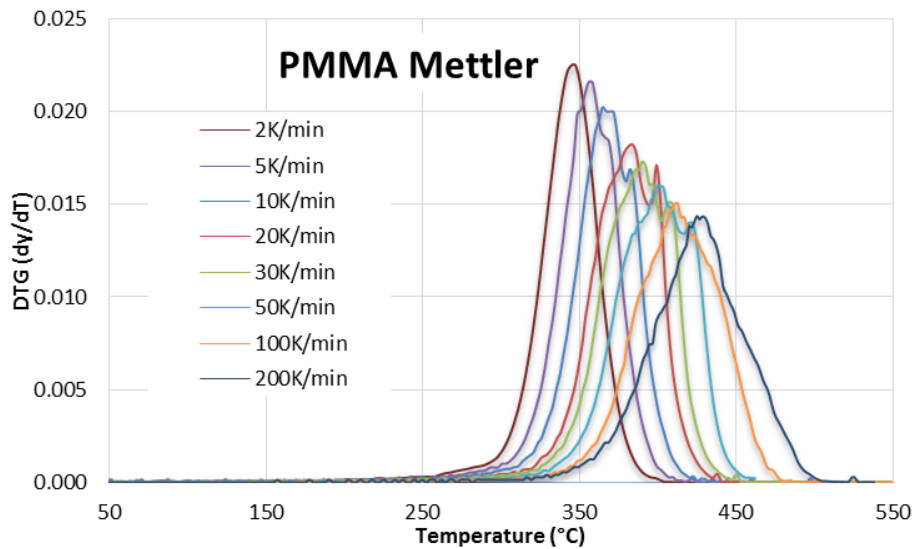


Figure 4.6: DTG plot of PMMA at various heating rates

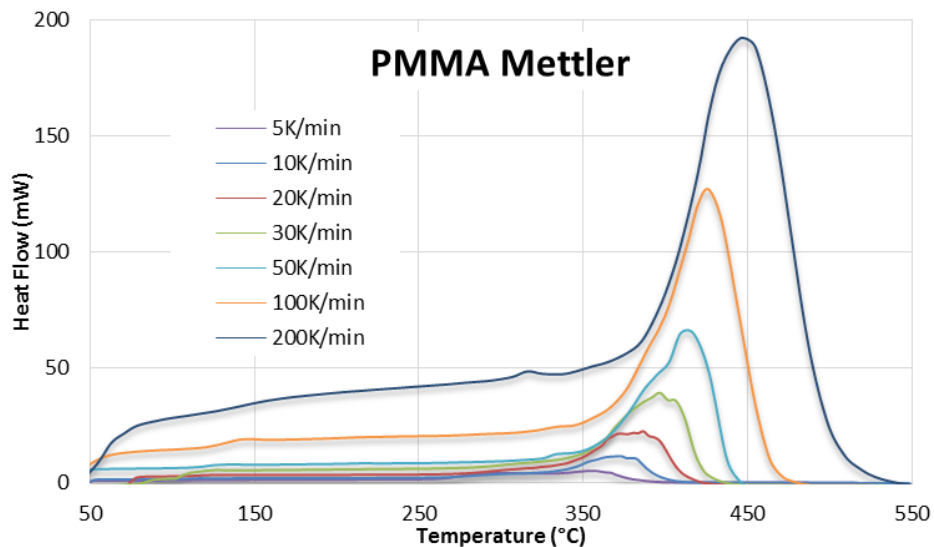


Figure 4.7: DSC thermograms of PMMA at various heating rates

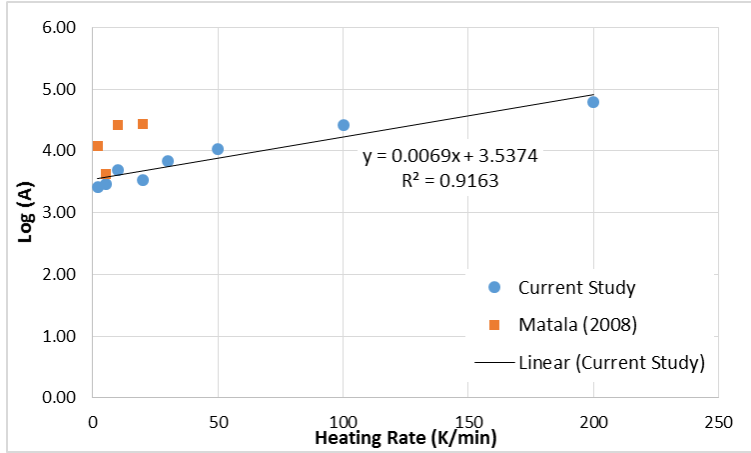
It should be noted that some models use a finite-order reaction where n is taken as unity. When the reaction order is forced to be unity, the kinetic parameters are somewhat controlled. A non-unity reaction order should be more realistic, because the kinetics are not forced to be of a certain order and subsequently, the other parameters obtained are also more accurate. Preliminary work in this area showed that with a unity reaction order, the simulation significantly deviated from the experimental result (Hasalova, Moinuddin & Abu-Bakar 2013).

4.2.1 Kinetic Parameters of Pine

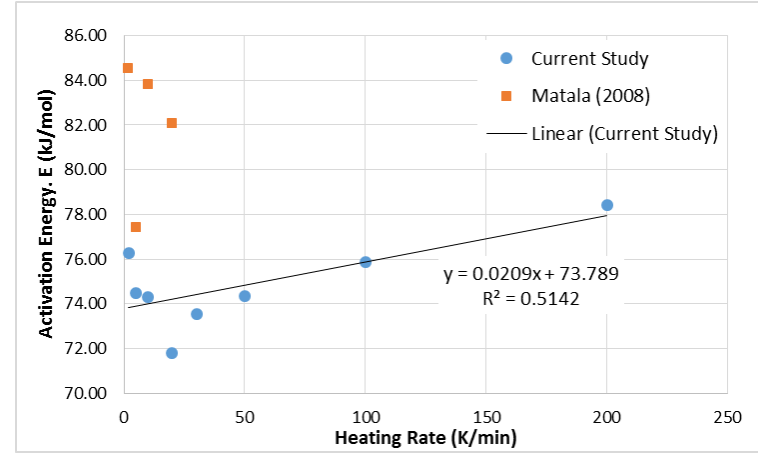
The kinetic parameters (activation energy, E , reaction order, n , and pre-exponential factor, A) for pine were derived from Figure 4.1 using the inflection point method and they are presented in Figure 4.8 as a function of heating rates (dT/dt). These figures show that the values of A , E and n vary with dT/dt which is consistent with the decomposition shift observed in Figure 4.1.

When a sample is heated it undergoes various physical and chemical changes. The physical changes may include melting or solid-phase transition (Vyazovkin 2015) and the chemical changes include molecular bond breakage which results in either endothermic or exothermic reactions. Examples of these changes occur during sample pyrolysis which converts organic materials into both a solid phase (char) and gases (Wampler 2006) which is the case for materials such as pine.

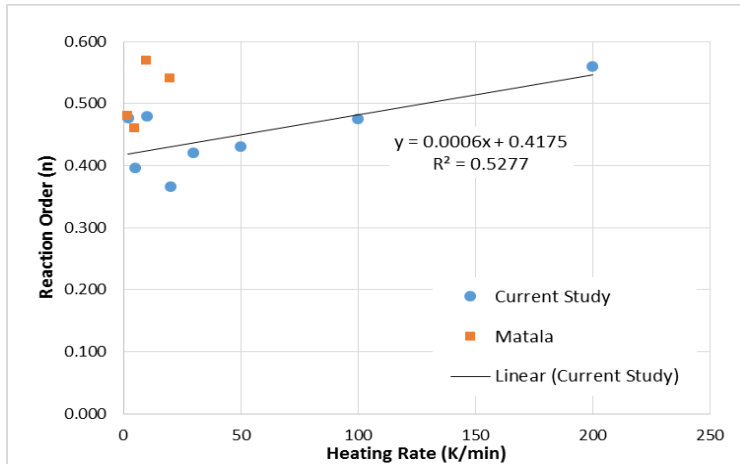
Matala (2008) studied these parameters comprehensively, however, an optimization technique (Lautenberger, Rein & Fernandez-Pello 2006) was used to study the kinetics of the experimental raw data. In this technique, an optimization algorithm performs permutations with combinations of the values of A , E and n . Then, with each set of kinetic values, simulations are run using a pyrolysis model with values of the model that match the best with the experimental result which are taken as the “model-specific” values. These are not true values as they may or may not be universally applied to all models and therefore, a different set of kinetic triplet values were obtained (Matala 2008). It is well known that there is a strong interdependence among the kinetic triplet (A , E , and n) (Opfermann 2000, Rein et al.2006). Applying two different set of triplets (one set from the current study and one set from (Matala 2008) to Equation (3.2) yields the same mass loss rate (to be discussed further in section 7.3.1 CHAPTER 7) which confirms this interdependence.



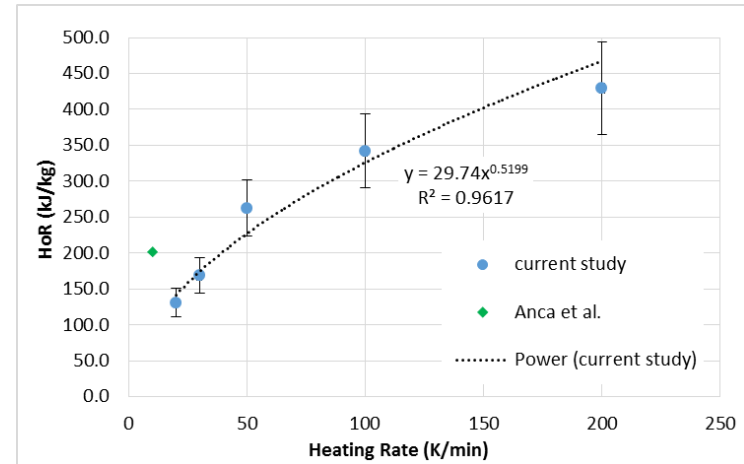
(a) Natural log of pre-exponential factor



(b) Activation energy, E (kJ/mol)

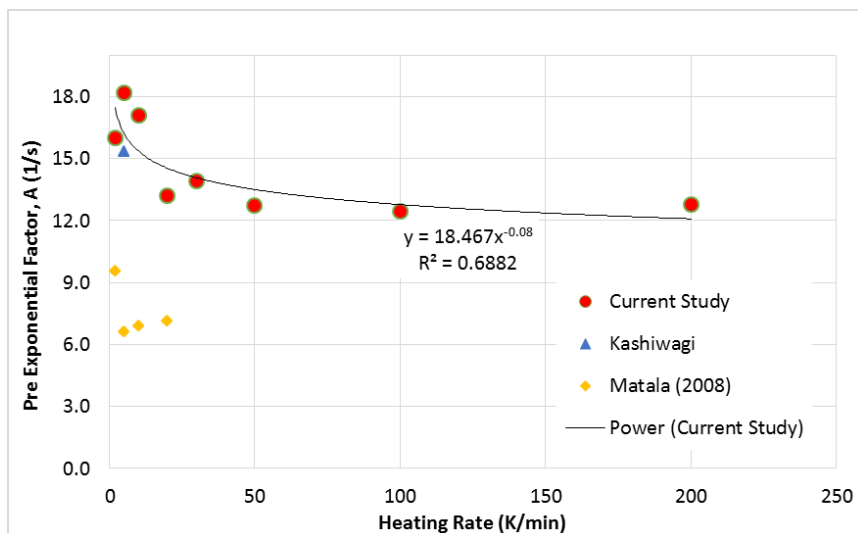


(c) Reaction order, n

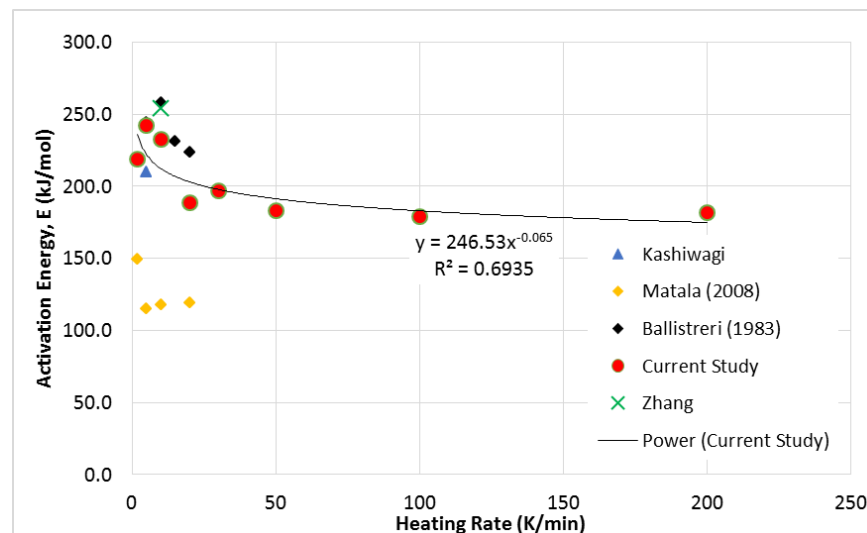


(d) Heat of reaction (kJ/kg)

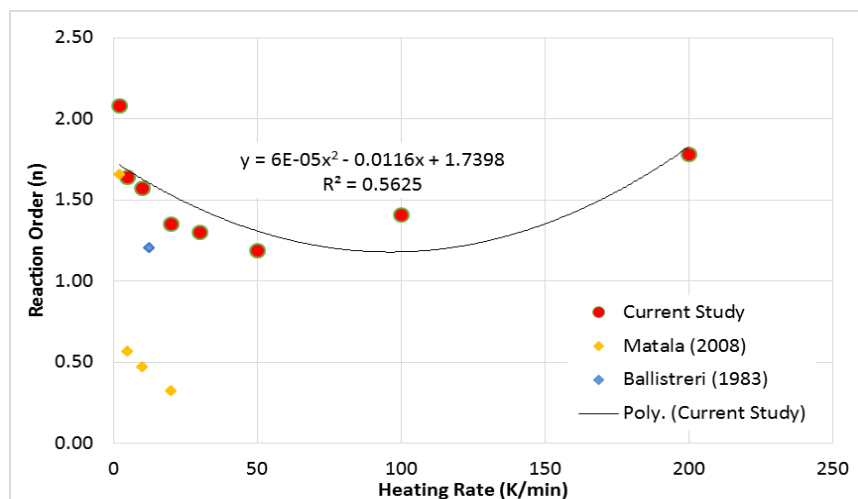
Figure 4.8: Kinetic parameters and HoR for pine



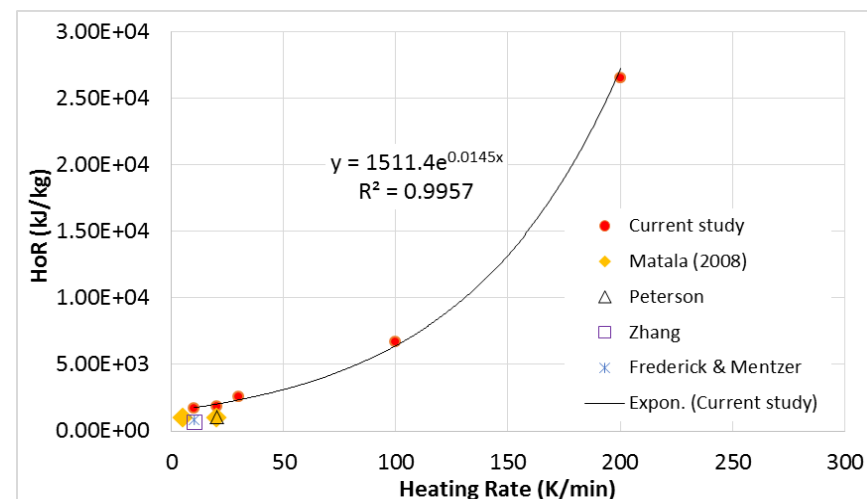
(a) Natural log of pre-exponential factor



(b) Activation energy, E (kJ/mol)



(c) Reaction order, n



(d) Heat of reaction (kJ/kg)

Figure 4.9: Kinetic parameters and HoR for PMMA

It is important to note that the data reported by Matala (2008) was obtained using relatively low heating rates (2 to 20 K/min). Due to the scarcity of reliable literature data obtained using high heating rates (50 to 200 K/min) the data from the current study could not be comprehensively compared.

Through regression analysis of the kinetic parameters for pine, a number of empirical formulae were obtained and are presented in Figure 4.8. For pine, some strong linear relationships with high correlation coefficients are observed, and overall, the kinetic parameters for pine show an increasing trend with an increasing heating rate. In particular, the pre-exponential factor (A) shows a strong linear relationship with respect to heating rate which is also indicative of a higher pyrolysis rate (Shi 2014, Cetin, Gupta & Moghtaderi 2005).

4.2.2 *HoR* of Pine

The *HoR* values as a function of heating rate for pine is presented in Figure 4.8(d). It is also important to note that the *HoR* is calculated based on the normalized enthalpy as expressed in Equation (3.21). For this material, a trend of increasing *HoR* values with respect to heating rate is observed, which has also been reported for the heating of waste materials (Missoum, Gupta & Cheng 1997). Anca et al. (2012) reported a *HoR* value for pine of around 200 kJ/kg measured at 10 K/min and this is higher than the value obtained in the current study measured at 20 K/min. In a comprehensive review of the literature, Haseli et al. (2011) arrived at the conclusion that the external heating rate of the material is one of the primary reasons for *HoR* variations. At high heating rates, more energy is required to volatilize the solid material into the gaseous phase whereas at lower heating rates, the transition from solid to gas is *via* a liquid phase which requires lower energy (Mui et al. 2008). A further explanation of additional heat flow needed for volatilisation at high heating rate is already discussed in Section 4.1.2. The *HoR* data in this work shows that a very strong power relationship exists for pine. This relationship is presented by the trend line and associated equation in Figure 4.8(d).

4.2.3 Kinetic Parameters of PMMA

The kinetic parameters (activation energy, E , reaction order, n , and pre-exponential factor, A) for PMMA was derived from Figure 4.6 using the inflection point method is presented in Figure 4.9 as a function of heating rates (dT/dt). Similar to pine, these

figures show that the values of A , E and n vary with dT/dt which is consistent with decomposition shift observed in Figure 4.6.

For some polymeric materials such as PMMA, physical and chemical processes occur when the heat is applied and consequently the material properties are also affected (Beyler & Hirschler 2002). The values obtained in the current study from Figure 4.9 were compared with those values observed in the literature. Similar to the results for pine, the values for kinetic parameters and HoR for PMMA at the higher heating used in this study have not been reported previously to the best of our knowledge. From a comparison of the data obtained in this work with that reported by other researchers, the values of the kinetic parameters and HoR lie within the range of values found in the literature.

The kinetic parameters of PMMA show a different trend compared to pine with the pre-exponential factor and activation energy declining as a function of heating rate. At lower heating rates, the chemical reaction is kinetically slow resulting in higher activation energies with the reverse occurring at higher heating rates (Shi 2014). It may be suggested that the activation energy (E) is controlled by the pyrolysis rate of the sample at the surface at higher heating rates whereas at lower heating rates, bond-breaking is the main contributor to the value of E (Ang & Pisharath 2012). In general, the kinetic triplet is observed to change significantly with a variation in heating rates and it has been suggested that this is influenced by physical and chemical changes of materials (Beyler & Hirschler 2002).

For PMMA, the relationship between $\log(A)$ and E with heating rate are empirically based on a power law, whereas for n , the relationship is more parabolic. In the equation presented in Figure 4.9(c), although the quadratic term is very small (6×10^{-5}), the fitting of a quadratic polynomial ($R^2=0.56$) has been observed to be much better than a linear function ($R^2=0.0041$) with the selection of average value of n (1.54).

The values obtained in the current study from Figure 4.9 were compared with those values observed in the literature. However, values for kinetic parameters and HoR for PMMA at the higher heating rate used in this study have not been studied to the best of our knowledge. From a comparison of the data obtained in this work with that reported by other researchers, the values of the kinetic parameters and HoR lie within the range of values found in the literature. For example, the A values obtained in the

current study and that reported by Kashiwagi et al. (1986) are very close. The A value reported by Matala (2008) is slightly lower compared to these two which may be due to the optimization technique used and the interdependence of the kinetic triplet discussed in Section 4.2.1. The E value obtained in the current study was compared with those reported by Kashiwagi et al. (1986), Matala (2008), Ballistreri et al. (1984) and Zhang (2004). With the exception of the E value obtained by Matala (2008), the values reported in the other studies agree well with the present study. Among these studies, only Ballistreri et al. (1984) and Matala (2008) considered non-unity n values and while the n value of the former is close to the value determined in the present study, the value reported in the latter work is lower. Similar reasons for the differences in the A value discussed previously can be attributed to the differences in the E and n values of Matala (2008). Since the literature values at low heating rates compare well, it may be suggested that values from the current study over the range of heating rates are reliable.

A summary of the trends and qualitative correlations of the relationships of all parameters for pine and PMMA with heating rate are presented in Table 4.1. The table shows that all kinetic parameters for pine materials increase with an increasing heating rate. The opposite is shown for PMMA with respect to A and E .

Table 4.1: Summary of kinetic parameters and HoR trends

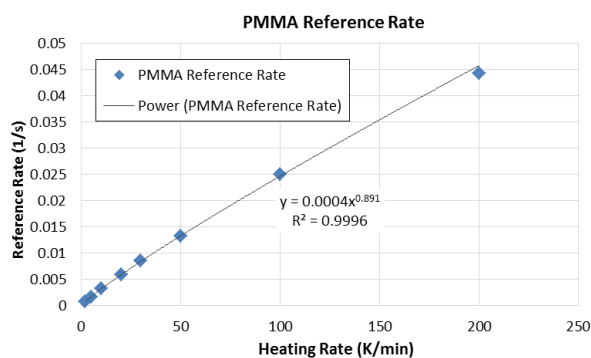
Material	Pine		PMMA	
Parameter	Trend	Strength	Trend	Strength
Log (A)	Linear (increasing)	Strong ($R^2=0.92$)	Power (decreasing)	Moderate ($R^2=0.69$)
E	Linear (increasing)	Poor ($R^2=0.51$)	Power (decreasing)	Moderate ($R^2=0.69$)
n	Linear (increasing)	Poor ($R^2=0.53$)	Parabolic (bottom vertex)	Poor ($R^2=0.56$)
HoR	Power (increasing)	Strong ($R^2=0.96$)	Exponential (increasing)	Strong ($R^2=1.0$)

Similar to the pine and PMMA kinetic parameters, those of moisture for virgin pine samples were also calculated using the inflection point method. However, no definite relationship with respect to the heating rate is observed with generally flat trends

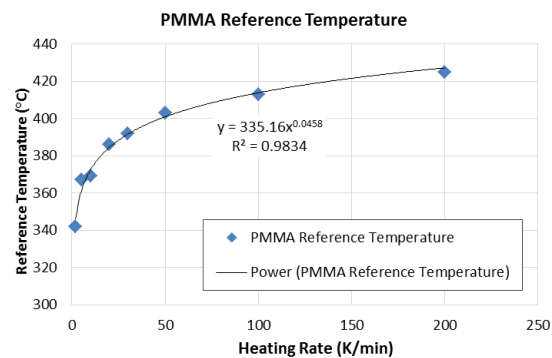
observed. The mean and standard deviation of the parameters across the various heating rates are presented in Table 4.2.

Table 4.2: Summary of kinetic parameters for moisture in virgin pine

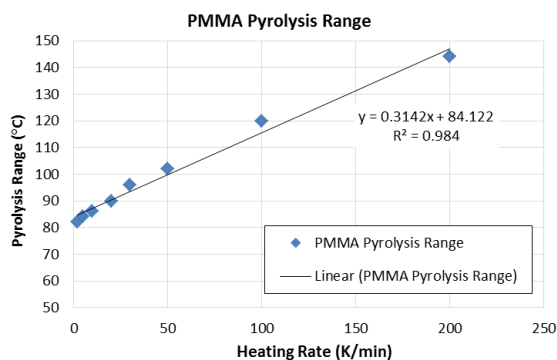
Parameter	Log (A)	E (kJ/mol)	n
Mean	8.78	76.5	1.64
Standard deviation	1.5	10.69	0.33



(a) Reference rate

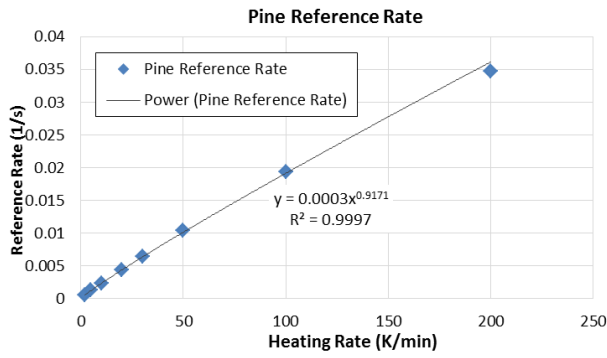


(b) Reference temperature

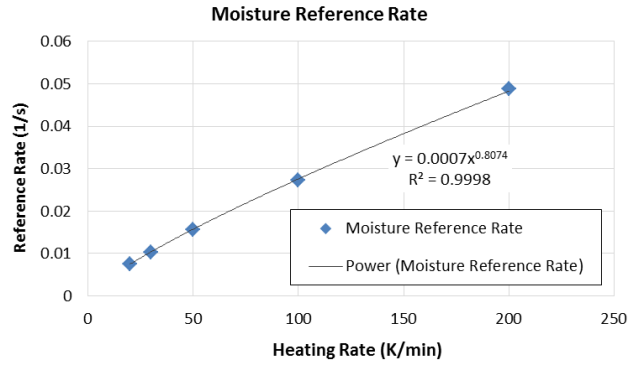


(c) Pyrolysis range

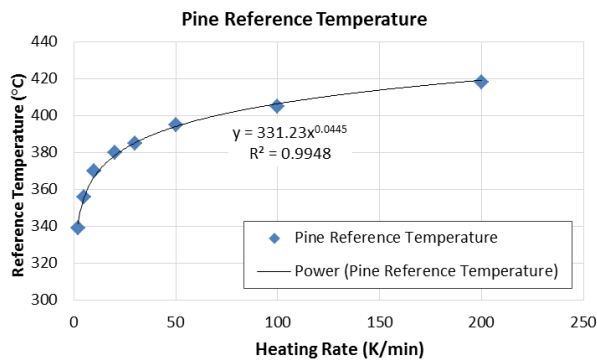
Figure 4.10: Reference temperature, reaction rate and pyrolysis range for PMMA



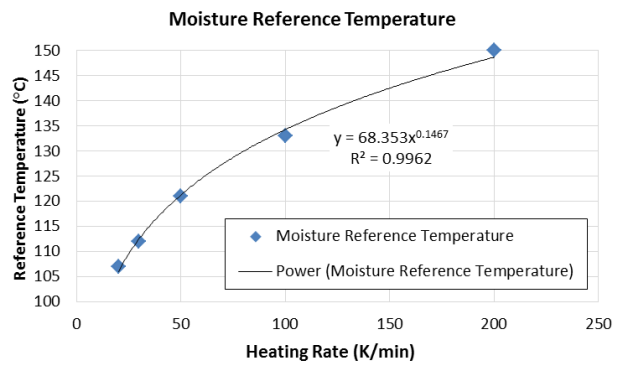
(a) Pine reference rate



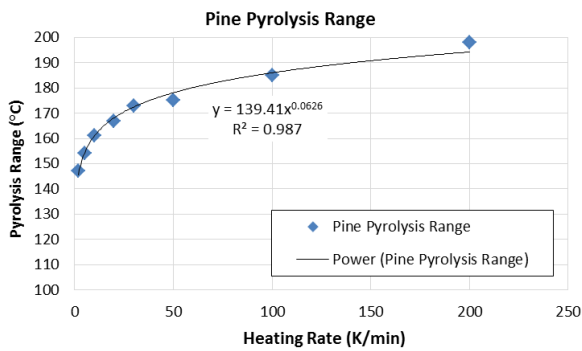
(b) Moisture reference rate



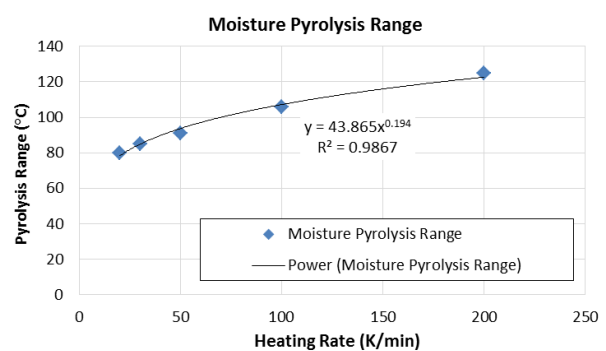
(c) Pine reference temperature



(d) Moisture reference temperature



(e) Pine pyrolysis range



(f) Moisture pyrolysis range

Figure 4.11: Reaction rate, reference temperature and pyrolysis range of pine

4.2.4 Alternative Kinetic Parameters for Pine and PMMA

The FDS model offers an alternative method for calculating the conversion rate by using a combination of the DTG peak location (REFERENCE_TEMPERATURE), peak value (REFERENCE_RATE= peak $dY/dT \times$ heating rate) and PYROLYSIS_RANGE (approximate width of the curves in Figure 4.1 and Figure 4.6 assuming its shape to be roughly triangular). The values from the DTG curves as a function of heating rate for PMMA are presented in Figure 4.10 and those of pine and moisture are presented in

Figure 4.11. The regression analyses of all three parameters for PMMA show power trends for the reference temperature and reference (reaction) rate and a linear trend for the pyrolysis range. A similar regression analysis of these parameters show power trends for both pine and moisture.

Other kinetic parameters, i.e. the yield of solid residue (v_s range) and the initial mass fraction, appear to be constant with respect to heating rate for pine and PMMA obtained from the TG plots of Figure 4.12 and Figure 4.5, respectively. The values of these parameters are summarised in Table 4.3.

Table 4.3: Yield of solid residue and initial mass fraction of pine and PMMA

Material	Property	Value
Pine	Yield of solid residue	0.185
	Initial mass fraction	0.965⁺
PMMA	Yield of solid residue	0
	Initial mass fraction	1

⁺ depending on moisture content

All TG and DSC tests were conducted in an inert atmosphere and as a result, the char carbonization appears to commence after ~71.5% of the mass of pine is pyrolysed when heated at 5 K/min and after ~81% when heated at 200 K/min. Thus the v_s range for virgin pine is found to be 0.19-0.285 with eventually only 18.5% of the char residue remaining. With respect to the bulk property of pine for the fire simulation, the yield of solid (char) residue can be taken as 0.185.

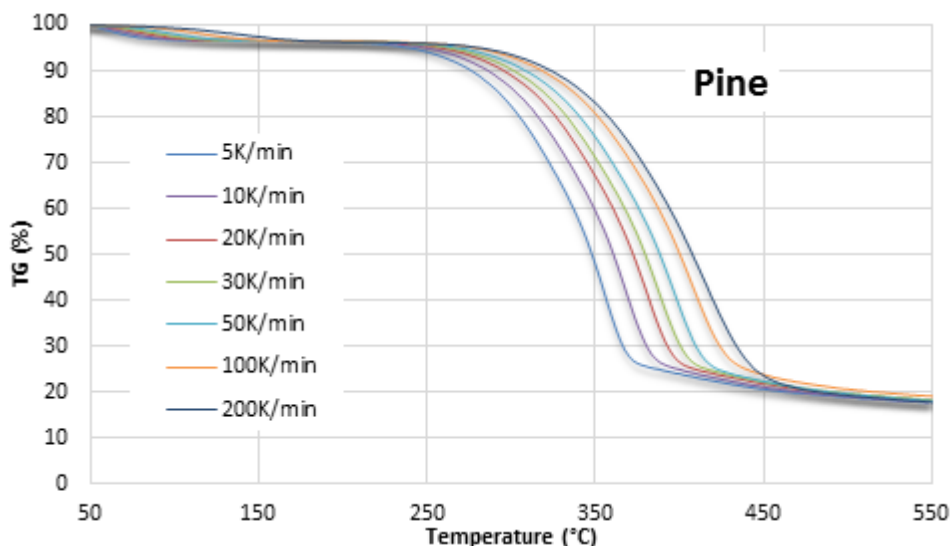


Figure 4.12: TGA thermograms of pine at various heating rates

4.2.5 *HoR* of PMMA

The *HoR* values as a function of heating rate for PMMA are presented in Figure 4.9 (d). The *HoR* of PMMA between 5 and 10 K/min obtained from the current study is close to the value of 1611 kJ/kg found by Tewarson and Pion (1976), however, they did not specify the heating rate utilised in their study. In other studies, Zhang (2004) reported a *HoR* value of 687 kJ/kg measured at a heating rate of 10 K/min and Peterson et al. (1999) obtained a *HoR* of 1080 kJ/kg at 20 K/min which are both lower than that in the current study. For the *HoR* data in this work, a through regression analyses shows very strong exponential relationship exists for PMMA. This relationship is presented by the trend line and associated equation in Figure 4.9(d).

4.3 Pyrolysis Parameters of Fabrics

In addition to the relatively “pure” materials, the effect of heating rate on the pyrolysis of two fabrics, cotton and wool, were explored. The results from experiments conducted with heating rates from 5 to 200 K/min are presented in Figure 4.13 to Figure 4.15 and Figure 4.24 to Figure 4.26 for cotton and wool respectively. Each figure presents the TG (Y as per Equation (3.1), DTG (dY/dT) and heat flow data.

4.3.1 Kinetic Parameters of Cotton

According to Faroq et al. (1994) the thermal decomposition of cotton can be observed over three separate stages where the first stage is the moisture release due to evaporation/dehydration. The second stage is the main decomposition of cotton which accounts for 75% of the overall weight loss and the subsequent char formation. Lastly, the third stage is attributed to the char removal or volatilisation of the sample. Similarly, Wakelyn et al. (2006) described three stages, namely evaporation/dehydration, transformation (accounting for 2% of dry weight of sample with the production of CO₂, CO and water vapour volatiles), and vacuum pyrolysis of pure cotton cellulose (80% of original sample mass).

The TG and DTG data for cotton are shown in Figure 4.13 and Figure 4.14 respectively. These figures show that dehydration of cotton occurs at below temperatures 150°C which is then followed by the pyrolysis process which takes place between 300-550°C. It is clear from these figures that multiple reactions result from the pyrolysis of cotton during the measurement. Beyond this range, where the pyrolysis is completed, a char residue remains as the final product. Overall, at each heating rate there are three reactions: one related to moisture evaporation (termed P1) with the remaining peaks related to the pyrolysis of cotton components with the first and second peaks expressed as Cotton 1 (P2) and Cotton 2 (P3) respectively. Unfortunately due to the reduced sensitivity of Mettler TGA under the test conditions, the moisture peak could not be properly resolved in Figure 4.14. From Figure 4.13, it can be determined that ~1.2% weight loss occurred during moisture evaporation (P1), with ~51.2% and ~32.5% weight loss during P2 and P3 respectively. In this case, P2 and P3 account for ~84% weight loss which is roughly 10% greater than the value reported by (Faroq, Price et al. 1994). Cao et al. (2010) and references therein described 59% weight loss for cellulosic and semi-cellulosic components and 14.5% lignin (non-cellulosic) decomposition. Therefore P2 and P3 most likely represent cellulosic and non-cellulosic decomposition, respectively. The char residue is consistently ~15% at all heating rates.

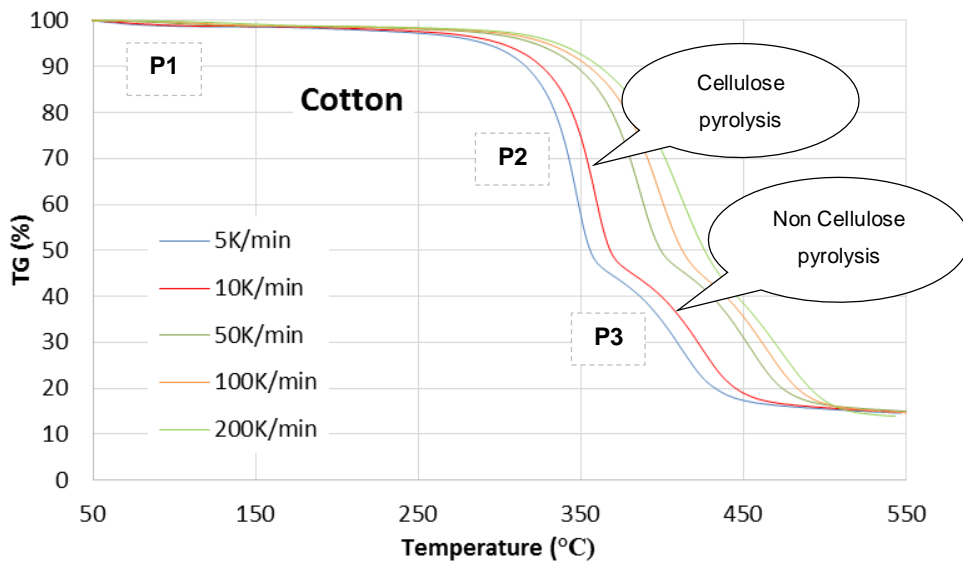


Figure 4.13: TG of cotton obtained using Mettler TGA

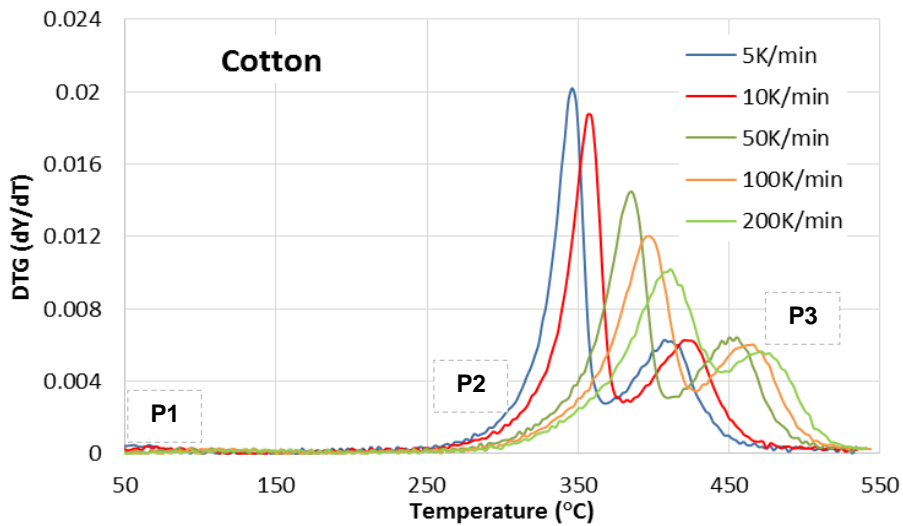


Figure 4.14: DTG of cotton obtained using Mettler TGA

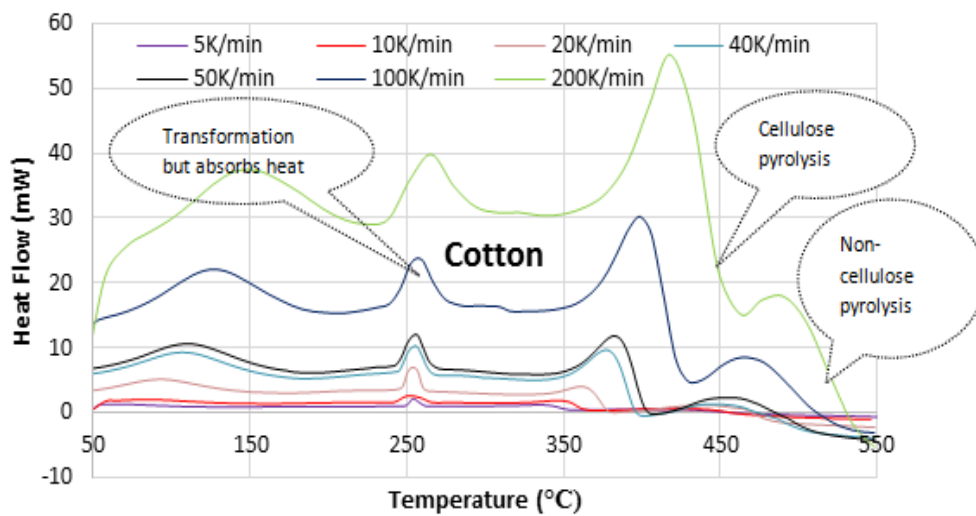


Figure 4.15: DSC heat flow of cotton obtained using Mettler DSC

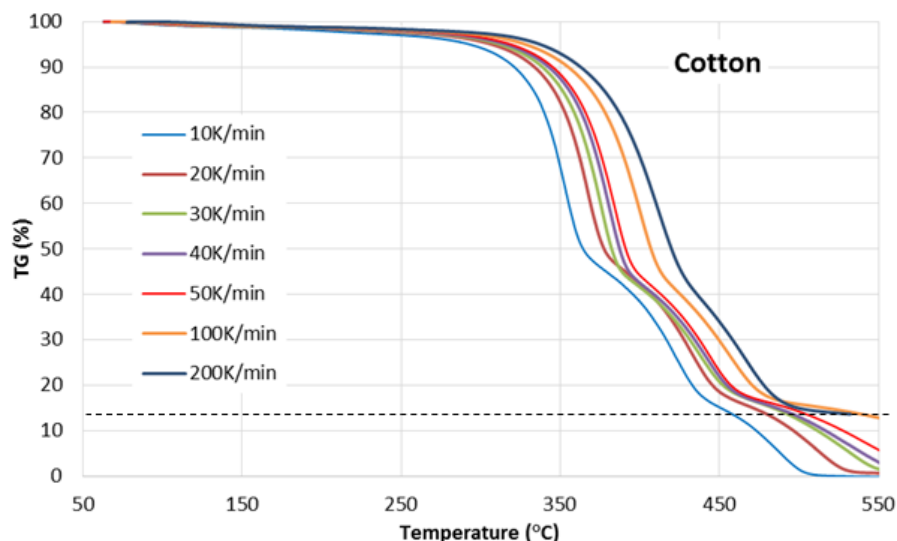
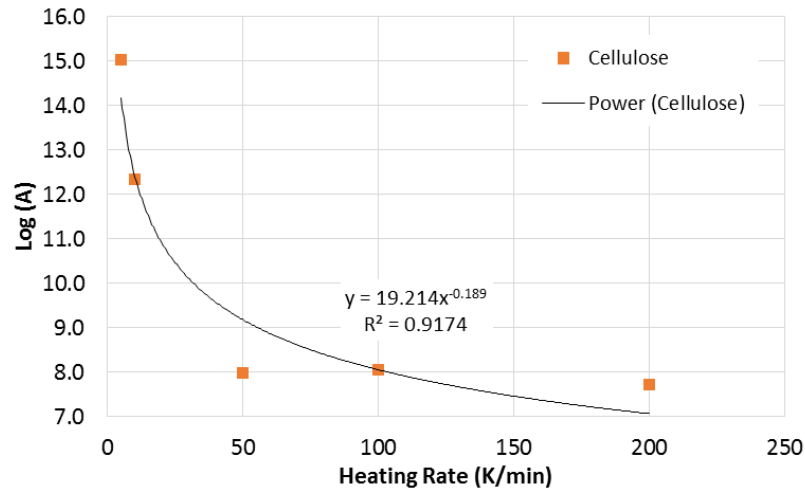


Figure 4.16: TG of cotton obtained using Perkin Elmer TGA

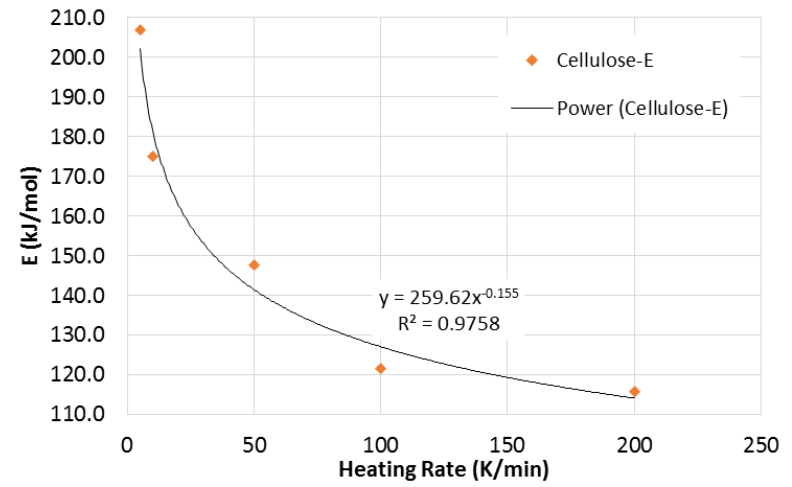
The higher sensitivity of the TGA data obtained using the Perkin Elmer instrument data shows a fourth pyrolysis peak commencing at 0.8 to 0.85 mass loss fraction followed by a complete loss of mass, especially at lower heating rates (Figure 4.16). Such a fourth peak is due to the char removal or volatilisation stage (Faroq et al. 1994) and detailed analysis of char removal is out of the scope of this study.

Unlike the TGA data, the DSC curves shown in Figure 4.15 depict four reactions including the moisture release occurring before 150°C. The second peak is attributed to the cellulose transformation with the remaining reactions attributed to the pyrolysis (cellulose and non-cellulose, respectively) over the temperature range 300-550°C.

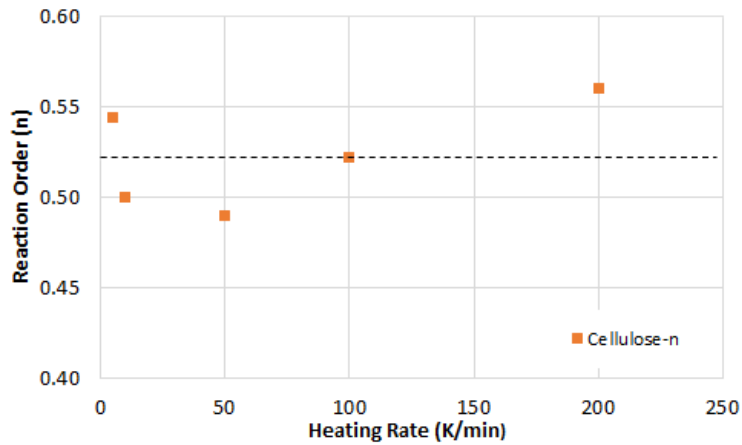
The TGA and DSC experiments enable the identification of at least two pyrolysis reactions in relation to cotton samples P2 and P3 (cellulose and non-cellulose, respectively). However, often ‘single effective’ kinetics are used in pyrolysis modelling due to the relative simplicity of this model. The kinetic parameters (activation energy, E , reaction order, n , and pre-exponential factor, A) derived from Figure 4.14 using the inflection point method are presented in Figure 4.17 to Figure 4.19 for cellulose, non-cellulose and ‘single effective’ kinetics as a function of heating rates (dT/dt). Through regression analysis of these various kinetics parameters the empirical formulae obtained are presented in the figures. From the seemingly flat trend observed in Figure 4.17(c), the average value of n for Cotton 1 (P2) is calculated as 0.52 with a standard deviation of 0.0029.



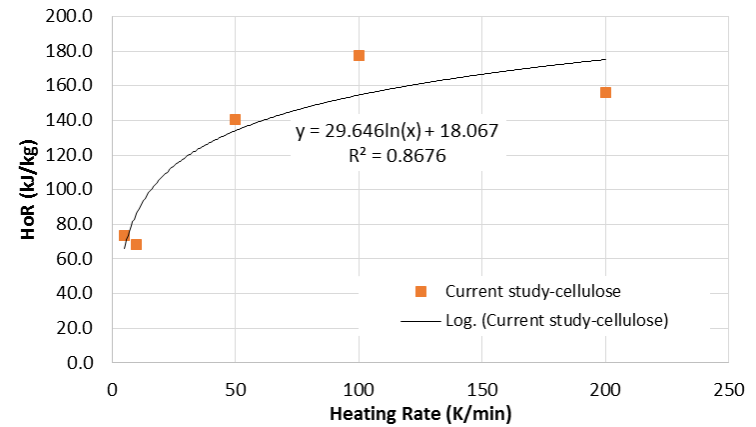
(a) Natural log of pre-exponential factor



(b) Activation energy, E (kJ/mol)

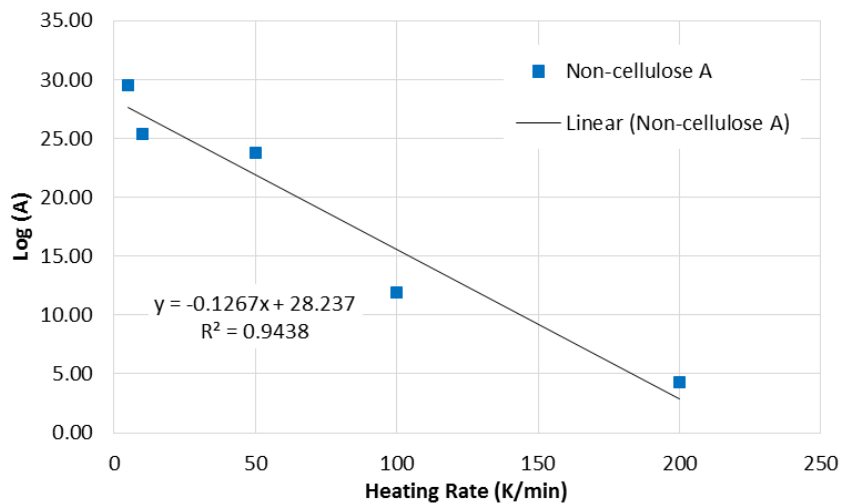


(c) Reaction order, n

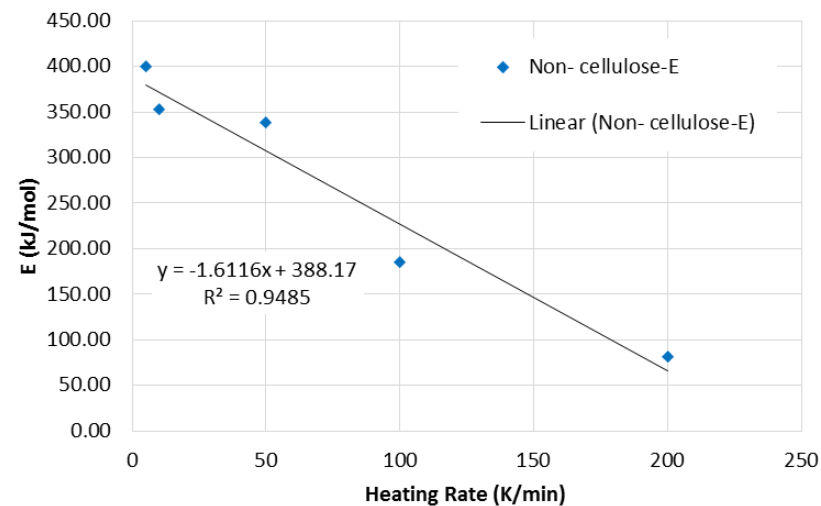


(d) : Heat of reaction (kJ/kg)

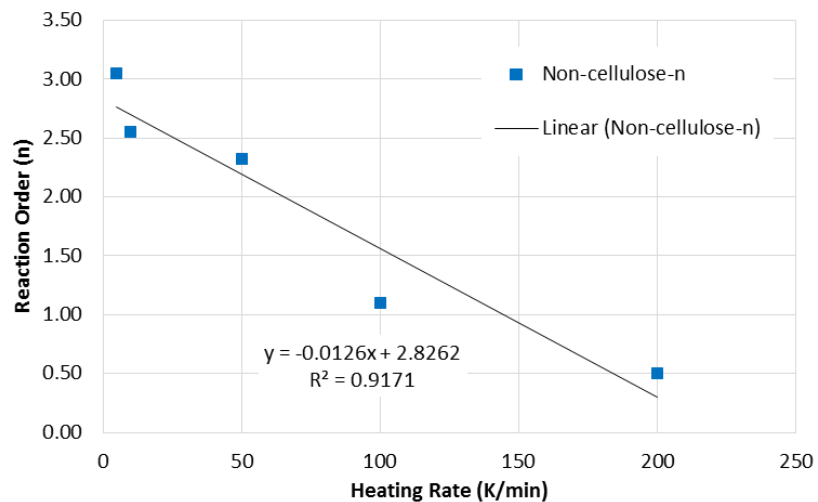
Figure 4.17: Kinetic parameters and HoR of Cotton 1 (P2)



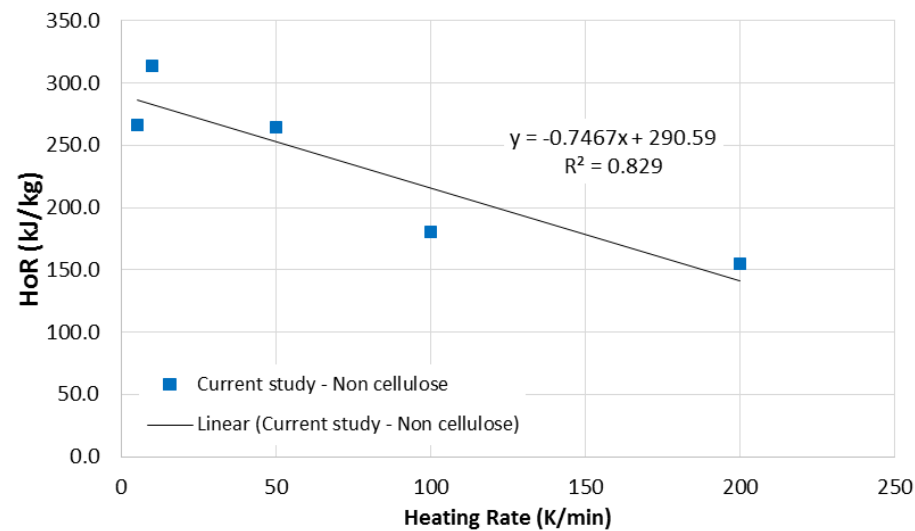
(a) Natural log of pre-exponential factor



(b) Activation energy, E (kJ/mol)

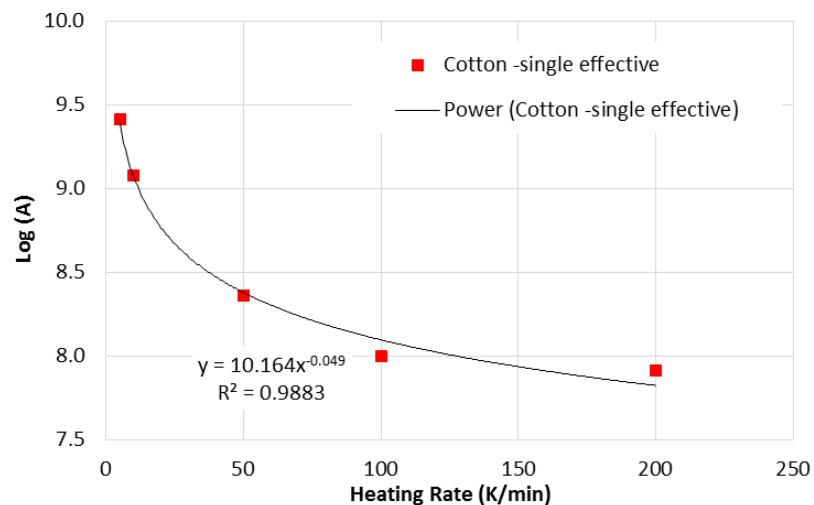


(c) Reaction order, n

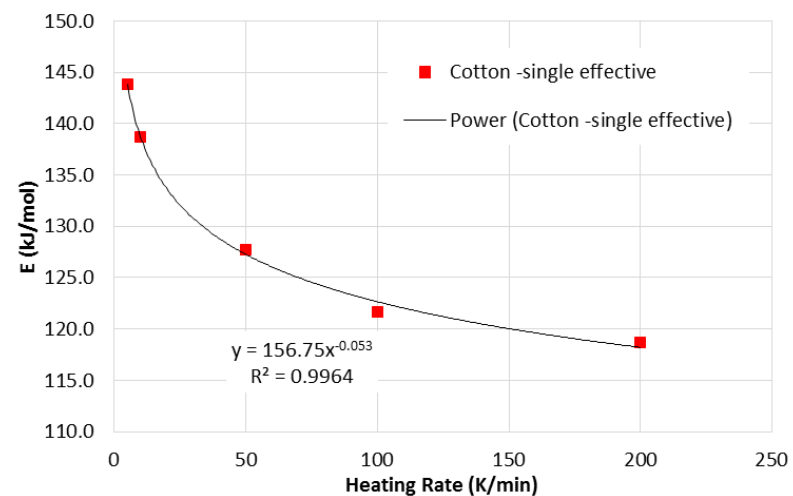


(d) Heat of reaction (kJ/kg)

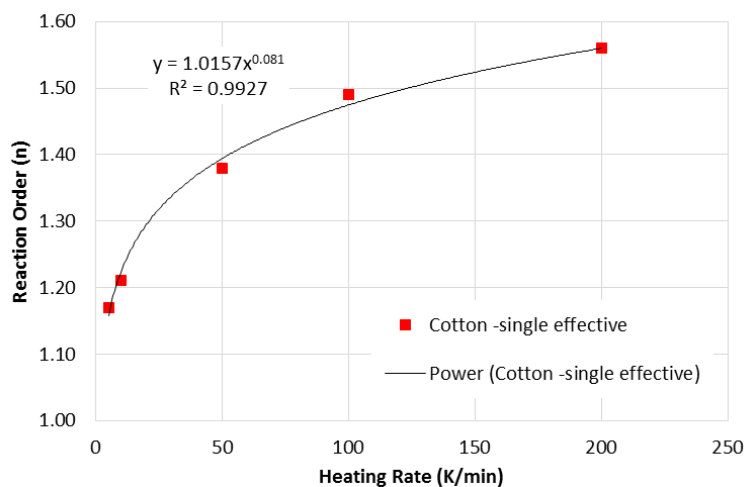
Figure 4.18: Kinetic parameters and HoR of Cotton 2 (P3)



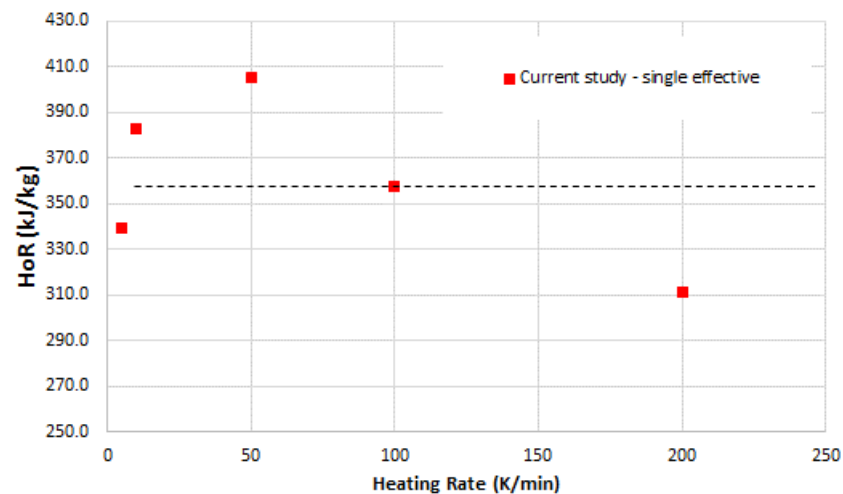
(a) Natural log of pre-exponential factor



(b) Activation energy, E (kJ/mol)

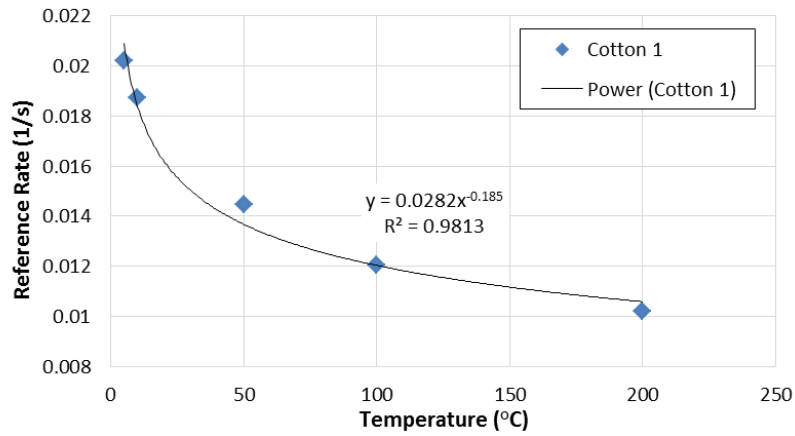


(c) Reaction order, n

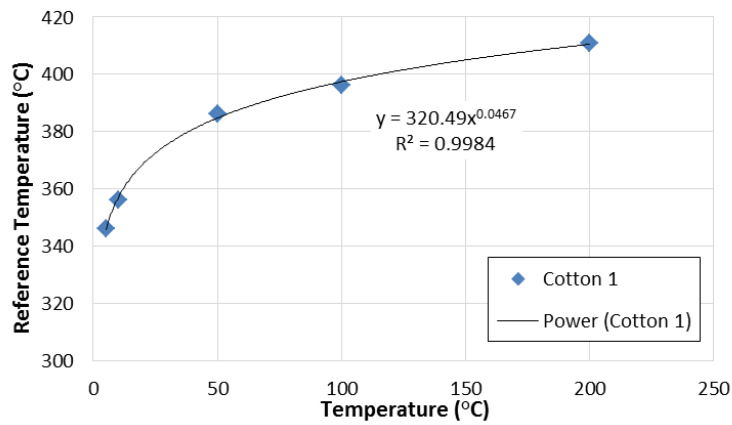


(d) Heat of reaction (kJ/kg)

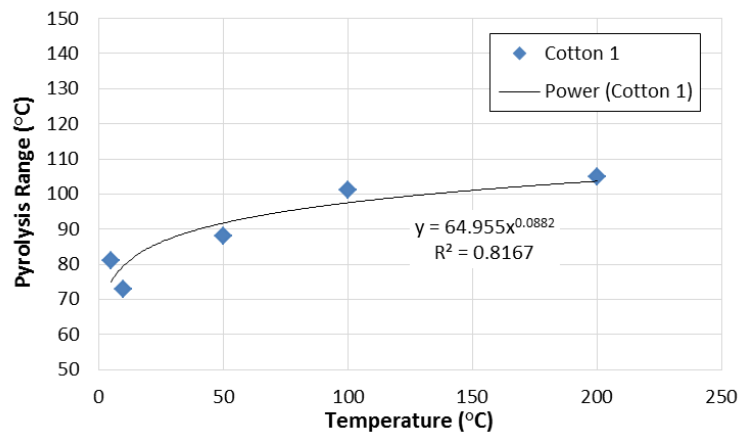
Figure 4.19: Kinetic parameters and HoR of Cotton ('single effective' method)



(a) Reference rate P2

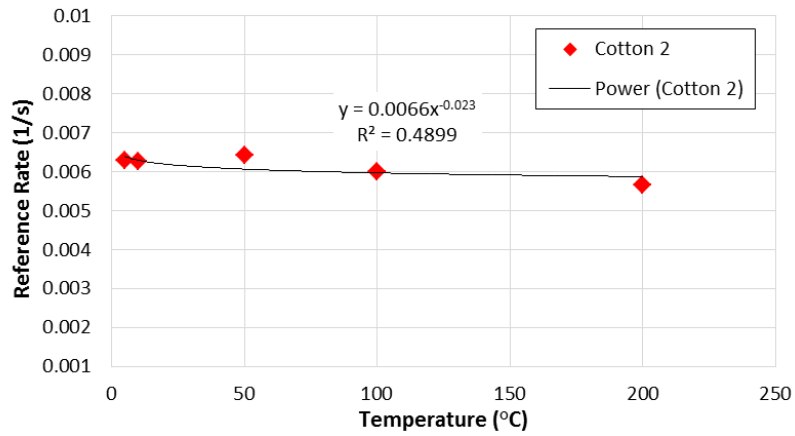


(b) Reference temperature P2

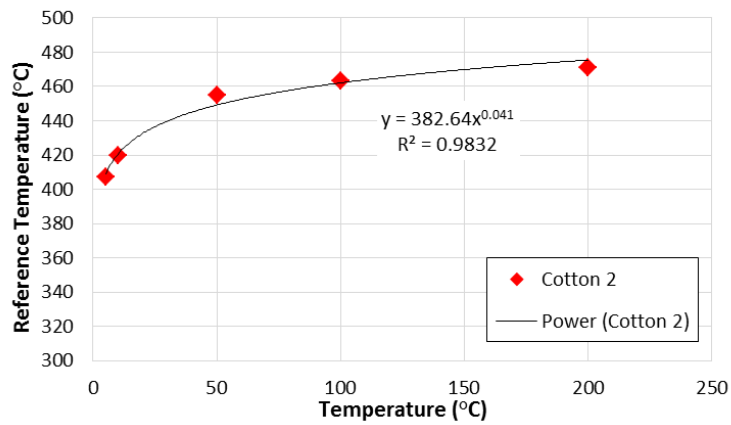


(c) Reference range P2

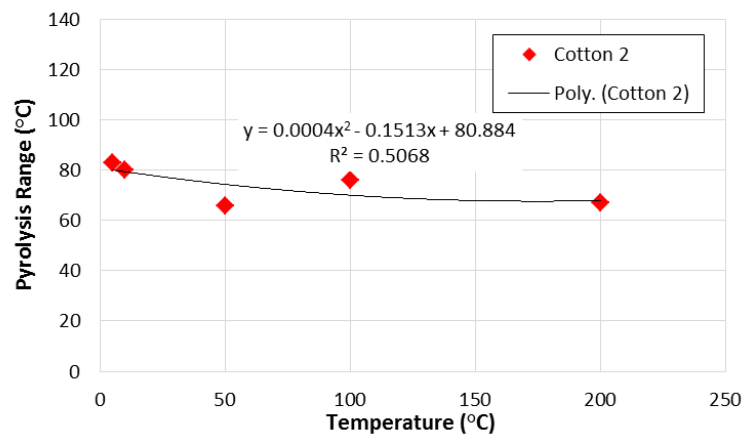
Figure 4.20: Kinetic parameters for Cotton 1



(a) Reference rate P3

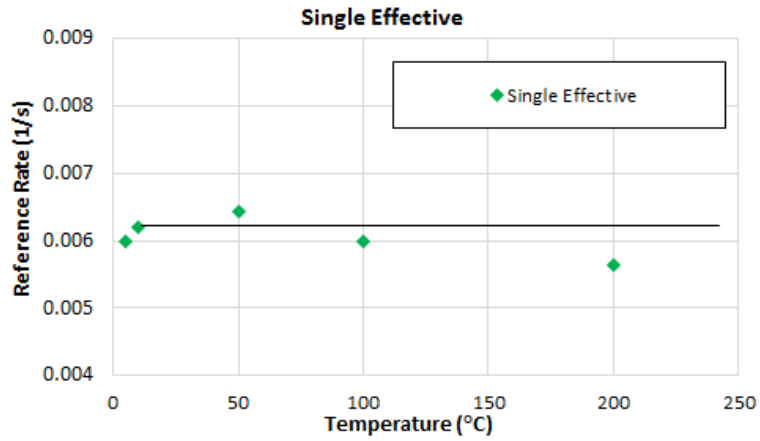


(b) Reference temperature P3

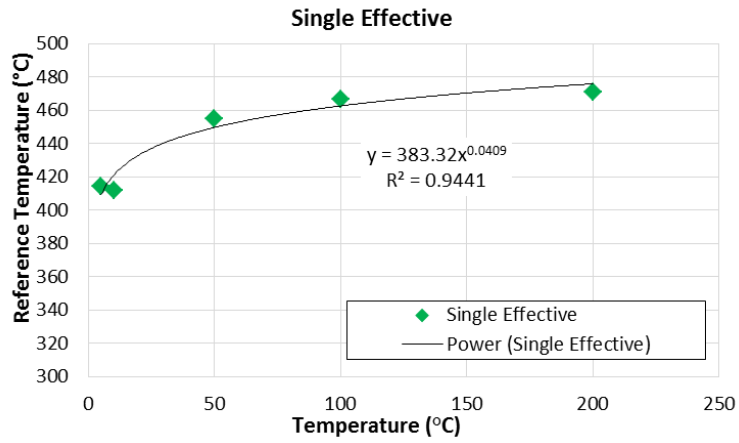


(c) Reference range P3

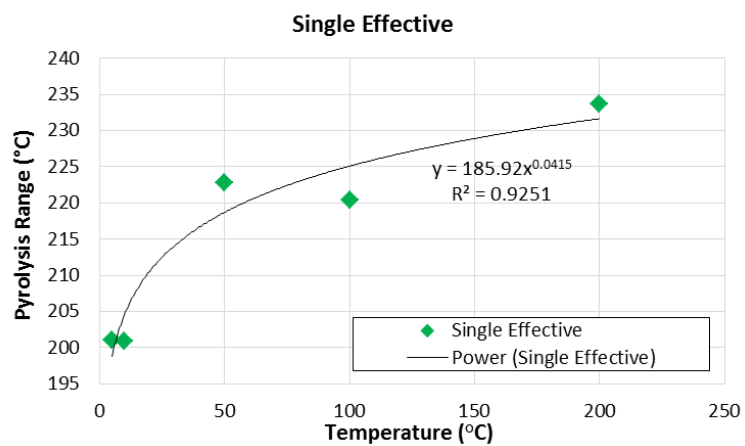
Figure 4.21: Kinetic parameters for Cotton 2



(a) Reference Rate 'single effective'



(b) Reference Temperature 'single effective'



(c) Reference Range 'single effective'

Figure 4.22: Kinetic parameters for Cotton 'single effective'

In some pyrolysis models, an alternative of three kinetic parameters, namely reference temperature, reaction rate and pyrolysis range are used. The details of this approach have been discussed in Section 4.2.4. The relationship of these parameters obtained for cotton is presented in Figures 4.20 to 4.22. As no trend is observed in Figure 4.22(a) for a 'single effective' reference rate, the average value is calculated as 0.0061 with a standard deviation of 0.0003.

4.3.2 *HoR* of Cotton

In Figure 4.23, the heat flow/unit mass vs temperature profile derived from the DSC and TGA data is presented by matching temperatures in the two sets of data. Here, the first peak represents moisture evaporation, the second peak represents transformation process which absorbs heat, the third peak represents cellulose pyrolysis and the fourth peak represents non-cellulose pyrolysis. To take into account of the heat absorption during transformation, the ΔH_{DSC} for cotton cellulose obtained from the areas under the curves of the second and third peaks are separately calculated using Equation (3.23) and then added in order to simplify numerical modelling and this is presented in Figure 4.17(d). Similarly, ΔH_{DSC} for the "single effective" model includes the sum of the areas under the curves of the second, third and fourth peaks as shown in Figure 4.19 (d). Conversely, the ΔH_{DSC} for non-cellulose is based only on the area under the curve of the fourth peak (presented in Figure 4.18d). To define the area under the peaks/curves, a spline function is used whereby tangents are drawn inward from the adjacent troughs, then they are connected with an approximate curve. Although this method is somewhat arbitrary, this conjecture is not uncommon for defining transitions in thermal analysis (Chizhik et al. 1979).

The *HoR* values as a function of heating rate for cotton cellulose, non-cellulose and the "single effective" model are presented in Figure 4.17(d), Figure 4.18(d) and Figure 4.19(d). An increasing trend of *HoR* values with respect to heating rate for P2 is observed whereas a decreasing trend is seen in P3. However, no definite trend is observed for the "single effective" model.

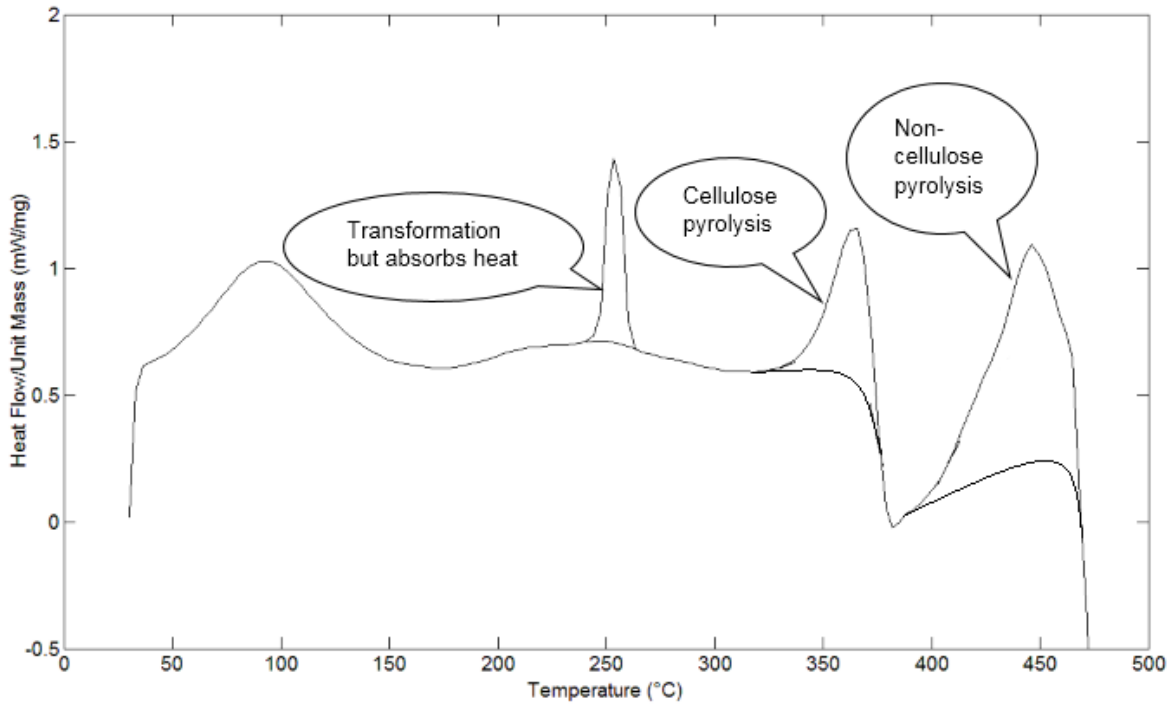


Figure 4.23: DSC/TGA temperature matched heat flow/mass for cotton (20 K/min)

Table 4.4: Summary of all kinetic parameters and *HoR* trends of cotton

Material	Cotton 1		Cotton 2		Cotton "Single Effective"	
Parameter	Trend	Strength	Trend	Strength	Trend	Strength
Log (A)	Power (decreasing)	Strong (R ² =0.92)	Linear (decreasing)	Strong (R ² =0.94)	Power (decreasing)	Strong (R ² =0.99)
E	Power (decreasing)	Strong (R ² =0.98)	Linear (decreasing)	Strong (R ² =0.95)	Power (decreasing)	Strong (R ² =1.0)
n	0.52 (average)	0.0029 (standard. deviation)	Linear (decreasing)	Strong (R ² =0.92)	Power (increasing)	Strong (R ² =1.0)
Reaction rate	Power (decreasing)	Strong (R ² =0.98)	Power (decreasing)	Poor (R ² =0.49)	0.0061 (average)	0.0003 (standard. deviation)
Reference temperature	Power (increasing)	Strong (R ² =1.0)	Power (increasing)	Strong (R ² =0.98)	Power (increasing)	Strong (R ² =0.94)
Pyrolysis range	Power (increasing)	Strong (R ² =0.82)	Polynomial (decreasing)	Poor (R ² =0.51)	Power (increasing)	Strong (R ² =0.93)
HoR	Logarithmic (increasing)	Strong (R ² =0.87)	Linear (decreasing)	Strong (R ² =0.83)	359.3kJ/kg (average)	36.57 kJ/kg (standard. deviation)

From the regression analysis of the data for cotton, the relationships between *HoR* and heating rates were obtained for cellulose and non-cellulose and are presented within the respective figures. The regression analysis of the ‘single effective’ model did not reveal any significant correlation; therefore the average value was calculated to be 359.3 kJ/kg with a standard deviation of 36.57 kJ/kg. A summary of the various trends and strengths of the relationships for all parameters is presented in Table 4.4. The table shows that for all kinetic parameters, decreasing trends with respect to increased heating rate are obtained with the exception of *n* for Cotton 1 and the “single effective” model where an increasing trend resulted.

4.3.3 Kinetic Parameters of Wool

Similar to cotton, the thermal decomposition of wool occurs in three stages (Tian et al. 1998) where the first stage is the moisture release is due to evaporation/dehydration. The second stage is the decomposition of wool and the final stage is attributed to the char volatilisation of the sample. Figure 4.24 and Figure 4.25 show the respective TG and DTG profiles of wool when heated from 10-200 K/min over the temperature range of 50-550°C. At lower heating rates (10K/min – 50K/min), dehydration occurred at below 150°C whereas at higher heating rates, dehydration is observed just below 200°C. The result observed at the lower heating rate has been reported previously with the first major TG mass loss attributed to moisture release between 30-120°C (Popescu & Augustin 1999). This is then followed by the wool pyrolysis process over the range of approximately 200-500°C. Horrocks and Price (2000) reported that the pyrolysis of wool starts at 225°C which is very close to the value found in the current study.

The results show that a single pyrolysis reaction occurs for the virgin wool sample and at lower heating rates (10-50 K/min), another peak is observed after pyrolysis which is attributed to the char volatilisation. Conversely, at higher heating rates, no char volatilisation is observed over the test heating range, rather a char residue is observed as the final product of the decomposition. It is also evident that greater char residue remains at the 100 K/min heating rate compare to the 200 K/min heating rate.

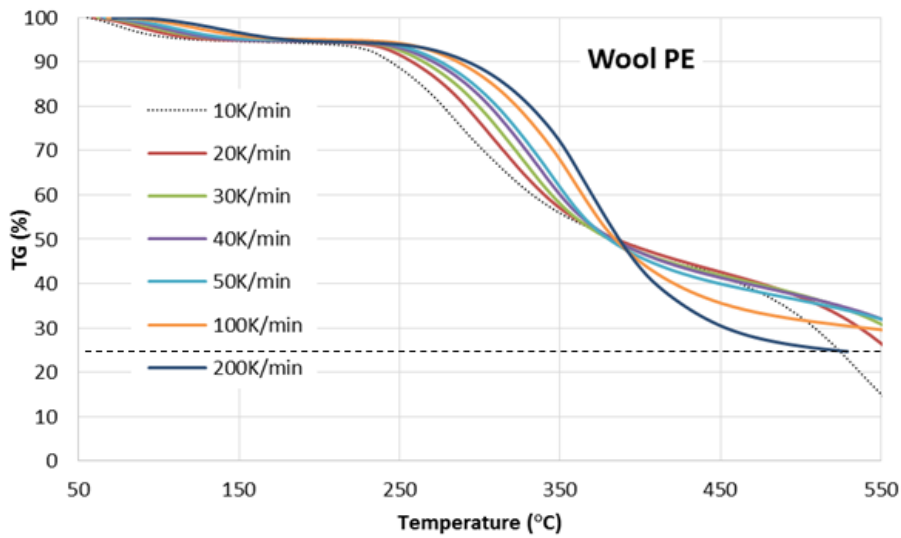


Figure 4.24: TG of wool obtained using Perkin Elmer TGA

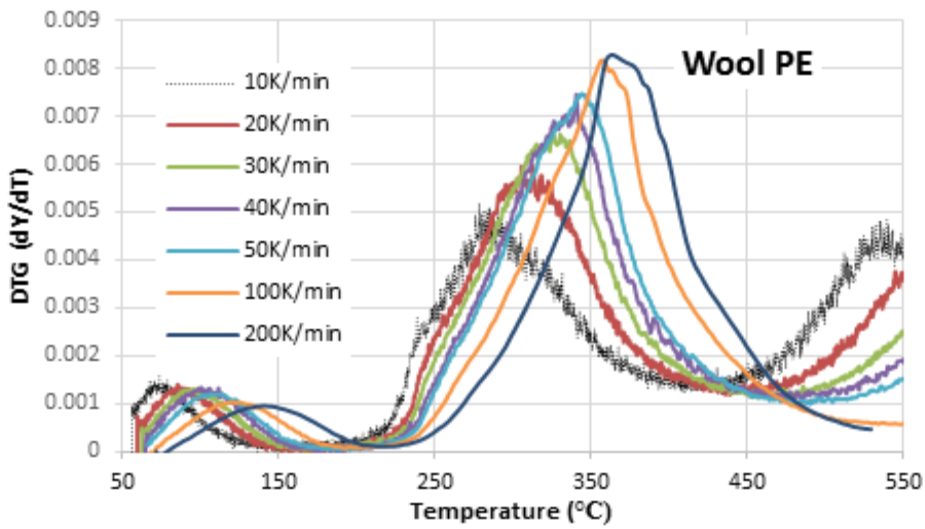


Figure 4.25: DTG of wool obtained using Perkin Elmer TGA

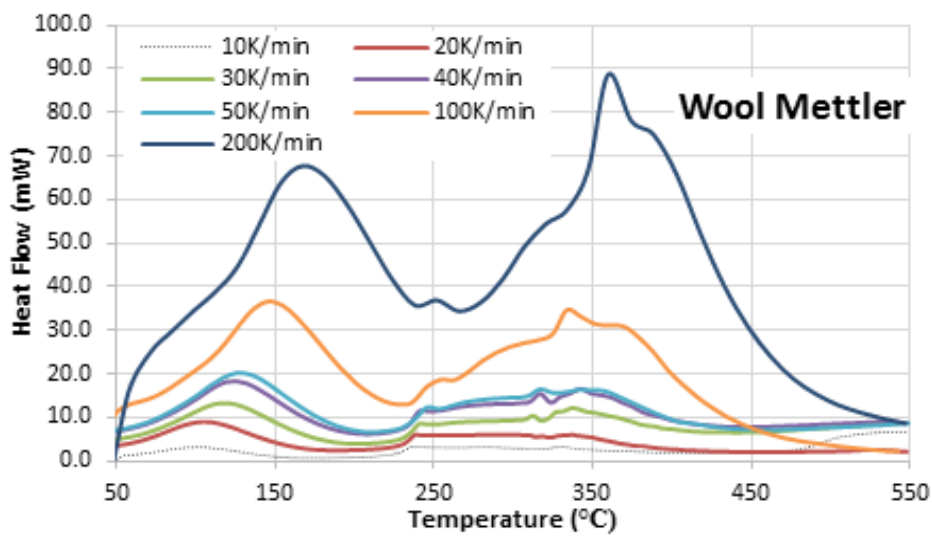


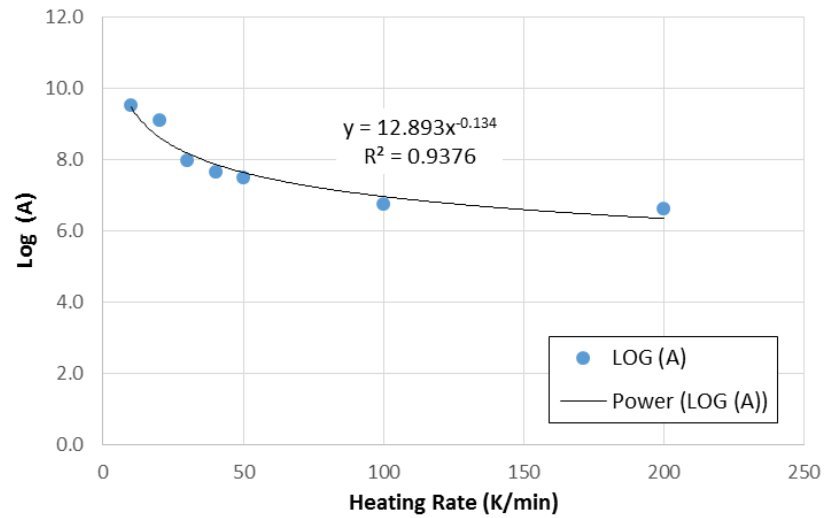
Figure 4.26: DSC heat flow of wool obtained using Mettler DSC

It has been observed that the pyrolysis of wool occurs via a single reaction. The kinetic parameters (activation energy, E , reaction order, n , and pre-exponential factor, A) derived from Figure 4.25 using the inflection point method are presented in Figure 4.27 as a function of heating rates (dT/dt). Additionally, the kinetic triplet of moisture in wool is presented in Table 4.5.

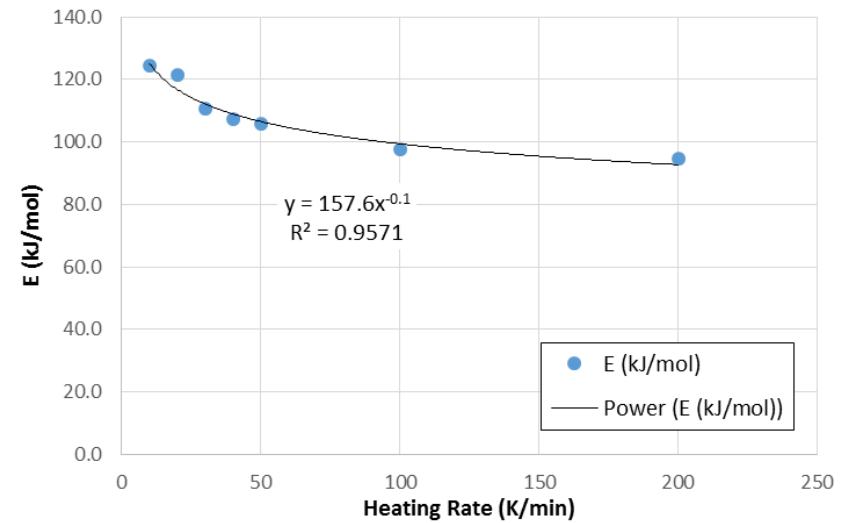
Table 4.5: Summary of kinetic parameters for moisture in wool

Parameter	Log (A)	E (kJ/mol)	n
Mean	6.8	58.68	1.53
Standard deviation	1.1	8.2	0.43

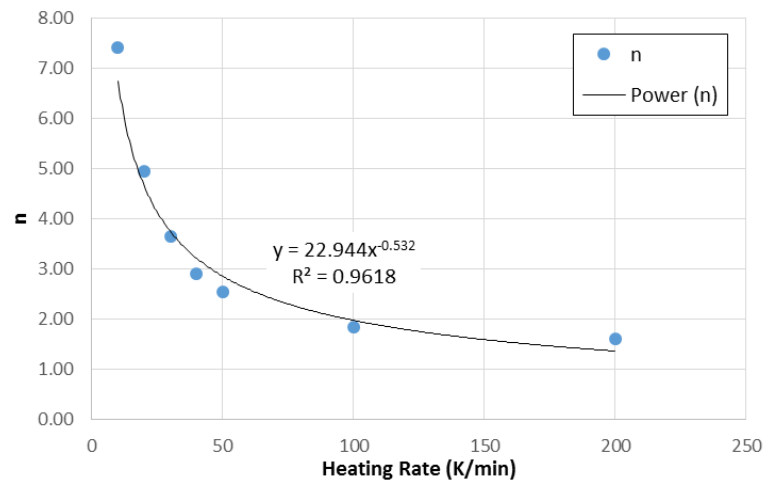
The values of reference temperature, reaction rate and pyrolysis range for wool at each heating rate are presented in (a) to (f). A strong power relationship is evident for all parameters relating to wool pyrolysis with a similar trend also observed for these parameters for moisture. Moreover, the results show that the reference rate, reference temperature and pyrolysis range increase as the temperature increases for wool. In contrast, the reference rate of moisture decreases with the increases in temperature. However, the trends are the same for moisture and wool with respect to reference temperature and pyrolysis range. The correlations for all the analyses are presented within respective figures.



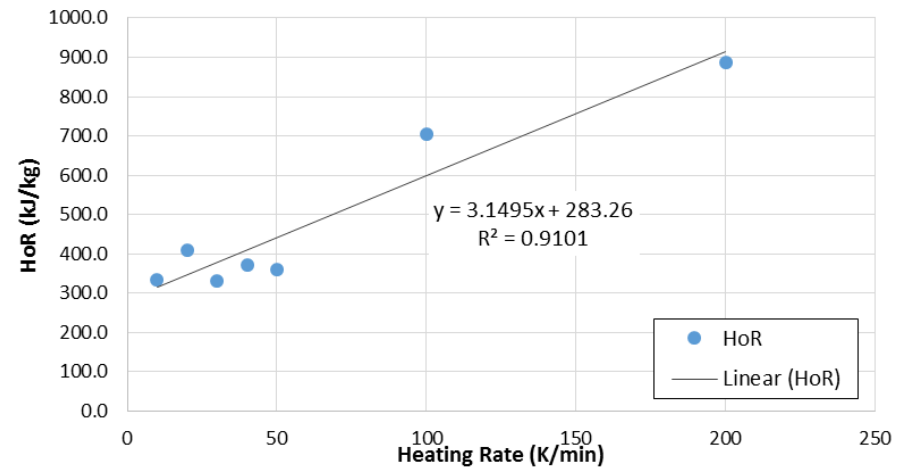
(a) Natural log of pre-exponential factor



(b) Activation energy, E (kJ/mol)

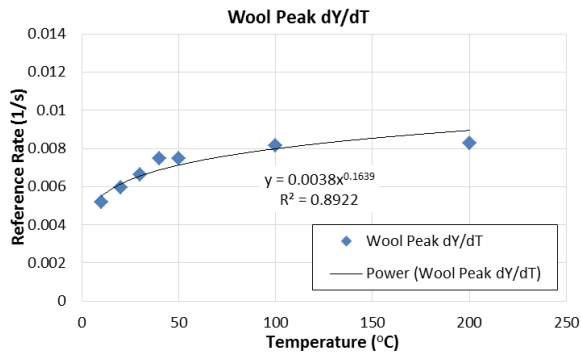


(c) Reaction order, n

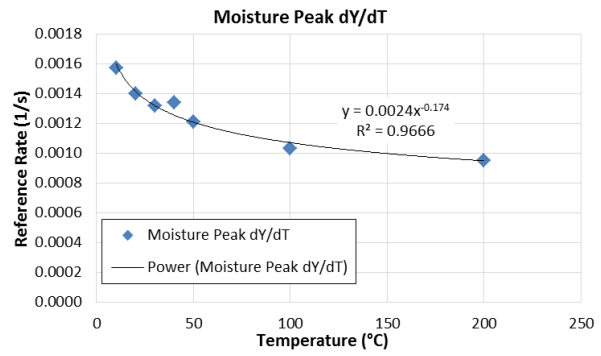


(d) Heat of reaction (kJ/kg)

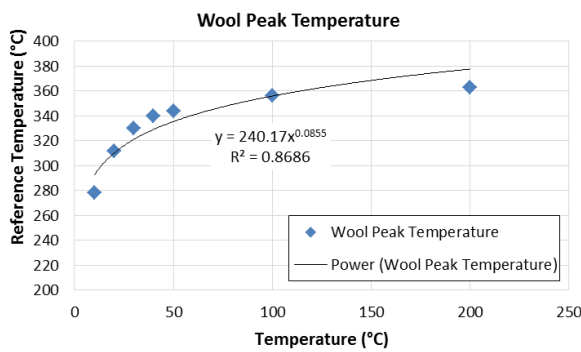
Figure 4.27: Kinetic parameters and HoR for wool



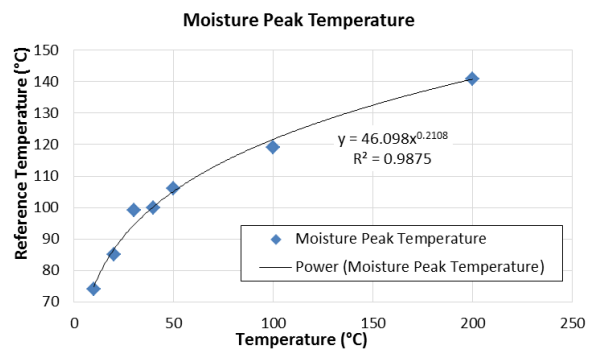
(a) Wool reference rate



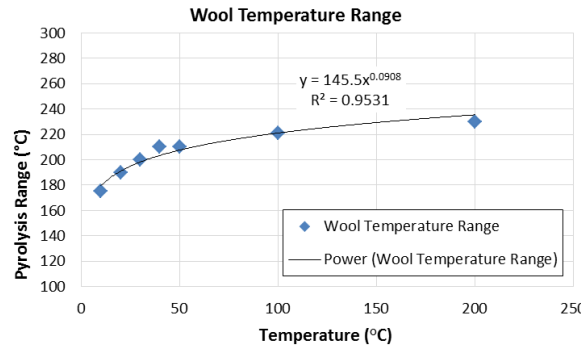
(b) Moisture reference rate



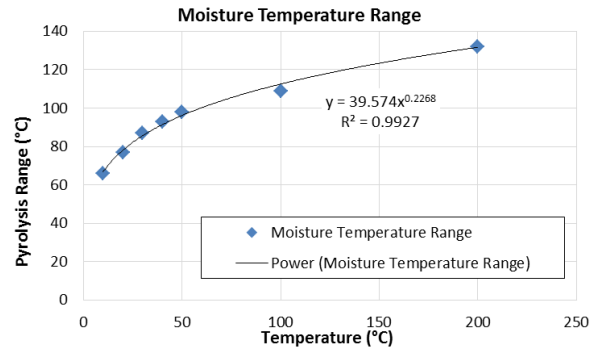
(c) Wool reference temperature



(d) Moisture reference temperature



(e) Wool reference range



(f) Moisture reference range

Figure 4.28: Kinetic parameters for wool and moisture

4.3.4 HoR of Wool

In Figure 4.29, a typical heat flow/unit mass vs temperature profile for wool is shown. Here the first peak represents the moisture evaporation which is clearly observed. However the peaks representing the wool pyrolysis are not as clear as those obtained for cotton. Upon closer observation of the heat flow data obtained from the DSC tests (Figure 4.26), it appears that the heat flows occur over a broad range of temperatures.

These ranges also correspond to the pyrolysis peak in the DTG profiles (Figure 4.25). Therefore the selected area under the curve in Figure 4.29 appears to adequately represent the ΔH_{DSC} and the HoR was subsequently calculated as per Section 3.3.4.

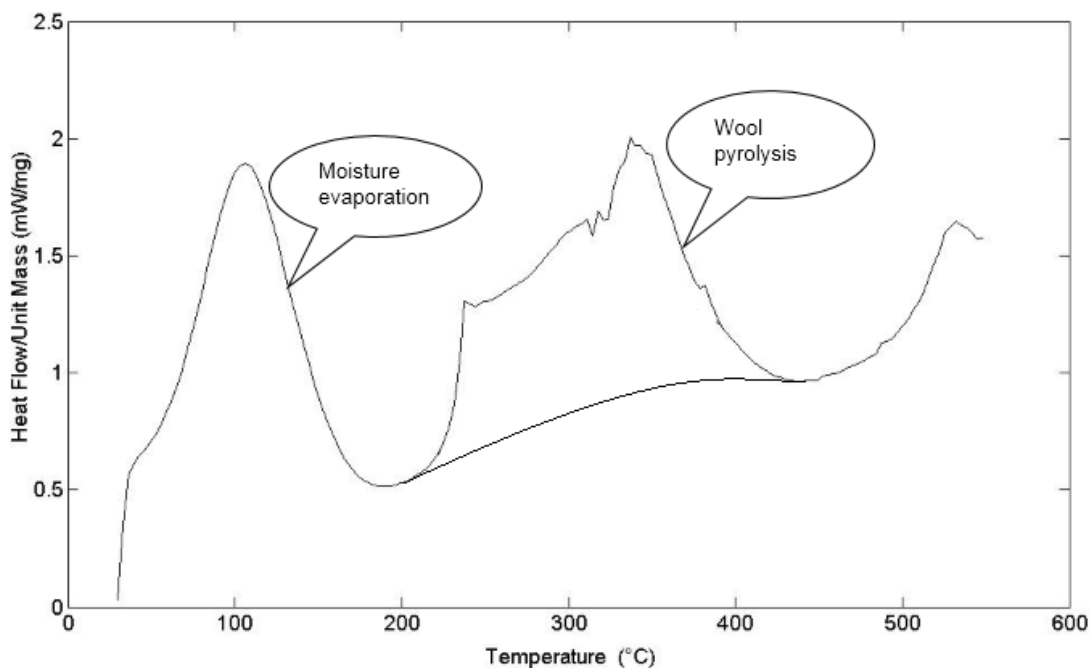


Figure 4.29: DSC/TGA temperature matched heat flow/mass for wool (20 K/min)

The HoR for wool as a function of heating rate presented in Figure 4.27 (d) shows an increasing trend with respect to heating rate with a very strong linear relationship resulting from the regression analysis. A summary of the trend and strength of the relationships for all parameters with temperature is presented in Table 4.6. In general, all kinetic parameters for wool show an increasing trend with increasing heating rates.

For cotton, and excluding char volatilization, the yield of solid residue (n_s) and initial mass fraction ($Y(0)$) appear to be constant with respect to heating rate (see TG plots in Figures 4.13 and 4.16). For wool, it appears that $Y(0)$ is independent of heating rate (see Figure 4.24), however, values for n_s cannot be clearly extracted, especially at low heating rates. Combining the data obtained using the Mettler TGA (see [Appendix A](#)), a generalized average value of n_s was determined and these values are given in Table 4.7.

Table 4.6: Summary of all kinetic parameters and *HoR* trends of wool and moisture

<i>Material</i> <i>Parameter</i>	<i>Wool</i>		<i>Moisture</i>	
	<i>Trend</i>	<i>Strength</i>	<i>Trend</i>	<i>Strength</i>
<i>Log (A)</i>	Power (decreasing)	Strong (R ² =0.94)	Logarithmic (increasing)	Fairly strong (R ² =0.59)
<i>E</i>	Power (decreasing)	Strong (R ² =0.96)	Logarithmic (increasing)	Fairly strong (R ² =0.63)
<i>n</i>	Power (decreasing)	Strong (R ² =0.96)	Logarithmic (increasing)	Very strong (R ² =0.86)
<i>reaction rate</i>	Power (increasing)	Very strong (R ² =0.89)	Power (decreasing)	Very strong (R ² =0.97)
<i>reference temperature</i>	Power (increasing)	Very strong (R ² =0.87)	Power (increasing)	Very strong (R ² =0.99)
<i>pyrolysis range</i>	Power (increasing)	Very strong (R ² =0.95)	Power (increasing)	Very strong (R ² =1.0)
<i>HoR</i>	Linear (increasing)	Strong (R ² =0.91)	260.2kJ/kg (average)	54.0kJ/kg (standard deviation)

Table 4.7: Yield of solid residue and initial mass fraction for fabrics

<i>Material</i>	<i>Properties</i>	<i>Value</i>
Cotton	Yield of solid residue	0.143
	Initial mass fraction	0.985*
Wool	Yield of solid residue	0.275
	Initial mass fraction	0.945*

* depending on moisture content

4.3.5 Heating Rate Effects

It is known that changes in heating rates can have a significant effect on the pyrolysis process (Wakelyn et al. 2006, Cao et al. 2010). From the DTG conversion rate profiles presented in Figure 4.14 and Figure 4.25, it is evident that as the heating rates increases, the curve is also shifted to a higher temperature. A similar trend is also observed in the heat flow profile, where the heat flow also increases as the heating rate is increased. The DSC profiles also show that the peak curve shifts to higher temperatures as the heating rate increases (see Figure 4.15 and Figure 4.26) and this phenomenon is discussed in Section 4.1.2.

4.4 Summary

In this chapter, the pyrolysis parameters of four materials were obtained experimentally, analysed and characterized in order to parameterize the FDS pyrolysis model variables. Significant variations in the obtained parameter values with respect to heating rate were observed and it can be suggested that this variation may be due to differences in the physical and chemical properties of each material which is even more complex for charring materials. As a non-charring polymer, PMMA physically undergoes glass transition and melting when exposed to heat. For charring materials, the char development process takes place when the material is exposed to higher temperatures. The variation of *HoR* with heating rates can be explained by the likelihood that a sample has less residence time for undergoing a volatilisation process at any particular temperature at higher heating rates. As a result, the volatiles are formed when the sample has reached higher temperature and therefore more heat flow is needed to assist this process at higher heating rates. These variations will be discussed in the Numerical Simulation chapter (CHAPTER 7). In the next chapter, a discussion of the parameterization of the FDS combustion model is presented.

CHAPTER 5

COMBUSTION MODEL PARAMETERIZATION

5.1 Introduction

The parameterization of the combustion model requires a detailed evaluation of properties such as: (i) the chemical composition of the combustible material through ultimate analysis; (ii) the yield of basic combustion products (i.e. CO, CO₂ and soot) and the heat of combustion via cone calorimetry; and (iii) the yield of other combustion products (i.e. those containing nitrogen, chlorine etc.). The latter is more suitable for complex materials and can be measured using Fourier-transform infrared (FTIR) spectroscopy (Fang et al. 2006, Gao et al. 2013). However, in this study, the materials selected are not overly complex with well characterized chemical compositions as shown in Table 5.1. As such, techniques such as FTIR spectroscopy are not essential for these analyses. In this chapter the parameterization of the more essential FDS combustion model variables as studied using the cone calorimeter is presented.

Table 5.1: Chemical composition of studied materials

Element (%)	Pine*	PMMA ⁺	Cotton [#]	Wool [~]
Carbon	54.9	59.1	40.7	50.5
Hydrogen	5.8	7.9	5.6	6.8
Oxygen	39.0	31.9	45.2	22.0
Nitrogen	0.2	<0.3		16.5
Others	0.1 (S)	<0.2 (S) 0.1 (Cl) 0.6 (H ₂ O)	~8.5 (N, ash, H ₂ O)	3.7 (S) 0.5 (ash)
Carbon to oxygen ratio	1.4	1.8	0.9	2.3

* (Ragland, Aerts & Baker 1991)

⁺ (Luche et al. 2011)

[#] (Moriani et al. 2014)

[~] (Bauer, Garbe & Surburg 1988)

The four materials in the current study were tested using a range of irradiance levels (i.e. 20 to 75 kW/m²) in accordance with the AS/NZS 3837 (1998) test protocol using a cone calorimeter. For each material, the HRR, MLR, SEA, CO, CO₂ are presented at

various heat flux levels and in addition, the char fraction of the charring materials is also analysed. The HRR is an important parameter as it influences the temperature and the spread of the fire (Mouritz, Mathys & Gibson 2006) and is also an important consideration when assessing fire hazards (Babrauskas & Peacock 1992). The MLR is also a significant consideration when studying the fire behaviour of a material. For example, a higher MLR indicates that the tested material can be readily pyrolysed resulting in more rapid flame spreading, thus increasing the fire risk. From the HRR and MLR, a very important combustion model parameter, the effective heat of combustion (EHoC) can be derived where $EHoC = HRR/MLR$.

The SEA describes the amount of smoke being produced per unit mass of the burning sample. For combustible materials, incomplete combustion releases CO and CO₂ whereas complete combustion releases CO₂. Both the CO and CO₂ yields are important parameters used to assess fire hazards in addition to the HRR and MLR. The variation of these properties at various heat fluxes is also presented in this chapter along with an evaluation of the relationships among the different variables.

5.2 PMMA Combustion Parameters

Initially, experiments using PMMA were conducted at the lowest heat flux of 10kW/m² but during the measurements, no flame was observed after 10 minutes and the test was abandoned in accordance with the AS/NZS 3837 (1998) test protocol. Subsequent tests using PMMA samples were conducted at higher heat fluxes over the range of 20 to 75kW/m².

5.2.1 Heat Release Rate

The HRR curves for PMMA are presented in Figure 5.1 at various external heat fluxes with the individual curve shown in this figure the average curve of multiple tests at each irradiance. The shape of the HRR curve observed for PMMA is similar to that described by Harper (2004) who tested a relatively thick sample of the non-charring polymer. A steady burning was reported for all PMMA samples and a bubbling phenomenon occurred as a result of the breakdown of PMMA molecular bonds during exposure to high temperatures with the releasing gasses causing the bubbles (Steinhaus 1999). During this stage in the present study, the flame was fully developed and this finding is in accordance with a similar study conducted by Zeng, Li and Chow (2002). Their study

also indicated that the steady state burning of PMMA may be due to the large thermal capacity of the material (Zeng, Li & Chow 2002).

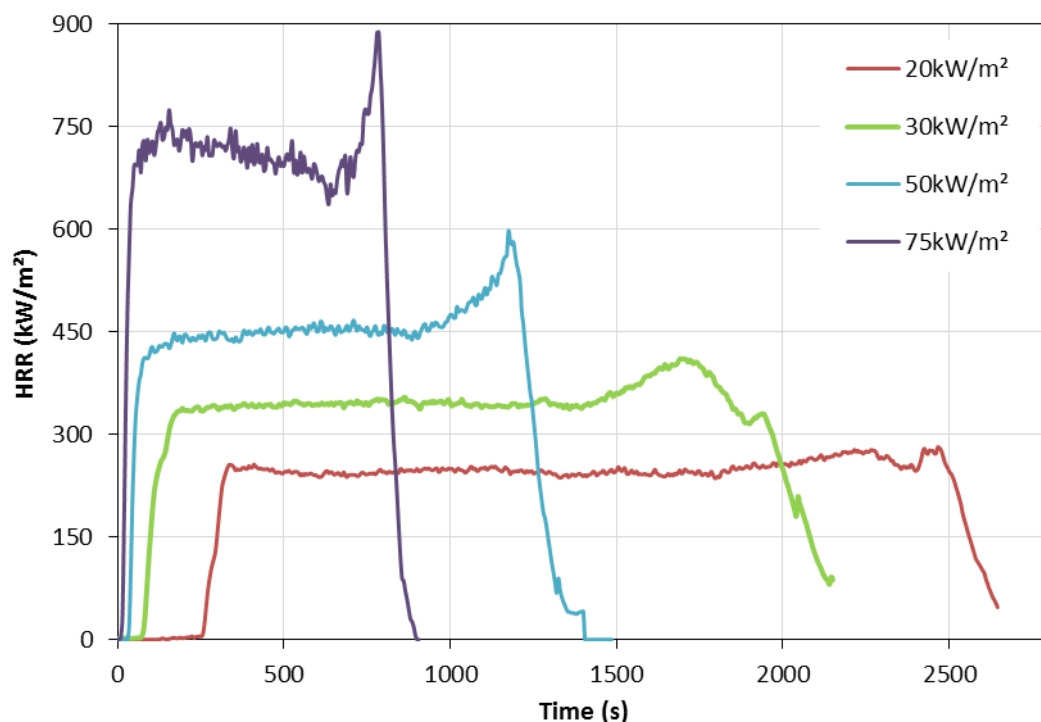


Figure 5.1: Average HRR for PMMA at various heat fluxes

A second peak in the HRR curve is observed at the end of the test and this is also reported in a number of other studies (Shi 2014, Tewarson 2002, Babrauskas, Twilley & Parker 1992). Brown, Braun and Twilley (1988) reported that this was a result of the thermal wave reaching the lower surface of the sample with a subsequent increase in the bulk temperature due to the small amount of the remaining sample. In another study, Babrauskas, Twilley and Parker (1992) proposed that this is due to a surface tension phenomenon.

Fundamentally, PMMA is a non-charring polymer that leaves little or no residue after burnout and this is in agreement with the findings of Luche et al. (2011) and Spearpoint and Quintere (2000). Shi (2014) suggested that the HRR of non-charring polymers is sensitive to thickness and heat flux and also reported similar findings in relation to heat flux variation discussed in the present work. However, it should be noted that the effect of sample thickness is outside of the scope of this study.

A rapid increase in the HRR immediately after ignition is observed for the PMMA sample tested at 75 kW/m², whereas the ignition time for the other heat fluxes varied between 30 and 250 seconds. Moreover, a greater heat exposure results in a higher HRR and this observation is consistent with the result obtained by Linteris et al. (2005). According to Shi (2014), the HRR of non-charring polymers varies with heat flux due to the increment in pyrolysis rate as the heat flux increases and more heat is absorbed. This HRR result of PMMA in the current study will be used as the benchmark for non-charring materials to validate the FDS after characterizing the remaining fire properties for the coupled pyrolysis and combustion model.

5.2.2 Mass Loss Rate

The MLR as a function of time at different heat flux values is shown in Figure 5.2 and similar to the HRR, the MLR of PMMA increases with increasing heat flux. This is also discussed by Shi (2014) who proposed that a non-charring polymer may be considered to be a pool fire that melts at a specific temperature, which is approximately 160°C for PMMA (Smith & Hashemi 2006).

The MLR curve shows a pattern similar to the curve of HRR at the corresponding heat flux which suggests that the MLR also achieves a steady state after ignition. This phenomenon is again observed at all heat flux levels. This has been observed by Jiang (2006) who described that HRR and MLR curves are similar for thick materials. An increase in MLR may also indicate that the burning period is shorter (Luche et al. 2011) and consequently, the MLR increases with an increase in the heat flux. The peak MLR is identified towards the end of each test and this is explained in the previous discussion of the HRR curves.

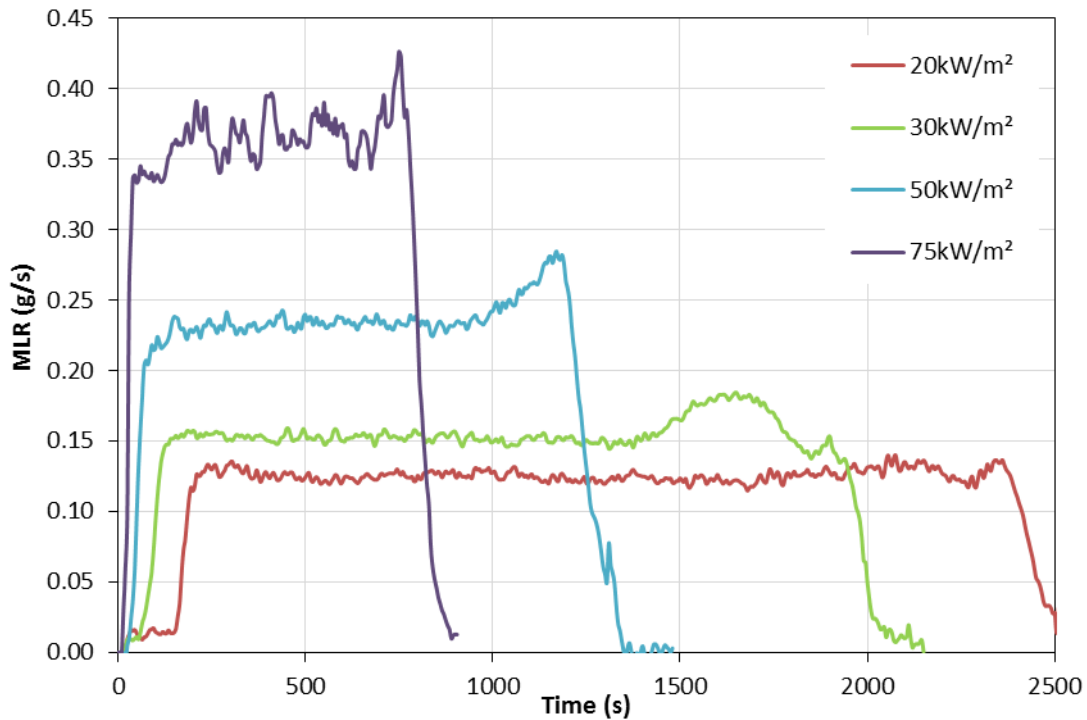


Figure 5.2: Average MLR of PMMA at various heat fluxes

5.2.3 Specific Extinction Area

Figure 5.3 illustrates the effect of heat flux on the SEA ratio and in all profiles the SEA curve shows a relatively steady phase throughout the burning period. Unlike the HRR and MLR, the SEA is somewhat constant through this steady phase across all heat fluxes and is slightly lower at 20 kW/m² irradiance. During the experiments, it was observed that quite a significant amount of smoke was released when burning the PMMA samples. Mouritz, Mathys and Gibson (2006) suggested that there is a strong relationship between HRR and SEA for fibre reinforced polymers (FRPs) and reported that this may be due to the endothermic decomposition which determines the amount of heat and smoke released. However, the result of the present study has shown that the heat flux and hence the HRR has little effect on SEA.

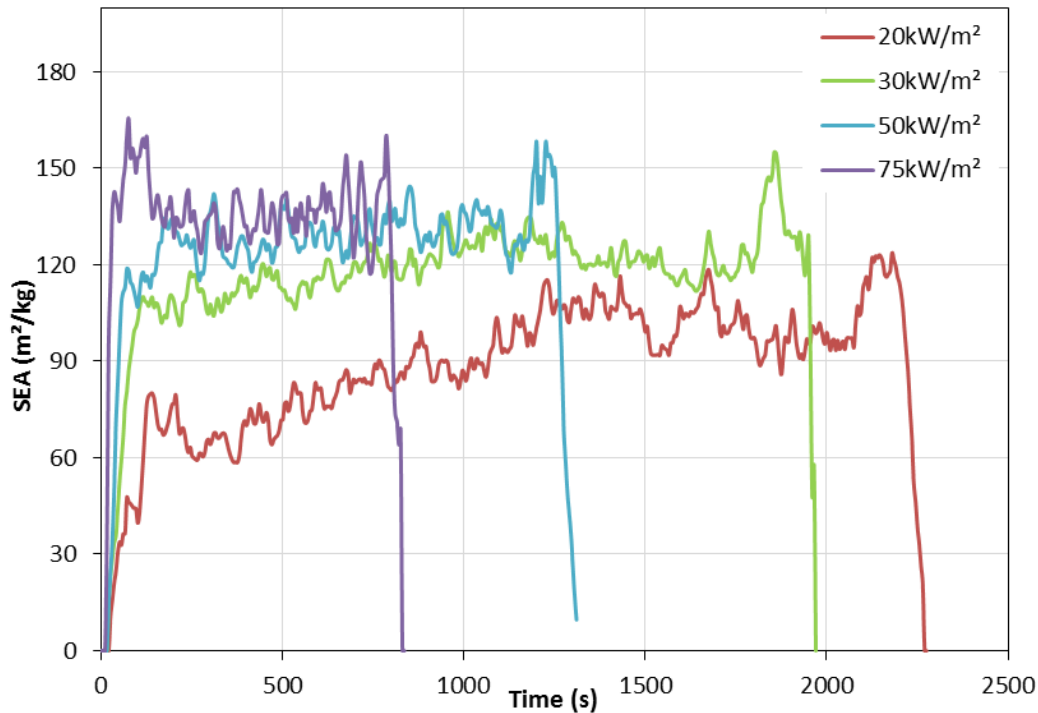


Figure 5.3: Comparison of SEA of PMMA at various heat fluxes

5.2.4 CO and CO₂ Yield

Figure 5.4 presents the CO yield as a function of time for the different heat fluxes during combustion of PMMA. The results show that, similar to the SEA, the CO is released over a steady phase until a peak occurs near the end of the test. Moreover, the CO yield increases as the heat flux is increased. In Figure 5.5, the CO₂ yield as a function of time for the combustion of PMMA is presented. In general, a steady state is observed with change for all heat fluxes with the exception of the 75 kW/m² irradiance where a slightly decreasing trend with burning period is observed. From Figure 5.5, it may be suggested that there is an increase in the production of CO₂ with the increasing of the heat flux. The average CO yield at 50kW/m² is 0.009 kg/kg and this is close to the value of 0.0098 kg/kg found in (Nelson & Jayakody 1998). Additionally, their recorded value for CO₂ yield is 1.64 kg/kg and the current study is 2.091 kg/kg. The CO and CO₂ release and yield from combustible products is believed to be related to the heat release rate properties as suggested by Babrauskas and Peacock (1992). This may explain the similar trends observed in Figures 5.4 and 5.5 although the CO₂ yield is observed to have less dependency on the HRR in comparison to the CO yield.

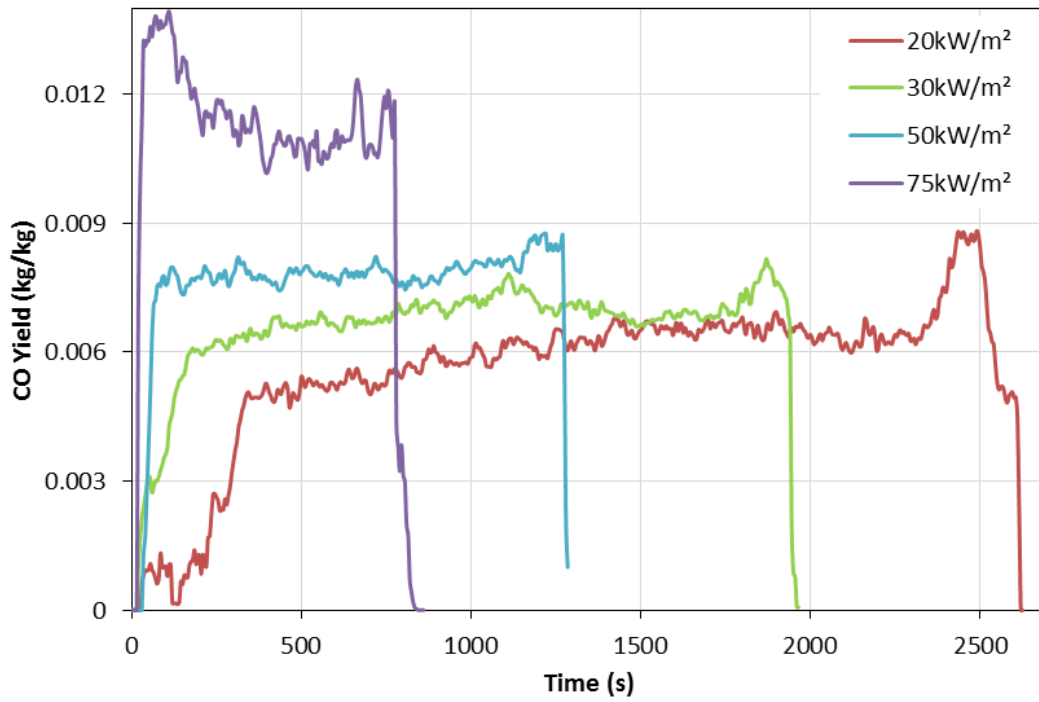


Figure 5.4: CO yield of PMMA at various heat fluxes

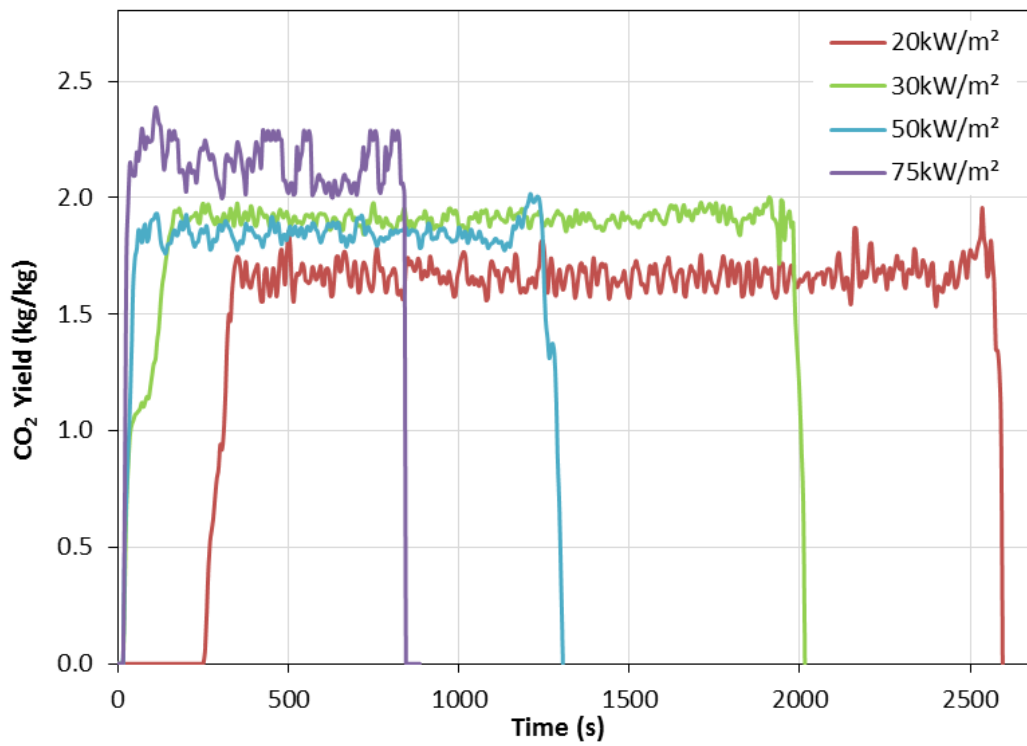
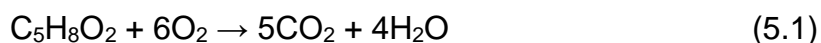


Figure 5.5: CO₂ yield of PMMA at various heat fluxes

The combustion of a single unit of PMMA under an oxygen environment follows:



Theoretically, for the combustion of 1 kg of PMMA, 2.2 kg of CO₂ will be evolved under these conditions (Wilson Jr et al. 2006) . Figure 5.5 shows that at 75 kW/m² heat flux approximately this amount of CO₂ is evolved. At other heat fluxes, the CO₂ yield is lower suggesting that other products are evolving in addition to CO₂.

Overall, the results show that for PMMA, the HRR, MLR, and CO yield is strongly dependent on the heat flux level. As expected for these parameters, the more heat that the PMMA is exposed to, the higher HRR, MLR and CO yield is obtained. Conversely, the SEA and CO₂ yield are nominally dependent and it is also observed that the yield of CO₂ is higher than that of CO indicating complete burning of PMMA dominates.

5.2.5 Correlation of Parameters

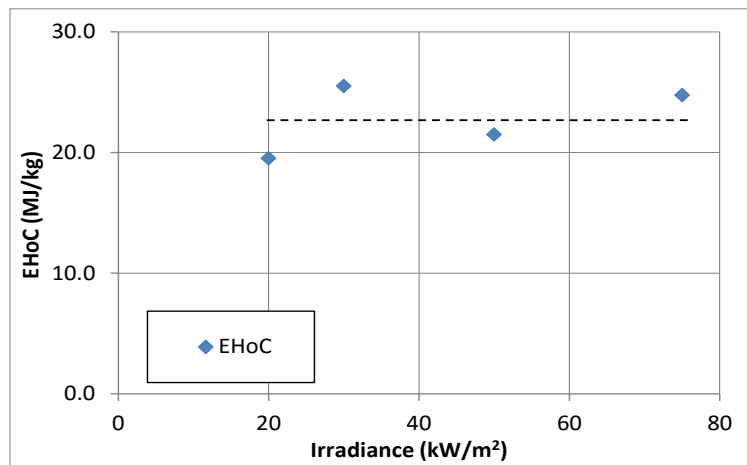
The cone calorimeter software provides averaged values of EHoC (or HRR/MLR), SEA, CO yield and CO₂ yield for six minutes after ignition. The soot yield is converted from the SEA by dividing with a constant value of 8700 (Mulholland & Croarkin 2000). From this software, the average values of EHoC, CO yield and soot yield as functions of heat fluxes for PMMA are presented in Figure 5.6. The average and standard deviations of EHoC are 22.79 and 2.8 MJ/kg respectively; whereas for CO₂ yield they are 1.97 and 0.2 kg/kg respectively. It should also be noted that the average and standard deviation values of EHoC in the current study are reasonably close to the value of 24.0 MJ/kg reported for 50 kW/m² in the study conducted by Nelson and Jayakody (1998).

Through regression analysis for the CO and soot yield of PMMA, a number of empirical formulae were obtained and are presented in the equations below:

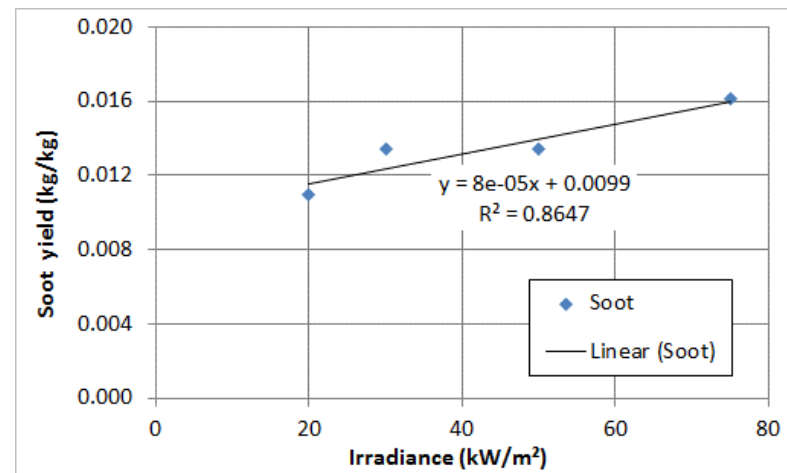
$$\text{CO yield} = 9E - 05(\dot{q}'') + 0.0044 \quad (5.2)$$

$$\text{soot yield} = 8E - 05(\dot{q}'') + 0.0099 \quad (5.3)$$

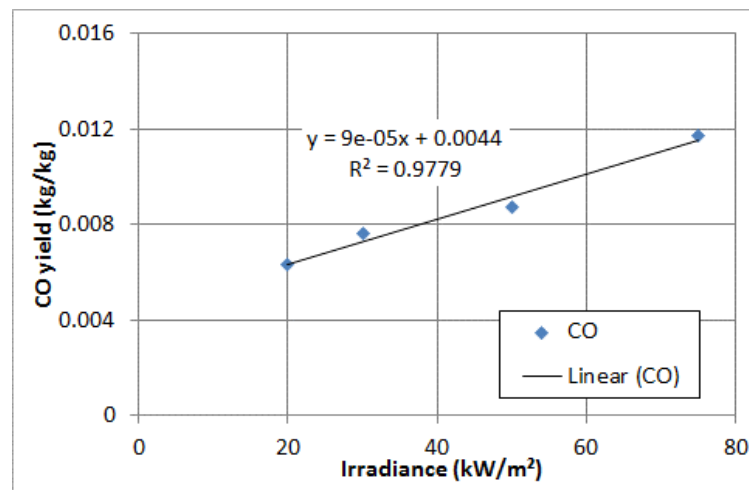
where \dot{q}'' represent the heat flux in kW/m². As shown in the Figure 5.6, the above equations show linear correlations.



(a) Effective heat of combustion



(b) Soot yield



(c) CO yield

Figure 5.6: Variation of combustion parameters of PMMA with respect to heat flux

5.3 Pine Combustion Parameters

5.3.1 Heat Release Rate

The heat release rate curves for pine are shown in Figure 5.7 at various external heat fluxes. During the pyrolysis phase, volatile gases are being released and when the sample area is exposed to sufficient amount of heat and fuel, the sample ignites. During this phase, a char has started to develop and this continues throughout the test. The critical heat flux is defined as the minimum heat flux that is required to cause ignition, and below which ignition cannot occur (Janssens 2003, Delichatsios, Paroz & Bhargava 2003). For charring materials, the critical heat flux has been reported to be over the range of 15 and 20 kW/m² (Delichatsios, Paroz & Bhargava 2003). In the present study, the pine sample was first tested at a heat flux of 10 kW/m² however ignition did not occur. At the next heat flux of 20kW/m², ignition occurred before 200 seconds but in this case, the sample only burned for approximately 600 seconds and then flameout was observed. This may have been due to the insufficient amount of heat flux to sustain pyrolysis.

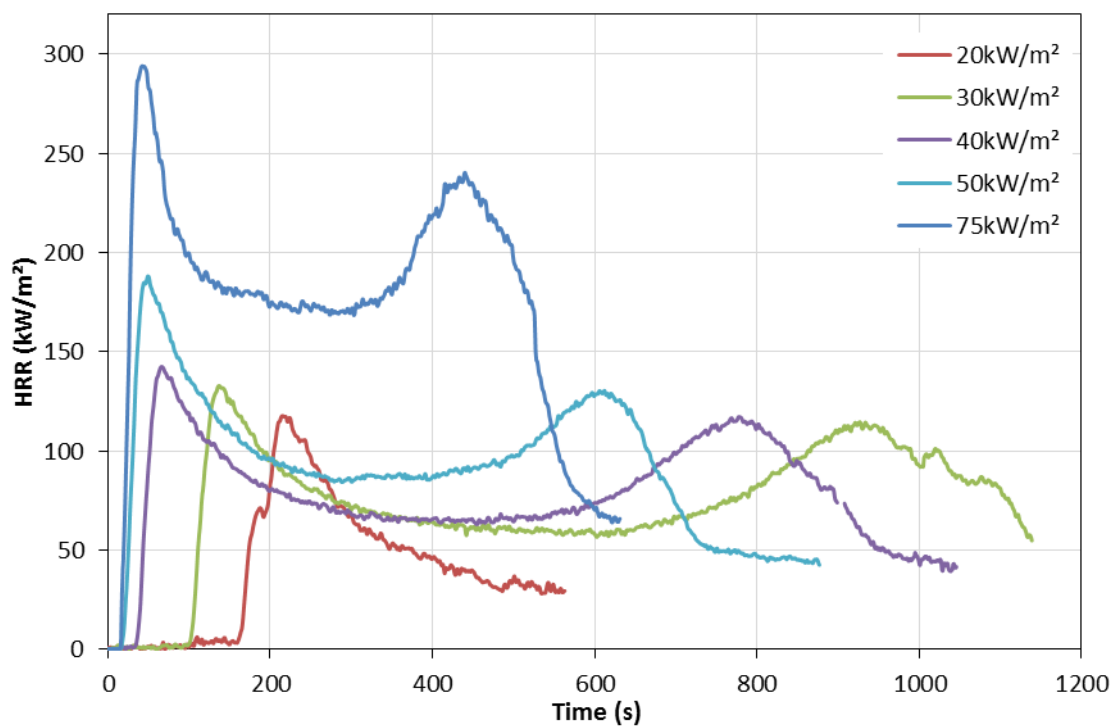


Figure 5.7: Average HRR of pine at various heat fluxes

Conversely, a sharp rise is observed with the first 20 seconds for the sample exposed to the highest heat flux of 75 kW/m². The HRR then reaches a quasi-steady phase which normally occurs for thick wood samples as reported by Tran (1992). A second peak prominently occurs towards the end of the test with theories explaining this observation reported by Brown, Braun and Twilley (1988) and Babrauskas, Twilley and Parker (1992) as discussed previously in Section 5.2.1. This phenomenon was also observed by Tran (1992) who suggested that as the charring process continues, the HRR increases due to an increased developing charring layer. In the current study, after the flameout of pine, the sample was not completely combusted and a char residue remained for all irradiances.

In summary, it can be concluded that the heat flux has a significant effect on the HRR of pine where higher heat fluxes on the surface, the higher the HRR is observed. For validation of the FDS model, the HRR results of pine will be used to benchmark charring materials after parameterization of the coupled pyrolysis and combustion models.

5.3.2 Mass Loss Rate

The MLR of pine presented in Figure 5.8 shows that at 20 kW/m² heat flux, a quasi-steady state is reached after 200 seconds. Prior to 100 seconds, the MLR is very low and this may be explained by the effects of the release of moisture and pyrolysis of inert gases before the ignition occurs, at approximately 160 seconds, as reported by Jiang (2006). It was also stated that a slowing of the MLR occurs as the char layer is forming, and this interferes with the heat and mass transfer until pyrolysis occurs and the moisture release increases due to the increasing surface temperature. As the heat flux is increased, the higher surface temperature of the sample promotes the speed of the heat and mass transfer as well as the pyrolysis. An early peak in MLR curves (similar to HRR curves in Fig 5.7) can be seen in 40, 50 and 75 kW/m² which indicates that the maximum mass loss occurs at an earlier stage when higher heat fluxes are used. Unlike HRR curves the second peak is not prominent in MLR curves at 30, 40 and 50 kW/m², rather a quasi-steady state is observed after 200 sec. However, in the MLR curve at 75 kW/m², a clear second peak (and in between two peaks a quasi-steady period) is observed. From all the tests performed at various heat fluxes, it can be suggested that the MLR of pine is directly influenced by the heat exposed to the sample in that the MLR increases as the heat flux is increased.

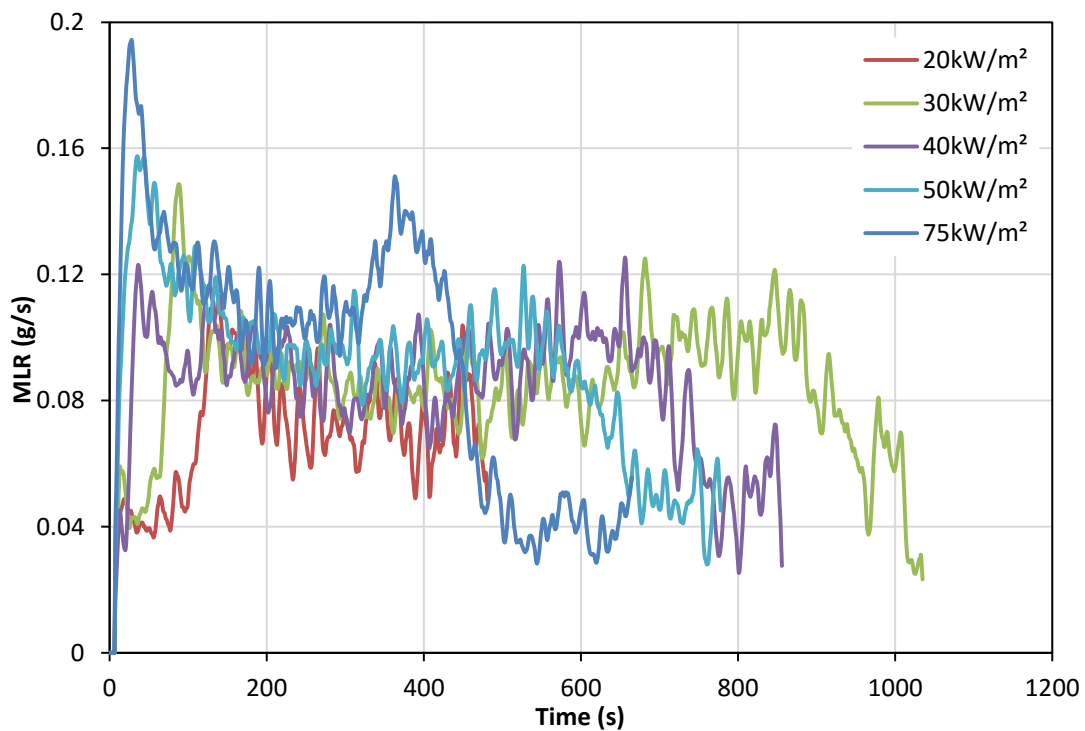


Figure 5.8: Average MLR of pine at various heat fluxes

5.3.3 Specific Extinction Area

The SEA of pine is presented in Figure 5.9 at all heat fluxes tested from 20 to 75 kW/m². With the exception of the 75 kW/m² very little variation in SEA is observed between the heat fluxes, especially between 30 and 800 sec. A consistent rise in the SEA curve is observed at 20 kW/m² prior to the ignition occurred. This can be explained by the fact that a significant amount of smoke that is produced during moisture evaporation and pyrolysis of inert gases. Second peaks are more prominent in 50 and 75 kW/m² curves. The first peak in SEA curves may be attributed to the pyrolysis process where the gaseous products were released (Mulholland 1995) whereas the latter may be to the smouldering of char residue as flaming ceased (Janssens & Douglas 2004). The average SEAs (over six minutes) at 20, 30, 40 and 75 kW/m² are 52.6, 38.23, 38.02 and 177.02 m²/kg respectively, implying that there may not be clear trend in the SEA relative to heat flux.

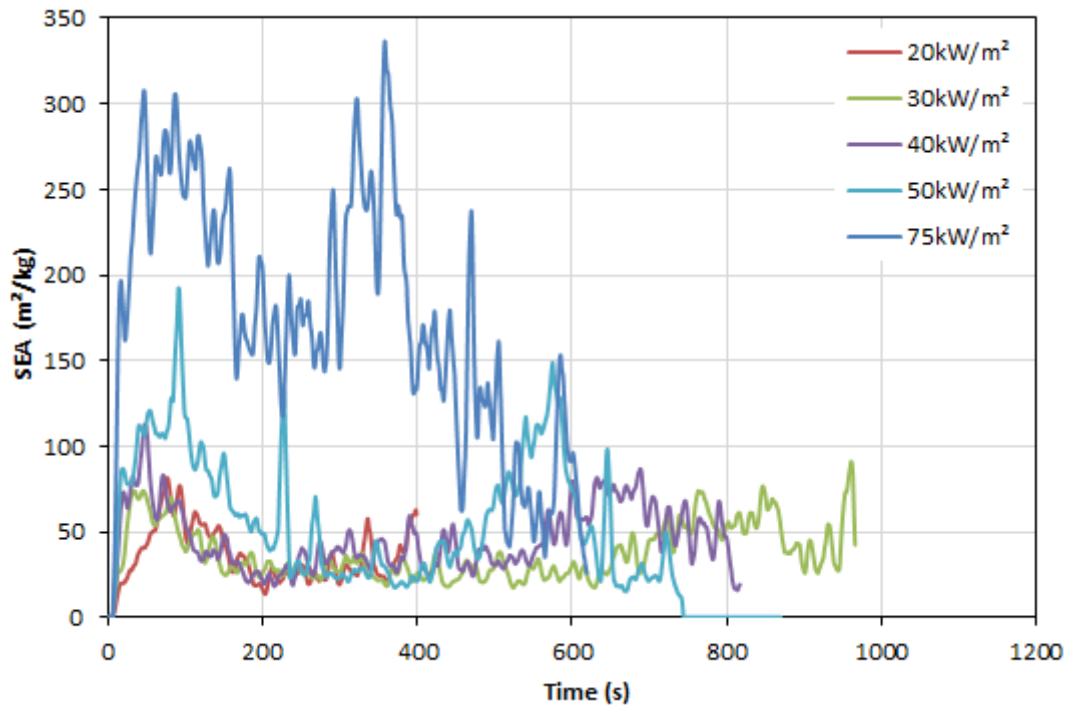


Figure 5.9: Comparison of SEA of pine at various heat fluxes

5.3.4 CO and CO₂ Yield

Figure 5.10 shows the CO yield of pine at the various heat flux levels and from this figure, it is evident that a sharp peak in the CO release occurs towards the end of each test. Jiang (2006) reported that this phenomenon is believed to be caused by the incomplete material combustion which is commonly observed in the combustion of timber by the time the virgin material is significantly burned out. The CO₂ yield of the pine is illustrated in Figure 5.11 at various heat fluxes and it appears that a low CO₂ yield occurs at 40 and 50 kW/m², whereas a higher yield is observed at 20, 30 and 75 kW/m². Similar to the SEA, there is no apparent trend in the CO₂ yield with respect to changing heat flux.

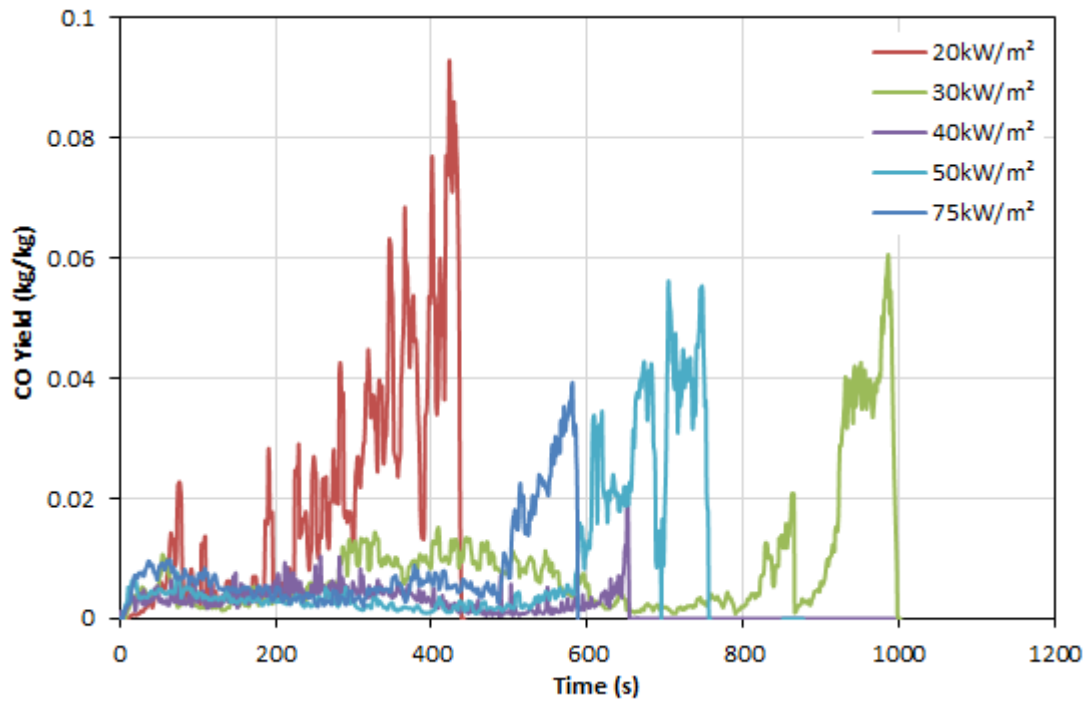


Figure 5.10: CO yield of pine at various heat fluxes

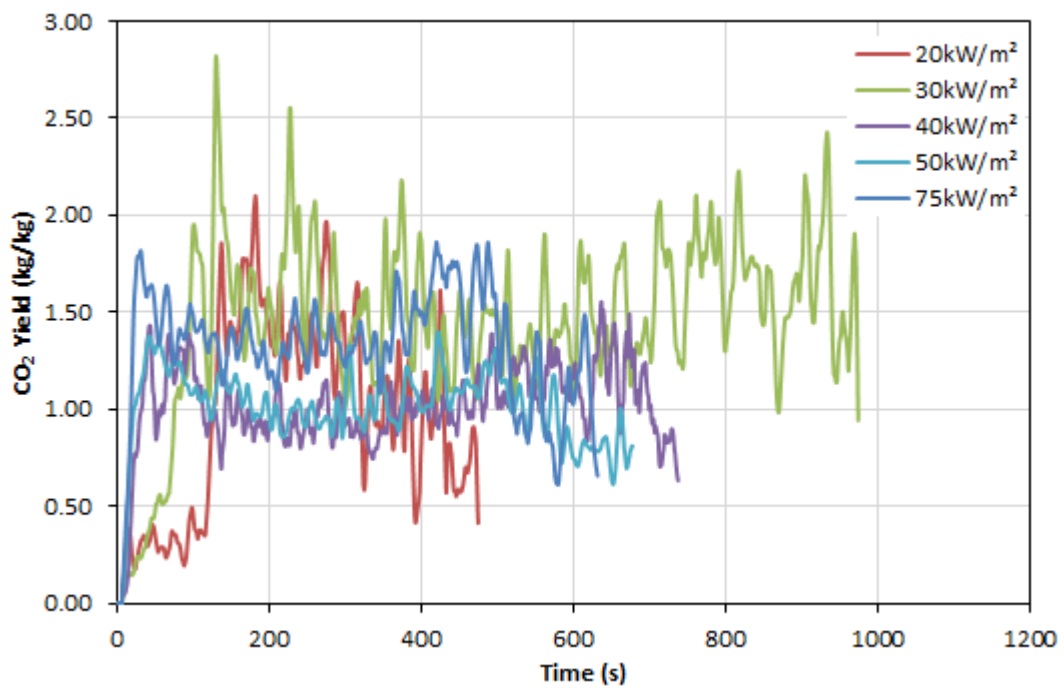


Figure 5.11: CO₂ yield of pine at various heat fluxes

5.3.5 Char residue

Charring materials produce gaseous vapours, tars and a solid residue, or char, when heated (Lowden & Hull 2013). For these materials, the char yield / char residue is an important parameter to the model pyrolysis processes. From the previous experiments using TG analysis, one set of char yield data was obtained (see CHAPTER 4). Although the TG experiments are essential for modelling mg scale experiments, it is uncertain whether the same data is applicable for much larger samples such as those tested by cone calorimetry (in oxidizing environment) which may be more representative of real life samples such as furniture and building components. This is the subject of the sensitivity study presented later in CHAPTER 7.

This char residue data is derived using:

$$\text{char residue} = \frac{W_{fc}}{W_{ic} \times (1 - MC)} \quad (5.4)$$

where, W_{fc} and W_{ic} are the final mass and initial mass of the sample in the cone calorimeter experiment respectively, and MC is the moisture content obtained from the TGA experiment.

Figure 5.12(c) shows the trend of char residue as a function of heat flux for pine. For the sample tested at 20 kW/m², complete burning was not achieved so this heat flux is not considered here. For this sample, only a small area of the top layer was charred while the bottom layer of the sample was still original virgin pine. From Figure 5.12(c), it is evident that the char residue increases linearly with the incident heat flux.

5.3.6 Correlation of Parameters

Significant variations in parameter values for each heat flux are observed. The values of EHoC, soot yield and CO₂ yield are averaged for the same period as PMMA. These are presented in Figure 5.12 along with char residue as a function of heat flux. These values are the averaged values obtained from multiple measurements at each heat flux level. Through regression analysis of these variables, a number of empirical formulae were obtained for pine and these are presented in the equations below:

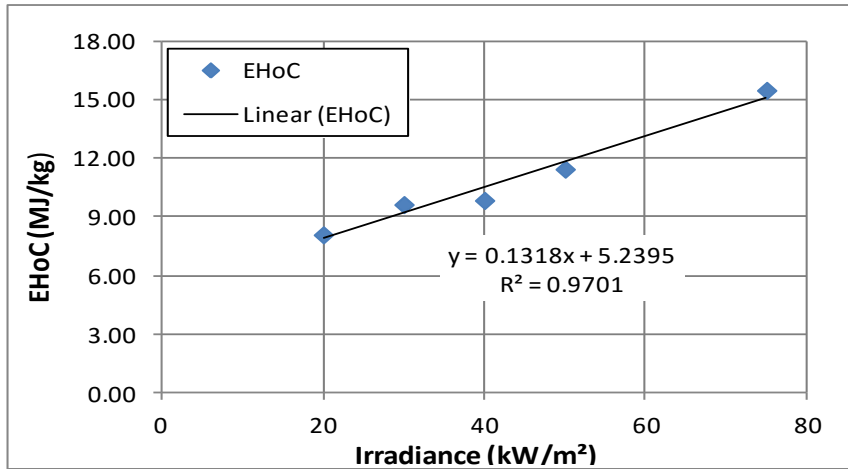
$$EHoC = 0.1318 (q'') + 5.2395 \quad (5.5)$$

$$Soot Yield = 0.0003 (q'') - 0.0034 \quad (5.6)$$

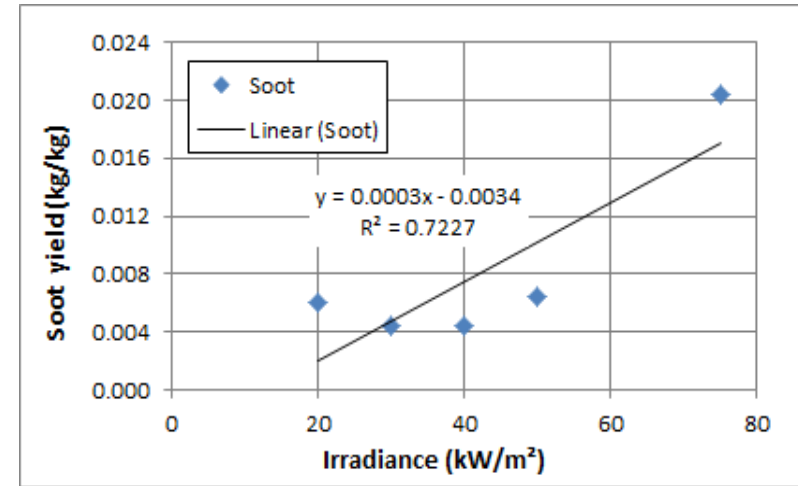
$$CO_2 = 0.0035(q'') + 0.9527 \quad (5.7)$$

$$Char residue = 0.0951(q'') + 7.8076 \quad (5.8)$$

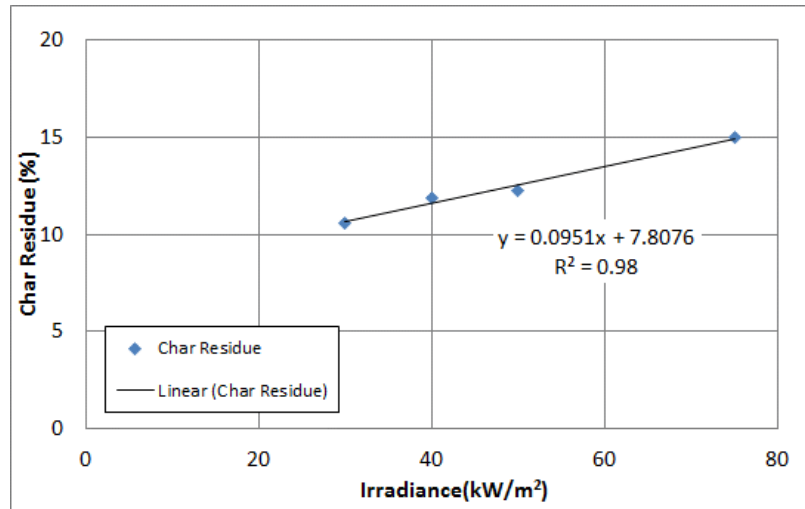
Linear correlations were obtained for all of these parameters with strong correlations observed for the EHoC, soot yield, char residue and CO₂ yield. The average EHoC measured at 50 kW/m² obtained in this study, 11.21 MJ/kg, is close to study conducted in (Park 2014) where a value of 12.94 MJ/kg was obtained. The same author reported the CO₂ yield of the same study at 1.39 kg/kg which compares reasonably well to that of the current study of 1.14 kg/kg. In addition, a CO yield of 0.019 kg/kg was reported with a comparative value in the current study of 0.007 kg/kg. It should be noted that there are numerous pine species across the world and comparisons should be made with this in mind.



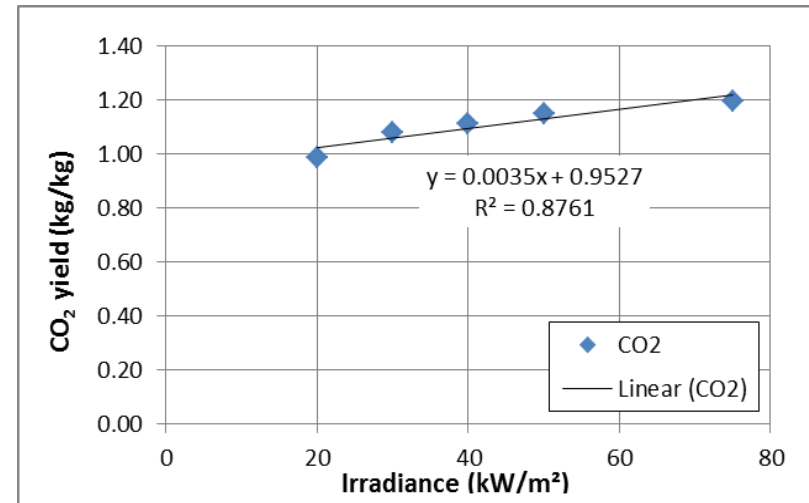
a) *Effective heat of combustion*



b) *Soot yield*



c) *Char residue*



d) *CO₂ yield*

Figure 5.12: Variation of combustion parameters of pine with respect to heat flux

5.4 Cotton Combustion Parameters

5.4.1 Heat Release Rate

The HRR curves of cotton are shown in Figure 5.13 at various external heat fluxes from 30 to 75 kW/m². Initially, the sample was tested at 10 kW/m² but due to the poor repeatability, this heat flux was excluded. According to Chen (2001), the critical heat flux for cotton is approximately 6 kW/m², however from the results of the present study, heat fluxes lower than 30 kW/m² commonly result in very poor reproducibility. Therefore, cotton samples were tested at a minimum of 30 kW/m² in this work which has shown good repeatability. From the results, only one peak occurs during the test and the HRR then decreases until the flameout. The peak value of the HRR is not influenced by the external heat flux at higher heat fluxes, however the time at which the peak occurs does vary with the heat flux. Of all the samples studied, cotton has the lowest burning time due to its thickness and comparatively low density.

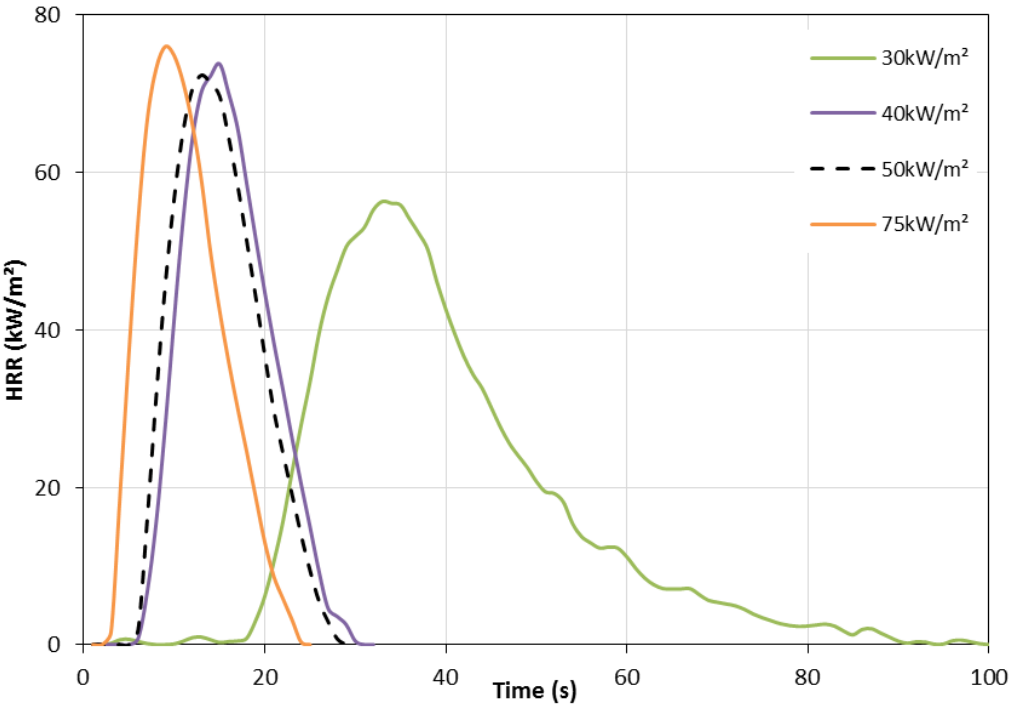


Figure 5.13: Average HRR of cotton at various heat fluxes

5.4.2 CO and CO₂ Yield

The CO and CO₂ yields of cotton are presented at various heat fluxes in Figure 5.14 and Figure 5.15 respectively. A higher CO yield is observed at the middle of the burning period as depicted by a bell shaped trend and it appears that the CO yield decreases with the increase of heat flux. For the CO₂ yield, no apparent trend in the yield with heat flux is observed and thus, the CO₂ yield has less dependency on the irradiance than the CO yield.

5.4.3 Correlation of Parameters

The average values of EHoC and CO₂ yield obtained from the cone calorimeter software along with char residue for cotton are presented in Figure 5.16. Through regression analysis of these parameters, a number of empirical formulae were obtained and are presented in the equations below.

$$EHoC = 10.798e^{-0.011(q''')} \quad (5.9)$$

$$CO_2 = -0.007(\dot{q}'') + 1.4548 \quad (5.10)$$

A linear correlation is obtained with a relatively good fit for the CO₂ yield. For the CO yield, the mean and standard deviation are 0.013 and 0.0022 kg/kg respectively and the average soot yield is 0.022 kg/kg with a standard deviation of 0.003 kg/kg and no significant trend is observed. This may be due to the tested cotton that is low in mass.

Comprehensive MLR and SEA results of cotton burning are not presented here as they did not show any significant trends with heat flux, however the data are presented in detail in [Appendix B](#).

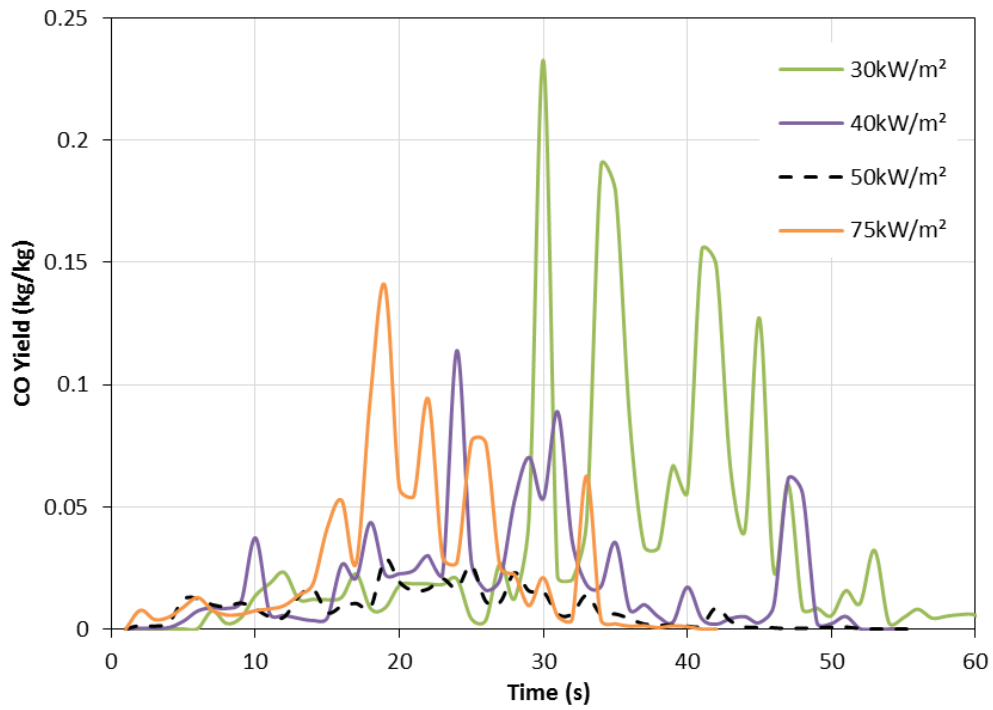


Figure 5.14: CO yield of cotton at various heat fluxes

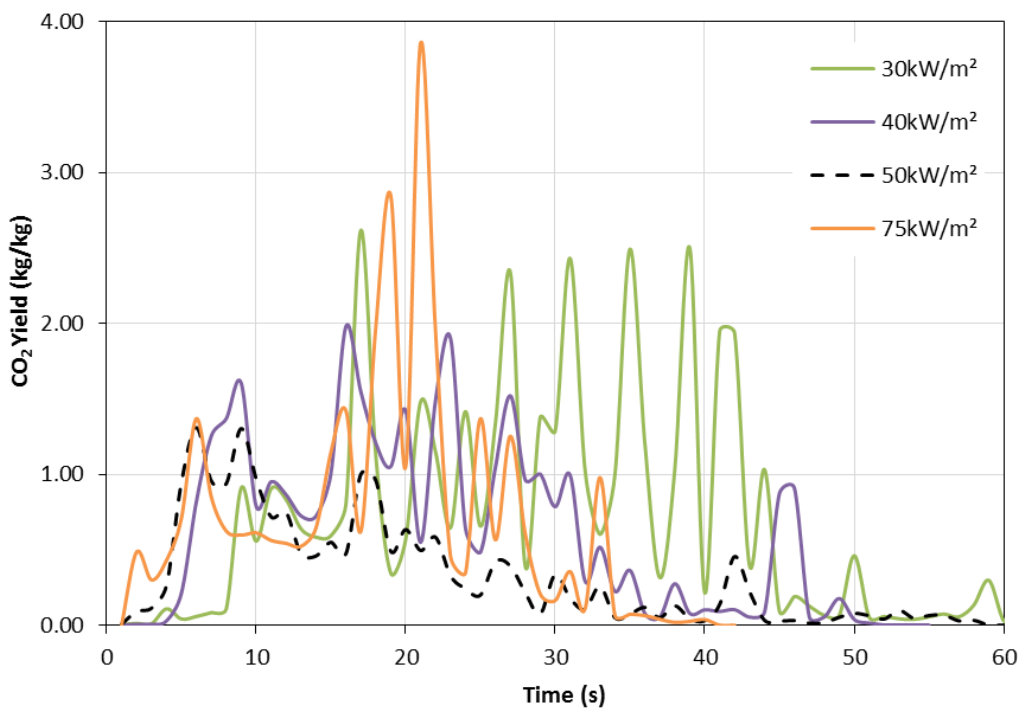
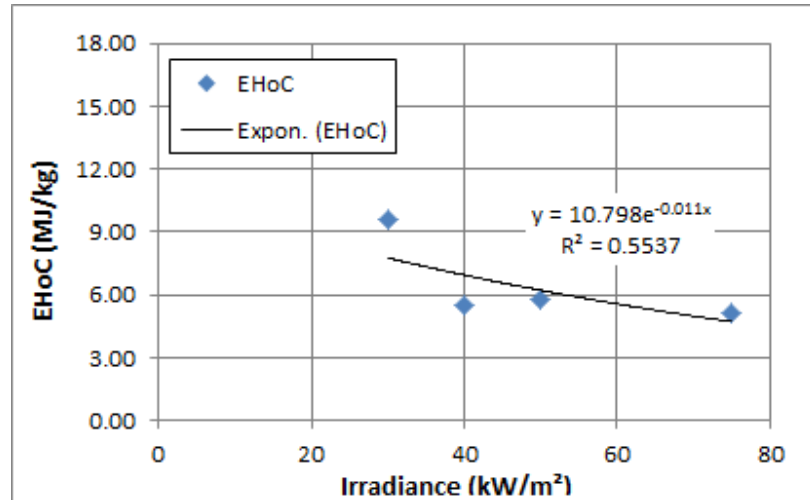
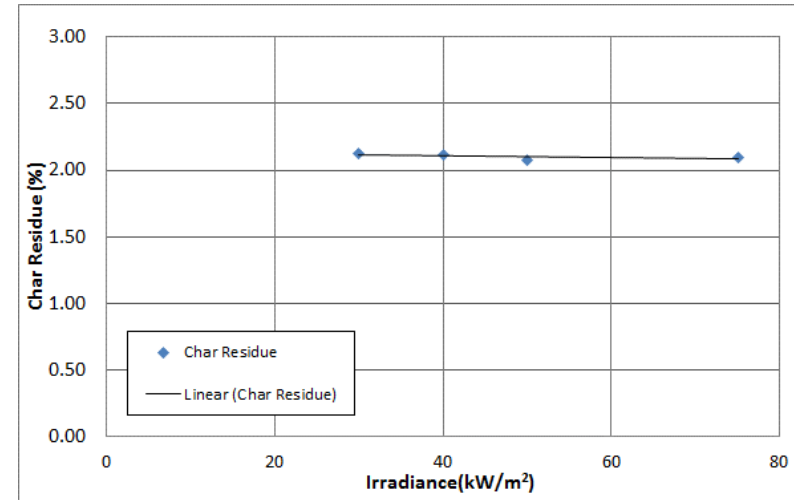


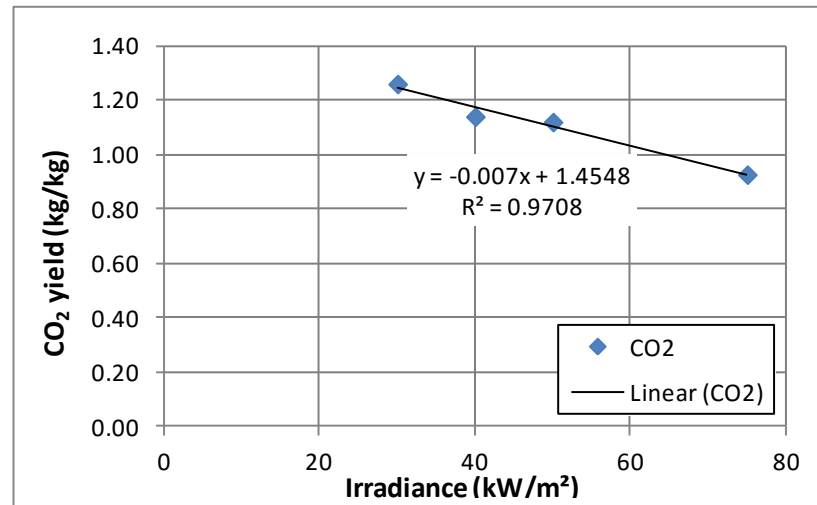
Figure 5.15: CO₂ yield of cotton at various heat fluxes



(a) Effective heat of combustion



(b) Char residue



(c) CO₂ yield

Figure 5.16: Variation of combustion parameters of cotton at various heat fluxes

5.5 Wool Combustion Parameters

5.5.1 Heat Release Rate

The HRR of wool as a function of time is shown in Figure 5.17 and it is clearly observed that only one peak occurs during the burning of the wool sample. Moreover, higher incident heat fluxes result in higher HRR and this appears to increase rapidly at higher heat fluxes thus resulting in shorter burning periods. This is also due to the thickness of the sample as reported by Tata et al. (2011). For similar reasons presented for cotton, the wool samples were only tested from 30 to 75 kW/m².

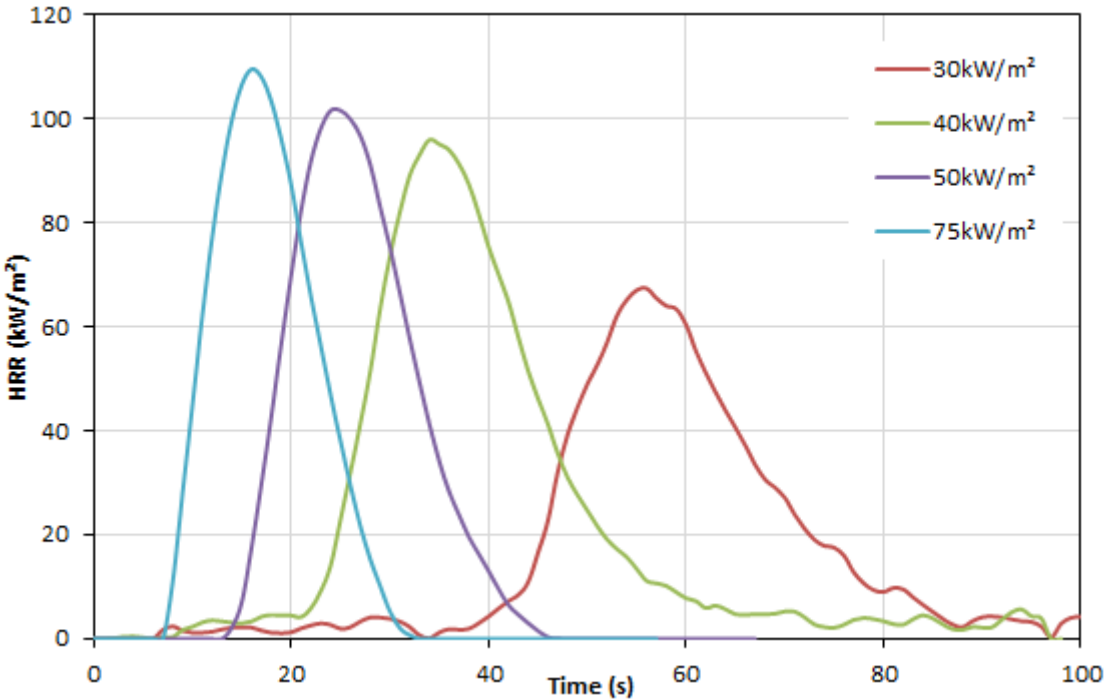


Figure 5.17: Average HRR of wool at various heat fluxes

5.5.2 Specific Extinction Area

The SEA of wool is presented in Figure 5.18 with a higher SEA observed at the middle of the burning period with apparent bell shaped trends. However, there is no clear trend in the SEA curves with time as a function of heat flux. A nominal range of 241 to 335 m²/kg is observed across all heat fluxes which is higher than the range observed for cotton and this is due to the differences in the amount of smoke released. This may be explained on the basis of the relative carbon content in these materials (see Table 5.1)

with wool containing more elemental carbon than cotton, thus more smoke is produced upon its combustion (Palanna 2009).

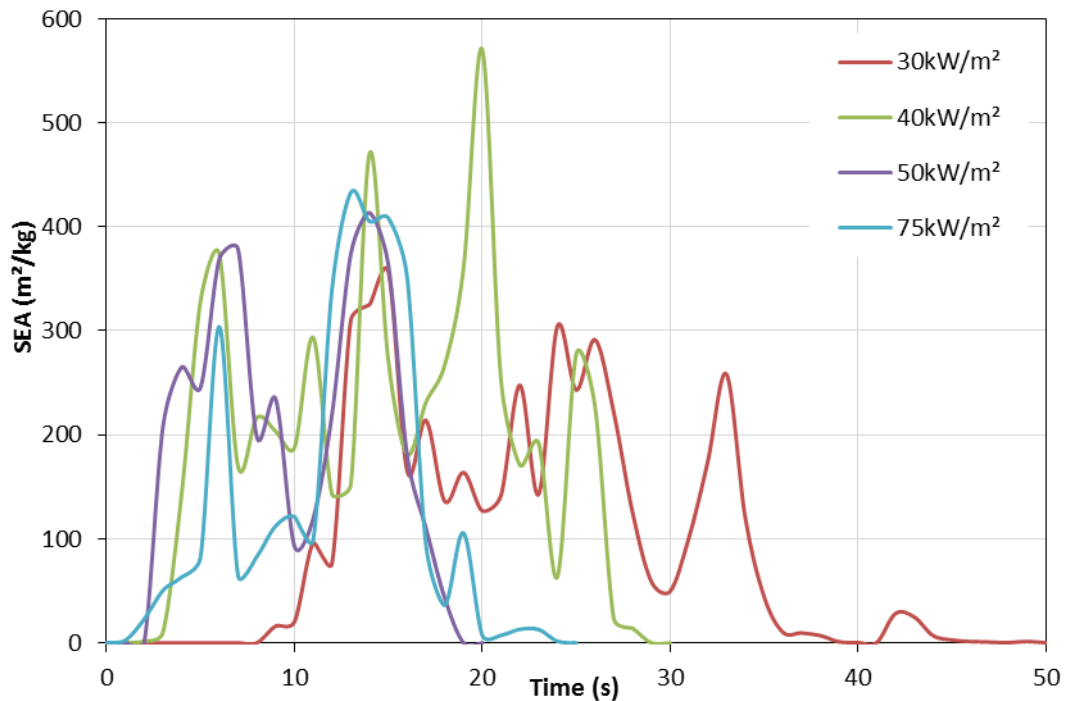


Figure 5.18: Average SEA of wool at various heat fluxes

5.5.3 CO and CO₂ Yield

The CO yield of wool is presented in Figure 5.19 with the CO₂ yield shown in Figure 5.20. For the CO yield, no clear trend over time is observed with the exception of the similar bell shaped profile as that observed for cotton. The CO yield observed with heat flux ranges from 0.007 to 0.011 kg/kg and it is evident that the CO yield of cotton is slightly higher than that of wool. The nominal CO₂ yield ranges between 1.0 to 1.3 kg/kg for wool and this is similar to that of cotton over the same heat flux range. In a similar study, Price et al. (2000) obtained a CO₂ yield at 35 kW/m² of 1.23 kg/kg which is slightly lower than that of the current study conducted at 30 kW/m² which was 1.37 kg/kg. The CO₂ yield is a result of complete sample combustion whereas CO yield represents an incomplete combustion (Jiang 2006). For both wool and cotton, the CO₂ yields are higher than CO yields which is an indication of the complete combustion of these two materials.

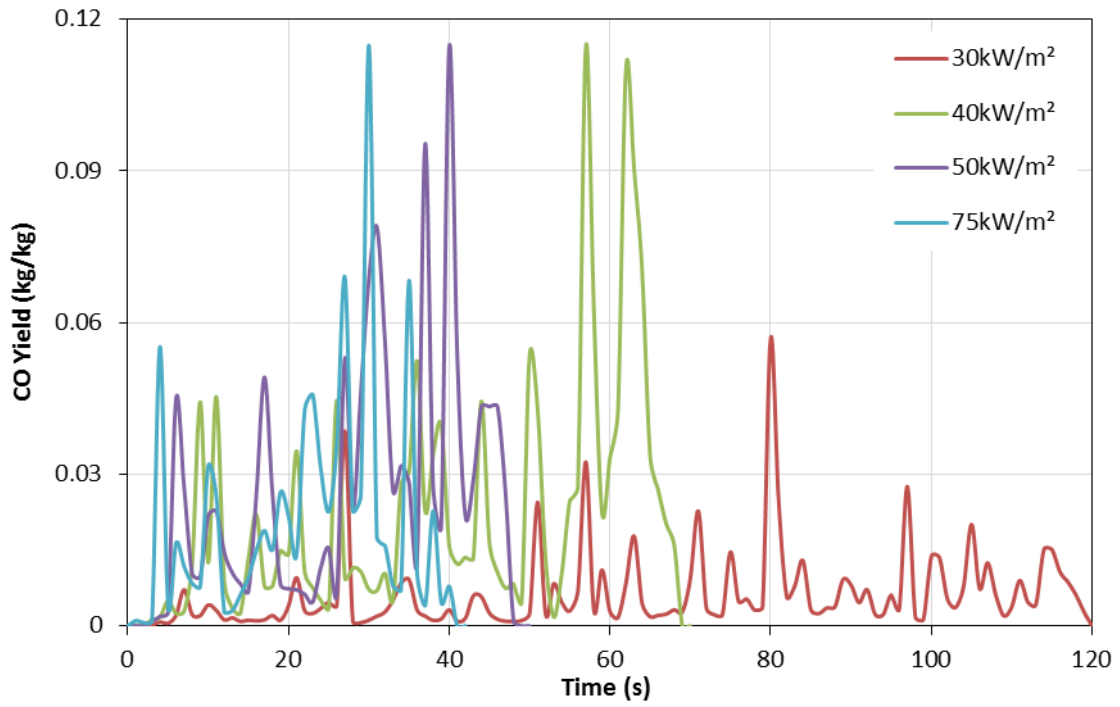


Figure 5.19: CO yield of wool at various heat fluxes

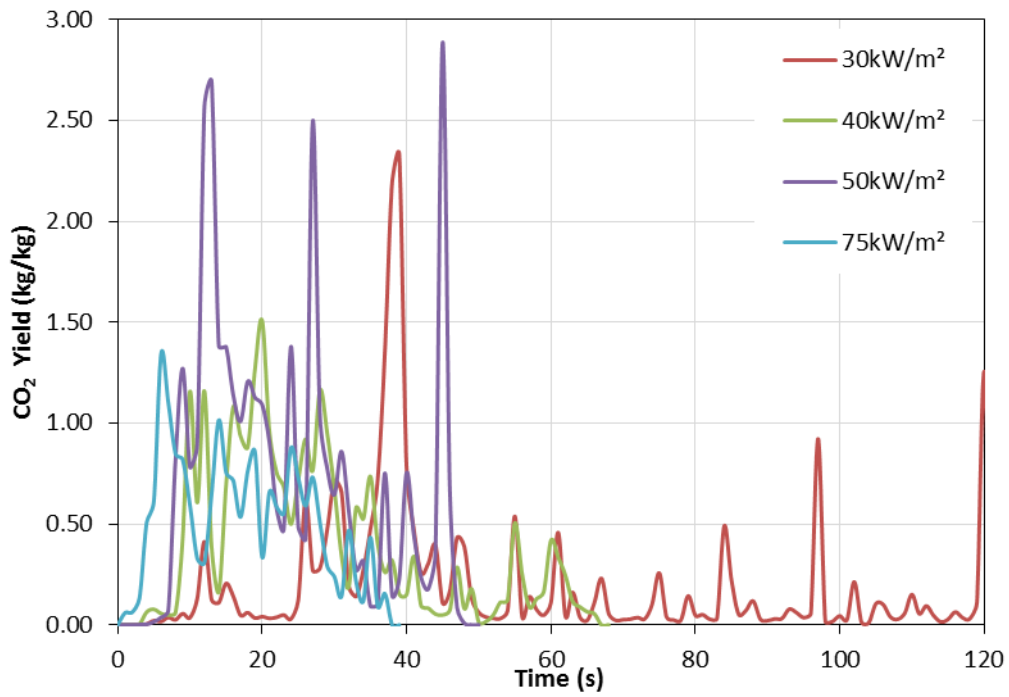
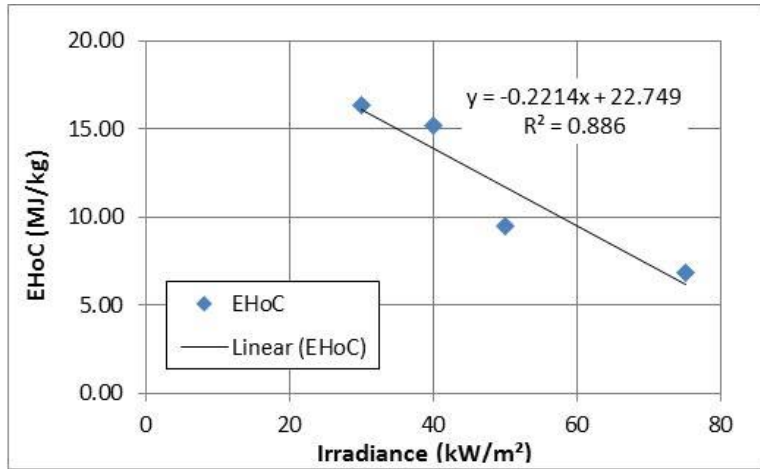
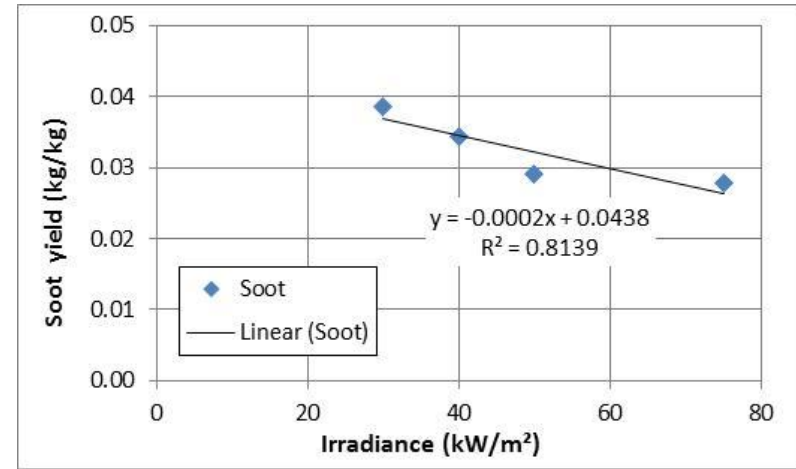


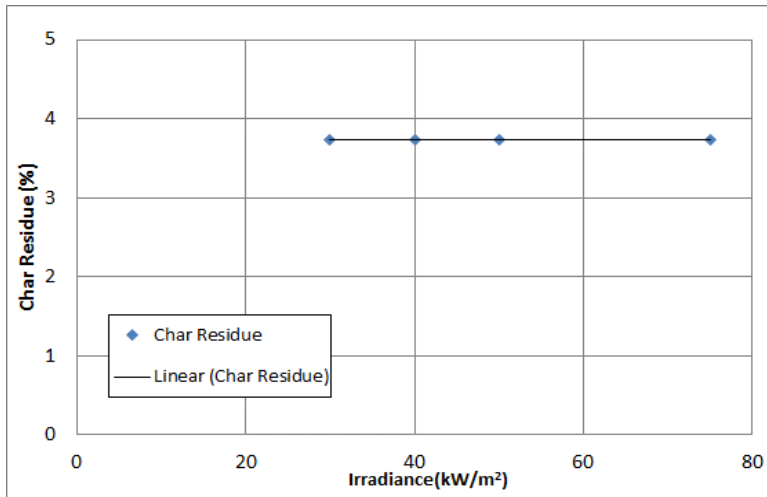
Figure 5.20: CO₂ yield of wool at various heat fluxes



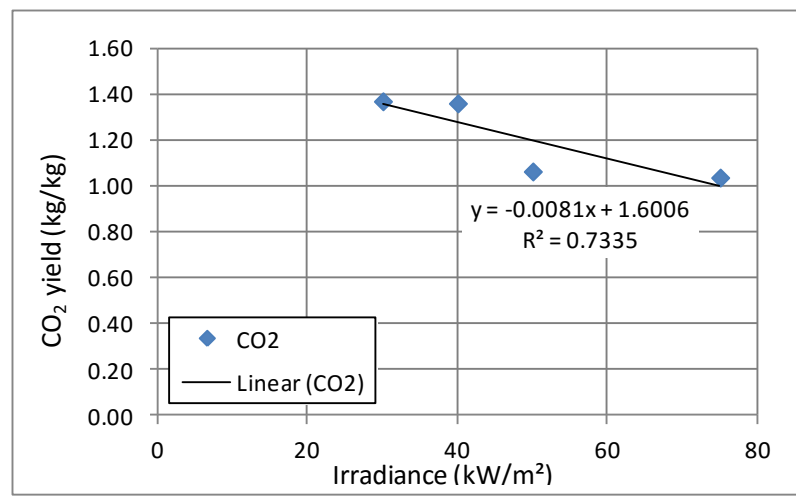
(a) Effective heat of combustion



(b) Soot yield



(c) Char residue



(d) CO₂ yield

Figure 5.21: Variation of combustion parameters of wool with respect to heat flux

5.5.4 Correlation of Parameters

Average values of EHoC, soot yield and CO₂ yield obtained from the cone calorimeter software along with char residue as functions of heat fluxes for wool are presented in Figure 5.21. The corresponding empirical formulae obtained for these functions via regression analysis are presented in the equations below:

$$EHoC = -0.2214(\dot{q}''') + 22.749 \quad (5.11)$$

$$Soot\ yield = -0.0002(\dot{q}''') + 0.0438 \quad (5.12)$$

$$CO_2 = -0.0081(\dot{q}''') + 1.6006 \quad (5.13)$$

Good to average linear correlations were obtained for each parameter and in addition, the average and standard deviation of the CO yield were 0.010 and 0.0018 kg/kg, respectively.

Similar to cotton, comprehensive MLR results for the burning of wool burning are not presented due to the lack of any significant trend, although this data is presented in [Appendix B](#). Wool also shows similar behaviour to cotton under burning with the production of a char (Pottel 1996). The values of char residue with respect to heat flux is presented in Figure 5.21(c) and no significant trend is observed.

5.6 Summary

The parameterization of the FDS combustion model variables for the different materials is presented in this chapter. Significant variations in parameter values with respect to the incident irradiance are observed. For PMMA and pine, values are averaged from normal measurements in the cone calorimeter over six minutes from the ignition at each irradiation level. For cotton and wool, the combustion period ranged from approximately 16 to 46 seconds and 22 to 89 seconds respectively, depending on heat flux, and this may be due to thin layer of the fabrics that are low in mass. It is observed that the parameter values for EHoC, CO yield, CO₂ yield and smoke yield vary with respect to changes in radiative heat flux and this is particularly evident for the charring materials. It is likely that the presence of high moisture contents and likely variations in char development with respect to incident radiation flux may influence these variations, especially for EHoC. Additionally, moisture evaporation and char development may not be uniform through the depth of the sample during the fire test. It is also found that

many parameters vary with time during the tests even under constant irradiation and this is more pronounced for charring materials. In the next chapter, characterization of material thermo-physical properties is presented.

CHAPTER 6

CHARACTERIZATION OF THERMO-PHYSICAL PARAMETERS

6.1 Introduction

Heat transfer models require the input of key material thermo-physical parameters such as thermal conductivity, specific heat capacity, density, emissivity and absorption coefficient. The first three parameters relate to the phenomena of conductive heat transfer while the latter two are related to radiative heat transfer. Most opaque combustible solids turn black quickly upon ignition leading to unity emissivity. For these materials, radiation is generally absorbed at the surface rendering the value of the absorption coefficient insignificant. The thermo-physical properties relevant to conductive heat transfer are characterised in this study through experimental results using a Hot Disk Analyser (HDA). Conversely, the primary parameter needed to determine convective heat transfer i.e. the convective heat transfer coefficient of a substance is not a characteristic material property.

A material's density is one critical parameter that has a significant impact on heat transfer. The bulk density of the various samples was determined by measuring the mass with an electronic scale and then dividing the mass by the volume. The data obtained is presented in Table 6.1

Table 6.1: Properties of the tested materials

Material	Description	Density (kg/m³)
PMMA	Acrylic polymer	1152-1210
Pine	Australian Radiata pine	412-472
Cotton fabric	100% cotton	~ 254
Wool fabric	100% wool	~ 211

In this chapter, the results of the HDA study are presented in relation to several of the key parameters as well as the density of the selected materials.

6.2 Thermal Conductivity

6.2.1 PMMA

The thermal conductivity (λ) of the non-charring PMMA from the current study is presented in Figure 6.1, along with comparative literature data. Although a sinusoidal pattern is observed, the λ value does not significantly change with temperature. Assael et al. (2005) reported that for PMMA, λ is relatively stable within the tested temperature range of their study. The average value in the current study was found to be 0.195 W/m.K with a standard deviation of 0.0045 W/m.K.

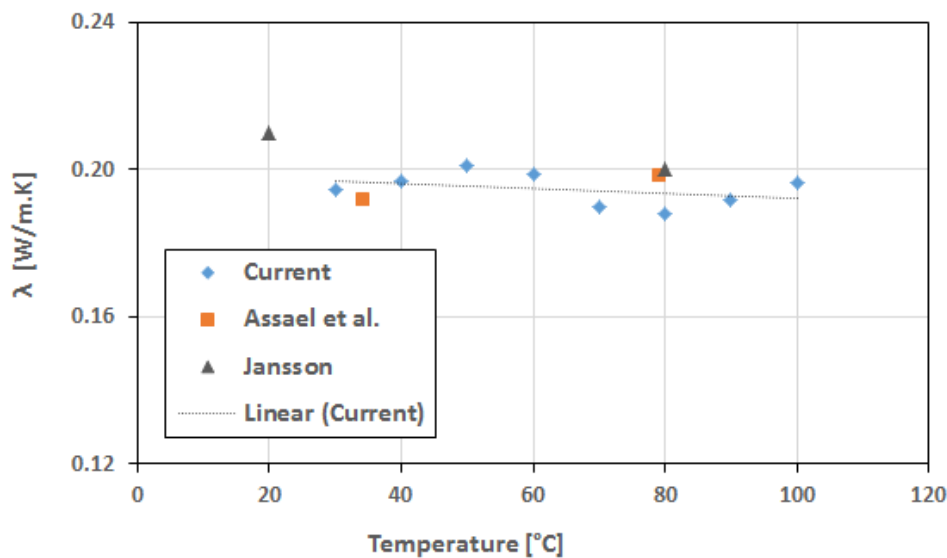


Figure 6.1: Thermal conductivity as function of temperature for PMMA

From this figure, it is evident that the data from the current study are consistent with that reported by other researchers. However, Assael et al. (2005) and Jansson (2004) measured the PMMA thermal conductivities at only two temperatures, 34 and 79°C, and 20 and 80°C respectively. The present study was performed over a wider temperature range between 30 and 100°C at 10°C increments. As a result, significantly more thermal conductivity data was collected. However, there is very little literature data available for thermal conductivities measured at temperatures greater than 80°C and therefore comparisons could not be made with the current data. Nevertheless, the

results are still within an acceptable range as they are closely matched with the literature data over the lower temperature range.

It is also important to note that it is not possible to measure the thermal conductivity of PMMA beyond 100°C as the polymer undergoes phase change above this point and begins to melt (Smith & Hashemi 2006). This is an inherent limitation of the equipment used to perform this measurement due to the construction of the sensor. However, the average value from the current study can be used as an input into the conductive heat transfer calculation and in the pyrolysis simulation.

6.2.2 Pine

The thermal conductivity of pine is presented separately in Figure 6.2. The first set, labelled “Current”, encompasses the entire data set including the moisture evaporation region which is highlighted by the hatched area. The second set, labelled “Current2”, excludes the moisture evaporation affected data. Further discussion of the moisture evaporation of the charring materials is presented later in Section 6.4. A regression analysis of the “Current2” data set shows a strong power relationship between the thermal conductivity and temperature with $R^2 = 0.82$. The empirical relationship is given in Equation (6.1):

$$\lambda = 0.139 T^{0.0658} \text{W/m.K} \quad (6.1)$$

where T is the temperature in °C. This relationship can be used in the conductive heat transfer calculations and the pyrolysis simulation. Pine is categorized as a softwood and it is reported that the thermal conductivity of softwoods increases linearly with temperature (Gupta, Yang & Roy 2003). Current2 data can also approximate a linear relationship, albeit with lower R^2 .

Figure 6.2 also includes thermal conductivities for pine reported in various literature sources. Using the same measurement methods, the value of thermal conductivity of 0.17 W/m.K reported by Ho (2007) matches well with that from the present study (0.18 W/m.K). Similar to the trend in the current study, the limited values reported by Fonseca and Barriera (2009) also show an apparent increasing trend in λ with temperature, although their values are comparatively lower.

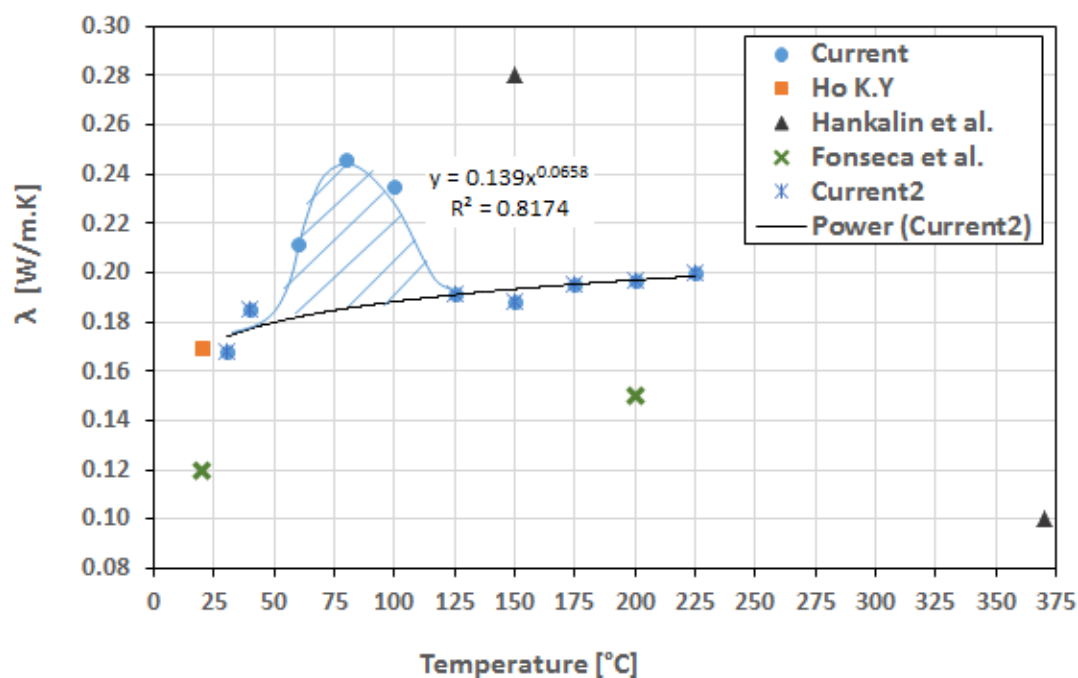


Figure 6.2: Thermal conductivity of pine as function of temperature

6.2.3 Pine Char

Unlike PMMA, wood undergoes charring when it is heated and therefore the thermal conductivity of char is also essential to include in fire simulation models. However, it is experimentally challenging to obtain the thermo-physical properties of char due to its tendency to break apart into irregular shapes. In this work, two types of pine char were measured including: (i) char from a burned flat pine slab obtained from a sample with a surface finish or coating (State Forests of New South Wales 1996) and (ii) char from burned structural furnishing pine. The thermal conductivities of charred pine from these two samples in the current study is presented in Figure 6.3 along with examples of literature data. It is evident that the conductivity of charred pine increases as the temperature increases. For the char obtained from flat pine, which is more representative of pine material characterized in this study, there is a strong incline from 0.07 W/m.K at ambient temperature up to the maximum test temperature of 120°C.

It is also evident that the thermal conductivity of flat pine is higher than that of structural pine and this may be explained by the density difference between these two materials. Gupta, Yang and Roy (2003) reported that density is one of the key influences in the thermal conductivity of materials.

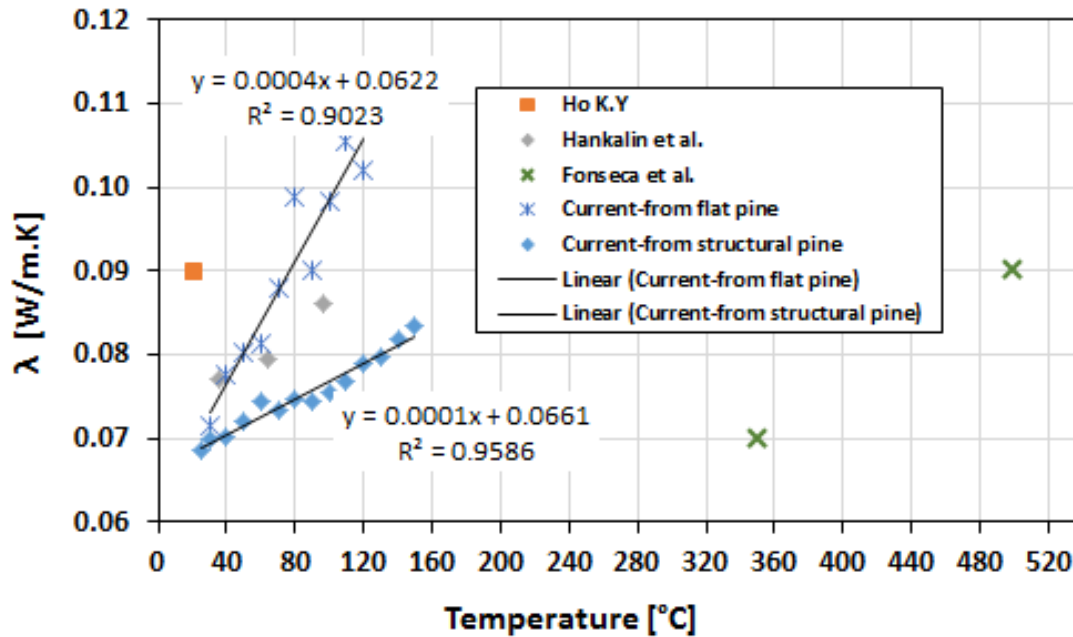


Figure 6.3: Thermal conductivity as function of temperature for pine char.

In Figure 6.3, the data of both Hankalin (2009) and Fonseca et al. (2009) shows a positive trend similar to that in the current research. The data are consistent with the values reported by Hankalin (2009) data and fit reasonably well with their trend. The values reported by Fonseca and Barriera (2009) were measured at much higher temperatures than that of any of the other studies including the present work.

The regression analysis shows a very strong ($R^2=0.9$) linear relationship between thermal conductivity and temperature for the 'char- from flat pine' sample in the current study data. Equation (6.2) representing the relationship is shown below and this relationship can be used in the state-of-the-art CFD-based fire models:

$$\lambda = -0.0004(T) + 0.0622 \text{ W/m.K} \quad (6.2)$$

6.2.4 Cotton

Similar to the results of pine, Figure 6.4 shows two different sets of thermal conductivity data for cotton measured in the current study are presented. The first set, labelled “Current”, presents all data including that in the hatched moisture evaporation region. The second set excludes the moisture evaporation affected data and is labelled “Current2”. The thermal conductivity of cotton is clearly affected by moisture between 50 and 150°C as shown in the previous DTG curve (Figure 4.14 in CHAPTER 4) where the endothermic reaction occurs. Further details are discussed later in Section 6.4. For the data in Figure 6.4, if the thermal conductivities of the moisture region are excluded, an increasing linear trend is observed. When the moisture region is included, the thermal conductivity is observed to increase from 30 to 40°C before it starts to fall when the moisture region is reached until a temperature of 90°C when it increases up until 150°C.

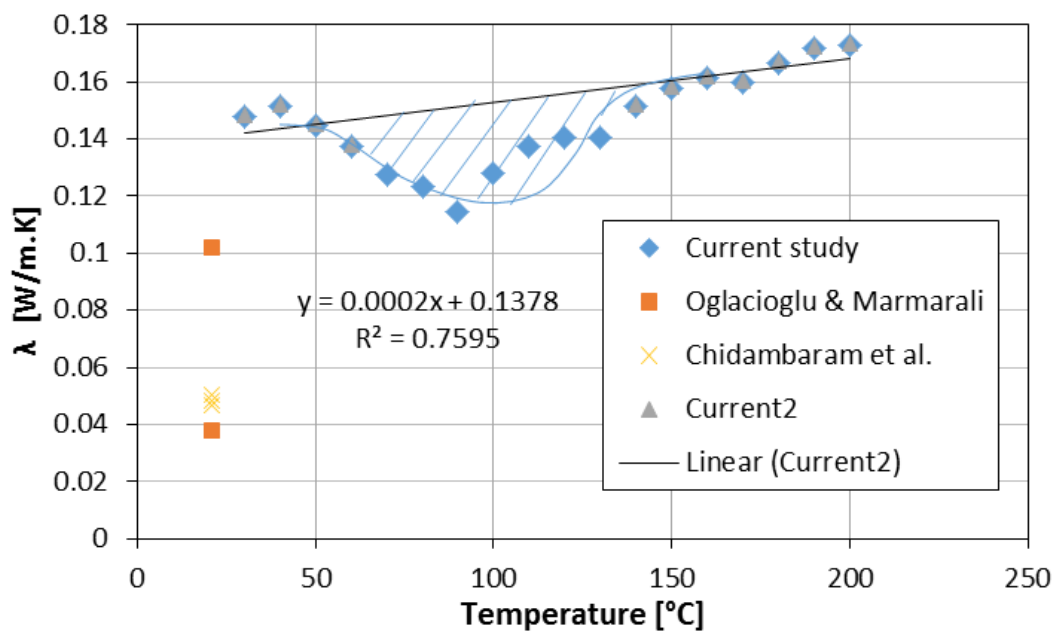


Figure 6.4: Thermal conductivity as function of temperature for cotton

A regression analysis of the “Current2” data shows a strong ($R^2=0.76$) power relationship between the thermal conductivity of cotton and temperature. Equation (6.3) representing this relationship is given by:

$$\lambda = 0.0002(T) + 0.1378 \text{ W/m.K} \quad (6.3)$$

The thermal conductivity data obtained from various literature sources is also presented in Figure 6.4. At 30°C, the thermal conductivity of cotton in the current study is approximately 0.15 W/m.K whereas Chidambaram, Govindan and Venkatraman (2012) reported lower values ranging between 0.0463 and 0.0501 W/m.K at 21°C for loose, medium and tight loop length cotton samples. The differences these results and those of the current study may be due to differences in the measured temperature as well as in the physical form of the sample itself such as variations in loop length. The thermal conductivity of cotton is not only vital in pyrolysis simulations, it is also important for other disciplines such as the textile industry where it can be used for many purposes such as the design of apparel.

6.2.5 Wool

In Figure 6.5, the thermal conductivity of wool studied over the temperature range of 30 to 200°C at 10°C intervals is shown. Like the other charring materials, the thermal conductivity data for wool is presented with (“Current”) and without (“Current2”) the moisture evaporation region. Similar to cotton, it is evident that the thermal conductivity of wool is affected by moisture between approximately 50°C and 150°C and evaporation in this region also seen in the previous DTG curve (see Figure 4.25 in CHAPTER 4). Beyond this temperature, the value of λ increases in a somewhat curvilinear trend.

A regression analysis of the “Current2” set shows a very strong ($R^2=0.92$) polynomial relationship between thermal conductivity and temperature and this relationship, which can be used in pyrolysis simulation, is given by Equation (6.4):

$$\lambda = 1E - 06(T)^2 - 0.002(T) + 0.0882 \quad (6.4)$$

It is important to note that to the best of our knowledge, there is no literature data for the thermal conductivity of wool. Thus, a comparison between the current study and comparative literature was not possible at this time.

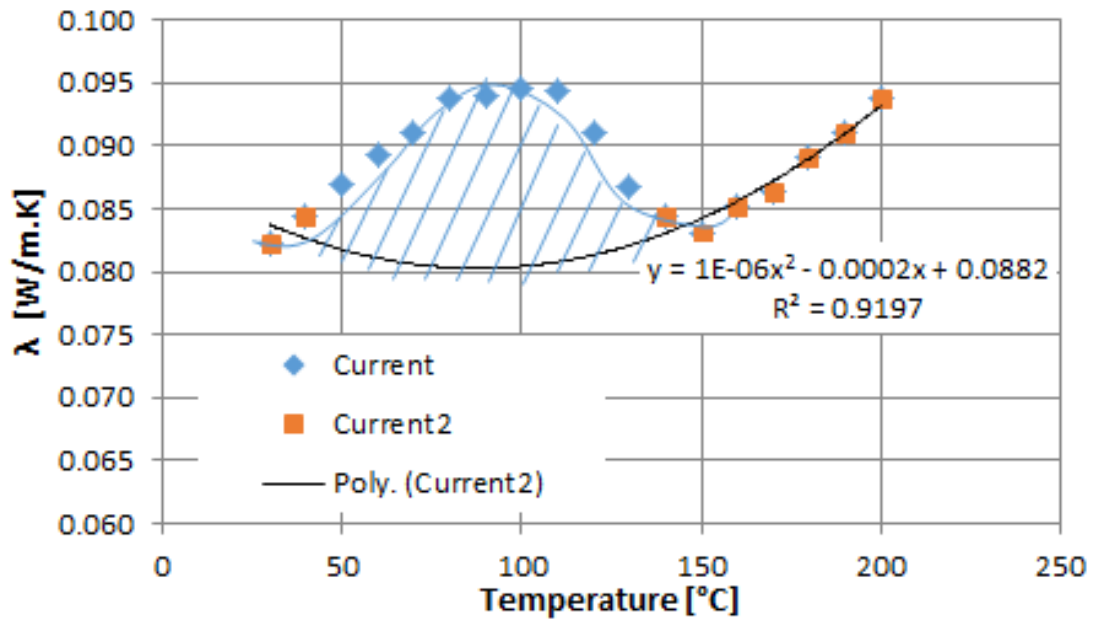


Figure 6.5: Thermal conductivity as function of temperature for wool

6.3 Specific Heat Capacity

6.3.1 PMMA

Figure 6.6 presents the specific heat capacity (C_p) of PMMA tested between 30 and 100°C. Reported literature data from Assael et al. (2005) and Jansson (2004) are also presented in the same figure. In the current study, the C_p values of PMMA range between 1400 and 1570 J/kg.K with an average value of 1471 ± 44 J/kg.K.

The literature values are similar to this data and although these examples only show limited data points, the trends imply increasing C_p with temperature. The current data, however, shows a flat trend suggesting there is no influence of C_p with temperature. Differences in these reported values and the present study may be due to differences in the type of PMMA used in the measurement and the equipment used.

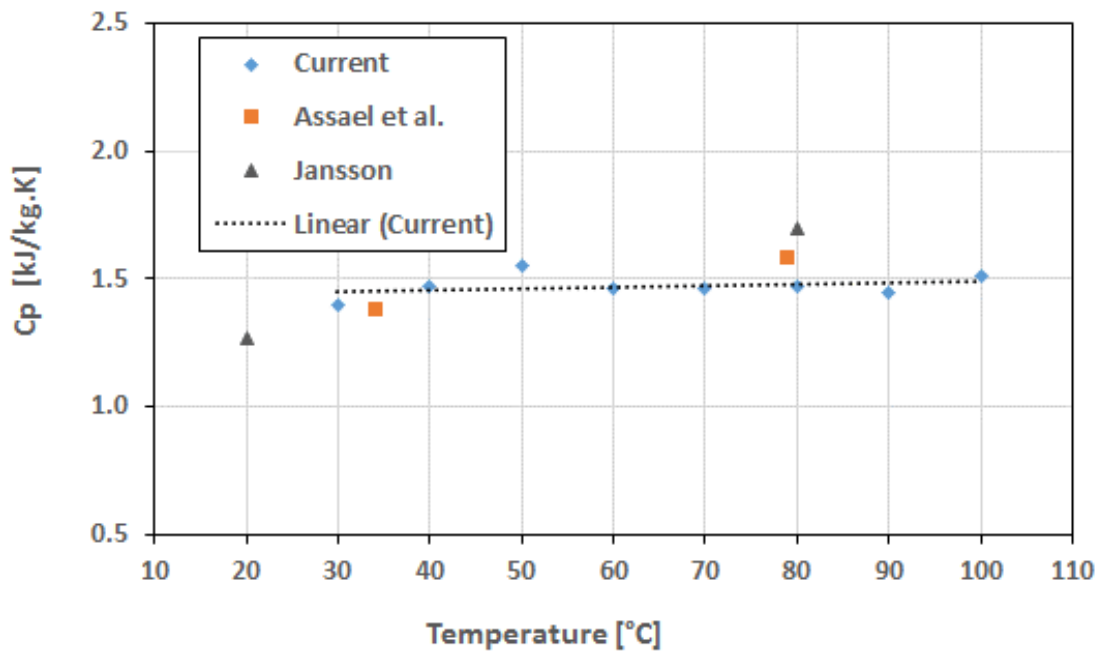


Figure 6.6: Specific heat as function of temperature for PMMA

6.3.2 Pine

Figure 6.7 shows the C_p vs. temperature profile of pine between 30°C and 225°C. In accordance with the previous thermal conductivity data, two sets are presented both inclusive (“Current”) and exclusive (“Current2”) of the moisture evaporation region. It is evident that the C_p of pine is affected by moisture evaporation between 70°C and 150°C then beyond this temperature, there is a slight increasing trend in the C_p value with respect to temperature. If the C_p values of this moisture region are excluded, a general increasing trend in C_p is observed as the temperature rises.

Literature examples reported by Gupta, Yan and Roy (2003) and Harada, Hata and Ishihara (1998) are also presented in Figure 6.7. These studies also show a similar positive trend with increasing temperature. Although the C_p values of Harada, Hata and Ishihara (1998) are similar to that of the current study, those of Gupta, Yan and Roy (2003) are roughly 0.15 kJ/kg.K higher at similar test temperatures. In another example, Ho (2007) reported a C_p value at ambient temperature of 0.50 kJ/kg.K which is significantly lower the values shown in Figure 6.7 for all studies. It is important to note that globally, a wide range of pine varieties exist and any variations may be due to differences in pine species as well as test equipment. The empirical relationship

between C_p and temperature is presented in Equation (6.5) for use in the pyrolysis simulation:

$$c_p = 587.51(T)^{0.1959} \tag{6.5}$$

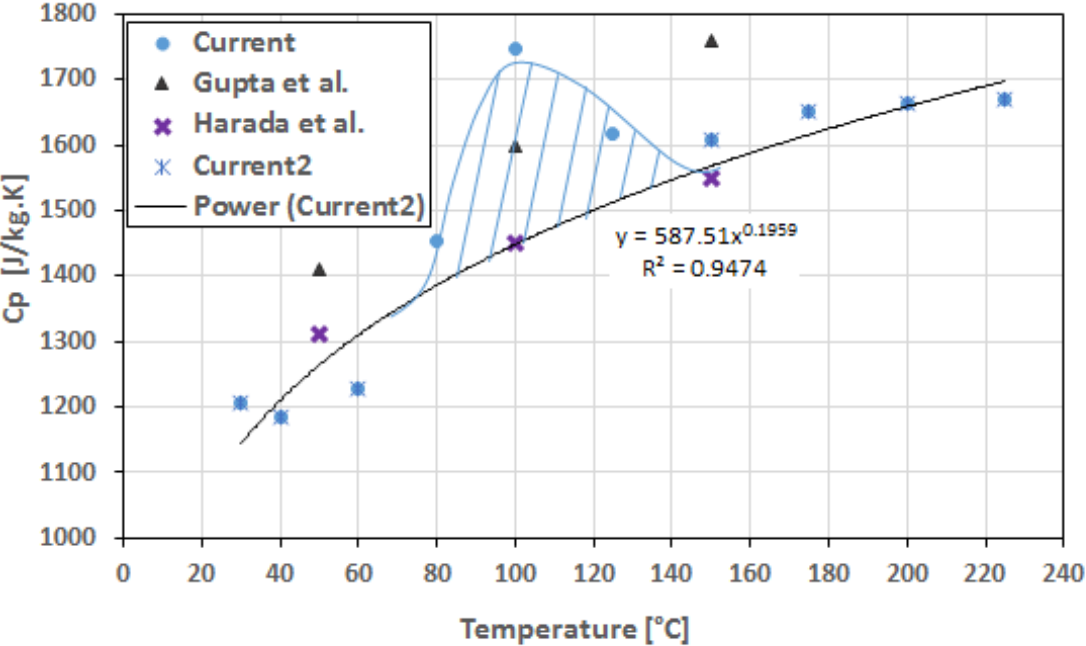


Figure 6.7: Specific heat as function of temperature for pine

6.3.3 Pine Char

In Figure 6.8, the specific heat of ‘char-from flat pine’ and ‘char-from structural pine’ samples used in the current study is presented over a temperature range from ambient to 120°C. For both materials, the C_p shows a general incline over this range, although the C_p of ‘char-from structural pine’ is higher than that of the flat pine. Although it was not possible to measure experimentally, this may be due to differences in the relative densities of these materials. As discussed in Section 1.1.2, a higher relative sample mass requires more energy to raise the sample temperature by 1°C (Goel 2008).

Various literature data reported by other researchers is also presented in Figure 6.8. The values of Gupta, Yan and Roy (2003) and Grønli (1996) show similar trends to the current results, however, the data of the former are generally lower than the values of the current study (‘char-from flat pine’) whilst those of the latter are generally higher.

Ho (2007) obtained a C_p value of 900 J/kg.K at ambient temperatures which is slightly higher than the value of the ‘char-from flat pine’ in the current study. Overall, the literature values for pine char are reasonably close to those for ‘char-from flat pine’ in the current study despite differences in the materials.

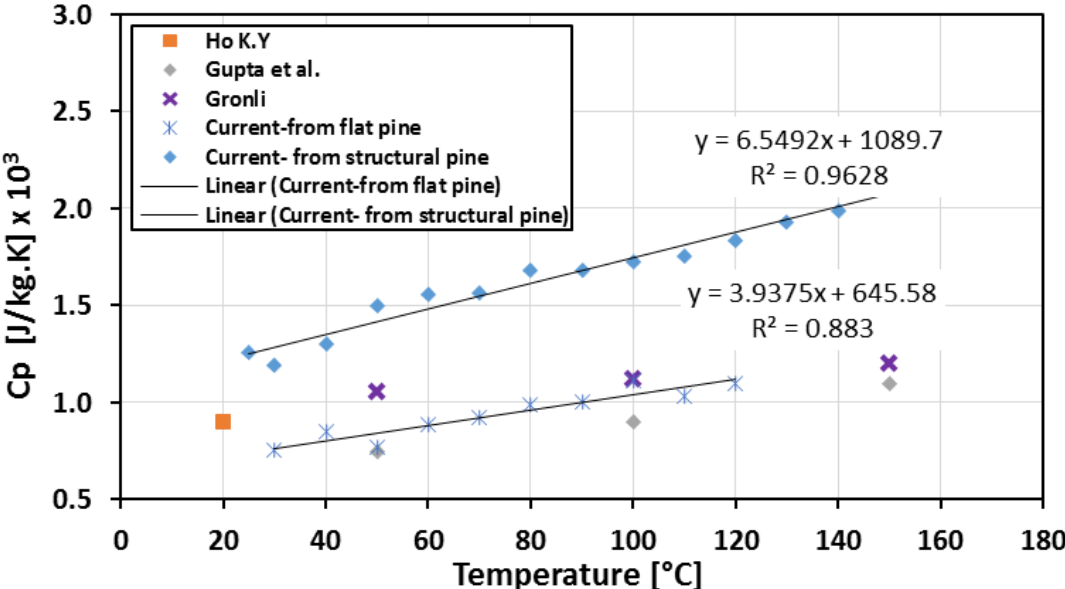


Figure 6.8: Specific heat as function of temperature for pine char

The regression analysis of the current data shows very strong ($R^2=0.88$ and 0.96) linear relationship between specific heat and temperature of pine char. Equation (6.6) represents the relationship for ‘char-from flat pine’ which is used for subsequent pyrolysis simulations:

$$c_p = 3.9375 (T) + 645.558 \tag{6.6}$$

6.3.4 Cotton

Figure 6.9 shows the trend in specific heat values with temperature for another charring material, cotton. Similar to the other charring materials, the moisture affected region is evident and therefore two sets of data presented: “Current” where the data are inclusive of the moisture evaporation region and “Current2” where the data exclude the moisture evaporation region. It is evident that the C_p of cotton is affected by moisture between 50°C and 150°C confirmed earlier in the DSC and DTG curves of Figure 4.15 and

Figure 4.14 respectively. Either side of this range, steadily increasing trends with temperature are observed. For this particular material, there is very limited literature data available for comparison with the exception of Harris (1956). This data is presented in the same figure and although only a single value is given, it is slightly lower than the current values.

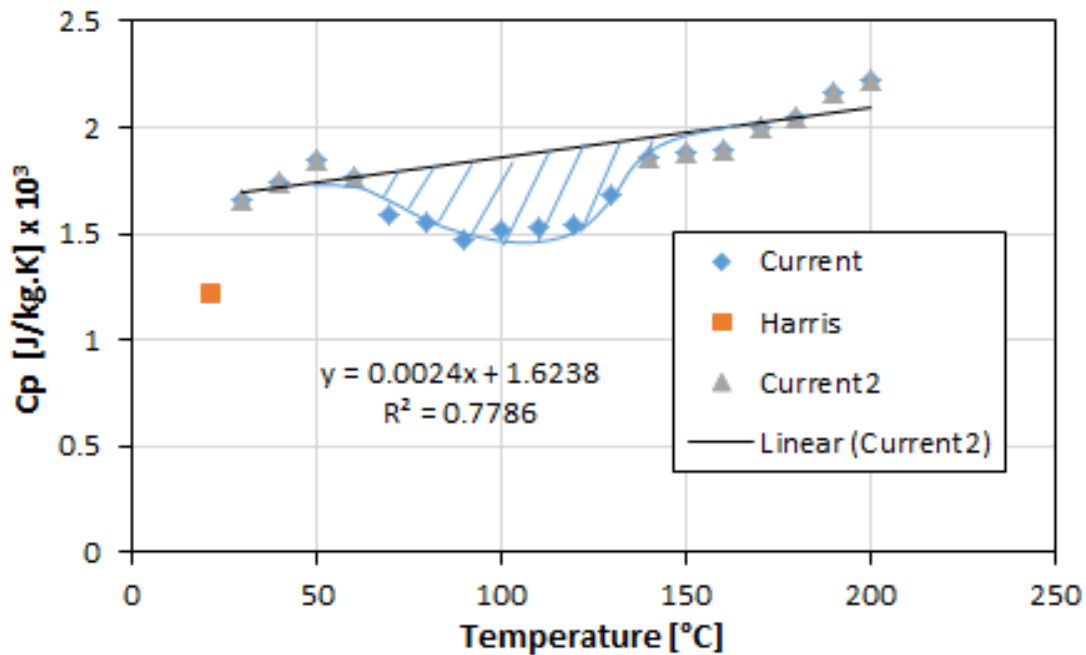


Figure 6.9: Specific heat as function of temperature for cotton

For use in pyrolysis simulation modelling, the linear relationship between specific heat and temperature based on “Current2” data is presented in Equation (6.7) below:

$$c_p = 0.0024(T) + 1.6238 \quad (6.7)$$

6.3.5 Wool

Figure 6.10 shows that, much like thermal conductivity, the specific heat of wool is affected by moisture evaporation over the test temperature range. The C_p is again presented separately as “Current” (inclusive of the moisture evaporation region) and “Current2” (exclusive of the moisture evaporation region) which is observed to be between approximately 40°C and 140°C. Similar to the thermal conductivity data,

beyond that region C_p increases in curvilinear trend. Interestingly, no literature data was found to enable a comparison with the current data.

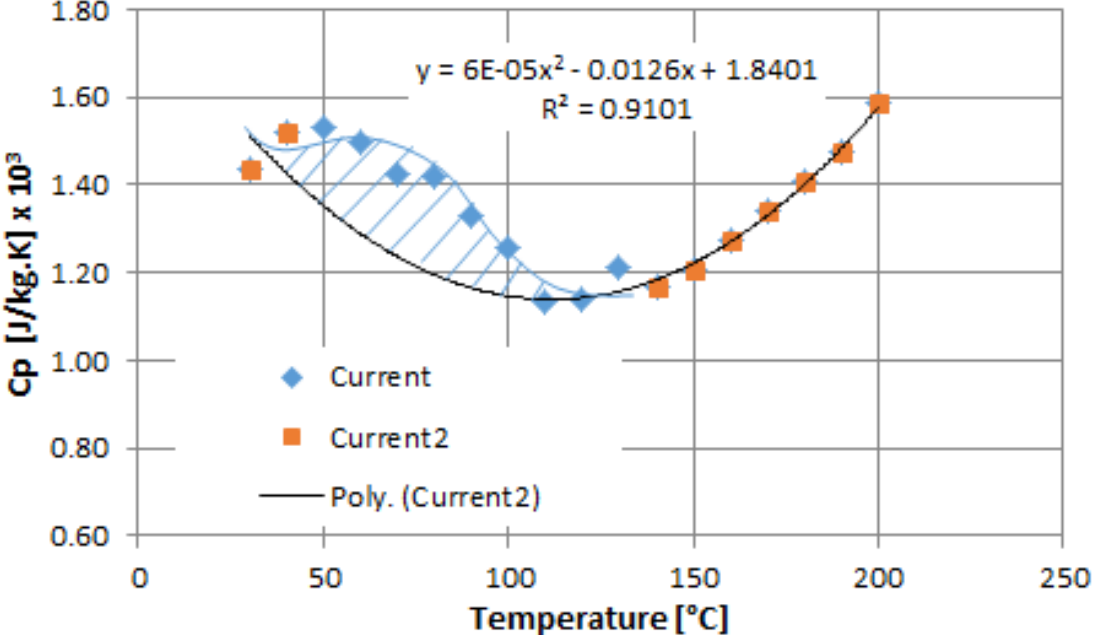


Figure 6.10: Specific heat as function of temperature for wool

The “Current2” data shows a very strong ($R^2=0.91$) polynomial relationship between specific heat and temperature as shown in Equation (6.8) presented below:

$$c_p = 6E - 05(T)^2 - 0.0126(T) + 1.8401 \tag{6.8}$$

6.4 Moisture Affected Region of Charring Materials

Thermal properties of fabrics are affected by a number of factors including humidity (Hes & Loghin 2009) and as such, the sample materials used in this study were conditioned at 23°C in 50% relative humidity (RH) prior to testing. Due to the volatile nature of water, the residual moisture present in some samples has resulted in evaporation thus influencing the measurement and the final result (Simile 2004). This phenomenon has been observed for the charring materials used in this study, particular the fabric samples tested. Indeed it has been reported that for synthetic fibers, the heat capacity and thermal conductivity are complex parameters dependent on many factors

including moisture content (Svetlov, Isaev & Svetlov 2014) so it is not surprising that the results in the current study are equally complex for natural fibers.

It is possible that the relative moisture contents of pine (Figure 6.2) and wool (Figure 6.5) has resulted in higher thermal conductivity in the moisture affected region. This may be due to the higher values of λ and C_p for water compared to these materials. This is in agreement with the findings of Abdou and Budaiwi (2013) and Hes and Loghin (2009) where higher thermal conductivities were attributed to higher moisture contents in the test samples. For pine and wool, the presence of moisture is shown in the respective DTG curves of Figure 4.4 and Figure 4.25 (CHAPTER 4) respectively and in relation to the TG analyses. Later, as the moisture is released from the samples, the thermal conductivities increase slightly as the temperature increases. Taking pine as an example, if the moisture affected region is excluded, a clear increasing trend becomes evident with increasing temperature (Figure 6.2). In addition to thermal conductivity, the moisture content of materials also influences C_p (Guerth-Schacher 2007) and this trend is also observed in pine, wool and cotton in the current work. In some cases, moisture can act as a heat sink and when the recondensation of moisture diminishes at higher temperature, a reduction in heat transfer within some fabrics may result (Guerth-Schacher 2007). This effect is observed for the λ and C_p of cotton, as shown in Figure 6.4 and Figure 6.9.

The chemical composition of materials may also influence the values of λ and C_p for various materials. For example, wool is naturally hydrophobic, or water repelling on the outer surface with a hydrophobic core (Carran, Ghosh & Dyer 2015) whereas cotton is primarily hydrophilic, or water absorbing (Hoshino, Wada & Nishizawa 1999). In their natural state, both fibres are hygroscopic but treatments such as scouring, cleaning, dyeing, heating etc. can significantly alter these properties. It is also reported that wool can absorb moisture due to the amino acid containing keratin in the fibers that have an inherent ability to bind together with water molecules (Chaudhuri 2004).

6.5 Summary

The thermo-physical properties of the materials studied in this work are characterized in this chapter. A summary of trends for all materials is presented in Table 6.2 for both thermal conductivity and specific heat properties with a range of trends observed for the different materials. With the exception of PMMA, the other materials demonstrate a strong relationship with respect to temperature and the results are in agreement with the findings of other researchers (Hankalin, Ahonen & Raiko 2009, Fonseca & Barreira 2009).

Table 6.2: Summary of the trend for all materials

Material	Conductivity	Specific heat
PMMA	Flat	Flat
Pine	Power (increasing)	Power (increasing)
Pine Char	Linear (increasing)	Linear (increasing)
Cotton	Linear (increasing)	Linear (increasing)
Wool	Curvilinear (increasing)	Curvilinear (increasing)

Overall the current data is similar to the literature data both in trends and nominal values. Therefore the current data is considered to be accurate, reliable and suitable for the next stage of the study. In this chapter, complete characterization of the fire properties for coupled pyrolysis and combustion modelling of the studied materials is completed. In the next chapter, these properties will be used as inputs into the FDS model followed by a simulation to check the validity of these properties as well as the validation of the FDS simulation.

CHAPTER 7

NUMERICAL SIMULATION AND OPTIMISED METHODS

7.1 Introduction

The CFD-based fire model, FDS, developed by the NIST was used to validate both the characterized fire properties of the studied materials and the CFD model. The open source FDS is commonly utilised to simulate fires in buildings and is widely used by a number of fire engineering researchers and professionals due to its unique features and availability from the NIST (2015).

The default mode of this model incorporates: a large eddy simulation (LES) turbulence model; a simple pyrolysis/evaporation model; a mixture-controlled combustion model; a one-dimensional conduction heat transfer model; a simple convective heat transfer model (a combination of natural and forced convection correlations); and a finite-volume radiative heat transfer model. In addition, an optional direct numerical simulation (DNS) hydrodynamic model and a finite-rate chemistry combustion model are also available. Complete details of these models can be found elsewhere (McGrattan et al. 2008) and in this chapter, an overview of the key sub-models used in this study is presented.

7.2 Governing Equations of FDS

7.2.1 Hydrodynamic Model

Numerous mathematical sub models are employed in the FDS including the LES turbulence model which has been further developed into the time-dependent three-dimensional flow model. This 3D model includes filtered and simplified continuity, as well as momentum and state equations (McGrattan et al. 2008). The density is solved by the continuity equation, whereas the momentum and state equations are applied in the determination of velocity and temperature values respectively throughout the domain.

Conservation of Mass (Continuity Equation)

The key in the conservation of mass is that the mass must remain constant in relation to time and the rate of mass flow change through the control surface is equal to changes in density of the system given by Equation (7.1):

$$\frac{\partial \bar{\rho}}{\partial t} + \frac{\partial}{\partial x_i} \left(\bar{\rho} \bar{u}_i \right) = 0 \quad (7.1)$$

In this equation, the first term represents the rate of change of mass, or more specifically density, within the control volume and the second term defines the nett mass flow through the control surface.

Conservation of Momentum

The momentum equation, also known as the Navier-Stokes equation, is fundamentally the application of the Newton's second law of motion. There are two approaches available in FDS that can be considered in modelling the conservation of momentum (inclusive of turbulence), namely the direct numerical simulation (DNS) and the large eddy simulation (LES).

A very fine numerical grid size in the order of 1 mm is required in the DNS approach (McGrattan et al. 2015), so this method is appropriate to model fundamental fluid and/or heat flows, very small-scale combustion etc. In the LES approach, it is assumed that the large eddies are controlling the momentum and turbulent kinetic energy in the flow field whereas the smaller eddies have a dissipative effect. In the LES method, the Navier-Stokes equation is filtered in order to separate the small eddies from the flow field with the large scale of fluid motion modelled by the filtered equation (White 2010) while the effect of small eddies are modelled. In this study, the LES method is employed and the filtered Navier-Stokes equation used is presented in Equation (7.2):

$$\bar{\rho} \left(\frac{\partial \bar{u}_i}{\partial t} + \bar{u}_j \frac{\partial \bar{u}_i}{\partial x_j} \right) = - \frac{\partial (\bar{p} - p_o)}{\partial x_i} + \frac{\partial}{\partial x_j} \left\{ \mu \left(\frac{\partial \bar{u}_i}{\partial x_j} + \frac{\partial \bar{u}_j}{\partial x_i} \right) \right\} + \bar{\rho} g \delta_{i3} - \frac{\partial \tau_{turb}}{\partial x_j} \quad (7.2)$$

In this equation, the left hand side represents the time-dependent term plus an advection term representing momentum and inertia forces, respectively. The right hand side comprises forces acting on a fluid represented by pressure (p), viscous diffusion, gravity (g) and turbulence terms. Additional forces such as drag can also applied.

In this equation, the term $\overline{u_i}$ represents the filtered velocity (approximately instantaneous) and the term τ_{turb} represents the filtered turbulence, also known as the sub grid scale Reynolds stress.

As mentioned in Chapter 1, version 6 of FDS used in the current study employs the default LES model based on the Deardoff model (Deardoff 1972) whereas in the previous edition, version 5, the default model was the constant Smagorinsky model (Smagorinsky 1963).

Equation of State and Poisson Equation

The FDS does not solve the (heat) energy equation but rather uses the ideal gas equation for temperature (although the energy equation itself is ideal), as well as the Poisson equation for pressure in order to achieve have faster simulations. Equation (7.3a) is used to solve for temperature:

$$\overline{p_0} = \overline{\rho} R \overline{T} \quad (7.3a)$$

where $\overline{p_0}$ is the background pressure, R is the molar gas constant (8.3145 kJ/kmol.K), and \overline{T} is the temperature.

For pressure, the Poisson equation is given by:

$$\nabla^2 H = -\frac{\partial(\nabla \cdot U)}{\partial t} - \nabla \cdot F ; F = -\overline{u_i} \times \omega - \tilde{p} \nabla \left(\frac{1}{\rho} \right) - \frac{1}{\rho} [(\rho - \rho_0)g + f_b + \nabla \cdot \tau_{ij}] \quad (7.3b)$$

Here, H is the total pressure, $(\overline{p_0} - \rho gh)$, where h is the height above ground level; $\overline{u_i}$ is the vector describing the instantaneous velocity in the u , v and w directions; F is referred to collectively as momentum flux; \tilde{p} is the pressure perturbation; ω represents vorticity; p_0 is the atmospheric pressure; g is the acceleration due to gravity; f_b is the external force vector (excluding gravity); and τ_{ij} is the viscous diffusion term and is described earlier in Equation (7.2) as the second term on the right hand side.

Conservation of Species

The equation describing the conservation of individual gaseous species, Y_i , is derived from the conservation of mass as follows:

$$\frac{\partial(\rho Y_i)}{\partial t} + \frac{\partial}{\partial x}(\rho u Y_i) + \frac{\partial}{\partial y}(\rho v Y_i) + \frac{\partial}{\partial z}(\rho w Y_i) = \nabla \cdot \rho D_i \nabla Y_i + w'' \quad (7.4)$$

where w'' is the mass production rate of a species within a control volume and D_i is the diffusion coefficient. The rate of mass change of species Y_i is presented by the term $\frac{\partial(\rho Y_i)}{\partial t}$ and the mass flow of this species through the control surface due to mass diffusion is presented via the sum of the second, third and fourth terms on the right hand side of the equation.

The above equations are simplifications with a low Mach number approximation, $M < 0.3$, which is considered to be valid for reacting flows. The following assumptions are made for simplification in the FDS model (Moinuddin & Thomas 2009):

- The speed of flow is lower than the speed of sound
- The variables of temperature and density are large
- The variation of pressure is low

7.2.2 Heat Transfer Model

Conduction

The modelling of the temperature of solid objects in FDS is presented in detail elsewhere (McGrattan et al. 2008), however, a brief description of the modelling of the temperature of combustible opaque solids (such as pine, fabric) is given here. A one dimensional heat transfer equation for the solid phase temperature $T_s(x; t)$ applied in the direction x pointing into the solid, where the point $x = 0$ represents the surface is given by:

$$\rho_s c_s \frac{\partial T_s}{\partial t} = \frac{\partial}{\partial x} k_s \frac{\partial T_s}{\partial x} \quad (7.5)$$

where k_s , ρ_s and c_s are the thermal conductivity, density and specific heat of the solid material, respectively.

The boundary condition to calculate the surface temperature of combustible solid facing the direction of fire is given by:

$$-k_s \frac{\partial T_s}{\partial n} = \dot{q}_r'' + \dot{q}_c'' - \dot{m}'' \Delta H_V \quad (7.6)$$

where T_s is the temperature of the solid, k_s is the thermal conductivity of the wall material, \dot{q}_c'' is the convective heat flux, \dot{q}_r'' is the radiative heat flux and \dot{m}'' is the volatile production rate. For the back facing surface, two possible boundary conditions may be prescribed:

- (a) if the back facing surface is assumed to be open to either an ambient void or another part of the computational domain, the back facing boundary condition is similar to that facing the front;
- (b) if the back facing side is assumed to be perfectly insulated, an adiabatic boundary condition is used given by:

$$k_s \frac{\partial T_s}{\partial x} = 0 \quad (7.7)$$

Convection

For equation (7.7), \dot{q}_c'' is obtained from a combination of natural and forced convection correlations:

$$\dot{q}_c'' = h\Delta T ; \quad h = \max \left[C|\Delta T|^{1/3}, \frac{k_g}{L} 0.037 \text{Re}^{4/5} \text{Pr}^{1/3} \right] \quad (7.8)$$

where h is the convective heat transfer coefficient ($\text{W}/\text{m}^2 \text{ /K}$), ΔT is the difference between the wall and the gas temperature (taken at the centre of the grid cell abutting the wall), C is the coefficient for natural convection (1.52 for a horizontal surface and 1.31 for a vertical surface) (Holman 1986), L is a characteristic length related to the size of the physical obstruction, k_g is the thermal conductivity of the gas, and the Reynolds number (Re) is based on the density and velocity of the gases in the middle of the first grid cell and the length scale L , and the Prandtl number (Pr) is assumed to be 0.7. Since Re is proportional to the characteristic length, L , the convective heat transfer coefficient (h) is weakly related to L . For this reason, L is taken as 1 m for all calculations.

Radiation

For opaque combustible solid materials, it is assumed that the thermal radiation from the surrounding gases is absorbed within an infinitely thin layer at its surface and the net radiative heat flux is given by:

$$\dot{q}_r = \sum_{i=1}^4 \varepsilon_i F_{i2} \sigma T_i^4 - \varepsilon_s \sigma T_s^4 \quad (7.9)$$

incident radiation outgoing radiation

where ε_i is the emissivity of the i^{th} flame or surrounding surface, ε_s is the emissivity of the surface whose temperature (T_s) is being calculated, F_i and T_i are the corresponding view factor and temperature respectively. For a semi-opaque material like PMMA, the absorption coefficient describes the depth up to which radiation is absorbed. The FDS also calculates radiative heat transport through air and combustion gases along with any absorption within those using a finite volume method which is in general very complicated (McGrattan et al. 2008).

The radiative transport equation is given by:

$$s \cdot \Delta I(x, s) = k(x) [I_b(x) - I(x, s)] \quad (7.10)$$

where S is the unit normal direction vector, $I(x, s)$ is the radiant intensity, $k(x)$ is the absorption coefficient (i.e. the gas absorption coefficient = 4.6 m^{-1}), and $I_b(x)$ is the radiant energy source equal to $\sigma T_{(x)}^4 / \pi$, where σ is the Stefan-Boltzmann coefficient.

7.2.3 Pyrolysis Model

The Arrhenius equation presented as Equation (3.2) in CHAPTER 3 is a valid assumption for pyrolysis reactions and has been used in a number of previous studies (Li, Gong & Stoliarov 2015, Li & Stoliarov 2013). The value of \dot{m}'' in Equation (7.6) is calculated using:

$$\dot{m}'' = m \frac{dY}{dt} = m\beta \frac{dY}{dT} \quad (7.11)$$

Here, dY/dt represents the reaction rate. In the FDS software (version 6), the reaction rate model is based on a slightly different form of the Arrhenius function given by Equation (3.2) (see CHAPTER 3) with an oxidation function to account for local oxygen concentration. Although Equation (3.2) is not exactly the same as the expression used in the FDS program, it may reduce to the same form in special cases, including those of the current study.

7.2.4 Mixture Controlled Combustion Model

The combustion model of a single fuel uses a default simple chemistry, mixing-controlled combustion model involving one gaseous fuel. In the FDS software, the transport equations apply to only the collective species (i.e. fuel and products such as O₂, CO₂, H₂O, N₂, CO and soot), which are solved and the default background for the collective species is air. However in FDS version 6, there options for: (i) complex modelling involving multiple fuels, (ii) specifying individual species instead of collective species, and (iii) finite-rate chemistry which requires very fine grid resolution making it impractical for large-scale fire applications.

In the mixture-controlled method, single fuel species that are composed primarily of C, H, O, and N react with oxygen in one mixing controlled step to form H₂O, CO₂, soot, and CO where the reaction of fuel and oxygen is considered to be infinitely fast. Semi-empirical rules are invoked by FDS to determine the rate of mixing of fuel and oxygen within a given mesh cell at a given time step. Each computational cell can be thought of as a batch reactor where only the mixed composition can react.

The variable, $\zeta(t)$, denotes the unmixed fraction, ranging from zero to one and is governed by the equation:

$$\frac{d\zeta}{dt} = \frac{-\zeta}{\tau_{mix}} \quad (7.12)$$

Here, τ_{mix} is the mixing time scale. The change in mass of a species is determined from the combination of mixing and the production/destruction rate of the chemical reaction.

If a cell is initially unmixed, $\zeta = 1$ by default and the combustion is considered non-premixed, however, if the cell is initially mixed, $\zeta = 0$ and the combustion is considered premixed. The FDS uses the chemical formation of the fuel to determine the amount of combustion products (CO₂, H₂O, N₂, CO and soot) that are formed. The heat release rate per unit volume (HRR_{puv} or $\dot{\mathcal{Q}}''$) is obtained by summing the combined species mass production rates (\dot{m}''_{α}) multiplied by their respective heats of formation

($\Delta H_{f,\alpha}$):

$$\dot{\mathcal{Q}}'' = -\sum_{\alpha} \dot{m}''_{\alpha} \Delta H_{f,\alpha} \quad (7.13)$$

Burning usually takes place at a distance from the fuel surface only where the fuel to oxygen ratio is at the optimum stoichiometric value.

7.3 Numerical Simulation

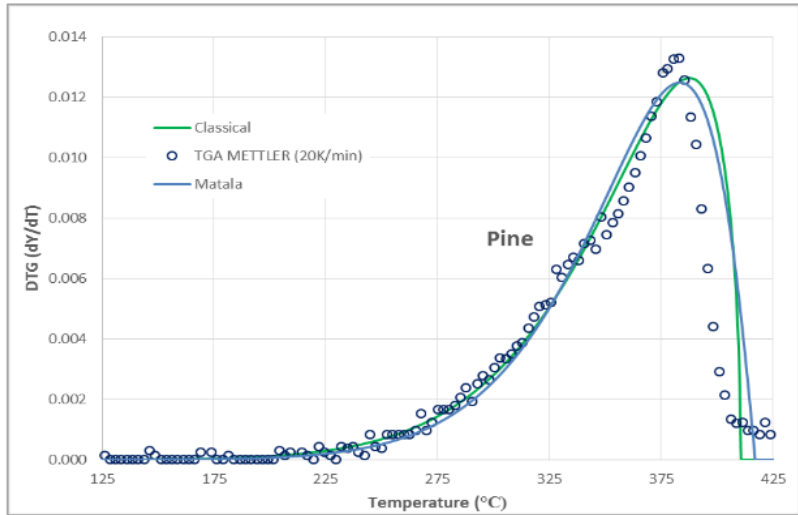
7.3.1 TGA simulation

Classical Theory (Arrhenius equation)

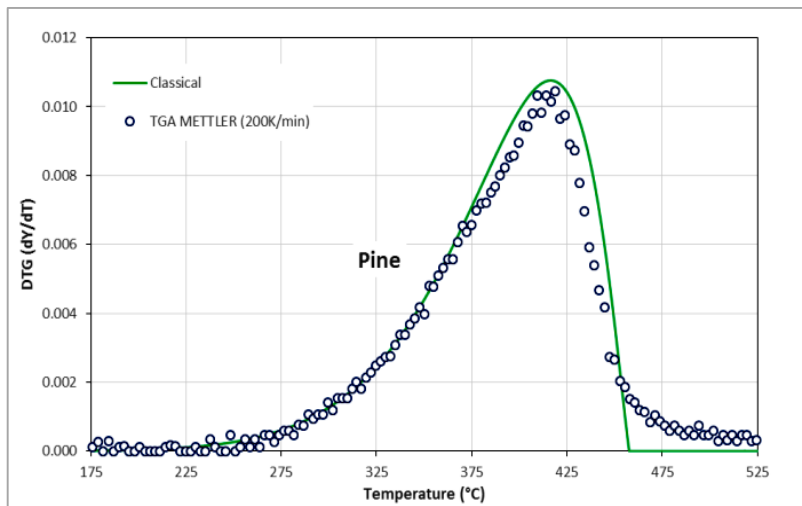
To check the validity of the values of A , E and n determined experimentally, dY/dT is calculated by solving Equation (3.2) (see CHAPTER 3). This was achieved using a classical forward differential method with a temperature step of 0.25 K (based on a sensitivity analysis) incorporating the kinetic values from Figure 4.8 in CHAPTER 4. In Figure 7.1, it is evident that the profiles obtained using this classical method are in strong agreement with the experimental results obtained at different heating rates. Similarly, in Figure 7.1(a), the profile calculated using the kinetic parameters of Matala (2008) also agree well with the experimental results of the current study. In addition, the use of parameters from Table 4.2 (CHAPTER 4), also provides a close match between the experimental moisture data and the simulated numerical profile. This provides further evidence of the quality of the experimental data as well as the adequacy of the inflection point method. This also suggests that the values of kinetic triplets are not unique however, applying them into Arrhenius equation; the experimental profile can be very closely reproduced. Vyazovkin (1992) proposed that the kinetic triplet is ambiguous and cannot adequately describe chemical kinetics, although it may be suitable for simple processes.

TGA Modelling Using FDS

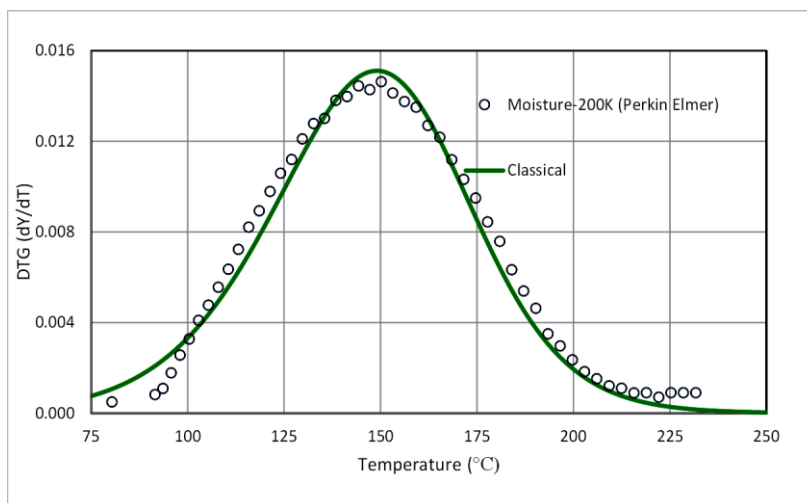
To confirm the efficacy of the kinetic values to serve as input parameters for the numerical simulation of pyrolysis, the FDS was used to perform several computations. In these simulations, FDS was tasked to simulate the solid phase only using the kinetic parameters from Figure 4.8 and Figure 4.9 of CHAPTER 4 and the sample was heated by radiation only. For these simulations, the sample was modelled as an obstruction of 2m long wide, 1m wide and 0.000001m thick placed horizontally at the bottom of a two-dimensional domain. It was heated (radiation only) from surrounding surfaces and only solid phase reaction was considered. The two-dimensional domain size was 4m x 1m and number of grids were 3 and 4 respectively. Sensitivity study showed that for solid phase only this resolution was adequate. The full input files of representative cases and a visualisation of the domain can be found in [Appendix C](#).



(a) 20 K/min

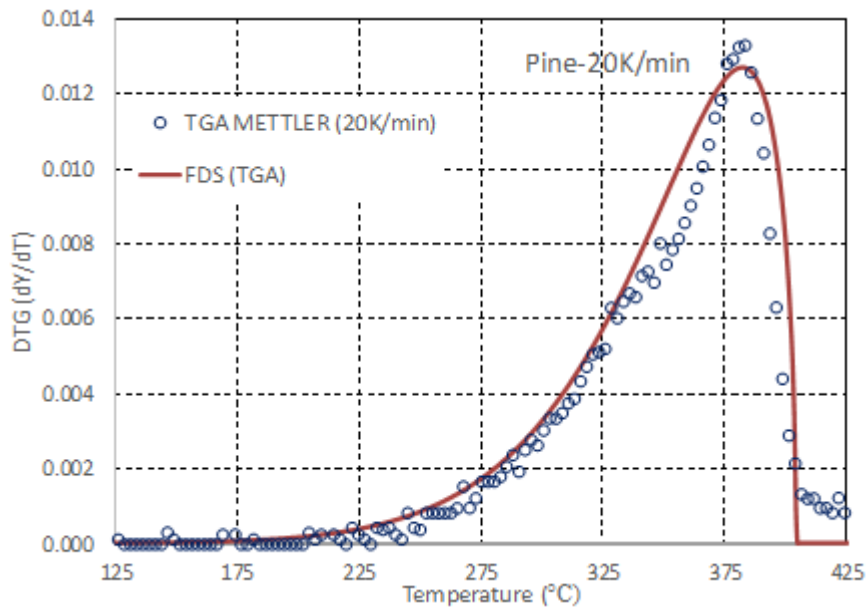


(b) 200 K/min

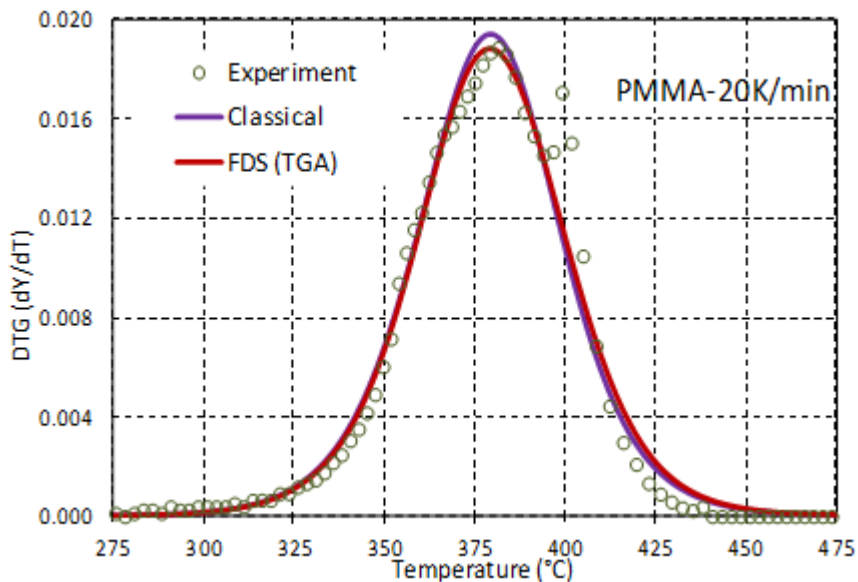


(c) Moisture

Figure 7.1: Simulation of pine DTG curve using experimental kinetic data



(a) Pine



(b) PMMA

Figure 7.2: Simulation of pine and PMMA DTG curves using experimental kinetic data at 20 K/min heating rate

The simulated DTG vs temperature profiles were calculated using representative sample masses and temperatures. The results from the FDS simulation of the TGA tests for pine and PMMA at 20 K/min heating rates are presented in Figure 7.2. From these results, it is evident that the TGA experiments are well predicted by the FDS using the experimental input parameters. A detailed study of char carbonization is out of the scope of the study and therefore is not presented.

7.3.2 Cone Calorimeter Simulation

For the cone calorimeter simulations, the FDS input data files are created to resemble the experimental set-up for the instrument. The burning of an appropriate sized sample is simulated with a specified heat flux to represent the effect of the cone heater without including the cone itself. The fuel-pan is modelled as an obstruction with dimensions similar to the actual size that is appropriately placed. The top face of the obstruction is used to simulate the fuel surface and the other faces are modelled as steel sheet. In all cases the back of the sample was considered to be insulated as they were encased or near insulated during the experiments with only the sample face exposed. Simulations were carried out at two irradiances, 30 and 50 kW/m², using a supercomputer employing four processors for each simulation. For these simulations, the sample was modelled as an obstruction of 100mm x 100mm x 25mm for PMMA and 100mm x 100mm x 19mm for pine placed horizontally at lower end. The overall domain size was 200mm x 200m x 1000mm which was open in all sides and cuboid grid sizes that were tested is discussed in the next page.

To model the coupled pyrolysis and combustion process, various input parameters are required for the FDS. These include combustion parameters (from the cone calorimeter), thermo-physical properties (from the HDA) and pyrolysis parameters (from the TGA and DSC) of the test materials. The prediction of HRR in the FDS model requires the input of multiple parameters but not all parameters were not measured directly such as emissivity and absorption coefficients. The experimentally derived parameters included one set of char yield data (from the TGA) and one set of char residue data (cone experiments), and multiple sets of pyrolysis data at various heating rates. Since various setting and options are available in FDS, a HRR prediction sensitivity analysis was conducted in accordance with that of Linteris (2011). The work of Linteris (2011) was focused extensively on the pyrolysis rate of PMMA. Here we performed a similar analysis, but we focussed upon the coupled pyrolysis and combustion simulation of pine.

The results of the cone calorimeter experiments of four combustion parameters obtained at 50kW/m² and used in the sensitivity study are listed in Table 7.1.

Table 7.1: Experimental combustion parameters

Properties	Pine	PMMA
Heat of combustion (kJ/kg)	11210	21463
Soot yield (kg/kg)	0.006	0.014
CO yield (kg/kg)	0.007	0.009
CO₂ yield (kg/kg)	1.140	2.091

The values of the input parameters are kept constant when performing the sensitivity study to simulation cone calorimeter experiments where these same input parameters are constant. It is also critical to obtain grid convergence of the numerical results to minimise or remove numerical error and therefore the sensitivity study was carried out by varying the grid, the thermo-physical properties and the pyrolysis parameters.

Grid Convergence

To test for convergence of the PMMA and pine fire HRR results, a number of simulations were conducted using various grid sizes. In all material burning simulations, the input parameters and boundary conditions were unchanged and only the grid size was altered. The grid sizes were initially coarse and were incrementally reduced by a factor of two. In Figure 7.3, the simulated HRR vs time profiles are presented for PMMA and pine. In each of these figures, only three simulation results using three finest grid sizes (10 mm, 5 mm and 2.5mm) are shown. The full input files of representative cases and a visualisation of the domain can be found in [Appendix D](#). It is evident that in for both materials, the 10 mm grid size resulted in a very high HRR compared to the other two cell sizes. The results of the simulations using the two smaller grid sizes were almost identical suggesting that the FDS result for the cone calorimeter test simulations numerically converges at a grid spacing of approximately 5 mm.

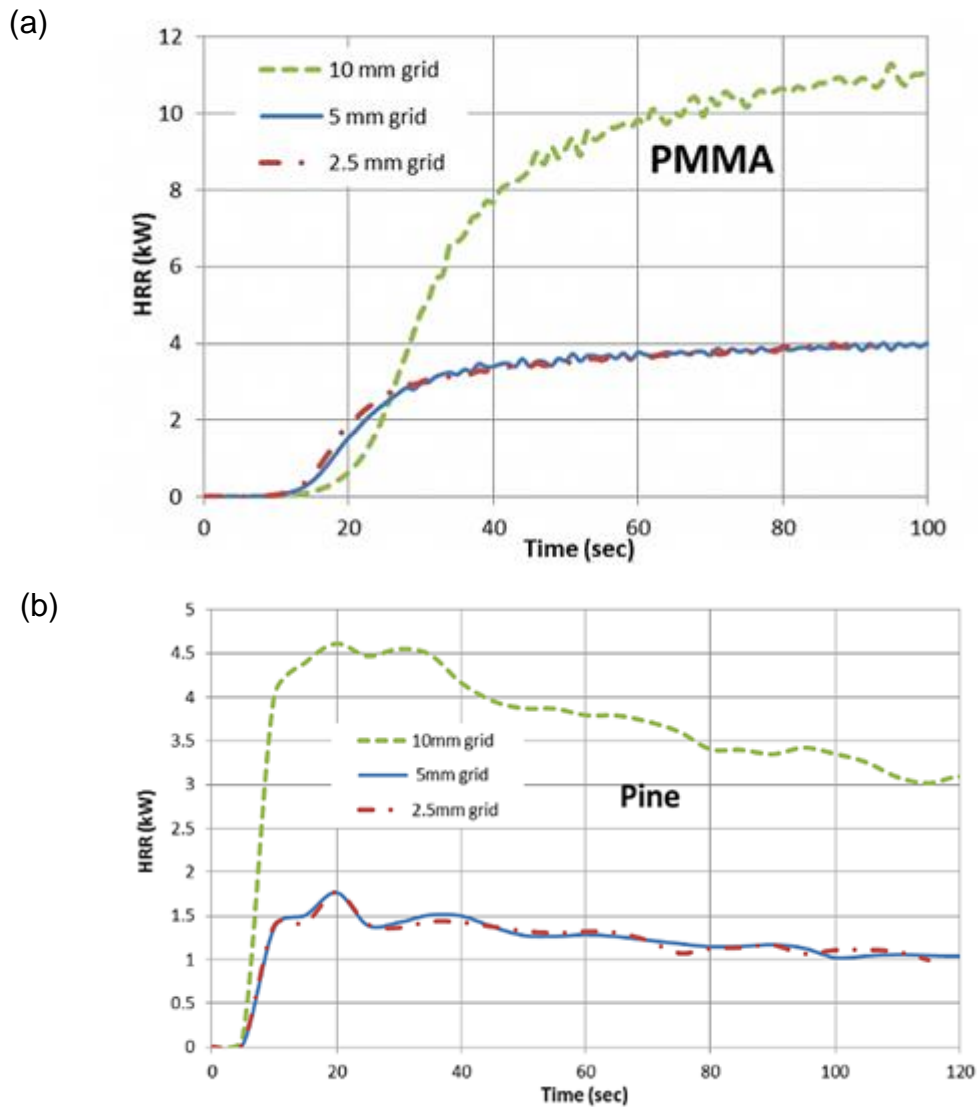


Figure 7.3: Grid convergence tests for PMMA and pine

Sensitivity of Thermo-physical Properties

The thermo-physical properties obtained in this study for PMMA and virgin pine that were input into the FDS simulation are presented in Table 7.2. As k and C_p values for pine vary with temperature, these were specified as functions of temperature in FDS using a piecewise function. This function can be implemented in FDS using the integrated RAMP function which allows users to control the behaviour of these two parameters as determined experimentally. This is described further in Section 7.4 with an example presented accordingly. Table 7.2 also presents literature values for steel, and since these values are so widely accepted, especially in fire research (McGrattan et al. 2012), these are not considered for sensitivity analysis. The values presented in

the table are held unchanged for the respective material simulations at the different irradiance levels.

Table 7.2: Specified thermo-physical properties

Property	Pine	PMMA	Steel [#]
	T = temperature , F = value of property		
Thermal conductivity (W/m.K)	T= 20., F=0.168 / T=225., F=0.2 /	0.195	T= 20, F=50. / T=677, F=30.6 /
Specific heat (kJ/kg.K)	T= 20., F=1.1 / T=60., F=1.23 / T=225., F=1.7/	1.47	T= 20., F=0.46/ T=377., F=0.60/ T=677., F=0.91/
Density (kg/m³)	460 (at 30 kW/m ²) 423 (at 50 kW/m ²)	1171 (at 30 kW/m ²) 1210 (at 50 kW/m ²)	7850

from (Incropera et al. 2006)

For the PMMA simulations, an emissivity of 0.85 (Hallman 1974) and an absorption coefficient of 2700 m⁻¹ was used (Tsilingiris 2003). Linteris (2011) did not observe a significant sensitivity of the absorption coefficient to the pyrolysis rate, especially for high irradiances and did not include emissivity in the sensitivity study. Similarly, these two parameters were also not significantly sensitive to the average pyrolysis rate in the study of Chaos (2013). Given these previous reports, it is acceptable to exclude them from the sensitivity study in the current work.

The sensitivity of some input parameters to various thermo-physical properties can be significant. By using FDS, Kempel et al. (2012) demonstrated that varying the input parameters (*k*, *C_p* etc.) as a function of temperature resulted in better agreement with experimental data. In other reports, the pyrolysis rate of PMMA has been observed to show sensitivity to *C_p* values (Chaos 2013, Linteris 2011) so therefore, the coupled pyrolysis and combustion model sensitivity to *C_p* values for PMMA were explored and are demonstrated in Figure 7.7(a).

For charring materials, the sensitivity to the properties of char can be significant. Chaos (2013) showed this to be the case for conductivity for low levels irradiance and to emissivity for high levels of irradiance. As discussed earlier, it is experimentally challenging to obtain the thermo-physical properties of char due to its tendency to break

into irregular shapes. For pine, three sets of k , C_p and ρ data were used for the sensitivity studies as shown in Table 7.3:

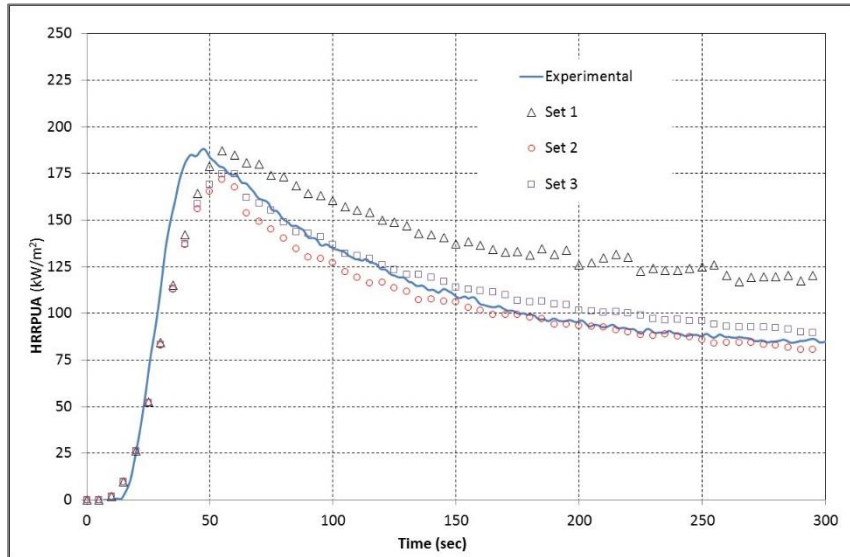
- Set 1: FDS (version 5) example of a charring solid (McGrattan et al. 2008) & low C_p (Grønli 1996)
- Set 2: Current study - flat pine (Figure 6.3 and Figure 6.8).
- Set 3: Current study - structural pine (Figure 6.3 and Figure 6.8).

In the sensitivity study, the emissivity is taken as 1 due to the black colour (carbon black) and the absorption coefficient of $50,000 \text{ m}^{-1}$ was used which represents the radiation absorbed at the surface. The same values were adopted for the blackened steel of the fuel pan.

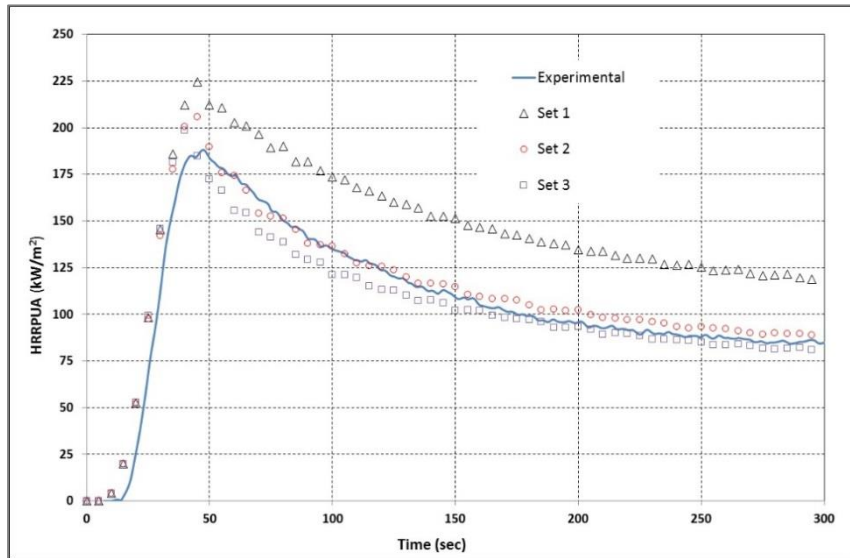
Table 7.3: Specified thermo-physical properties

Properties	Unit	Set 1	Set 2	Set 3	
Density	kg/m ³	140	FDS5 example	110	163
Thermal conductivity	W/m/K	T= 20., F=0.08 / T=900., F=0.25 /	charring solid (McGrattan, Hostikka et al. 2008)	T= 20., F=0.069 / T=120., F=0.102 /	T= 25., F=0.069 / T=150., F=0.083 /
Specific heat	kJ/kg/K	0.43	(Grønli 1996)	T= 20.,F=0.724 / T=120.,F=1.097 /	T= 25.,F=1.256 / T=150.,F=2.118 /

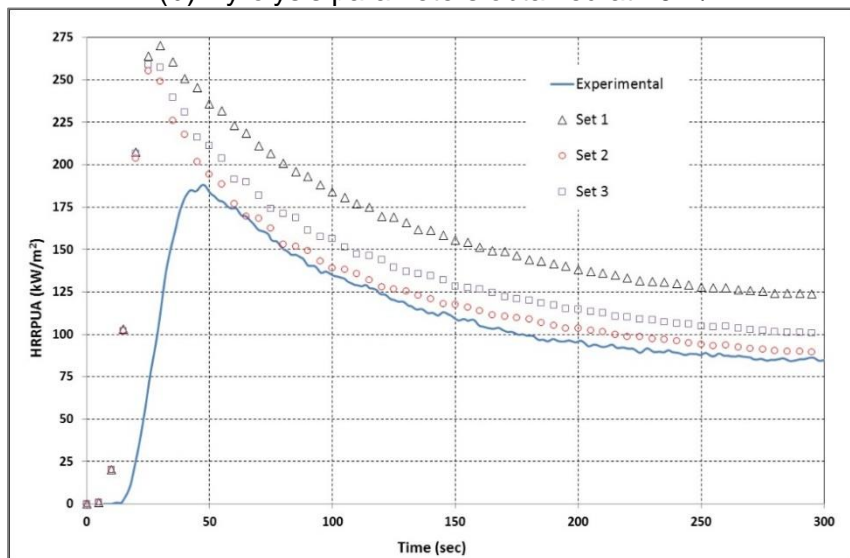
For each pine slab burning simulation based on the cone-calorimeter test, 3.5% moisture content determined experimentally was used (see CHAPTER 4) along with a char residue of 12.6% (see Figure 5.12 in CHAPTER 5). Using these and the other parameters shown in Table 7.3, nine simulations at a 50 kW/m^2 irradiance level were conducted for a period up to 300 seconds. The solution domain and the boundary conditions were the same as given in page 138-9 and 5 mm grid size were used (the visualisation representation is the same as Figure D.1). The full input files of representative cases can be found in [Appendix E](#). In the first three simulations, pyrolysis parameters obtained at 5 K/min along with one set of char properties (from Table 7.3) were used in each simulation and the results are presented in Figure 7.4(a). Similarly, the results in Figure 7.4(b) were determined using the pyrolysis parameters obtained at 20 K/min with varied char properties. Finally, the results shown in Figure 7.4(c) were obtained when char properties were varied while keeping the pyrolysis parameters obtained at 200 K/min unchanged (see Figure 4.8 of CHAPTER 4). In each case, the real experimental result is also plotted.



(a) Pyrolysis parameters obtained at 5 K/min



(b) Pyrolysis parameters obtained at 20 K/min



(c) Pyrolysis parameters obtained at 200 K/min

Figure 7.4: Fire simulation sensitivity to pine char properties (50 kW/m² irradiance)

For all three sets, it is evident that with Set 1 char properties, the HRR per unit area (HRR_{PUA}) predictions are significantly high. Conversely, the difference between the results obtained using Set 2 and Set 3 char properties is not significant and they are relatively closer to the experimental results obtained. However their effects on HRR_{PUA} prediction are different among three sets. For example, in Figure 7.4 (a) and (c), a higher HRR_{PUA} is predicted for Set 3 compared to Set 2 and this trend is reversed in Figure 7.4 (b). It should be noted that Set 2 represents results obtained for the burning of the pine slab in the cone calorimeter tests.

The sensitivity to emissivity and absorption coefficient of virgin pine was conducted as very few comparative sensitivity studies with respect to the pyrolysis rate of pine involving these two parameters. This is an important consideration despite the rapid blackening of the pine surface upon ignition and that the radiation is mostly likely to be absorbed at the surface. It should be noted that pine char residue of 10.6% and 12.6% remained unburned after the cone calorimeter test with irradiance levels of 30 and 50 kW/m^2 respectively. However, a higher char yield of 18.5% remained after the TGA test thus numerical simulations with both char yield/ residue were conducted as part of the sensitivity study. Using the pyrolysis parameters obtained at 20 K/min heating rate the char properties (Set 2 in Table 7.3) simulations at 50 kW/m^2 irradiance were conducted by varying the parameters outlined in Table 7.4. The results of this sensitivity analysis are presented in Figure 7.5 where Set 2 in Figure 7.4(b) is considered to be the baseline result for this analysis.

Table 7.4: Physical properties for sensitivity analysis

Properties	Nominal Value	Varied Value
Emmissivity	1	0.4
Absorption Coefficient (m^{-1})	50,000 (default)	9990
Char yield/ residue	12.6% (at 50kW/m ²)	18.5%

It is evident from Figure 7.5 that a 60% reduction in emissivity resulted in an increased HRR prediction by nearly 25%. The reason may be that if the emissivity of the sample is lower, once it is heated, radiation from it to the surrounding air is also lower and as a result the sample retains more heat leading to higher pyrolysis. A 5-fold decrease in the absorption coefficient resulted in an increase in HRR by approximately 35%

whereas changing the char yield/residue from 12.6% to 18.5% resulted in a 30% decrease of the HRR values. The variation with experimental values is the most significant for the results obtained with 18.5% char yield based on the TGA test. Therefore, for this study, the char residue from the cone calorimeter test were selected as the best candidates for the input variables to conduct representative simulations.

Selection of Pyrolysis Parameters

The HRR_{PUA} measured for pine and PMMA slabs exposed to irradiance levels of 30 and 50 kW/m² in the cone calorimeter were considered as benchmark experimental values for FDS validation. The results of these validations are presented in Figure 7.6 and Figure 7.7 where full duration FDS simulations were carried out using combustion data from Figures 5.6 and 5.12, thermo-physical parameters from

Sensitivity of Thermo-physical Properties

The thermo-physical properties obtained in this study for PMMA and virgin pine that were input into the FDS simulation are presented in Table 7.2. As k and C_p values for pine vary with temperature, these were specified as functions of temperature in FDS using a piecewise function. This function can be implemented in FDS using the integrated RAMP function which allows users to control the behaviour of these two parameters as determined experimentally. This is described further in Section 7.4 with an example presented accordingly. Table 7.2 also presents literature values for steel, and since these values are so widely accepted, especially in fire research (McGrattan et al. 2012), these are not considered for sensitivity analysis. The values presented in the table are held unchanged for the respective material simulations at the different irradiance levels.

Table 7.2, and other properties discussed above as input parameters. The computational domain was extended to capture all of the combustion activity as shown in Figure 7.8 and Figure 7.9.

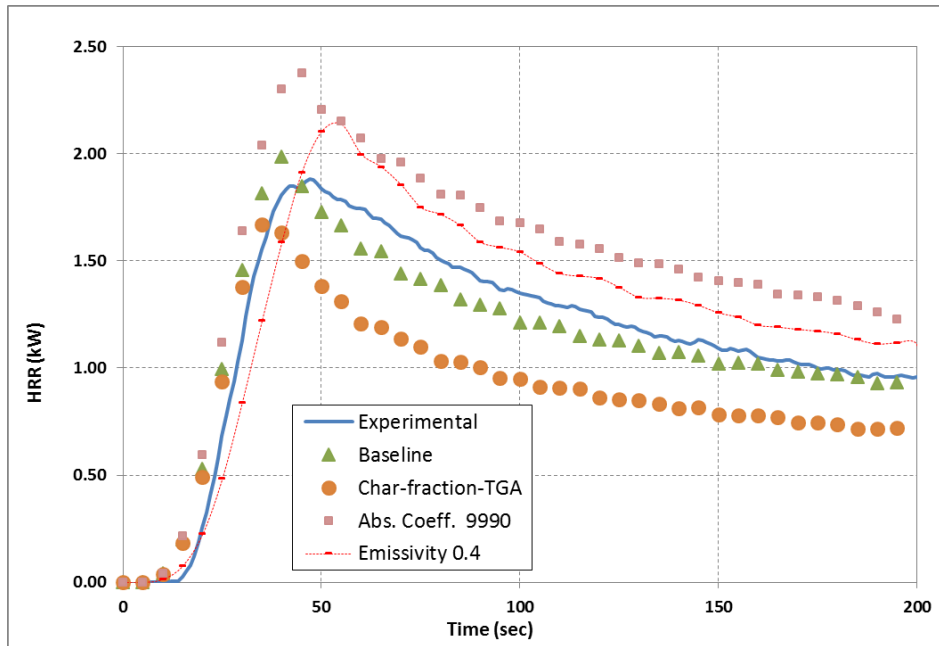


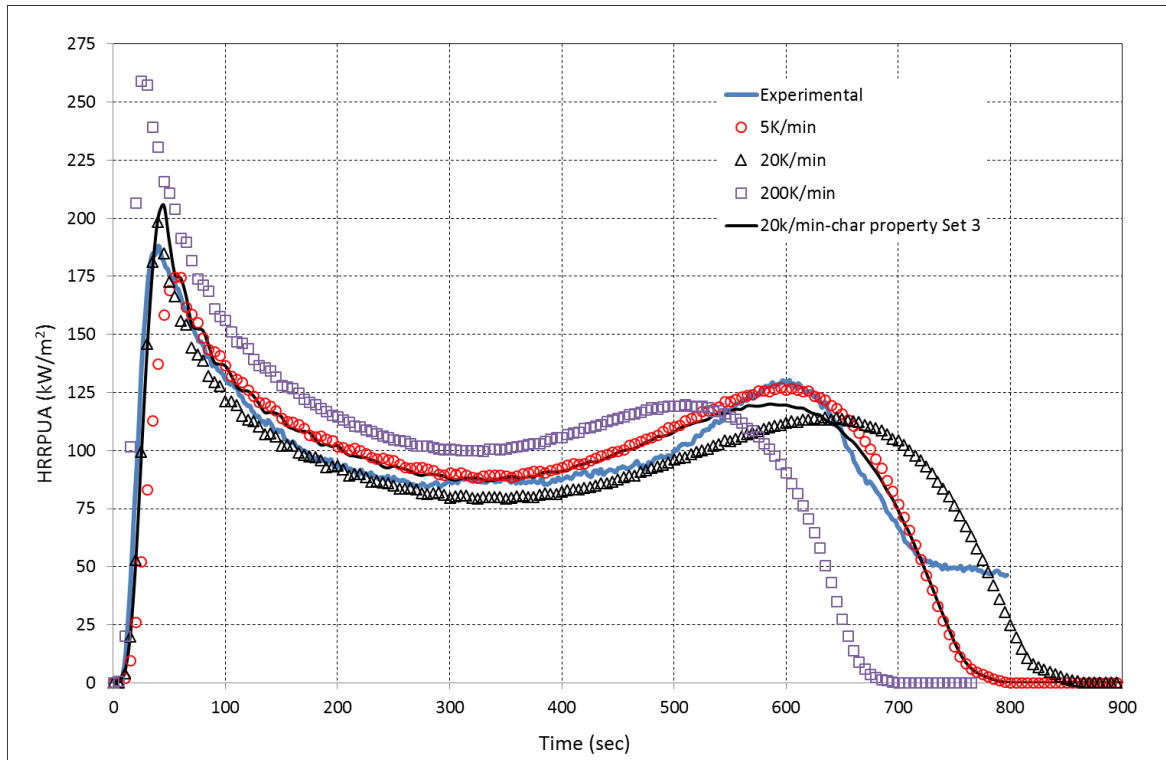
Figure 7.5: Variation of emissivity, absorption coefficient and char fraction (irradiance 50 kW/m²)

Several pine fire simulations were conducted for each experimental condition using kinetic and *HoR* data obtained at different heating rates from Figure 4.8 of CHAPTER 4 and the numerical HRR_{PUA} results are presented in Figure 7.6 with the corresponding experimental result. In Figure 7.6(a), where the 50 kW/m² irradiance results are shown, two simulation results with different char properties are presented. Comparing the HRR profiles obtained using input parameters from three heating rates, it can be observed that up to ~300 seconds the closest simulation is obtained using input parameters obtained from the 20 K/min heating rate. However, after 300 seconds, the closest result is obtained using input parameters from the 5 K/min heating rate, especially in the region of the second peak. It is likely that the 20 K/min heating rate is closely associated with the 50 kW/m² irradiance level in the early part of the burning process, whereas at 5 K/min heating rate, with a faster rate of rise in HRR_{PUA} , is better associated in the later part. It can also be seen that the results of the char properties outlined in Set 3 of Table 7.3 show closeness with the experimental results throughout and this confirms the high sensitivity of HRR_{PUA} to char properties.

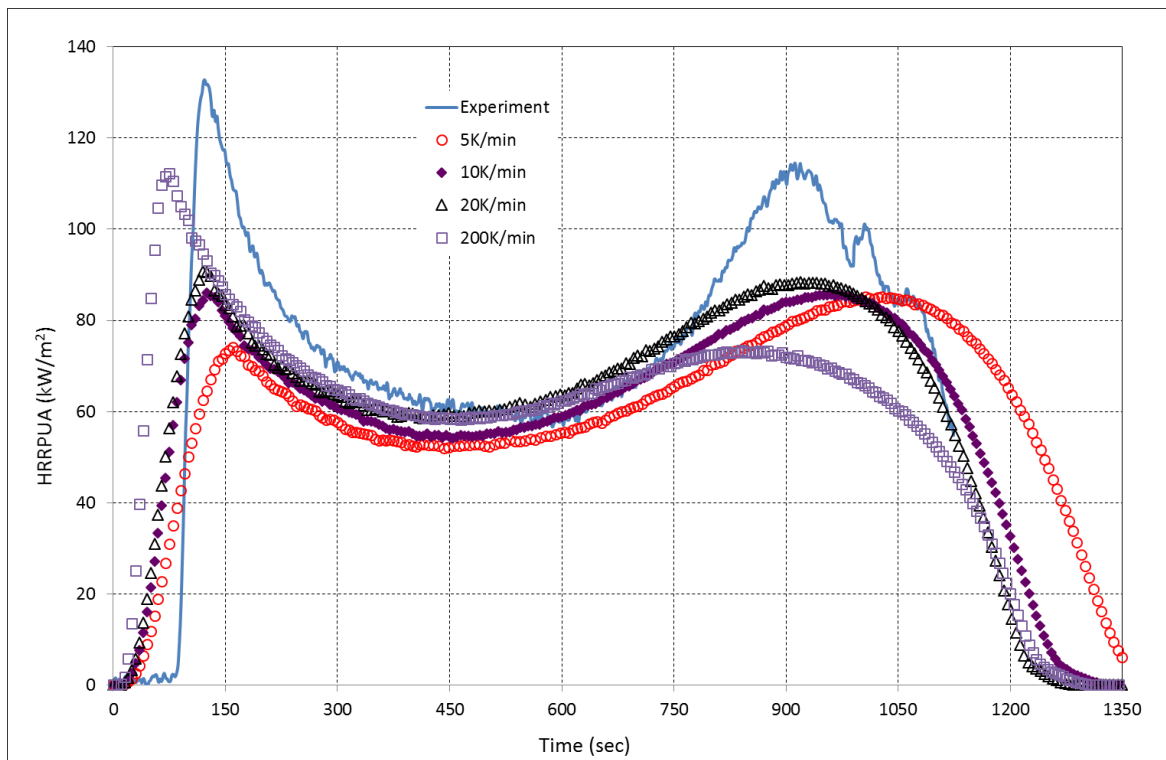
In Figure 7.6(b), the experimental and numerical results associated with the 30 kW/m² irradiance obtained separately using pyrolysis parameters at different heating rates are presented. It is evident that the results obtained using data from the 10 and 20 K/min heating rates are quite close to experimental results beyond ~500 seconds. However,

to capture the first peak very high heating rates (≥ 200 K/min) are needed but this may not adequately capture the second peak.

Overall, it can be concluded from Figure 7.6 that the burning of the pine slab in the cone calorimeter is reasonably predicted by the FDS coupled pyrolysis and combustion model when appropriate values are used as input parameters. It can even predict the second peak reasonably well which until now has been elusive for such models. The first peak, in this case, appears to correspond with the initial pyrolysis of the top layer of the material. Hagge, Bryden and Dietenberger (2004) suggested that the second peak phenomenon is caused by the pyrolysis of the bottom of the material due to the rapid increase of heat transfer to the remaining virgin wood. Since the temperature increase only involves a small area of the sample, this leads to the release of the pyrolysis gases. They also observed that the secondary peak is not as pronounced in the numerical simulation as it is in the cone calorimeter data. Another theory is that the second peak is caused by the thermal wave of the fuel reaching the lower surface of the sample (Brown, Braun & Twilley 1988) as discussed previously in CHAPTER 5.

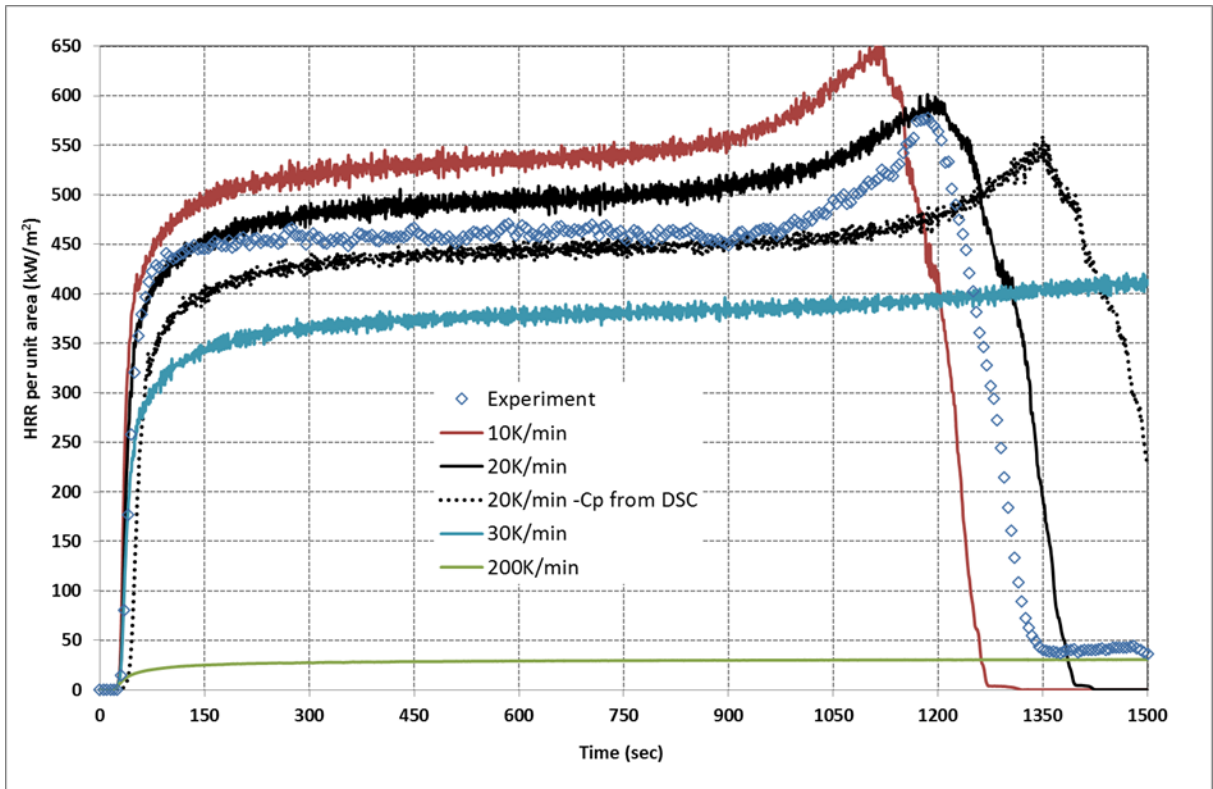


(a) 50 kW/m²

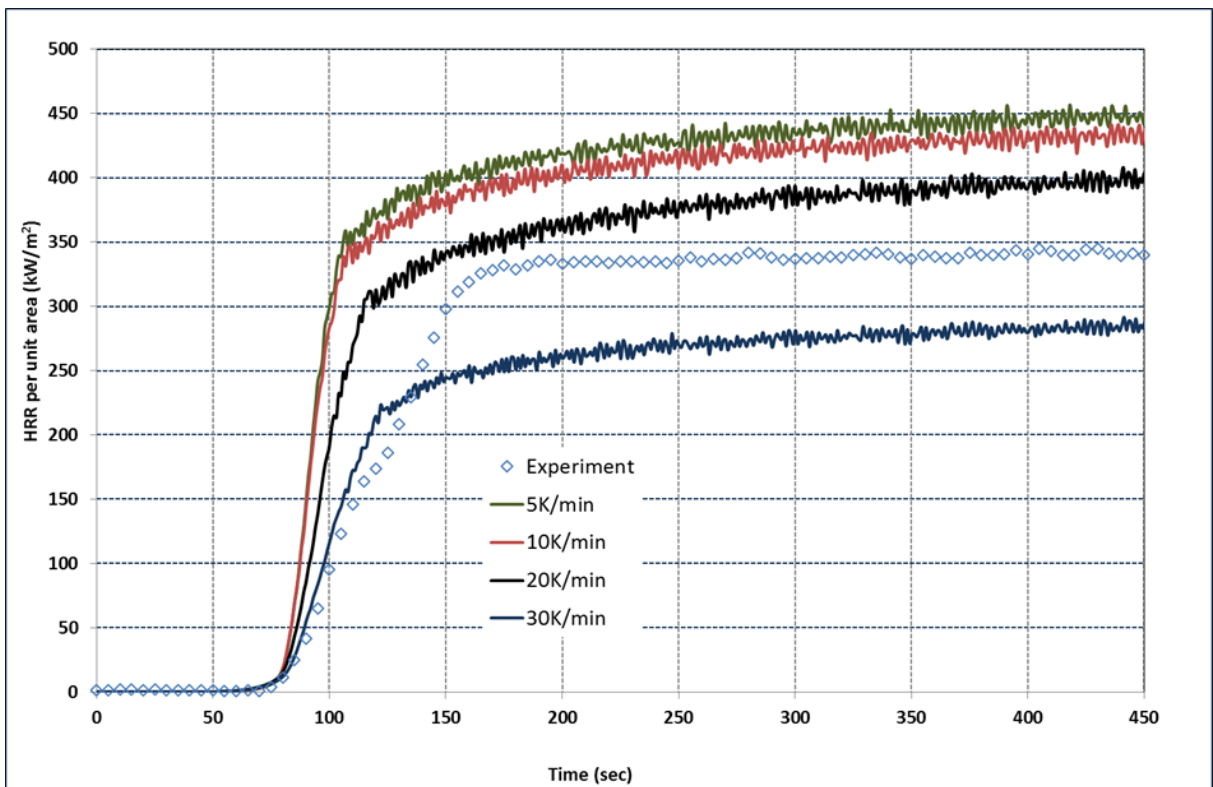


(b) 30 kW/m²

Figure 7.6: Experimental and simulation results obtained using kinetic triplets and HoR at various heating rates for pine



(a) 50 kW/m²



(b) 30 kW/m²

Figure 7.7: Experimental and simulation results for PMMA at various heating rates

The results of a non-prescribed fire simulation of a burning PMMA sample are shown Figure 7.7, which also shows the experimental result for comparison. The simulation results at 50 kW/m² irradiance using the kinetic triplets and *HoR* obtained with 10, 20, 30 and 200 K/min heating rates (from Figure 4.9 of CHAPTER 4) for PMMA are presented in Figure 7.7 (a). Input values of *k* and *C_p* were taken from the HDA measurement in the current study, with the exception of one simulation (“20K/min-*C_p* from DSC”) where the Perkin Elmer DSC value for *C_p* and the HDA value of *k* were used (Abu-Bakar & Moinuddin 2012). This figure shows that the simulation results with parameters obtained at lower heating rates yield higher HRR values. Comparison of the results from simulations showed that experimental heat release rate profile lies across numerical profiles predicted by FDS. This is also observed for the pine simulation shown in Figure 7.6(b), but not as strong as in PMMA simulation shown in Figure 7.7(a).

Not unlike the first part of pine fire simulations using the 50 kW/m² irradiance level, it is again observed that the closest result to the experimental data for PMMA is obtained using input parameters from the 20 K/min heating rate. The “20K/min-*C_p* from DSC” simulation results in an even closer fit to the experimental result, especially between 500 and 950 seconds. The difference between the “20K/min” and “20K/min-*C_p* from DSC” results also confirm the sensitivity of the HRR prediction to *C_p* as observed by Linteris (2011) and Chaos (2013) to the pyrolysis rate. In Figure 7.7(a), although a steady burning trend is observed between 250 and 900 seconds in the experimental result, a gentle slope is observed in the simulation results over that same time period. A peak only occurs during the final stages of burning in the cone calorimeter test and this is due to the extinguishment/flameout of the sample. This event is reasonably captured in the modelling (please refer to the profile associated with kinetic triplets and *HoR* obtained at 10 and 20 K/min heating rates).

The PMMA fire simulation obtained using a 30 kW/m² irradiance along with the parameters obtained using 5, 10, 20 and 30K/min heating rates are presented in Figure 7.7 (b). Similar to the 50 kW/m² irradiance case, the experimental HRR_{PUA} profile mainly lies between predicted profiles associated with parameters obtained at 20 and 30K/min heating rates.

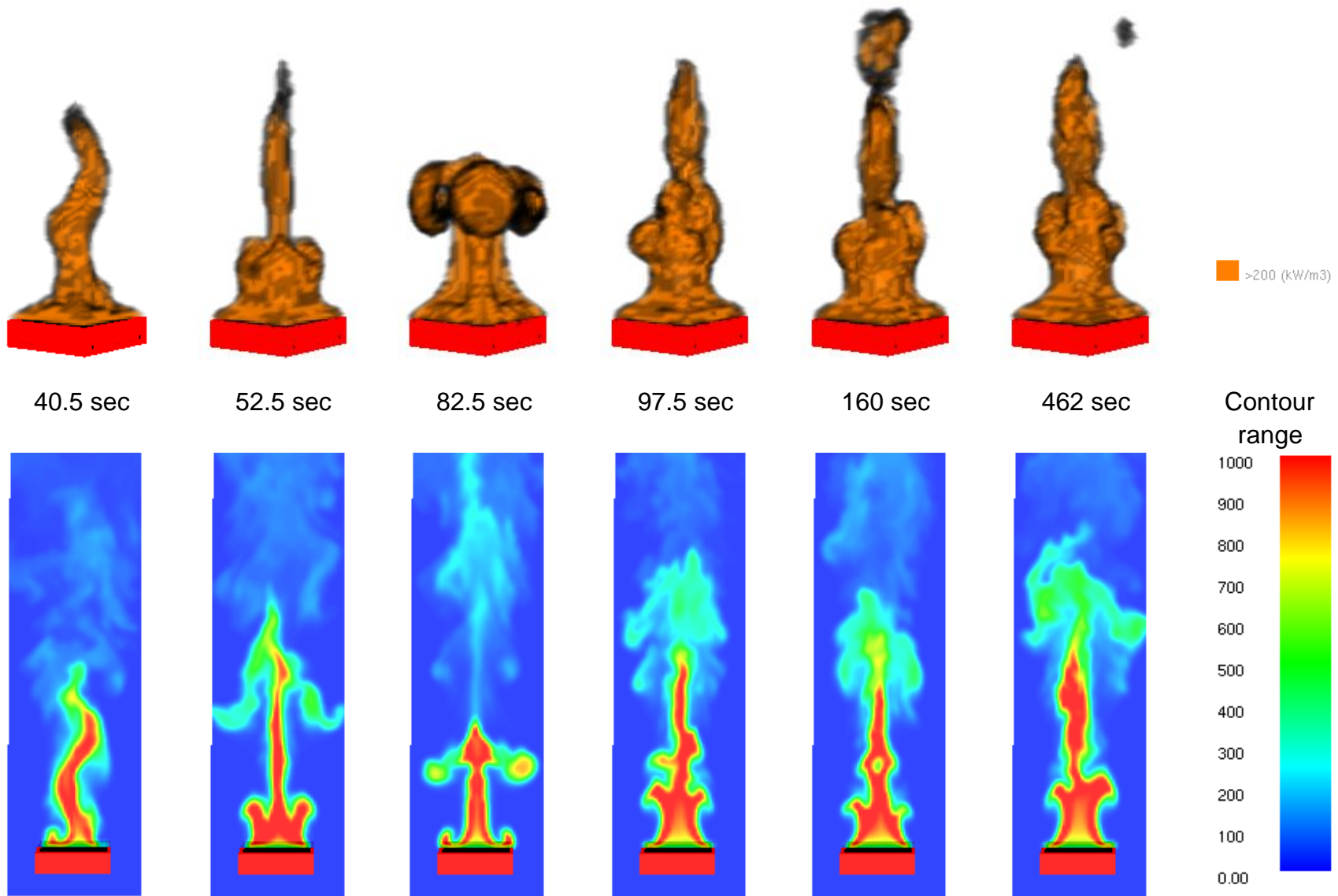


Figure 7.8: Modelled flaming combustion of PMMA slab using FDS

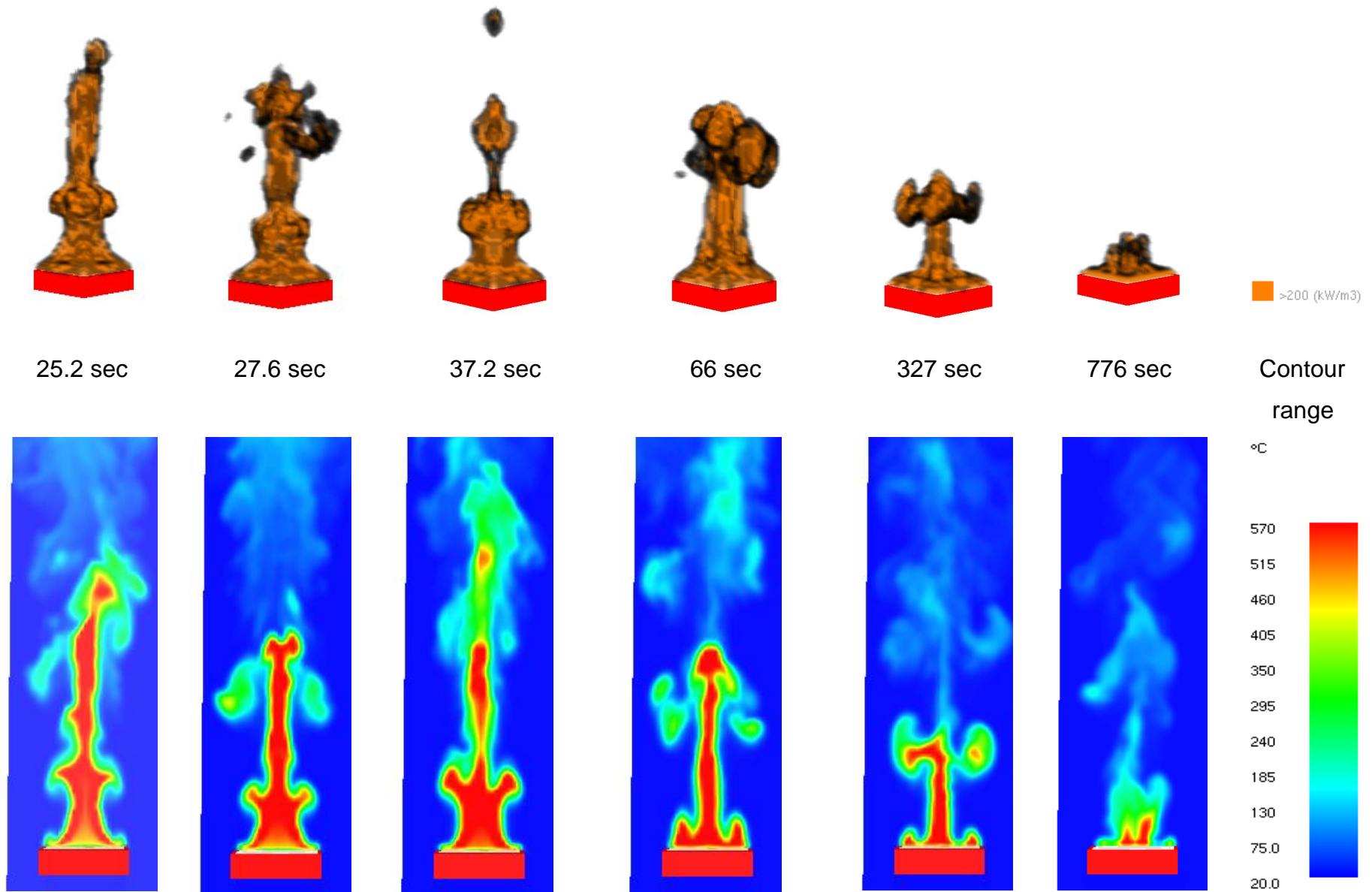


Figure 7.9: Modelled flaming combustion of Pine slab using FDS

It is also likely that if the values of the kinetic triplet and *HoR* relevant to changing heating rates are used to simulate the growth or burnout of a fire, more appropriate predictions can be obtained. Although this aspect is not well addressed in the literature, there are two kinds of approaches to investigate this possibility that which will be discussed further in Section 7.4. Until a detailed model is developed, gross estimates can be roughly modelled with parameters associated with 20 K/min heating rates which can be useful for practical engineering analysis.

In Figures 7.8 and 7.9, snapshots rendered using the FDS companion program, Smokeview, are presented showing the characteristic stages of PMMA and pine burning respectively, similar to the analysis presented by Mell et al. (2009). In both figures, the input parameters were obtained from the 20 K/min heating rate test data. The top row of these figures shows the three-dimensional flame represented a HRR_{PUV} greater than 200 kW/m³ and temperature slice files representing thermal contours are shown along the bottom row.

Very fine grid resolution has resulted in a clear depiction of fine structures in the flames. The temperature slice files reveal that much higher temperatures of flame are reached in the PMMA fire simulation than in the pine fire. This consistent with Figure 7.7 which shows that higher HRR_{PUA} is measured and predicted for the PMMA fire.

7.4 Optimised Use of Input Parameters

As the fire grows in a real fire event, the combustible materials exposed to fire receive different irradiance levels and are heated at different rates (dT/dt). Ideally, simulations should be performed by using appropriate values for temperature, heating rate, and irradiance at each computational node or cell for the fire conditions.

For pyrolysis simulations, Donskoi and McElwain (1999) proposed a method for altering the values of the *A* and *E* relevant to changing heating rates. In another method, Li et al. (2014) coupled Kissinger's method (1956) with an optimisation method to obtain a single kinetic triplet across three heating rates; the triplet was then extrapolated to a fourth heating rate and reasonable agreement with experimental data was found. Furthermore, it is possible to determine kinetic triplets for various reaction paths or for various components within the sample by an optimisation process (Shi &

Chew 2013). However, none of these methods is expanded to include the effects of HoR or C_p as functions of heating rate, and are not applied to fire scenarios where solid and gas phase reactions are coupled.

Optimisation methods are also proposed by Lautenberger et al. (2006) to obtain an optimised single set of all properties including kinetic triplets and HoR to match cone calorimeter measurements, where the solid phase is directly modelled and a fixed gas phase heat source is considered. It would be tremendously computationally “expensive” to include the gas phase reaction modelling in the optimisation process. For example, in the FDS simulations conducted in this study, a 1200 second (physical time) simulation of PMMA fire required 600 CPU hours using 4 Open MPI processors (on a cluster with 64 nodes, each node corresponds to 16 AMD Opteron(tm) 6128 CPUs, which run at 2GHz, and has 2GB per CPU), whereas for the pine fire simulations over the same duration, 175 CPU hours across 4 processors was required. Therefore, to use an optimisation method such as a genetic algorithm with 200 generations and a population size of 250 (Abu-Bakar, Moinuddin 2013), and over a similar simulation duration, enormous computational resources will be required.

From the current study of experimental and numerical results, it appears that the method described by Donskoi & McElwain (1999) can be expanded for modelling coupled solid and gas phase reactions by altering the values of the kinetic triplet and the HoR relevant to changing heating rates. This method for the FDS fire model by using built-in RAMP and tabular functions is described in Section 7.4.1 and 7.4.2 respectively. This alternative method is not limited to the kinetic triplet and HoR only, but it is also applicable to the thermal properties such as C_p that can vary with heating rate and to combustion parameters that can vary with incident radiation.

7.4.1 RAMP Function

Existing RAMP Function for Thermal Properties

Currently, with the RAMP function, the thermal properties (specific heat, C_p and thermal conductivity, k) can be specified as functions of temperature. The RAMP function allows users to control the behaviour of these two parameters that are found experimentally. The behaviour can be linear or non-linear and some examples are given below:

```

Cp_steel(T)  {
    Case 1: T= 20., F=0.45 / implies Cp=0.45 kJ/kg/K when 20°C≥T
    Case 2: T=677., F=0.85 / implies Cp=0.00083T+0.6 when 377°C≤T≤677
°C and
                                                    Cp=0.85 when T≥677°C
    }
k_steel(T)   {
    Case 1: T= 20., F=48. / implies k=48 W/m/K when 20°C≥T
    Case 2: T=677., F=30. / implies k=-0.0274T+48 when 20°C≤T≤677 °C
    and
                                                    k=30 when T≥677°C
    }

```

It is to be noted that for values of temperature: (i) below and above the given range, FDS will assume a constant value equal to the first or last F specified, and (ii) between two consecutive temperatures, parameter values increase or decrease linearly. With this setting, the fire growth and development is being simulated by using a set of thermo-physical property values at various temperatures.

Proposed RAMP Function for Chemical Kinetics

It was shown previously in Figure 4.8 and Figure 4.9 (CHAPTER 4) that parameter values of A , E , n and HoR vary with dT/dt for pine and PMMA. Similar to the approach of Donskoi and McElwain (1999), provisions can be made for specifying the dT/dt dependent values of parameters in FDS. However, similar to the temperature RAMP function described above, the heating rate RAMP functions: (ACTIVATION_ENERGY_RAMP, HEAT_OF_REACTION_RAMP, PREEXPONENTIAL_FACTOR_RAMP and REACTION_ORDER_RAMP) can be used in FDS. As the heating rate increases or decreases, the RAMP function will provide appropriate material property values representing actual conditions. As the FDS calculates the temperature history of each solid cell, it is possible to calculate dT/dt for every time-step. For simplicity, FDS may need to use parameter values of the previous time-step for the current time-step.

The cone calorimeter experimental results in CHAPTER 5 shows the variation in parameter values for EHoC, CO yield, CO₂ yield and smoke yield with respect to a change in radiative heat flux (especially for charring materials). As the FDS calculates radiative heat flux on each solid surface, it is possible to introduce an IRRADIANCE_RAMP function for every time-step.

It has been observed that those parameters vary with time during the tests even under constant irradiation. It may be argued that a more complicated algorithm needs to be developed to reflect the changes in values with respect to irradiance, time, material thickness, char fraction etc. However, the method proposed in this study can offer the first steps towards improved usage of bench scale data. It is expected that in the future, more advanced algorithms will be developed in relation to gas and soot yields.

7.4.2 Tabular Function

Existing Tabular Function

To account for the multi-dimensional variation of input quantities, the FDS uses the TABL function. Currently, it is only used for prescribing a sprinkler spray pattern via the SPRAY_PATTERN_TABLE command. An example is given below:

```
&PROP ID='K-11',  
    QUANTITY='SPRINKLER LINK TEMPERATURE',  
    OFFSET=0.10,  
    PART_ID='water_drops',  
    FLOW_RATE=60.,  
    SPRAY_PATTERN_TABLE='TABLE1',  
    SMOKEVIEW_ID='sprinkler_upright',  
    DROPLET_VELOCITY=10. /
```

```
&TABL ID='TABLE1', TABLE_DATA=independent parameter1 set1, independent  
parameter2 set2, dependent parameter1, dependent parameter2/
```

```
&TABL ID='TABLE1', TABLE_DATA=independent parameter1 set2, independent  
parameter2 set2, dependent parameter1, dependent parameter2/
```

Here, the two dependent variables of droplet velocity and fractional volume flow rate vary with the two sets of independent variables bound of latitude and bound of longitude. In the next section a new tabular function is proposed, where multiple dependent variables vary with one independent variable.

Proposed Tabular Function for Thermal Properties and Kinetics

It has been observed that the specific heat-temperature profiles vary with the heating rate as shown in Figure 7.10 (Kousksou et al. 2011). This phenomenon is unlikely to be modelled by the SPECIFIC_HEAT_RAMP function only. However, since the single variable is dependent, two relatively independent variables, T and dT/dt , render it possible for FDS developers to develop a new tabular SPECIFIC_HEAT_TABLE function. An example is given below:

```
&TABL ID='TABLE1', TABLE_DATA= HEATING_RATE1, TEMP_S1, TEMP_E1,
SPECIFIC_HEAT_M1/
&TABL ID='TABLE1', TABLE_DATA= HEATING_RATE2, TEMP_S2, TEMP_E2,
SPECIFIC_HEAT_M2/
```

The variables TEMP_S, TEMP_E and SPECIFIC_HEAT_M represent the start temperature, T_s , end temperature, T_e , and peak value at the end temperature, $C_{p,max}$, respectively. For any material temperature, T_i , between the start and end temperatures at a specific heating rate, the specific heat capacity, $C_{p,i}$ can be calculated using:

$$C_{p,i} = C_{p,max} \times \frac{T_i - T_s}{T_e - T_s} \quad (7.14)$$

For heating rates not listed in the table, values of T_s , T_e and $C_{p,max}$ can be selected as average values of the previous and the next heating rate. However, below and above the given range of the heating rate, constant values equal to the first or last set of heating rates are assumed.

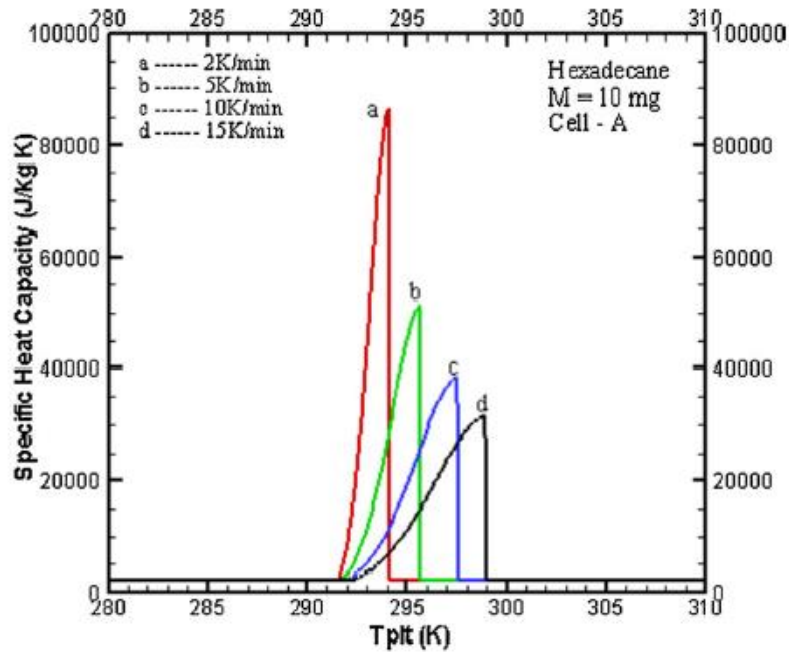


Figure 7.10: Specific heat-temperature profile from (Kousksou et al. 2011)

7.4.3 Systematic Approach

Input values from the experimental study can be stored in a database to be used with an optimisation tool. Such data be used as input values into the optimisation tool to make the best use of the data under appropriate fire conditions. The optimisation tool can be linked with FDS or any CFD-based fire model to enable the model to access appropriate values from the database at each computational node or cell, and assess the conditions of material temperature, heating rate and irradiance for the fire conditions being simulated. A schematic diagram of the operation of the optimisation tool is shown in Figure 7.11.

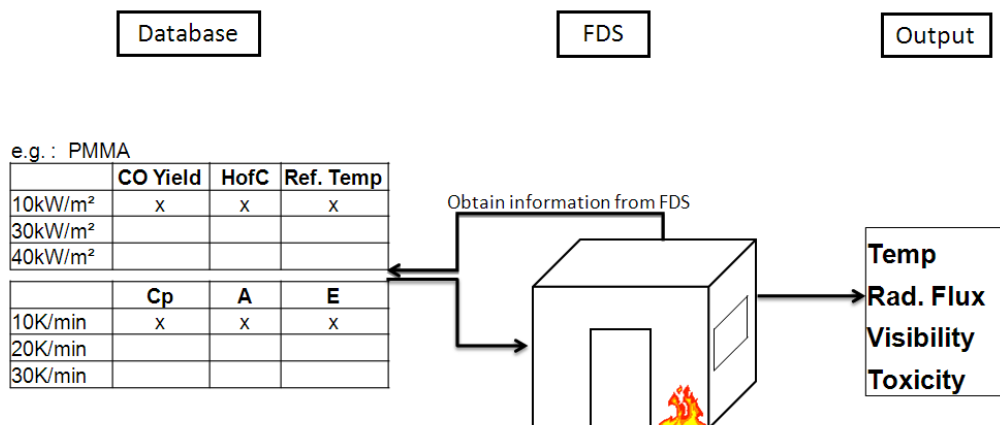


Figure 7.11: Optimisation tool linked to the CFD-based fire model to assess appropriate fire condition

7.5 Summary

It should be noted that both methods discussed above are, to some degree, based on curve-fitting of TGA and/or cone calorimeter data. It can be argued that the method presented in here is less reliant on curve fitting since the kinetic triplet, *HoR*, combustion parameters etc., are initially obtained at a specific heating rate or irradiance using well-established post-processing methods. However, this alternative method may be limited to very few reaction pathways, making it ideally suitable for bulk thermal degradation processes involving fuel, moisture and char due to the experimental limitations. Both methods should be tested against real fire experiments with mid-scale samples rather than bench-scale experiments such as TGA or cone calorimeter tests. Such medium scale experiments are the subject of future studies.

CHAPTER 8

SUMMARY AND CONCLUSIONS

8.1 Introduction

The overarching objective of this study is to characterize the fire properties of a representative set of materials, for coupled pyrolysis and combustion simulations and to explore a method for the optimised use of those properties as input variables in a CFD model. Accurate characterization and optimized use of fire properties can provide a better and more reliable simulation of real fire scenarios that invariably involve coupled pyrolysis and combustion phenomena. These are required for the development and approval of performance-based design and has been partially demonstrated for bench-scale fire simulations in this study.

This research was performed in a number of stages that commenced with developing an understanding of the existing experimental techniques and the development/refinement of new methods. This was followed by the selection and implementation of data post-processing methods and the development of new methods where required. Detailed characterization of fire properties, implementation of coupled pyrolysis and combustion simulations using input data using these properties, sensitivity studies for selected parameters, and an evaluation of the optimized use of fire properties completed the work.

8.2 Experimental Techniques

Several new experimental techniques used to characterize and measure fire properties of materials have been established in this study. Prior to this work, the only established experimental technique utilized in our research group was the measurement of combustion parameters by means of a cone calorimeter. In the current study, techniques for measuring various for thermal properties via TGA and DSC analysis and using a hot disc analyser (HDA) have been established.

The use of appropriate experimental techniques is critical to establish an understanding of the nature of decomposition processes and to obtain the pyrolysis parameters of combustible materials. The protocols for determining the kinetic parameters using TGA and DSC by combining data sets obtained from a mass loss

curves (TGA) and *HoR* (DSC) have been established. The first case is well established in the literature where DTG curves are widely used. In this study, the technique has been established using both old and new TGA instruments from different manufacturers. In addition, a semi-established technique for determining the *HoR* of combustible materials utilizing the newer instrument was comprehensively explored. An idealized experimental technique, directed towards normalizing the sample masses in TGA and DSC experiments, and the corresponding test protocol is documented in this work.

To characterize thermal properties, a new HDA instrument was utilized with significant efforts focused on self-learning techniques for measuring specific heat capacity and thermal conductivity using Transient Plane Source techniques. As a result, a test protocol has been developed for measuring the properties for thin and thick solid materials and this is a crucial pathway for ensuring the quality of the results and also the reproducibility of each parameter tested. The key strategy to obtain accurate, representative experimental results is to identify the most appropriate probing depth which has been investigated and reported in this study.

8.3 Data Post-Processing

Appropriate post-processing techniques to obtain fire properties from the raw experimental data are extremely important. Whilst the cone calorimeter and HDA instruments have in-built software for data post-processing, this is not the case for TGA and DSC which typically provide mass loss and heat flow curves as a function of temperature or time respectively. Therefore, the raw data obtained from the TGA and DSC experiments require further processing in order to obtain the chemical kinetic parameters and *HoR* values and several established data reduction methods were investigated. For obtaining chemical kinetic parameter from TGA experiments, a MATLAB program utilizing the inflection point method was developed in this work. For the determination of *HoR*, an established technique for matching sample masses from TGA and DSC experiments at the same sample temperatures was found to be adequate. This technique has also been expanded in this study to include the case where the initial sample masses for TGA and DSC experiments are different. These methods for determining *HoR* from the raw experimental data were also automated using MATLAB code developed for this purpose.

8.4 Characterization of Fire Properties

Unlike other reported studies, this work was been conducted using a wider range of heating rates, heat fluxes and temperatures. The characterization of various pyrolysis, combustion and thermo-physical parameters of four combustible materials commonly in buildings, namely non-charring PMMA, and charring pine, cotton and wool was undertaken in this study.

8.4.1 Effect of Heating Rate on Pyrolysis Parameters

The kinetic parameters and *HoR* values, were determined over a wide heating rate between 5 and 200 K/min. The kinetic data obtained for PMMA at the lower heating range was in good agreement with literature values. However, significant variations of these values with respect to heating rate were observed and this may be due to the physical and chemical properties of each tested material. For some materials such as pine, a char can develop when the material is exposed to higher temperatures. For non-charring polymers such as PMMA, samples will undergo a number of phase changes including glass transition and melting. Similarly, differences in the chemical composition of the materials can contribute to the thermal decomposition process and similar trends have also been reported by other researchers, particularly with respect to the relationship between pyrolysis and heating rate.

For each material studied, relationships between each material parameter and heating rate were proposed through regression analysis. The trends and relative fit of the relationships for each parameter and for all four materials were evaluated and it is clear that all kinetic parameters of pine materials show increasing trends with respect to increasing heating rates. This is the reverse of the corresponding trends found for PMMA, wool and cotton (single effective) with respect to *A* and *E*. For *n*, there was a moderate parabolic (lower vertex) trend for PMMA, a very strong decreasing power trend for wool and a very strong increasing power trend for cotton (single effective). For simplicity, the average value of *n* across the heating range for each material may be considered.

The summary presented in Table 8.1 shows that *HoR* values generally increase with an increasing heating rate for all materials which is also consistent with comparative literature findings. This appears to be attributed to the shifting of DTG and DSC peaks

to higher temperatures as the heating rate is increased and it may be suggested that there is a reduced residence time for volatiles released from the material within the vicinity of any specific temperature at the higher heating rates. Therefore, by the time the volatiles are formed, the sample has reached a higher temperature and thus, more heat flow is needed to assist the formation of volatiles quickly at higher heating rates.

8.4.2 Effects of Irradiance on Combustion Parameters

The variation in heat flux with various combustion parameters was also investigated. In this case, observed variations are most likely due to the moisture content in the tested samples, particularly the natural materials pine, cotton and wool. The presence of moisture has a significant effect on the variation of *EHoC* of pine and wool and this is particularly the case for the charring materials which may also be influenced by moisture content when exposed to various conditions of heat flux. For these charring materials, a likely variation in char development with respect to incident radiation flux may also have some influence, particularly in the case of thick and denser samples. Additionally, moisture evaporation and char development may not be uniform through the depth of the sample during the fire test. For PMMA, no significant trend is observed in *EHoC* and this may be attributed to the absence of moisture and the subsequent lack of char formation.

A summary of the relative trends and strength of the relationships for all parameters measured for each of the four materials is presented in Table 8.2. For these combustion parameters, the *EHoC*, soot yield, CO₂ yield and char residue of pine increased with heat flux. The soot yield and the CO yield of PMMA is increasing whereas the *EHoC* and CO₂ yield for cotton is decreasing with an increase in heat flux. For wool the *EHoC*, soot yield, CO₂ yield is decreasing with an increase in heat flux. Another important factor that may contribute to these observations is related to the vast differences in the chemical composition of the materials. As expected, each material reacts differently depending on the physical and chemical properties which may also explain the differences observed between charring and non-charring materials and even within the different charring materials studied.

Table 8.1: Summary of kinetic parameters and *HoR* trends of tested materials

Material →	PMMA	Pine	Wool	Cotton (cellulose)	Cotton (non-cellulose)	Cotton (single effective)
Parameter ↓						
Log (<i>A</i>)						
<i>E</i>						
<i>N</i>						
Reaction rate						
Reference temperature						
Pyrolysis Range						
<i>HoR</i>						

Key:

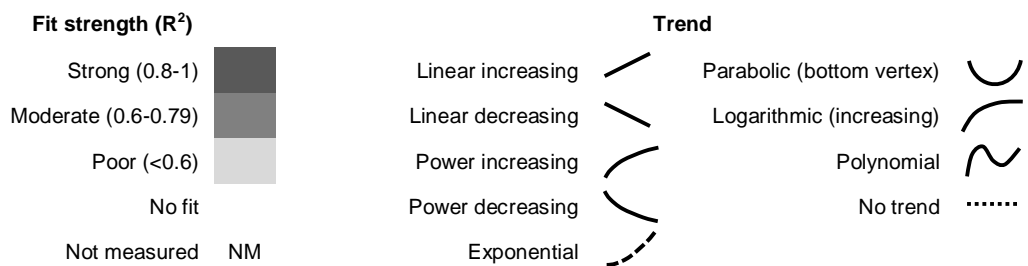
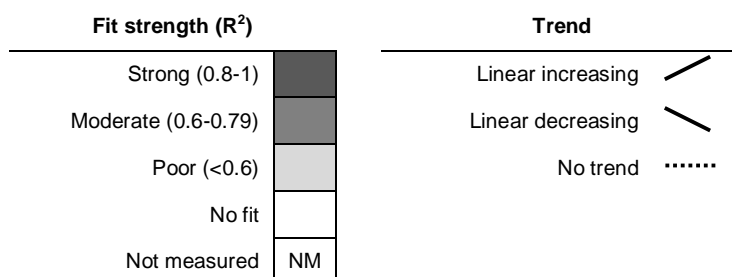


Table 8.2: Summary of combustion parameters trends of materials

Material →	PMMA	Pine	Cotton	Wool
Parameter ↓				
<i>E</i> H _o C	↗	↘	↘
CO yield	↗
CO ₂ yield	↗	↘	↘
Soot yield	↗	↗	↘
Char residue	NM	↗	↘

Key:



8.4.3 Effects of Temperature on Thermal Properties

Thermal conductivity and specific heat capacity were determined over a relatively wide temperature range of 40 to 200°C. The results showed that the thermal conductivity and specific heat for the charring materials were significantly varied with temperature. For the non-charring PMMA, these parameters did not demonstrate any significant effect with changing temperature. As suggested for the effect of irradiance, these properties may vary due to the differences between the charring and non-charring materials based on their chemical and physical compositions as well as moisture content. The case of PMMA may be the exception to this observation since non-combustible metals which are also non-charring can also demonstrate this variation with temperature. A summary of all of the relative trends and strengths of the

relationships of the thermal parameters with temperature the tested materials is presented in Table 8.3.

Table 8.3: Summary of all thermal properties trends of materials

Material →	PMMA	Pine	Pine char - flat	Pine char - structural	Cotton	Wool
Parameter ↓						
Thermal conductivity					
Specific heat capacity					

Key:

Fit strength (R^2)	Trend
Strong (0.8-1)	No trend
Moderate (0.6-0.79)	Power increasing
Poor (<0.6)	Linear increasing
No fit	Curvilinear (polynomial)
Not measured	

8.5 Fire Simulation Using Post-Processed Data as Input Variables

The post-processed data obtained from the experimental work was used in the fire modelling. Simulations of reactions involving two relatively “pure” materials (pine and PMMA) were conducted to assess the level of agreement between the numerically simulated and the experimental HRR values. This part of the study is crucial as it can verify the accuracy of experimental and post-processing techniques as well as validate the CFD-based fire used in the simulations.

The numerical simulation of the pyrolysis to emulate TGA experiments and the coupled pyrolysis and combustion simulation to emulate the cone calorimeter experiments were performed using the CFD-based fire model, FDS. In the FDS simulation, the coupled solid and gas phase reactions were simulated, and the results

were uniquely found to be converged as the spatial resolution increased to the order of mm. A sensitivity analysis and comparison of the results from simulations of non-prescribed fires showed that experimental HRR profile can be reasonably predicted if appropriate input parameters are used. Moreover, by using the kinetic parameters and *HoR* values which vary with heating rates in the simulations, a more accurate prediction of fire behaviour may be obtained. In this work, variations in thermal properties with respect to temperature were implemented, however, variations in combustion parameters with respect to irradiance were not tested in the scope of the study.

Overall, this simulation study presents a reliable model for comprehensively quantifying the representative fire properties for an unknown or novel material, which can provide adequate simulations of at least bench-scale fire scenarios. In addition to those studied in this work, other output parameters are known to follow trends with HRR. More accurate HRR prediction can lead to improved prediction of these other output parameters including toxic gas release from combustible materials, radiant heat and temperature exposure, which can be a major threat to human life.

8.6 Future Optimised Data Use

Optimum use of experimentally obtained material property data is required as the FDS and other CFD-based fire models generally use only single values of pyrolysis and combustion parameters regardless of the fire condition being modelled. At different stages of a fire, values such as heat flux levels and heating rates of the combustible material vary and similarly, pyrolysis and combustion parameters can vary with these values.

Two approaches have been discussed to improve coupled pyrolysis and combustion reaction simulations: (i) an optimisation method using genetic algorithm (Li et al. (2014), Lautenberger, Rein & Fernandez-Pello (2006) and FDS validation guide (McGrattan et al. 2015) and (ii) the method proposed by Donskoi and McElwain (1999) and its expanded version proposed in CHAPTER 7. Both approaches have the potential to be further expanded to include the effects of pyrolysis parameters or specific heat as a function of heating rate, and the effects of combustion parameters

as a function of heat flux. These can then be applied to simulate real fire scenarios where solid and gas phase reactions are coupled.

8.7 Recommendations for Future Studies

8.7.1 FDS Simulation of Fabric Fire

Accurate simulation of fabric fire is crucial for fire safety in buildings where considerable amounts of furnishing and other items are comprised of various fabric materials. These simulations are often under-reported in the literature so it is therefore important to address this in future studies. In the current work, the properties obtained can be employed in representative fire simulation studies where combustion properties, chemical kinetics and thermal properties of some materials are already obtained. Additionally, the FDS model can be used to confirm the fire properties of fabric samples obtained from the experiments concurrent with further sensitivity analyses which may include a study of grid and thermo-physical property sensitivities.

8.7.2 Development of an Optimisation Tool

An optimisation tool as outlined in Figure 7.11 may be developed to: (i) access appropriate parameter values from a database, and (ii) assess the conditions of material temperature, heating rate and irradiance on the parameter values. Such a tool along with the database can be linked to FDS or any CFD-based fire model to further enhance the capabilities of the existing models.

The principal method proposed to develop this tool and further the research is illustrated in Figure 8.1. However, it should be noted that this method is only applicable for bulk fire properties such as those measured in this study. This method can also be widely expanded to include other combustible and flammable materials that burn in buildings or in other fire scenarios such as bushfire or chemical fires. In the simulation of such fire scenarios, the FDS model provides output parameters such as gas and solid temperatures, radiation flux, levels of CO, CO₂, smoke and other toxic gases. These parameters are largely dependent on the fire properties of the combustible materials present in the building and surrounding environment. It is therefore essential to use appropriate values depending on the temperature, heating rate, and irradiance

level at each computational node or cell for the fire conditions as aforementioned output parameters can pose a major threat to human life.

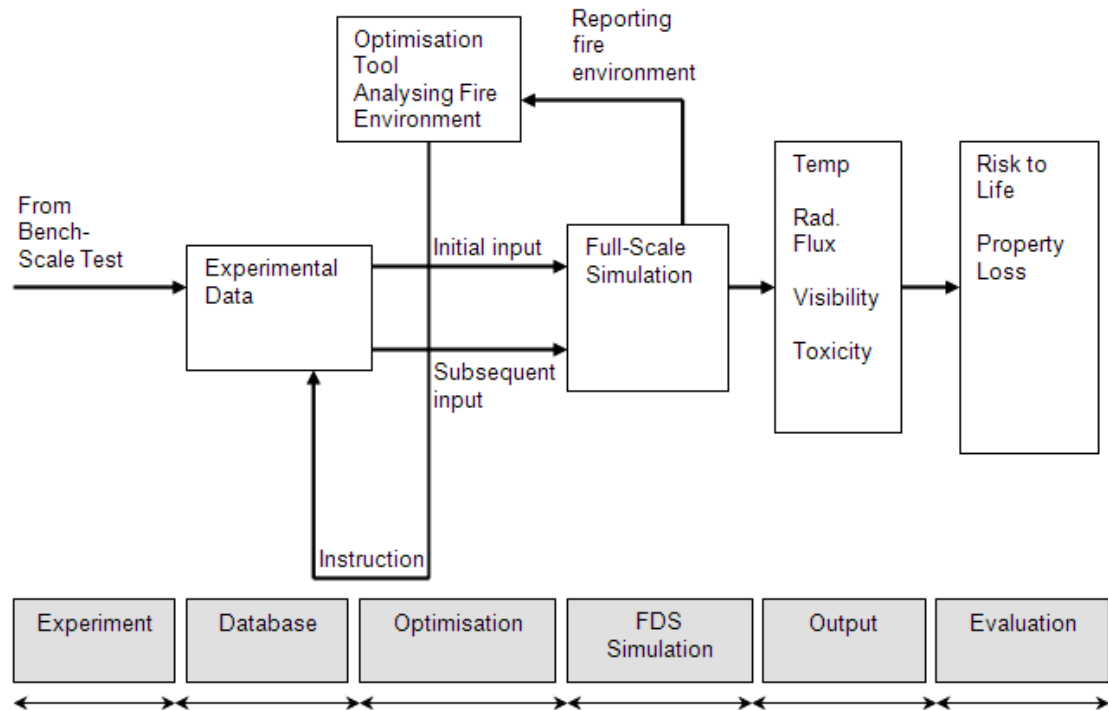


Figure 8.1: Proposed method for future studies

8.7.3 Optimization Study

The approach of optimization to account for variations in fire properties should be explored in future studies. The raw experimental data obtained from this study can be employed optimization techniques such as a genetic algorithm (GA) and/or artificial neural network (ANN) to obtain fire properties using the methods of Li et al. (2014), Lautenberger, Rein and Fernandez-Pello (2006), and the FDS validation guide (McGrattan et al. 2015) among others. The use of the GA/ANN techniques could lead to the enhancement of the raw data by using as the input data to determine kinetic triplets for various reaction paths or for various components within the sample as discussed by Shi and Chew (2013) using optimisation processes. It has also been emphasized that the TG analysis at multiple heating rates is an important key to

determine kinetics triplets and to predicting pyrolysis behaviour, which the advance search by GA is currently incapable of achieving (Li et al. 2014).

It will also be a key advancement to incorporate the observed shifting phenomena of thermal events (i.e. decomposition) in the numerical modelling of fire behaviour as well as the variation in combustion parameters with respect to irradiance. In future studies, both approaches should be tested experimentally with larger mid-scale samples rather than the smaller bench-scale experiments performed using the TGA or cone calorimeter. These proposed studies may lead to a more accurate estimation of the risk to life and property loss by improved use of FDS and other CFD-based fire models. As a result, safer and more economical buildings could be constructed.

8.7.4 Other Studies

In general, the modelling and simulation of fire is data intensive but there are few input parameters that are specific to material properties. Future studies could incorporate a more detailed analysis or characterization of these properties that may offer solutions to some of the key observations that appear to be material specific such as moisture content. In addition, advances in analytical techniques and the hybridization of one or more existing techniques can lead to further revelations of the material properties. For example, techniques combining combustion (cone calorimeter) or pyrolysis (TGA) with analytical tools such as infrared spectroscopy are now available and this is the subject of future study.

Due to lack of computational resources, a simulation of a real fire using the developed properties could not be conducted. Future works may include room burning experiments with mock-up furniture built from the studied materials and simulate those experiments with FDS.

REFERENCES

- ABDOU, A. and BUDAIWI, I., 2013. The variation of thermal conductivity of fibrous insulation materials under different levels of moisture content. *Construction and Building Materials*, 43(0), pp. 533-544.
- ABU-BAKAR, A.S. and MOINUDDIN, K.A.M., 2013. *The State of Art model Fire Dynamics Simulator: Feasibility of Introduction of New RAMP and Tabular Functions*. Discussion Paper edn. Melbourne: Victoria University.
- ABU-BAKAR, A.S. and MOINUDDIN, K.A.M., 2012. Effects of Variation in Heating Rate, Sample Mass and Nitrogen Flow on Chemical Kinetics for Pyrolysis, AFMC COMMITTEE, ed. In: *18th Australasian Fluid Mechanics Conference*, 3-7 December 2012 2012, Australasian Fluid Mechanics Society, pp. 1.
- ADL-ZARRABI, B., BOSTRÖM, L. and WICKSTRÖM, U., 2006. Using the TPS method for determining the thermal properties of concrete and wood at elevated temperature. *Fire and Materials*, 30(5), pp. 359-369.
- AMERICAN SOCIETY FOR TESTING AND MATERIALS, 2015. *ASTM WK49591 Determining Thermal Conductivity and Thermal Diffusivity Using the Transient Plane Source or Hot Disc Method*. USA: .
- AMERICAN SOCIETY FOR TESTING AND MATERIALS, 2014. *ASTM E1933 - 14 Standard Practice for Measuring and Compensating for Emissivity Using Infrared Imaging Radiometers*. USA: .
- AMERICAN SOCIETY FOR TESTING AND MATERIALS, 2007. *ASTM E1641-07 Standard Test Method for Decomposition Kinetics by Thermogravimetry (TGA)*. USA: .
- AMERICAN SOCIETY FOR TESTING AND MATERIALS, 2005. *ASTM E1269-05 Standard Test Method for Determining Specific Heat Capacity by Differential Scanning Calorimetry*. USA: .
- AMERICAN SOCIETY FOR TESTING AND MATERIALS, 2004a. *ASTM E1354-4a Standard Test Method for Heat Release Rates for Materials and Product Using an Oxygen Consumption Calorimeter*. USA: .

AMERICAN SOCIETY FOR TESTING AND MATERIALS, 2004b. *ASTM E2160-04 Standard Test Method for Heat of Reaction of Thermally Reactive Materials by Differential Scanning Calorimetry*. USA: .

ANCA-COUCÉ, A., ZOBEL, N., BERGER, A. and BEHRENDT, F., 2012. Smouldering of pine wood: Kinetics and reaction heats. *Combustion and Flame*, 159(4), pp. 1708-1719.

ANDERSON, H., STREY, R., KEMMLER, A. and HABERLAND, D., 1997. Effective search of starting values for kinetic parameters estimation. *Journal of Thermal Analysis*, 49(3), pp. 1565-1569.

ANG, H.G. and PISHARATH, S., 2012. *Energetic polymers*. John Wiley & Sons.

ASSAEL, M., BOTSIOS, S., GIALOU, K. and METAXA, I., 2005. Thermal conductivity of polymethyl methacrylate (PMMA) and borosilicate crown glass BK7. *International Journal of Thermophysics*, 26(5), pp. 1595-1605.

ASSAEL, M. and GIALOU, K., 2003. Measurement of the Thermal Conductivity of Stainless Steel AISI 304L up to 550 K. *International Journal of Thermophysics*, 24(4), pp. 1145-1153.

BABRAUSKAS, V., BAROUDI, D., MYLLYMÄKI, J. and KOKKALA, M., 1997. The cone calorimeter used for predictions of the full scale burning behaviour of upholstered furniture. *Fire and Materials*, 21(2), pp. 95-105.

BABRAUSKAS, V. and PEACOCK, R.D., 1992. Heat release rate: the single most important variable in fire hazard. *Fire Safety Journal*, 18(3), pp. 255-272.

BABRAUSKAS, V., TWILLEY, W.H. and PARKER, W.J., 1992. The Effects of Specimen Edge Conditions on Heat Release Rate. *October 9th, 1992*, 17, pp. 51-63.

BALLISTRERI, A., MONTAUDO, G. and PUGLISI, C., 1984. Reliability of the volatilization method for determination of the activation energy in the thermal decomposition of polymers. *Journal of Thermal Analysis*, 29(2), pp. 237-241.

BAUER, K., GARBE, D. and SURBURG, H., 1988. Ullmann's encyclopedia of industrial chemistry. *Ullmann's Encyclopedia of Industrial Chemistry*, 11.

BAXTER, S., 1946. The thermal conductivity of textiles. *Proceedings of the Physical Society*, 58(1), pp. 105.

BECK, P., GORDON, P. and INGHAM, P., 1976. Thermogravimetric analysis of flame-retardant-treated wools. *Textile Research Journal*, 46(7), pp. 478-483.

BERGMAN, T.L., INCROPERA, F.P. and LAVINE, A.S., 2011. Radiation: Processes and Properties. *Fundamentals of heat and mass transfer*. John Wiley & Sons, pp. 762-763.

BEYLER, C.L. and HIRSCHLER, M.M., 2002. Thermal decomposition of polymers. *SFPE handbook of fire protection engineering*, 2.

BILBAO, R., ARAUZO, J. and SALVADOR, M.L., 1995. Kinetics and modeling of gas formation in the thermal decomposition of powdery cellulose and pine sawdust. *Industrial & Engineering Chemistry Research*, 34(3), pp. 786-793.

BLACK SATURDAY BUSHFIRES, 2015, 2015-last update, Black Saturday Bushfires [Homepage of Black Saturday Bushfires], [Online]. Available: <http://www.blacksaturdaybushfires.com.au/> [01/19, 2015].

BRESCIANINI, C., YEOH, G., CHANDRASEKARAN, V. and YUEN, R., 1997. A numerical model for pilot ignition of PMMA in a cone calorimeter. *Combustion Science and Technology*, 129(1-6), pp. 321-345.

BROWN, J.E., BRAUN, E. and TWILLEY, W.H., 1988. Cone Calorimeter Evaluation of the Flammability of Composite Materials.

CAO, X., SHEN, B., LU, F. and YAO, Y., 2010. Catalytic Pyrolysis of Cotton Straw by Zeolites and Metal Oxides, *Proceedings of the 20th International Conference on Fluidized Bed Combustion 2010*, Springer, pp. 648-652.

- CARRAN, R.S., GHOSH, A. and DYER, J.M., 2015. Modification of surface properties of wool fabric with linde type a nano-zeolite. *Journal of Applied Polymer Science*, 132(32),.
- CELINA, M., GILLEN, K. and ASSINK, R., 2005. Accelerated aging and lifetime prediction: review of non-Arrhenius behaviour due to two competing processes. *Polymer Degradation and Stability*, 90(3), pp. 395-404.
- CELINA, M.C., 2013. Review of polymer oxidation and its relationship with materials performance and lifetime prediction. *Polymer Degradation and Stability*, 98(12), pp. 2419-2429.
- CETIN, E., GUPTA, R. and MOGHTADERI, B., 2005. Effect of pyrolysis pressure and heating rate on radiata pine char structure and apparent gasification reactivity. *Fuel*, 84(10), pp. 1328-1334.
- CHAOS, M., 2013. Application of sensitivity analyses to condensed-phase pyrolysis modeling. *Fire Safety Journal*, 61, pp. 254-264.
- CHATTERJEE, P.K. and CONRAD, C.M., 1966. Kinetics of the pyrolysis of cotton cellulose. *Textile Research Journal*, 36(6), pp. 487-494.
- CHAUDHURI, S.K., 2004. Taking wool into the future – Through innovations, *21st National Textile Technicians Congress*, 7-11 September 2004 2004.
- CHEN, F.F., 2001. *Radiant Ignition of New Zealand Upholstered Furniture Composites*, Canterbury University New Zealand.
- CHIDAMBARAM, P., GOVINDAN, R. and VENKATRAMAN, K.C., 2012. Study of thermal comfort properties of cotton/regenerated bamboo knitted fabrics. *African Journal of Basic & Applied Sciences*, 4(2), pp. 60-66.
- CHIZHIK, A.I., SHABES, S.V., TSYUI, L.L. and TETEREVA, N.G., 1979. The use of spline approximation for the interpretation of results of thermal analysis. *Polymer Science U.S.S.R.*, **21**(7), pp. 1846-1850.

CHOW, C.L., CHOW, W.K., FONG, N.K., JIANG, Z. and HAN, S.S., 2004. Assessing Fire Behaviour of Common Building Materials with a Cone Calorimeter. Volume 5(4), pp. 91-98.

CHOW, W., 2002. Assessment on heat release rate of furniture foam arrangement by a cone calorimeter. *Journal of Fire Sciences*, 20(4), pp. 319-328.

CHUNG, T.K. and DRYSDALE, D., 2002. Using cone calorimeter data for the prediction of fire hazard. *October 2002*, 37(7), pp. 697-706.

CNN INTERNATIONAL, October 22, 2007, 2007-last update, 265,000 flee as massive wildfires char Southern California [Homepage of CNN International], [Online]. Available:

<http://edition.cnn.com/2007/US/10/22/wildfire.ca/index.html?eref=yahoo> [1/19, 2015].

COLES, A.R., 2001. Flammability of upholstered furniture using the cone calorimeter.

COMMONWEALTH OF AUSTRALIA , BUREAU OF METEOROLOGY, 2015, 2015-last update, Ash Wednesday, February 1983 [Homepage of Commonwealth of Australia , Bureau of Meteorology], [Online]. Available: <http://www.bom.gov.au/lam/climate/levelthree/c20thc/fire5.htm> [01/19, 2015].

DEARDOFF, J.W., 1972. Numerical Simulation and Neutral and Unstable Planetary Boundary Layers. *1972*, 29, pp. 91.

DELICHATSIOS, M., PAROZ, B. and BHARGAVA, A., 2003. Flammability properties for charring materials. *Fire Safety Journal*, 38(3), pp. 219-228.

DELICHATSIOS, M.A., 2005. Piloted ignition times, critical heat fluxes and mass loss rates at reduced oxygen atmospheres. *Fire Safety Journal*, 40(3), pp. 197-212.

DENIZE, H., 2000. The combustion behaviour of upholstered furniture materials in New Zealand.

DIETENBERGER, M., 2012. Pyrolysis kinetics and combustion of thin wood by an advanced cone calorimetry test method. *J Therm Anal Calorim*, 109, pp. 1215-1228.

DIETENBERGER, M.A. and GREXA, O., 2000. Correlation of smoke development in room tests with cone calorimeter data for wood products.

DONSKOI, E. and MCELWAIN, D.L.S., 1999. Approximate modelling of coal pyrolysis. *May 1999*, 98(7), pp. 825.

EDELMAN, P., OSTERLOH, J., PIRKLE, J., CAUDILL, S.P., GRAINGER, J., JONES, R., BLOUNT, B., CALAFAT, A., TURNER, W., FELDMAN, D., BARON, S., BERNARD, B., LUSHNIAK, B.D., KELLY, K. and PREZANT, D., 2003. Biomonitoring of chemical exposure among New York City firefighters responding to the World Trade Center fire and collapse. *Environmental health perspectives*, 111(16), pp. 1906-1911.

FANG, M.X., SHEN, D.K., LI, Y.X., YU, C.J., LUO, Z.Y. and CEN, K.F., 2006. Kinetic study on pyrolysis and combustion of wood under different oxygen concentrations by using TG-FTIR analysis. *Journal of Analytical and Applied Pyrolysis*, 77(1), pp. 22-27.

FAROQ, A., PRICE, D., MILNES, G. and HORROCKS, A., 1994. Thermogravimetric analysis study of the mechanism of pyrolysis of untreated and flame retardant treated cotton fabrics under a continuous flow of nitrogen. *Polymer Degradation and Stability*, 44(3), pp. 323-333.

FATEH, T., ROGAUME, T. and RICHARD, F., 2014. Multi-scale modeling of the thermal decomposition of fire retardant plywood. *Fire Safety Journal*, 64(0), pp. 36-47.

FERRIOL, M., GENTILHOMME, A., COCHEZ, M., OGET, N. and MIELOSZYNSKI, J., 2003. Thermal degradation of poly (methyl methacrylate)(PMMA): modelling of DTG and TG curves. *Polymer Degradation and Stability*, 79(2), pp. 271-281.

FIRE TESTING TECHNOLOGY, 1998. *User's Guide for the Cone Calorimeter*. User's Guide edn. United Kingdom: FTT.

FLAMBARD, X., BOURBIGOT, S., FERREIRA, M., VERMEULEN, B. and POUTCH, F., 2002. Wool/para-aramid fibres blended in spun yarns as heat and fire resistant fabrics. *Polymer Degradation and Stability*, 77(2), pp. 279-284.

FLYNN, J.H. and WALL, L.A., 1966. A quick, direct method for the determination of activation energy from thermogravimetric data. *Journal of Polymer Science Part B: Polymer Letters*, 4(5), pp. 323-328.

FONSECA, E. and BARREIRA, L., 2009. Charring rate determination of wood pine profiles submitted to high temperatures.

FONT, R., CONESA, J., MOLTÓ, J. and MUNOZ, M., 2009. Kinetics of pyrolysis and combustion of pine needles and cones. *Journal of Analytical and Applied Pyrolysis*, 85(1), pp. 276-286.

FOROUHARSHAD, M., MONTAZER, M., MOGHADAM, M.B. and SALIGHEH, O., 2011. Flame retardant wool using zirconium oxychloride in various acidic media optimized by RSM. *Thermochimica Acta*, 516(1), pp. 29-34.

FOUNDA, D. and GIANNAKOPOULOS, C., 2009. The exceptionally hot summer of 2007 in Athens, Greece—a typical summer in the future climate? *Global and Planetary Change*, 67(3), pp. 227-236.

FREDERICK, W.J. and MENTZER, C.C., 1975. Determination of heats of volatilization for polymers by differential scanning calorimetry. *Journal of Applied Polymer Science*, 19(7), pp. 1799-1804.

FUJINO, J. and HONDA, T., 2007. Measurement of the Specific Heat capacity of Plastic Waste/Fly Ash Recycled Composite Using a Differential Scanning Calorimeter. *October 17, 2007*, 36(7), pp. 435-448.

GAAN, S. and SUN, G., 2009. Effect of nitrogen additives on thermal decomposition of cotton. *Journal of Analytical and Applied Pyrolysis*, 84(1), pp. 108-115.

GAO, N., LI, A., QUAN, C., DU, L. and DUAN, Y., 2013. TG–FTIR and Py–GC/MS analysis on pyrolysis and combustion of pine sawdust. *Journal of Analytical and Applied Pyrolysis*, 100, pp. 26-32.

GOEL, V.K., 2008. Thermal Expansion and Calorimetry. *Fundamentals Of Physics*. XI edn. Tata McGraw-Hill Publishing Company Limited, .

GREXA, O., JANSSENS, M., WHITE, R. and DIETENBERGER, M., 1996. Fundamental thermophysical properties of materials derived from the cone calorimeter measurements. *Wood and Fire Safety*, .

GRØNLI, M.G., 1996. *A theoretical and experimental study of the thermal degradation of biomass*, The Norwegian University of Science and Technology.

GRØNLI, M.G., ANTAL, J., M.J. and VARHEGYI, G., 1999. A Round-Robin Study of Cellulose Pyrolysis Kinetics by Thermogravimetry. *April 27th, 1999*, 38(6), pp. 2238–2244.

GUERTH-SCHACHER, C.C., 2007. *Evaluation of the Effects of Moisture on the Thermal Protective Performance of Fire Protective Clothing in Low Level Heat Exposures*. ProQuest.

GUPTA, M., YANG, J. and ROY, C., 2003. Specific heat and thermal conductivity of softwood bark and softwood char particles. *Fuel*, 82(8), pp. 919-927.

GUSTAFSSON, S.E., 1991. Transient plane source techniques for thermal conductivity and thermal diffusivity measurements of solid materials. *Review of Scientific Instruments*, 62(3), pp. 797.

GUSTAVSSON, M., KARAWACKI, E. and GUSTAFSSON, S.E., 1994. Thermal conductivity, thermal diffusivity, and specific heat of thin samples from transient measurements with hot disk sensors. *Review of Scientific Instruments*, 65(12), pp. 3856-3859.

HAGEN, M., HEREID, J., DELICHATSIOS, M.A., ZHANG, J. and BAKIRTZIS, D., 2009. Flammability assessment of fire-retarded Nordic Spruce wood using thermogravimetric analyses and cone calorimetry. *Fire Safety Journal*, 44(8), pp. 1053-1066.

HAGGE, M.J., BRYDEN, K.M. and DIETENBERGER, M.A., 2004. Effects of backing board materials on wood combustion performance , *Wood & fire safety : proceedings, 5th international scientific conference* , April 18-22 2004, Faculty of Wood Sciences and Technology, pp. 51-58.

HALLMAN, J.R., 1974. Polymer surface reflectance-absorptance characteristics. 14(10), pp. 717.

HANKALIN, V., AHONEN, T. and RAIKO, R., 2009. On thermal properties of a pyrolysing wood particle. *Finnish-Swedish Flame Days*, 16.

HARADA, T., HATA, T. and ISHIHARA, S., 1998. Thermal constants of wood during the heating process measured with the laser flash method. *Journal of wood science*, 44(6), pp. 425-431.

HARPER, C.A., 2004. *Handbook of building materials for fire protection*. New York McGraw-Hill.

HASALOVÁ, L., IRA, J. and JAHODA, M., 2012. Measurement and evaluation of experimental data for modelling thermal decomposition of solid materials. 29, pp. 1405-1410.

HASALOVA, L., MOINUDDIN, K.A.M. and ABU-BAKAR, A.S., 2013. Chemical kinetics of combustible materials - is the single "effective" reaction kinetics the best practice? , ACFM COMMITTEE, ed. In: *The 14th Asian Congress of Fluid Mechanics (14 ACFM)*, October 15 - 19, 2013 2013, ACFM.

HASELI, Y., VAN OIJEN, J.A. and DE GOEY, L.P.H., 2011. Modeling biomass particle pyrolysis with temperature-dependent heat of reactions. *Journal of Analytical and Applied Pyrolysis*, 90(2), pp. 140-154.

HES, L. and LOGHIN, C., 2009. Heat, moisture and air transfer properties of selected woven fabrics in wet state. *Journal of Fiber Bioengineering and Informatics*, 2(3), pp. 141-149.

HILLIER, J., BEZZANT, T. and FLETCHER, T.H., 2010. Improved Method for the Determination of Kinetic Parameters from Non-isothermal Thermogravimetric Analysis (TGA) Data. *April 23, 2010*, 24(5), pp. 2841–2847.

HO, K.W., 2007. *Flame Spread Modelling Using FDS4 CFD Model* , Canterbury University.

HOFFMAN, R. and PAN, W., 1990. Combining DSC and TG data for measuring heats of reaction. *Thermochimica acta*, 166, pp. 251-265.

HOLMAN, J.P., 1986. *Heat Transfer*. Singapore: Mc Gran–Hill.

HOSHINO, E., WADA, Y. and NISHIZAWA, K., 1999. Improvements in the hygroscopic properties of cotton cellulose by treatment with an endo-type cellulase from *Streptomyces* sp. KSM-26. *Journal of Bioscience and Bioengineering*, 88(5), pp. 519-525.

HOSTIKKA, S., 2012. *Personal Communication*.

HSHIEH, F. and BEESON, H.D., 1995. Flammability Testing of Pure and Flame Retardant-treated Cotton Fabrics. *June 24th, 1995*, 19(5), pp. 233-239.

HU, M., YU, D. and WEI, J., 2007. Thermal conductivity determination of small polymer samples by differential scanning calorimetry. *Polymer Testing*, 26(3), pp. 333-337.

HUGGETT, C., 1980. Estimation of rate of heat release by means of oxygen consumption measurements. *Fire and Materials*, 4(2), pp. 61-65.

INCROPERA, F.P., DEWITT, D.P., Bergman and T.L., L., A.S., 2006. *Fundamental of Heat and Mass Transfer*. 6th edn. Wiley.

INSTITUTION OF FIRE ENGINEERS, 2014, 2014-last update, Fire Engineering [Homepage of Institution of Fire Engineers], [Online]. Available: <http://www.ife.ca/fire-engineering.html> [01/2014, 2014].

INTERNATIONAL ORGANIZATION FOR STANDARDIZATION (ISO), 2002. *ISO 5660 -1 : 2002 Reaction-to-fire tests -- Heat release, smoke production and mass loss rate -- Part 1: Heat release rate (cone calorimeter method)*. Switzerland: .

JANSSENS, M. and DOUGLAS, B., 2004. Wood and Wood Products. In: C.A. HARPER, ed, *Handbook of Building Materials for Fire Protection*. McGraw-Hill, pp. 7.1-7.58.

JANSSENS, M.L., 2003. Improved method for analyzing ignition data from the cone calorimeter in the vertical orientation. *Fire Safety Science*, 7, pp. 803-814.

JANSSON, R., 2004. Measurement of thermal properties at elevated temperatures- brandforsk project 328-031. *SP Report*, 46.

JIANG, G., NOWAKOWSKI, D.J. and BRIDGWATER, A.V., 2010. A Systematic Study of Kineticsof Lignin Pyrolysis. 2010, 498(1–2), pp. 61–66.

JIANG, Y., 2006. *Decomposition, Ignition and Flame Spread on Furnishing Materials*, Victoria University Australia.

KASHIWAGI, T., INABA, A. and BROWN, J., 1986. Differences In Pmma Degradation Characteristics And Their Effects On Its Fire Properties. *Fire Safety Science*, 1, pp. 483-493.

KEMPEL, F., SCHARTEL, B., LINTERIS, G.T., STOLIAROV, S.I., LYON, R.E., WALTERS, R.N. and HOFMANN, A., 2012. Prediction of the mass loss rate of polymer materials: Impact of residue formation. *Combustion and Flame*, 159(9), pp. 2974-2984.

KIM, E., LAUTENBERGER, C. and DEMBSEY, N., 2009. Property estimation for pyrolysis modeling applied to polyester FRP composites with different glass contents. *Fire and Material*, .

KIM, S. and PARK, J.K., 1995. Characterization of thermal reaction by peak temperature and height of DTG curves. *Thermochimica acta*, 264, pp. 137-156.

KIM, S., KIM, J., PARK, Y. and PARK, Y., 2010. Pyrolysis kinetics and decomposition characteristics of pine trees. *Bioresource technology*, 101(24), pp. 9797-9802.

KISSINGER, H.E., 1956. Variation of peak temperature with heating rate in differential thermal analysis. *Journal of Research of the National Bureau of Standards*, 57(4), pp. 217-221.

KODUR, V.K.R. and HARMATHY, T.Z., 2002. Properties of Building Materials. In: P.J. DINENNO, D. DRYSDALE, C.L. BEYLER, W.D. WALTON, R.L.P. CUSTER,

J.R.J. HALL and J.M.J. WATTS, eds, *SFPE Handbook of Fire Protection Engineering*. Third edn. National Fire Protection Association, pp. 155-181.

KOUSKSOU, T., JAMILB, A., OMARIA, K.E., ZERAOULIA, Y. and LE GUERA, Y., 2011. Effect of heating rate and sample geometry on the apparent specific heat capacity: DSC applications. *20 May 2011*, 519(1–2), pp. 59–64.

LAUTENBERGER, C., REIN, G. and FERNANDEZ-P, C., 2006. The application of a genetic algorithm to estimate material properties for fire modeling from bench-scale fire test data. *April 2006*, 41(3), pp. 204–214.

LE BRAS, M., WILKIE, C.A. and BOURBIGOT, S., 2005. *Fire retardancy of polymers: new applications of mineral fillers*. Royal Society of Chemistry.

LEE, W.I., LOOS, A.C. and SPRINGER, G.S., 1982. Heat of reaction, degree of cure, and viscosity of Hercules 3501-6 resin. *Journal of Composite Materials*, 16(6), pp. 510-520.

LEE, Y. and VISWANATH, D.S., 2000. Degradation of poly (methyl methacrylate)(PMMA) with aluminum nitride and alumina. *Polymer Engineering & Science*, 40(11), pp. 2332-2341.

LESNIKOVICH, A. and LEVCHIK, S., 1983. A method of finding invariant values of kinetic parameters. *Journal of Thermal Analysis and Calorimetry*, 27(1), pp. 89-93.

LI, K., HUANG, X., FLEISCHMANN, C., REIN, G. and JI, J., 2014. Pyrolysis of medium-density fiberboard: optimized search for kinetics scheme and parameters via a genetic algorithm driven by Kissinger's method. *Energy & Fuels*, 28(9), pp. 6130-6139.

LI, J., GONG, J. and STOLIAROV, S.I., 2015. Development of pyrolysis models for charring polymers. *Polymer Degradation and Stability*, 115(0), pp. 138-152.

LI, J., GONG, J. and STOLIAROV, S.I., 2014. Gasification experiments for pyrolysis model parameterization and validation. *International Journal of Heat and Mass Transfer*, 77(0), pp. 738-744.

LI, J. and STOLIAROV, S.I., 2013. Measurement of kinetics and thermodynamics of the thermal degradation for non-charring polymers. *Combustion and Flame*, 160(7), pp. 1287-1297.

LINTERIS, G., 2011. Numerical simulations of polymer pyrolysis rate: effect of property variations. *Fire and Materials*, 35(7), pp. 463-480.

LINTERIS, G., GEWUERZ, L., MCGRATTAN, K. and FORNEY, G., 2005. Modeling solid sample burning, *Fire Safety Science--Proceedings of the Eight International Symposium, International Association for Fire Safety Science, Boston, MA 2005*.

LOWDEN, L.A. and HULL, T.R., 2013. Flammability behaviour of wood and a review of the methods for its reduction. *Fire science reviews*, 2(1), pp. 1-19.

LUCHE, J., ROGAUME, T., RICHARD, F. and GUILLAUME, E., 2011. Characterization of thermal properties and analysis of combustion behavior of PMMA in a cone calorimeter. *Fire Safety Journal*, 46(7), pp. 451-461.

MARQUIS, D.M., PAVAGEAU, M., GUILLAUME, E. and CHIVAS-JOLY, C., 2013. Modelling decomposition and fire behaviour of small samples of a glass-fibre-reinforced polyester/balsa-cored sandwich material. *Fire and Materials*, 37(6), pp. 413-439.

MATALA, A., 2008. *Estimation of Solid Phase Reaction Parameters for Fire Simulation*, Helsinki University of Technology.

MCGRATTAN, K. and FORNEY, G., 2006. *Fire Dynamics Simulator (Version 4) - User's Guide*. 4 edn. Washington DC, USA: National Institute of Technology and Standard.

MCGRATTAN, K., HOSTIKKA, S., MCDERMOTT, R., FLOYD, J., WEINSCHENK, C. and OVERHOLT, K., 2015. *Fire Dynamics Simulator (Version 6.2.0) Technical Reference Guide Volume 3 - Validation*. USA: National Institute of Standard and Technology.

MCGRATTAN, K., FLOYD, J., FORNEY, G., HOSTIKKA, S., KORHONEN, T., MCDERMOTT, R., and WEINSCHENK, C., 2012. *Fire Dynamics Simulator (Version 6.0.9) - User's Guide*. USA: National Institute of Standard and Technology.

MCGRATTAN, K., KLEIN, B., HOSTIKKA, S. and FLOYD, J., 2009a. *Fire Dynamics Simulator (Version 5.3) - User's Guide*. Washington DC USA: National Institute of Standard and Technology.

MCGRATTAN, K., KLEIN, B., HOSTIKKA, S. and FLOYD, J., 2009b. *Fire Dynamics Simulator (Version 5) - User's Guide*. Washington, USA: National Institute of Standard and Technology.

MCGRATTAN, K., HOSTIKKA, S., FLOYD, J., BAUM, H. and REHM, R., 2008. *Fire Dynamics Simulator (Version 5) - Technical Guide*. Gaithersburg, MD USA: National Institute of Standards and Technology.

MELL, W., MARANGHIDES, A., MCDERMOTT, R. and MANZELLO, S.L., 2009. Numerical simulation and experiments of burning douglas fir trees. *October 2009*, 156(10), pp. 2023.

METTLER-TOLEDO, 2012. *TGA 1 User's Manual*. User Guide edn. Switzerland: .

METTLER-TOLEDO, 2011. *DSC1 User's Manual*. User Guide edn. Switzerland: .

MILOSAVLJEVIC, I., OJA, V. and SUUBERG, E.M., 1996. Thermal effects in cellulose pyrolysis: relationship to char formation processes. *Industrial & Engineering Chemistry Research*, 35(3), pp. 653-662.

MISSOUM, A., GUPTA, A.K. and CHEN, J., 1997. Global kinetics of the thermal decomposition of waste materials, *Energy Conversion Engineering Conference, 1997. IECEC-97., Proceedings of the 32nd Intersociety 1997*, IEEE, pp. 636-641.

MOGHADDAM, A., MOINUDDIN, K., THOMAS, I., BENNETTS, I. and CULTON, M., 2004. Fire Behaviour Studies of Combustible Wall Linings Applying Fire Dynamics Simulator.

MOGHTADERI, B., NOVOZHILOV, V., FLETCHER, D. and KENT, J., 1997. A new correlation for bench-scale piloted ignition data of wood. *Fire Safety Journal*, 29(1), pp. 41-59.

MOGHTADERI, B., DLUGOGORSKI, B.Z., KENNEDY, E.M. and FLETCHER, D.F., 1998. Effects of the structural properties of solid fuels on their re-ignition characteristics. *Fire and Materials*, 22(4), pp. 155-165.

MOINUDDIN, K.A. and THOMAS, I.R., 2009. An experimental study of fire development in deep enclosures and a new HRR–time–position model for a deep enclosure based on ventilation factor. *Fire and Materials*, 33(4), pp. 157-185.

MOLTÓ, J., FONT, R., CONESA, J.A. and MARTÍN-GULLÓN, I., 2006. Thermogravimetric analysis during the decomposition of cotton fabrics in an inert and air environment. *Journal of Analytical and Applied Pyrolysis*, 76(1), pp. 124-131.

MORIANA, R., VILAPLANA, F., KARLSSON, S. and RIBES, A., 2014. Correlation of chemical, structural and thermal properties of natural fibres for their sustainable exploitation. *Carbohydrate Polymers*, 112, pp. 422-431.

MOURITZ, A., MATHYS, Z. and GIBSON, A., 2006. Heat release of polymer composites in fire. *Composites Part A: Applied science and manufacturing*, 37(7), pp. 1040-1054.

MUI, E.L., CHEUNG, W., LEE, V.K. and MCKAY, G., 2008. Kinetic study on bamboo pyrolysis. *Industrial & Engineering Chemistry Research*, 47(15), pp. 5710-5722.

MULHOLLAND, G.W. and CROARKIN, C., 2000. Specific extinction coefficient of flame generated smoke. *Fire and Materials*, 24(5), pp. 227-230.

MULHOLLAND, G.W., 1995. Smoke production and properties. *SFPE handbook of fire protection engineering*, 3, pp. 2-258.

MURALIDHARA, K. and SREENIVASAN, S., 2010. Thermal Degradation Kinetic Data of Polyester, Cotton and Polyester-Cotton Blended Textile Material. *World Applied Sciences Journal*, 11(2), pp. 184-189.

NATIONAL INSTITUTE OF STANDARD AND TECHNOLOGY, 2015-last update, Fire Dynamics Simulator (FDS) and Smokeview (SMV) [Homepage of National Institute of Standard and Technology], [Online]. Available: <http://www.fire.nist.gov/fds/>. [5/19, 2015].

NAZARÉ, S., KANDOLA, B. and HORROCKS, A.R., 2002. Use of Cone Calorimetry to Quantify the Burning Hazard of Apparel Fabrics. *December 2002*, 26(4-5), pp. 191-199.

NELSON, G.L. and JAYAKODY, C., 1998. Flame Retardant Polyurethane, FIRE RETARDANT CHEMICALS ASSOCIATION, ed. In: *Flame Retardant Polymeric: Electrical/Electronic Applications*, October, 4th-7th 1998, Fire Retardant Chemicals Association, pp. 1.

OPFERMANN, J., 2000. Kinetic analysis using multivariate non-linear regression. I. Basic concepts. *Journal of thermal analysis and calorimetry*, 60(2), pp. 641-658.

ÖSTMAN, B.A.-. and TSANTARIDIS, L.D., 1995. Heat release and classification of fire retardant wood products. *Fire and Materials*, 19(6), pp. 253-258.

OZAWA, T., 1975. Critical investigation of methods for kinetic analysis of thermoanalytical data. *Journal of Thermal Analysis and Calorimetry*, 7(3), pp. 601-617.

OZAWA, T., 1970. Kinetic analysis of derivative curves in thermal analysis. *Journal of Thermal Analysis and Calorimetry*, 2(3), pp. 301-324.

PALANNA, O., 2009. *Engineering chemistry*. Tata McGraw-Hill.

PARK, D., 2014. Evaluation of the Combustion Characteristics of Railroad Waste using a Cone Calorimeter. *February 20, 2014*, 2(1), pp. 27-35.

PAU, D.S.W., 2013. *A comparative study on combustion behaviours of polyurethane foams with numerical simulations using pyrolysis models*, University of Canterbury. Civil and Natural Resources Engineering.

PAU, D., FLEISCHMANN, C., SPEARPOINT, M. and LI, K., 2014. Thermophysical properties of polyurethane foams and their melts. *Fire and Materials*, 38(4), pp. 433-450.

PERKIN ELMER, 1997. *Pyris User Manual*. User Guide edn. USA: Perkin Elmer.

PETERSON, J.D., VYAZOVKIN, S. and WIGHT, C.A., 1999. Kinetic study of stabilizing effect of oxygen on thermal degradation of poly (methyl methacrylate). *The Journal of Physical Chemistry B*, 103(38), pp. 8087-8092.

POPESCU, C. and AUGUSTIN, P., 1999. Effect of chlorination treatment on the thermogravimetric behaviour of wool fibres. *Journal of thermal analysis and calorimetry*, 57(2), pp. 509-515.

POTTEL, H., 1996. The accumulation of flammable gases in cone calorimeter tests is responsible for flash ignition of wool and cotton samples. *Fire and Materials*, 20(2), pp. 107-109.

PRICE, D., LIU, Y., HULL, T.R., MILNES, G.J., KANDOLA, B.K. and HORROCKS, A.R., 2000. Burning behaviour of fabric/polyurethane foam combinations in the cone calorimeter. *Polymer International*, 49(10), pp. 1153-1157.

QUAN, C., LI, A. and GAO, N., 2009. Thermogravimetric analysis and kinetic study on large particles of printed circuit board wastes. *Waste Management*, 29(8), pp. 2353-2360.

RAGLAND, K., AERTS, D. and BAKER, A., 1991. Properties of wood for combustion analysis. *Bioresource technology*, 37(2), pp. 161-168.

RATH, J., WOLFINGER, M.G., STEINER, G., KRAMMER, G. and BARONTINI, F.C., V., 2003. Heat of Wood Pyrolysis. *January 2003*, 82(1), pp. 81–91.

REIN, G., LAUTENBERGER, C., FERNANDEZ-PELLO, A.C., TORERO, J.L. and URBAN, D.L., 2006. Application of genetic algorithms and thermogravimetry to determine the kinetics of polyurethane foam in smoldering combustion. *Combustion and Flame*, 146(1), pp. 95-108.

RHODES, B.T. and QUINTIERE, J.G., 1996. Burning rate and flame heat flux for PMMA in a cone calorimeter. *April 1996*, 26(3), pp. 221-240.

RICCIO, A., DAMIANO, M., ZARRELLI, M. and SCARAMUZZINO, F., 2013. Three-dimensional modeling of composites fire behavior. *Journal of Reinforced Plastics and Composites*, , pp. 0731684413512226.

SENECCA, O., 2007. Kinetics of pyrolysis, combustion and gasification of three biomass fuels. *January 2007*, 88(1), pp. 87-97.

SHAFIZADEH, F., BRADBURY, A.G., DEGROOT, W.F. and AANERUD, T.W., 1982. Role of inorganic additives in the smoldering combustion of cotton cellulose. *Industrial & Engineering Chemistry Product Research and Development*, 21(1), pp. 97-101.

SHALAEV, E.Y. and STEPONKUS, P.L., 2000. Correction of the sample weight in hermetically sealed DSC pans. *Thermochimica acta*, 345(2), pp. 141-143.

SHI, L., 2014. *Pyrolysis and Combustion Processes of Combustible Materials Under External Heat Flux*, National University of Singapore.

SHI, L. and CHEW, M.Y.L., 2013. A review of fire processes modeling of combustible materials under external heat flux. *Fuel*, 106, pp. 30-50.

SIBULKIN, M., 1986. Heat of gasification for pyrolysis of charring materials, *Fire Safety Science: Proceedings of the First International Symposium 1986*, CRC Press, pp. 391.

SIMILE, C.B., 2004. Critical evaluation of wicking in performance fabrics.

SLOPIECKA, K., BARTOCCI, P. and FANTOZZI, F., 2012. Thermogravimetric analysis and kinetic study of poplar wood pyrolysis. *Applied Energy*, 97, pp. 491-497.

SMAGORINSKY, J., 1963. General circulation experiments with the primitive equations: I. the basic experiment *March 1963*, 91(3), pp. 99.

SMITH, W.F. and HASHEMI, J., 2006. Polymeric Materials. *Foundations of Materials Science and Engineering*. Fifth edn. Mcgraw-Hill Publishing, pp. 515-516.

SPEARPOINT, M. and QUINTIERE, J., 2000. Predicting the piloted ignition of wood in the cone calorimeter using an integral model - effect of species, grain orientation and heat flux. *Combustion and Flame*, 123(3), pp. 308-325.

STANDARDS AUSTRALIA & STANDARDS NEW ZEALAND, 1998. *AS/NZS 3837 Cone Calorimeter standards (ISO 5660–1 ASTM E 1354)*.

STATE FORESTS OF NEW SOUTH WALES, 1996. *Finishes for Exterior Timber Surfaces*. State Forests of New South Wales.

STEINHAUS, T., 1999. *Evaluation of the Thermophysical Properties of Poly(Methylmethacrylate) : A Reference Material for Development of A Flammability Test for Micro-Gravity Environments*, University of Maryland.

STOLIAROV, S.I. and WALTERS, R.N., 2008. Determination of the heats of gasification of polymers using differential scanning calorimetry. *Polymer Degradation and Stability*, 93(2), pp. 422-427.

SU, Y., LUO, Y., WU, W., ZHANG, Y. and ZHAO, S., 2012. Characteristics of pine wood oxidative pyrolysis: degradation behavior, carbon oxide production and heat properties. *Journal of Analytical and Applied Pyrolysis*, 98, pp. 137-143.

SULEIMAN, B., LARFELDT, J., LECKNER, B. and GUSTAVSSON, M., 1999. Thermal conductivity and diffusivity of wood. *Wood Science and Technology*, 33(6), pp. 465-473.

SUUBERG, E.M., MILOSAVLJEVIC, I. and OJA, V., 1996. Two-regime global kinetics of cellulose pyrolysis: the role of tar evaporation, *Symposium (International) on Combustion 1996*, Elsevier, pp. 1515-1521.

SVETLOV, D., ISAEV, V. and SVETLOV, Y.V., 2014. Heat Capacity and Thermal Conductivity of Fabrics Based on Chemical Fibers. *Fibre Chemistry*, 46(1), pp. 45-50.

SWANN, J., HARTMAN, J. and BEYLER, C., 2008. Study of radiant smoldering ignition of plywood subjected to prolonged heating using the cone calorimeter, TGA,

and DSC, *The ninth international symposium on fire safety science, German 2008*, pp. 98-102.

TATA, J., ALONGI, J., CAROSIO, F. and FRACHE, A., 2011. Optimization of the procedure to burn textile fabrics by cone calorimeter: part I. Combustion behavior of polyester. *Fire and Materials*, 35(6), pp. 397-409.

TEWARSON, A., 2002. Generation of heat and chemical compounds in fires. In: DINENNO ET AL., ed, *SFPE Handbook of Fire Protection Engineering*. 3 edn. Massachusetts, USA: National Fire Protection Association, pp. 3.82.

TEWARSON, A. and PION, R.F., 1976. Flammability of plastics—I. Burning intensity. *Combustion and Flame*, 26(0), pp. 85-103.

THERMTEST INC., 2012. *Hot Disk Thermal Constants Analyser Instruction Manual*. Application Note edn. Canada: Thermtest Inc.

TIAN, C., ZHANG, H., XU, J., PANG, X., GUO, H., SHI, J. and SHI, Z., 1998. Studies on the flame retardation and thermal degradation of wool.

TRAN, H.C., 1992. Experimental Data on Wood Materials. In: V. BABRAUSKAS and S.J. GRAYSON, eds, *Heat Release Rate in Fires*. New York: Elsevier Applied Science, pp. 357.

TSAI, K., 2009. Orientation effect on cone calorimeter test results to assess fire hazard of materials. *Journal of hazardous materials*, 172(2-3), pp. 763-772.

TSILINGIRIS, P.T., 2003. Comparative evaluation of the infrared transmission of polymer films. *November 2003*, 44(18), pp. 2839.

VISWANATH, S.G. and GUPTA, M.C., 1996. Estimation of nonisothermal kinetic parameters from a TG curve by the methods of overdetermined system and inflection point. *Thermochimica Acta*, 285(2), pp. 259-267.

VYAZOVKIN, S., 2015. *Isoconversional Kinetics of Thermally Stimulated Processes*. Switzerland: Springer.

VYAZOVKIN, S., BURNHAM, A.K., CRIADO, J.M., PÉREZ-MAQUEDA, L.A., POPESCU, C. and SBIRRAZZUOLI, N., 2011. ICTAC Kinetics Committee recommendations for performing kinetic computations on thermal analysis data. *Thermochimica Acta*, 520(1), pp. 1-19.

VYAZOVKIN, S. and WIGHT, C.A., 1998. Isothermal and non-isothermal kinetics of thermally stimulated reactions of solids. *International Reviews in Physical Chemistry*, 17(3), pp. 407-433.

VYAZOVKIN, S., 1992. Alternative description of process kinetics. *Thermochimica acta*, 211, pp. 181-187.

WAKELYN, P.J., BERTONIERE, N.R., FRENCH, A.D., THIBODEAUX, D.P., TRIPLETT, B.A., ROUSSELLE, M., GOYNES JR, W.R., EDWARDS, J.V., HUNTER, L. and MCALISTER, D.D., 2006. Chapter 9 Cotton Fibers. In: M. LEWIN, ed, *Handbook of Fiber Chemistry*. Third Edition edn. CRC Press, pp. 612.

WAMPLER, T.P., 2006. *Applied pyrolysis handbook*. CRC Press.

WANG, G., LI, W., LI, B. and CHEN, H., 2008. TG study on pyrolysis of biomass and its three components under syngas. *Fuel*, 87(4), pp. 552-558.

WHITE, N., 2010. *Fire Development in Passengers Train*, Victoria University Melbourne.

WILSON JR, E.W., KELLER, B.D., HARKNESS, K.M., SMEAL, C.S., EASTERLY, M.S. and MACKEY, J.E., 2006. Ultraviolet-Visible Spectrometry Characterization of Combustion in Hybrid Rocket Motors, *42nd AIAA/ASME/SAE/ASEE Joint Propulsion Conference & Exhibit 2006*, pp. 4343.

YANG, L., CHEN, X., ZHOU, X. and FAN, W., 2003. The pyrolysis and ignition of charring materials under an external heat flux. *Combustion and Flame*, 133(4), pp. 407-413.

ZENG, W.R., LI, S.F. and CHOW, W.K., 2002. Preliminary studies on burning behavior of polymethylmethacrylate (PMMA). *Journal of Fire Sciences*, 20(4), pp. 297-317.

ZHANG, H., 2004. *Fire-safe polymers and polymer composites*. Washington: Federal Aviation Administration.

ZHANG, Z., YANI, S., ZHU, M., LI, J. and ZHANG, D., 2013. Effect of temperature and heating rate in pyrolysis on the yield, structure and oxidation reactivity of pine sawdust biochar.

ZHU, P., SUI, S., WANG, B., SUN, K. and SUN, G., 2004. A study of pyrolysis and pyrolysis products of flame-retardant cotton fabrics by DSC, TGA, and PY-GC-MS. *Journal of Analytical and Applied Pyrolysis*, 71(2), pp. 645-655.

APPENDIX A - ADDITIONAL TGA DATA

This is a supplementary data of pine, PMMA and cotton data from Perkin Elmer TGA data is presented in Figure A.1 to A.4 at various heating rates. Additionally, data from Mettler TGA for wool is presented in Figure A.5 and A.6. This is a supplementary data that is presented in CHAPTER 4.

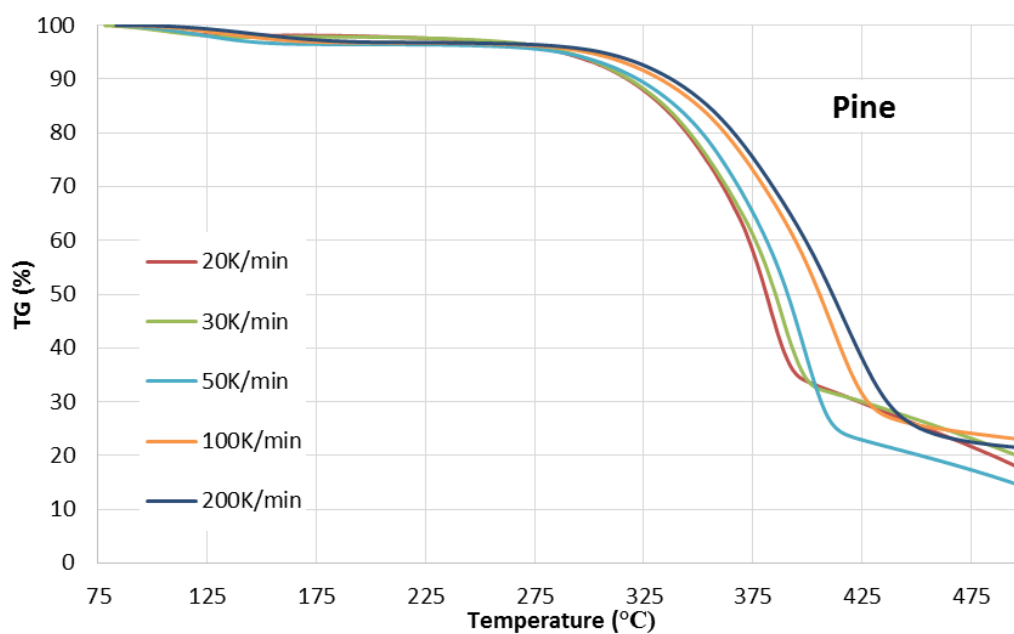


Figure A.1: TGA PE thermograms of pine at various heating rates

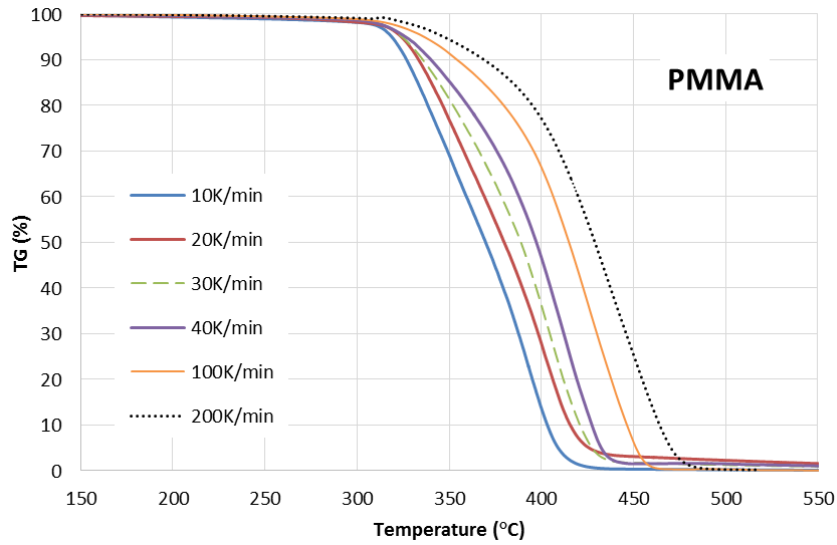


Figure A.2: TGA PE thermograms of PMMA at various heating rates

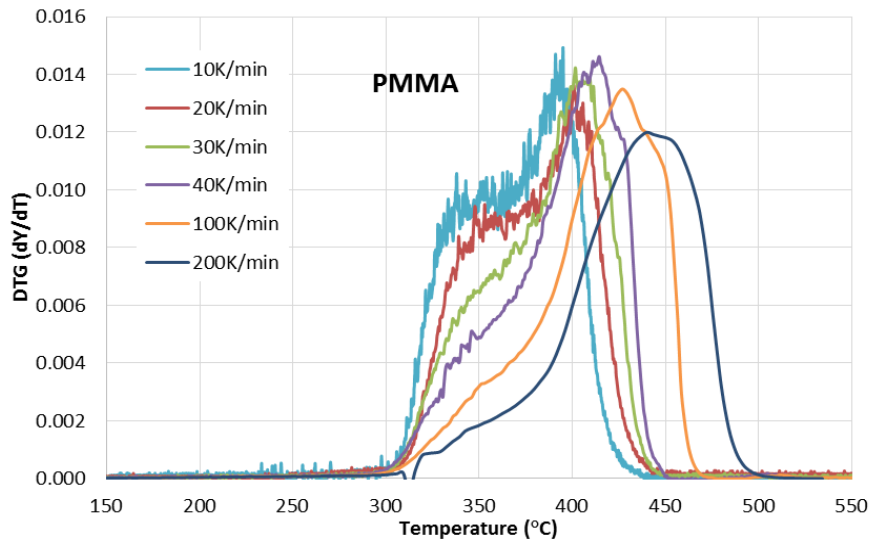


Figure A.3: DTG PE thermograms of PMMA at various heating rates

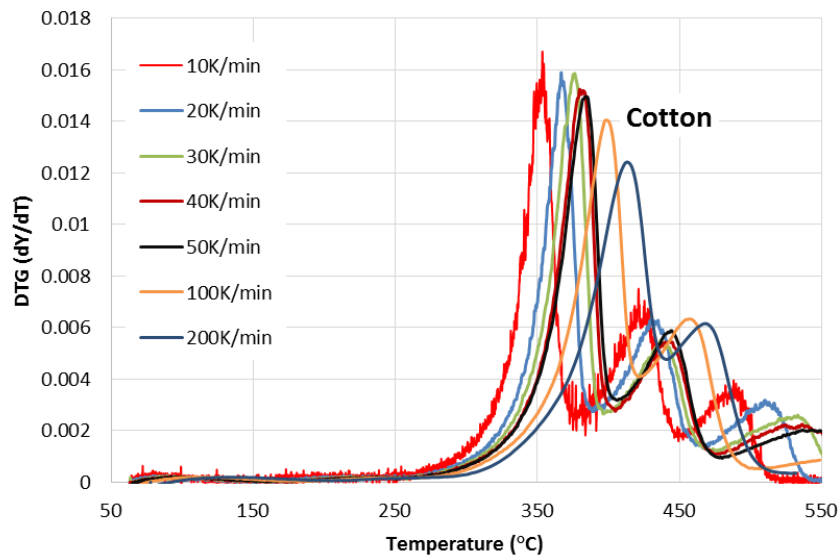


Figure A.4: DTG PE thermograms of Cotton at various heating rates

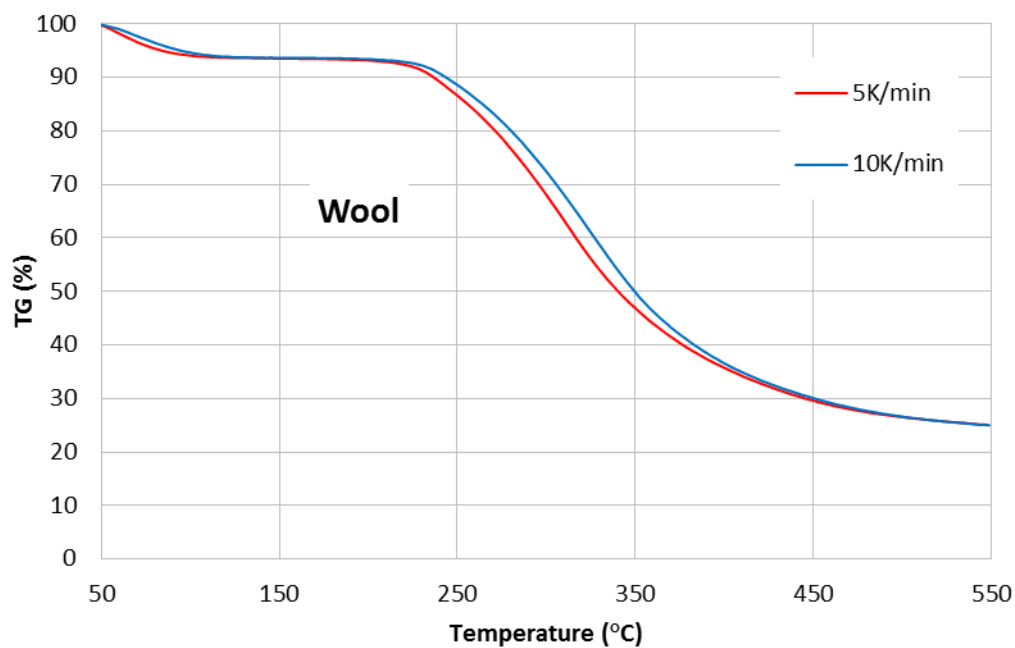


Figure A.5: TGA Mettler thermograms of Wool at various heating rates

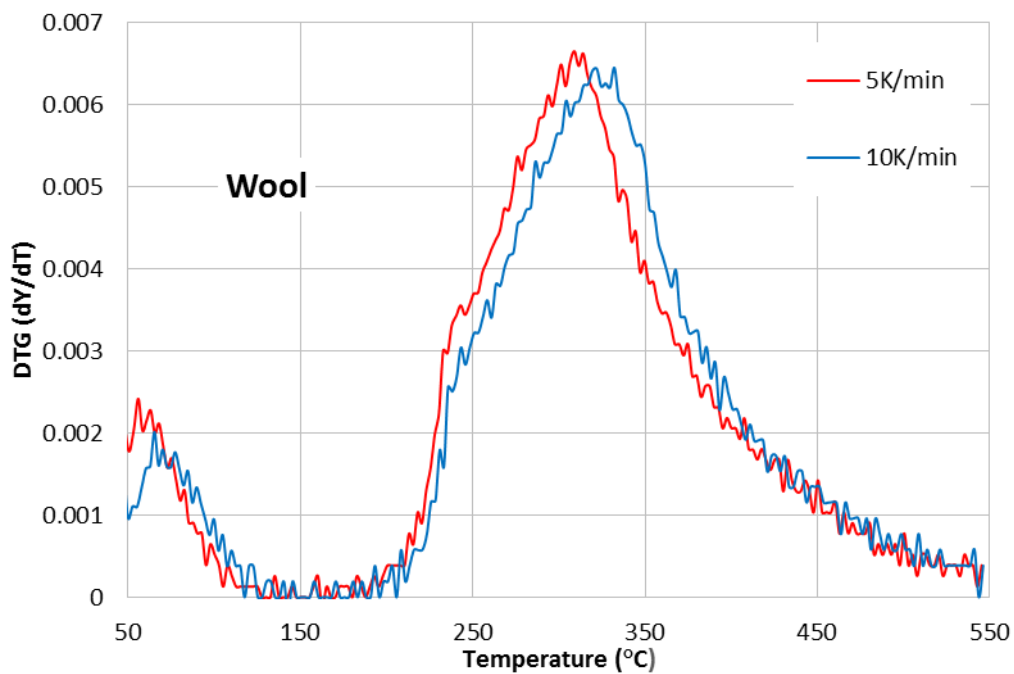


Figure A.6: DTG Mettler thermograms of Wool at various heating rates

APPENDIX B – CONE CALORIMETER DATA

MLR and SEA profile vs time of cotton are presented at various heat fluxes in Figure B.1 and Figure B.2, respectively. This is a supplementary data that is presented in Section 5.4. On the other hand, the MLR data of wool is presented in Figure B.3 as an additional data from Section 5.5.

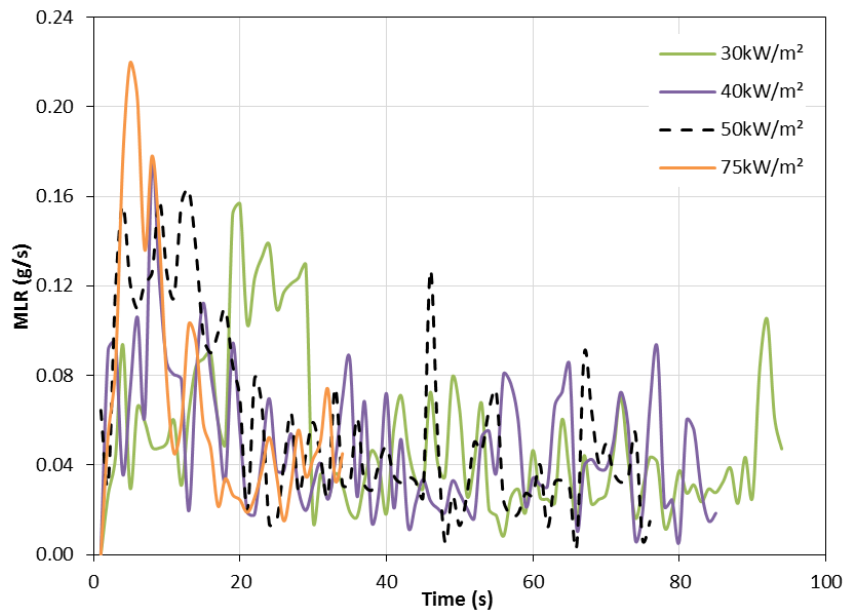


Figure B.1: MLR of Cotton at various heat fluxes

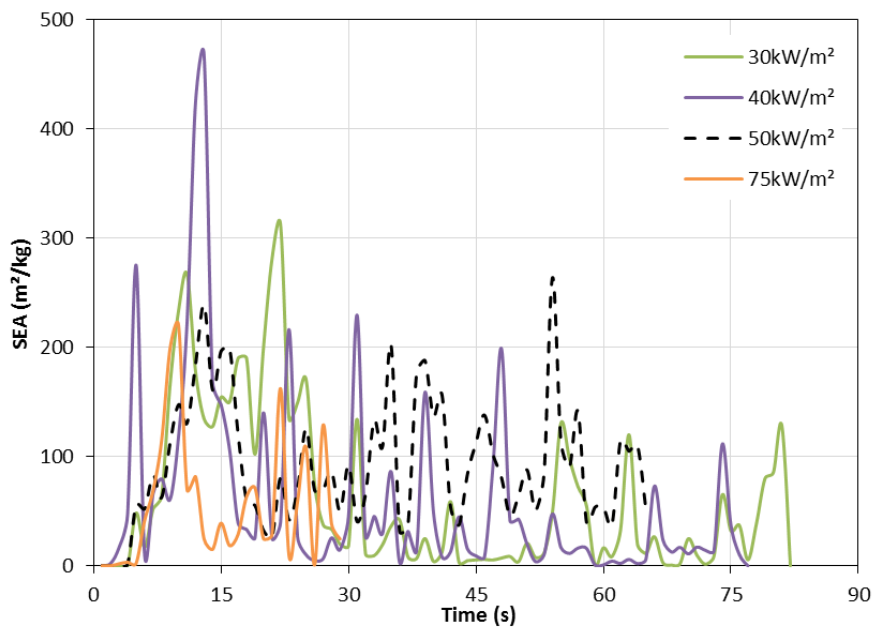


Figure B.2: SEA of Cotton at various heat fluxes

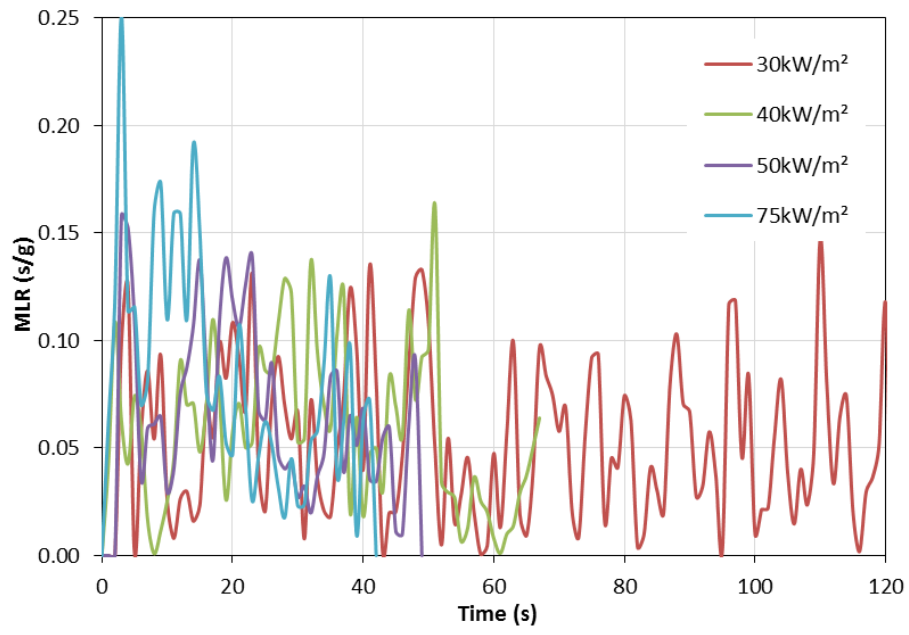


Figure B.3: MLR of Wool at various heat fluxes

APPENDIX C– DETAILS OF TGA SIMULATION USING FDS

C.1 FDS input file for TGA simulation of Pine at 20 K/min

```
&HEAD CHID='Pine-TGA-20K', TITLE='Case to simulate TGA test-pine' /
&MESH IJK=3,1,4, XB=-2.0,2.0,-0.5,0.5,0.0,1.0 /
&TIME T_END= 1466.0, DT = 0.0500, WALL_INCREMENT = 1 /
&MISC TMPA= 125.1, SOLID_PHASE_ONLY=.TRUE., Y_O2_INFITY=0.01 /
&RADI TIME_STEP_INCREMENT=1,NUMBER_RADIATION_ANGLES = 100 /
&REAC FUEL='METHANE', C=1., H=4., CRITICAL_FLAME_TEMPERATURE=2000. /

&VENT XB = -1,1,-0.5,0.5,0.0,0.0, SURF_ID = 'SAMPLE', COLOR = 'BLUE' /

&VENT MB='XMIN', SURF_ID='HOT' /
&VENT MB='XMAX', SURF_ID='HOT' /
&VENT MB='ZMAX', SURF_ID='HOT' /

&VENT XB = -2,-1,-0.5,0.5,0.0,0.0, SURF_ID = 'HOT' /
&VENT XB = 1,2,-0.5,0.5,0.0,0.0, SURF_ID = 'HOT' /

&SURF ID = 'HOT'
EMISSIVITY = 1.0
RGB      = 250,0,0
TMP_FRONT = 1000.
HEAT_TRANSFER_COEFFICIENT = 0.
RAMP_T      = 'T_RAMP' /

&RAMP ID = 'T_RAMP' T = 0., F = 0.00000 /
&RAMP ID = 'T_RAMP' T = 1466.00, F = 0.6081 /

&MATL ID          = 'PINE'
  CONDUCTIVITY_RAMP='k_PINE'
  DENSITY          = 360.00
  SPECIFIC_HEAT_RAMP='c_PINE'
  EMISSIVITY      = 1.0
  SPEC_ID(01,01)  = 'METHANE'
  NU_SPEC(01,01)  = 0.815
  A(01)           = 2.66E+03
  E(01)           = 70.34E+03
  N_S(01)         = 0.348
  THRESHOLD_TEMPERATURE(01)= 0.00
  HEAT_OF_REACTION(01) = 100.00
  N_REACTIONS     = 01
  MATL_ID = 'CHAR'
  NU_MATL = 0.185
  ALLOW_SHRINKING=.FALSE.
  ALLOW_SWELLING=.FALSE./

&MATL ID = 'CHAR', EMISSIVITY = 1.0, DENSITY = 285.,
CONDUCTIVITY=0.08,SPECIFIC_HEAT=0.43/

&RAMP ID='c_PINE', T= 20., F=1.1 /
```

```

&RAMP ID='c_PINE', T=50., F=2.3 /
&RAMP ID='c_PINE', T=90., F=4.0 /

&RAMP ID='k_PINE', T= 20., F=0.17 /
&RAMP ID='k_PINE', T=110., F=0.02 /

&SURF ID = 'SAMPLE', THICKNESS = 0.00001, STRETCH_FACTOR = 1.0000,
MINIMUM_LAYER_THICKNESS =1E-9, MATL_ID(1,01) = 'PINE',
HEAT_TRANSFER_COEFFICIENT = 0.000, BACKING = 'INSULATED' /

&DUMP DT_DEVC= 2.0000, DT_PROF= 1.0000, DT_HRR = 1E6, DT_PL3D = 1E6,
SMOKE3D = .FALSE. /

&DEVC XYZ = 0.0,0.0,1.0, IOR = -3, QUANTITY = 'WALL TEMPERATURE' /
&DEVC XYZ = 0.0,0.0,0.0, IOR = 3, QUANTITY = 'WALL TEMPERATURE' /
&DEVC XYZ = 0.0,0.0,0.0, IOR = 3, QUANTITY = 'SURFACE DENSITY' /
\&DEVC XYZ = 0.0,0.0,0.0, IOR = 3, QUANTITY = 'NORMALIZED MASS' /
\&DEVC XYZ = 0.0,0.0,0.0, IOR = 3, QUANTITY = 'NORMALIZED MASS LOSS RATE'
SPEC_ID = 'METHANE' /

&TAIL /

```

C.2 FDS input file for TGA simulation of PMMA at 20 K/min

```

&HEAD CHID='PMMA-TGA-20K', TITLE='Case to simulate TGA test-PMMA' /
&MESH IJK=3,1,4, XB=-2.0,2.0,-0.5,0.5,0.0,1.0 /
&TIME T_END= 1466.0, DT = 0.0500, WALL_INCREMENT = 1 /
&MISC TMPA= 125.1, SOLID_PHASE_ONLY=.TRUE., Y_O2_INFITY=0.01 /
&RADI TIME_STEP_INCREMENT=1, NUMBER_RADIATION_ANGLES = 100 /
&REAC FUEL='METHANE', C=1., H=4., CRITICAL_FLAME_TEMPERATURE=2000. /

&VENT XB = -1,1,-0.5,0.5,0.0,0.0, SURF_ID = 'SAMPLE', COLOR = 'BLUE' /
&VENT MB='XMIN', SURF_ID='HOT' /
&VENT MB='XMAX', SURF_ID='HOT' /
&VENT MB='ZMAX', SURF_ID='HOT' /
&VENT XB = -2,-1,-0.5,0.5,0.0,0.0, SURF_ID = 'HOT' /
&VENT XB = 1,2,-0.5,0.5,0.0,0.0, SURF_ID = 'HOT' /

&SURF ID = 'HOT'
EMISSIVITY = 1.0
RGB = 250,0,0
TMP_FRONT = 1000.
HEAT_TRANSFER_COEFFICIENT = 0.
RAMP_T = 'T_RAMP' /

&RAMP ID = 'T_RAMP' T = 0., F = 0.00000 /
&RAMP ID = 'T_RAMP' T = 1466.00, F = 0.625 /

&MATL ID = 'PMMA'
CONDUCTIVITY = 0.195
DENSITY = 1210.00

```

```

SPECIFIC_HEAT      = 1.47
EMISSIVITY         = 0.85
ABSORPTION_COEFFICIENT = 0.9E+9
SPEC_ID(01,01)    = 'METHANE'
NU_SPEC(01,01)   = 1.000
A(01)             = 4.26E+17
E(01)             = 2.41E+05
N_S(01)           = 1.73
THRESHOLD_TEMPERATURE(01)= 0.00
HEAT_OF_REACTION(01) = 1000.00
N_REACTIONS       = 01 /

&SURF ID          = 'SAMPLE'
THICKNESS         = 0.00001
STRETCH_FACTOR    = 1.0000
MINIMUM_LAYER_THICKNESS =1E-9
MATL_ID(1,01) = 'PMMA',
HEAT_TRANSFER_COEFFICIENT = 0.000,
BACKING           = 'INSULATED' /

&DUMP DT_DEVC= 2.0000, DT_PROF= 1.0000, DT_HRR = 1E6, DT_PL3D = 1E6,
SMOKE3D = .FALSE. /

&DEVC XYZ = 0.0,0.0,1.0, IOR = -3, QUANTITY = 'WALL TEMPERATURE' /
&DEVC XYZ = 0.0,0.0,0.0, IOR = 3, QUANTITY = 'WALL TEMPERATURE' /
&DEVC XYZ = 0.0,0.0,0.0, IOR = 3, QUANTITY = 'SURFACE DENSITY' /
\&DEVC XYZ = 0.0,0.0,0.0, IOR = 3, QUANTITY = 'NORMALIZED MASS' /
\&DEVC XYZ = 0.0,0.0,0.0, IOR = 3, QUANTITY = 'NORMALIZED MASS LOSS RATE',
SPEC_ID = 'METHANE' /

&TAIL /

```

C.3 Visualisation of the domain

A visualisation of a typical domain modelled for TGA test simulation is given in Figure C1 where blue represents the sample and red represents radiative heating from surrounding.

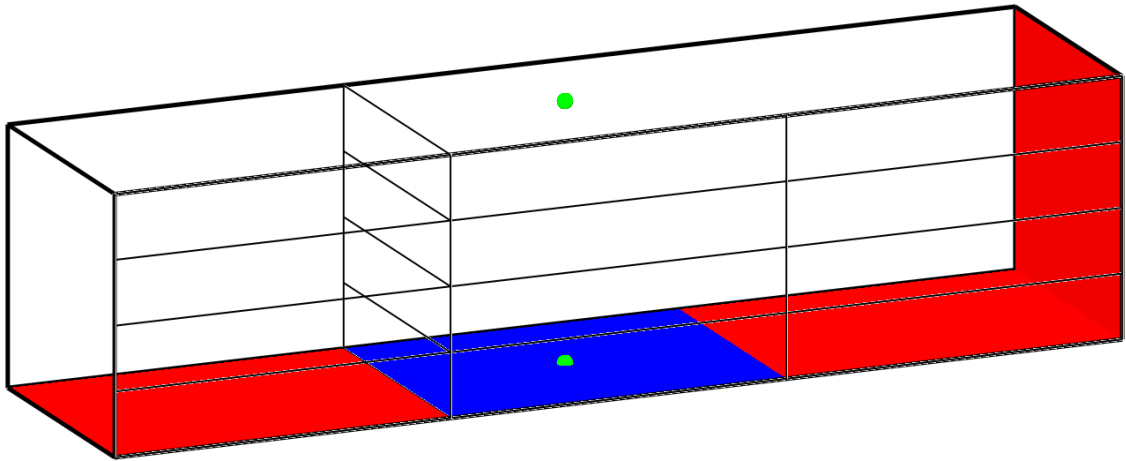


Figure C.1: Visualisation of typical domain: blue represents the sample and red represents radiative heating from surrounding.

APPENDIX D— DETAILS OF CONE CALORIMETER SIMULATION USING FDS FOR GRID SENSITIVITY

D.1 FDS input file for Cone Calorimeter simulation of Pine for grid sensitivity

```
&CHID='PINE', TITLE='Cone calorimeter'/ for 50kW/m2, 10mm grid

&MESH IJK=10,10,70, XB = 0.15,0.25,0.15,0.25,0,0.7/
&MESH IJK=10,10,70, XB = 0.25,0.35,0.15,0.25,0,0.7/
&MESH IJK=10,10,70, XB = 0.15,0.25,0.25,0.35,0,0.7/
&MESH IJK=10,10,70, XB = 0.25,0.35,0.25,0.35,0,0.7/

&TIME T_END=120, WALL_INCREMENT=1., DT=0.01/
&DUMP DT_HRR = 5.0, DT_DEVC = 5.0, DT_RESTART=20. /

&OBST XB=0.215,0.285,0.215,0.285,0.05,0.075 ,SURF_ID = 'PINE'/
&OBST XB=0.2,0.215,0.2,0.3,0.05,0.075 ,SURF_ID = 'PINE2'/
&OBST XB=0.285,0.3,0.2,0.3,0.05,0.075 ,SURF_ID = 'PINE2'/

&OBST XB=0.2,0.3,0.2,0.215,0.05,0.075 ,SURF_ID = 'PINE2'/
&OBST XB=0.2,0.3,0.285,0.3,0.05,0.075 ,SURF_ID = 'PINE2'/

&OBST XB=0.2,0.3,0.2,0.3,0.05,0.047,SURF_ID='STEEL'/
&OBST XB=0.197,0.303,0.197,0.2,0.047,0.075,SURF_ID='STEEL' /
&OBST XB=0.197,0.2,0.197,0.303,0.047,0.075,SURF_ID='STEEL'/
&OBST XB=0.3,0.303,0.197,0.303,0.047,0.075,SURF_ID='STEEL'/
&OBST XB=0.197,0.303,0.3,0.303,0.047,0.075,SURF_ID='STEEL'/

&SPEC ID='WATER VAPOR' /

&SURF ID = 'PINE',MATL_ID= 'PINE','STEEL', MATL_ID(1,1) = 'PINE',MATL_ID(1,2)
= 'MOISTURE', MATL_MASS_FRACTION(1,:) = 0.94,0.06, EXTERNAL_FLUX= 50.,
COLOR = 'WHITE',BACKING = 'INSULATED',THICKNESS=
0.0188,0.0007,CELL_SIZE_FACTOR=0.5,STRETCH_FACTOR=1,BURN_AWAY = .TRUE./

&SURF ID = 'PINE2',MATL_ID= 'PINE','STEEL',MATL_ID(1,1) = 'PINE',MATL_ID(1,2)
= 'MOISTURE', MATL_MASS_FRACTION(1,:) = 0.94,0.06, EXTERNAL_FLUX= 50.,
COLOR = 'WHITE',BACKING = 'EXPOSED', THICKNESS=
0.0188,0.0007,CELL_SIZE_FACTOR=0.5,STRETCH_FACTOR=1,BURN_AWAY = .TRUE./

&REAC ID = 'PINE_FUEL',C = 3.4,H = 6.2,O = 2.5, CO_YIELD = 0.007, SOOT_YIELD =
0.006,HEAT_OF_COMBUSTION = 11210., IDEAL=.FALSE./

&RADI RADIATION=.TRUE. /

&MATL ID='PINE', CONDUCTIVITY_RAMP='k_PINE',SPECIFIC_HEAT_RAMP='c_PINE',
DENSITY=360., Emissivity= 1.0, N_REACTIONS=1,
SPEC_ID='PINE_FUEL',NU_SPEC=0.85,MATL_ID = 'CHAR',NU_MATL = 0.15,
HEAT_OF_REACTION=97., E=107.26E3, N_S=0.717,A=4.4E7/
```

&RAMP ID='c_PINE', T= 20., F=1.1 /
&RAMP ID='c_PINE', T=50., F=2.3 /
&RAMP ID='c_PINE', T=90., F=4.0 /

&RAMP ID='k_PINE', T= 20., F=0.17 /
&RAMP ID='k_PINE', T=110., F=0.02 /

&MATL ID = 'MOISTURE', EMISSIVITY = 1.0, DENSITY = 1000., CONDUCTIVITY = 0.6,
SPECIFIC_HEAT = 4.19,N_REACTIONS = 1,A = 1.82E4,E = 38.92E3,N_S = 0.11,
SPEC_ID = 'WATER VAPOR', NU_SPEC = 1.0, HEAT_OF_REACTION= 2260. /

&MATL ID = 'CHAR', EMISSIVITY = 1.0, DENSITY = 285.,
CONDUCTIVITY=0.08,SPECIFIC_HEAT=0.43/

&SURF ID= 'STEEL', MATL_ID = 'STEEL',COLOR = 'RED',BACKING =
'EXPOSED',THICKNESS= 0.003 /

&MATL ID = 'STEEL', EMISSIVITY = 0.9, DENSITY = 7850., SPECIFIC_HEAT_RAMP =
'c_steel', CONDUCTIVITY_RAMP = 'k_steel'/

&RAMP ID='c_steel', T= 20., F=0.45 /
&RAMP ID='c_steel', T=377., F=0.60 /
&RAMP ID='c_steel', T=677., F=0.85 /

&RAMP ID='k_steel', T= 20., F=48. /
&RAMP ID='k_steel', T=677., F=30. /

&VENT MB='XMIN',SURF_ID='OPEN'/
&VENT MB='XMAX',SURF_ID='OPEN'/
&VENT MB='YMIN',SURF_ID='OPEN'/
&VENT MB='YMAX',SURF_ID='OPEN'/
&VENT MB='ZMAX' SURF_ID='OPEN'/
&VENT MB='ZMIN' SURF_ID='OPEN'/

&SLCF PBX=0.25, QUANTITY='TEMPERATURE'/
&SLCF PBY=0.25, QUANTITY='TEMPERATURE'/

&BNDF QUANTITY='WALL TEMPERATURE'/
&BNDF QUANTITY='NET HEAT FLUX'/
&BNDF QUANTITY='RADIATIVE HEAT FLUX'/

&DEVC ID= 'Temperature', XYZ=0.255,0.255,0.075, QUANTITY= 'WALL
TEMPERATURE',IOR=3/
&DEVC ID= 'Inside Temperature1', XYZ=0.255,0.255,0.07375, QUANTITY= 'INSIDE
WALL TEMPERATURE',IOR=3/
&DEVC ID= 'Inside Temperature2', XYZ=0.255,0.255,0.0725, QUANTITY= 'INSIDE
WALL TEMPERATURE',IOR=3/
&DEVC ID= 'Inside Temperature3', XYZ=0.255,0.255,0.07125, QUANTITY= 'INSIDE
WALL TEMPERATURE',IOR=3/
&DEVC ID= 'Inside Temperature4', XYZ=0.255,0.255,0.07, QUANTITY= 'INSIDE
WALL TEMPERATURE',IOR=3/
&DEVC ID= 'Inside Temperature5', XYZ=0.255,0.255,0.06875, QUANTITY= 'INSIDE
WALL TEMPERATURE',IOR=3/

```

&DEVC      ID= 'Inside Temperature6', XYZ=0.255,0.255,0.0675, QUANTITY= 'INSIDE
WALL TEMPERATURE',IOR=3/
&DEVC      ID= 'Inside Temperature7', XYZ=0.255,0.255,0.06625, QUANTITY= 'INSIDE
WALL TEMPERATURE',IOR=3/
&DEVC      ID= 'Inside Temperature8', XYZ=0.255,0.255,0.065, QUANTITY= 'INSIDE
WALL TEMPERATURE',IOR=3/
&DEVC      ID= 'Inside Temperature9', XYZ=0.255,0.255,0.06375, QUANTITY= 'INSIDE
WALL TEMPERATURE',IOR=3/
&DEVC      ID= 'Inside Temperature10', XYZ=0.255,0.255,0.0625, QUANTITY= 'INSIDE
WALL TEMPERATURE',IOR=3/

```

```

&DEVC ID= 'RADIATIVE HEAT', XYZ=0.255,0.255,0.075,
QUANTITY='RADIATIVE_FLUX',IOR=3/
&DEVC ID= 'CONVECTIVE HEAT', XYZ=0.255,0.255,0.075,
QUANTITY='CONVECTIVE_FLUX',IOR=3/
&DEVC      ID= 'Thickness', XYZ=0.255,0.255,0.075, QUANTITY='WALL
THICKNESS',IOR=3 /

```

```

&MISC TMPA=20/,RESTART=.TRUE./

```

```

&TAIL/

```

D.2 FDS input file for Cone Calorimeter simulation of PMMA for grid sensitivity

```

&CHID='PMMA', TITLE='Cone calorimeter'/ for 50kW/m2, 5mm

```

```

&MESH IJK=20,20,200 , XB = 0.15,0.25,0.15,0.25,0,1/
&MESH IJK=20,20,200 , XB = 0.25,0.35,0.15,0.25,0,1/
&MESH IJK=20,20,200 , XB = 0.15,0.25,0.25,0.35,0,1/
&MESH IJK=20,20,200 , XB = 0.25,0.35,0.25,0.35,0,1/

```

```

&TIME T_END=100, WALL_INCREMENT=1., DT=0.01/
&DUMP DT_HRR = 1.0, DT_DEVC = 1.0, DT_RESTART=10.0 /

```

```

&OBST XB=0.215,0.285,0.215,0.285,0.05,0.075 ,SURF_ID = 'PMMA SHEET'/
&OBST XB=0.2,0.215,0.2,0.3,0.05,0.075 ,SURF_ID = 'PMMA SHEET2'/
&OBST XB=0.285,0.3,0.2,0.3,0.05,0.075 ,SURF_ID = 'PMMA SHEET2'/

```

```

&OBST XB=0.2,0.3,0.2,0.215,0.05,0.075 ,SURF_ID = 'PMMA SHEET2'/
&OBST XB=0.2,0.3,0.285,0.3,0.05,0.075 ,SURF_ID = 'PMMA SHEET2'/

```

```

&OBST XB=0.2,0.3,0.2,0.3,0.05,0.047,SURF_ID='STEEL'/
&OBST XB=0.197,0.303,0.197,0.2,0.047,0.075,SURF_ID='STEEL' /
&OBST XB=0.197,0.2,0.197,0.303,0.047,0.075,SURF_ID='STEEL'/
&OBST XB=0.3,0.303,0.197,0.303,0.047,0.075,SURF_ID='STEEL'/
&OBST XB=0.197,0.303,0.3,0.303,0.047,0.075,SURF_ID='STEEL'/

```

&SURF ID = 'PMMA SHEET',MATL_ID= 'PMMA','STEEL',EXTERNAL_FLUX = 50.,
COLOR = 'BLACK',BACKING = 'INSULATED',THICKNESS=
0.025,0.0007,CELL_SIZE_FACTOR=0.5,STRETCH_FACTOR=1,BURN_AWAY = .TRUE./

&SURF ID = 'PMMA SHEET2',MATL_ID = 'PMMA','STEEL',EXTERNAL_FLUX= 50.,
COLOR = 'BLACK',BACKING = 'EXPOSED',THICKNESS=
0.025,0.0007,CELL_SIZE_FACTOR=0.5,STRETCH_FACTOR=1,BURN_AWAY = .TRUE./

&REAC ID = 'PMMA_FUEL',C = 5.,H = 8.,O = 2.,CO_YIELD = 0.007, SOOT_YIELD =
0.014,HEAT_OF_COMBUSTION=20630., IDEAL=.FALSE./

&RADI RADIATION=.TRUE. /

&MATL ID='PMMA',
CONDUCTIVITY_RAMP='k_pmma',SPECIFIC_HEAT_RAMP='c_pmma', DENSITY=1210.,
Emissivity= 0.95, N_REACTIONS=1,
SPEC_ID='PMMA_FUEL',NU_SPEC=1.,HEAT_OF_REACTION=2007., E=99.4E3,
N_S=0.79,A=3.54E6/

&RAMP ID='c_pmma', T= 20., F=1.55 /
&RAMP ID='c_pmma', T=100., F=1.96 /
&RAMP ID='c_pmma', T=280., F=2.36 /

&RAMP ID='k_pmma', T= 20., F=0.185 /
&RAMP ID='k_pmma', T=100., F=0.113 /

&SURF ID= 'STEEL', MATL_ID = 'STEEL',COLOR = 'RED',BACKING =
'EXPOSED',THICKNESS= 0.003 /

&MATL ID = 'STEEL', EMISSIVITY = 0.9, DENSITY = 7850., SPECIFIC_HEAT_RAMP =
'c_steel', CONDUCTIVITY_RAMP = 'k_steel'/

&RAMP ID='c_steel', T= 20., F=0.45 /
&RAMP ID='c_steel', T=377., F=0.60 /
&RAMP ID='c_steel', T=677., F=0.85 /
&RAMP ID='k_steel', T= 20., F=48. /
&RAMP ID='k_steel', T=677., F=30. /

&VENT MB='XMIN',SURF_ID='OPEN'/
&VENT MB='XMAX',SURF_ID='OPEN'/
&VENT MB='YMIN',SURF_ID='OPEN'/
&VENT MB='YMAX',SURF_ID='OPEN'/
&VENT MB='ZMAX' SURF_ID='OPEN'/
&VENT MB='ZMIN' SURF_ID='OPEN'/

&SLCF PBX=0.25, QUANTITY='TEMPERATURE'/
&SLCF PBY=0.25, QUANTITY='TEMPERATURE'/

&BNDF QUANTITY='WALL TEMPERATURE'/
&BNDF QUANTITY='NET HEAT FLUX'/
&BNDF QUANTITY='RADIATIVE HEAT FLUX'/

```

&DEVC      ID= 'Temperature', XYZ=0.255,0.255,0.075, QUANTITY= 'WALL
TEMPERATURE',IOR=3/
&DEVC      ID= 'Inside Temperature1', XYZ=0.255,0.255,0.07375, QUANTITY= 'INSIDE
WALL TEMPERATURE',IOR=3/
&DEVC      ID= 'Inside Temperature2', XYZ=0.255,0.255,0.0725, QUANTITY= 'INSIDE
WALL TEMPERATURE',IOR=3/
&DEVC      ID= 'Inside Temperature3', XYZ=0.255,0.255,0.07125, QUANTITY= 'INSIDE
WALL TEMPERATURE',IOR=3/
&DEVC      ID= 'Inside Temperature4', XYZ=0.255,0.255,0.07, QUANTITY= 'INSIDE
WALL TEMPERATURE',IOR=3/
&DEVC      ID= 'Inside Temperature5', XYZ=0.255,0.255,0.06875, QUANTITY= 'INSIDE
WALL TEMPERATURE',IOR=3/
&DEVC      ID= 'Inside Temperature6', XYZ=0.255,0.255,0.0675, QUANTITY= 'INSIDE
WALL TEMPERATURE',IOR=3/
&DEVC      ID= 'Inside Temperature7', XYZ=0.255,0.255,0.06625, QUANTITY= 'INSIDE
WALL TEMPERATURE',IOR=3/
&DEVC      ID= 'Inside Temperature8', XYZ=0.255,0.255,0.065, QUANTITY= 'INSIDE
WALL TEMPERATURE',IOR=3/
&DEVC      ID= 'Inside Temperature9', XYZ=0.255,0.255,0.06375, QUANTITY= 'INSIDE
WALL TEMPERATURE',IOR=3/
&DEVC      ID= 'Inside Temperature10', XYZ=0.255,0.255,0.0625, QUANTITY= 'INSIDE
WALL TEMPERATURE',IOR=3/

&DEVC ID= 'RADIATIVE HEAT', XYZ=0.255,0.255,0.075,
QUANTITY='RADIATIVE_FLUX',IOR=3/
&DEVC ID= 'CONVECTIVE HEAT', XYZ=0.255,0.255,0.075,
QUANTITY='CONVECTIVE_FLUX',IOR=3/
&DEVC      ID= 'Thickness', XYZ=0.255,0.255,0.075, QUANTITY='WALL
THICKNESS',IOR=3 /

```

```

&MISC TMPA=20/,RESTART=.TRUE./

```

```

&TAIL/

```

D.3 Visualisation of the domain

A visualisation of a typical domain modelled for cone calorimeter test simulation is given in Figure D1 where black represents the sample and red represents the steel casing.

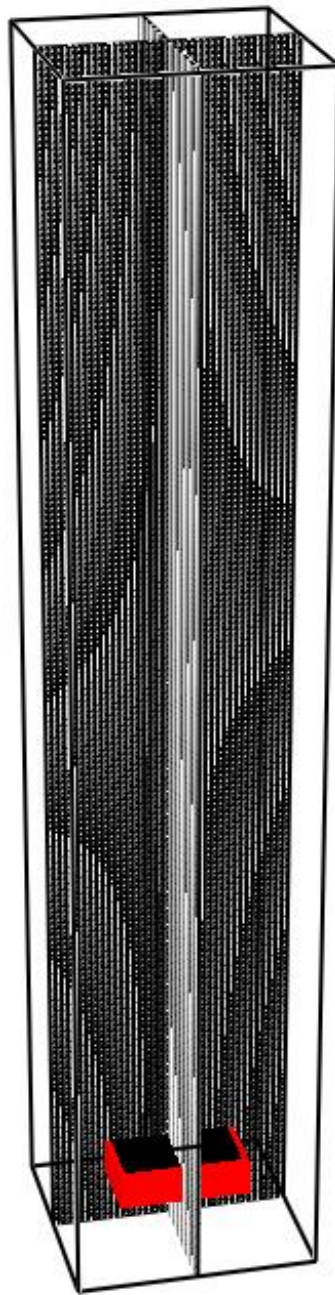


Figure D.1: Visualisation of typical domain: black represents the sample and red represents the steel casing.

APPENDIX E— REPRESENTATIVE FULL INPUT FILES FOR CONE CALORIMETER SIMULATION USING FDS WITH IN-HOUSE INPUT DATA

E.1 FDS input file for Cone Calorimeter simulation of Pine with in-house input data

```
&CHID='PINE-Insul', TITLE='Cone calorimeter'/ for 50kW/m2, with 20k/min heating rate data
```

```
&MESH IJK=20,20,140, XB = 0.15,0.25,0.15,0.25,0,0.7/  
&MESH IJK=20,20,140, XB = 0.25,0.35,0.15,0.25,0,0.7/  
&MESH IJK=20,20,140, XB = 0.15,0.25,0.25,0.35,0,0.7/  
&MESH IJK=20,20,140, XB = 0.25,0.35,0.25,0.35,0,0.7/
```

```
&TIME T_END=1200, WALL_INCREMENT=1., DT=0.01/  
&DUMP DT_HRR = 5.0, DT_DEVC = 5.0, DT_RESTART=20. /
```

```
&OBST XB=0.215,0.285,0.215,0.285,0.05,0.07 ,SURF_ID = 'PINE'/  
&OBST XB=0.2,0.215,0.2,0.3,0.05,0.07 ,SURF_ID = 'PINE2'/  
&OBST XB=0.285,0.3,0.2,0.3,0.05,0.07 ,SURF_ID = 'PINE2'/
```

```
&OBST XB=0.2,0.3,0.2,0.215,0.05,0.07 ,SURF_ID = 'PINE2'/  
&OBST XB=0.2,0.3,0.285,0.3,0.05,0.07 ,SURF_ID = 'PINE2'/
```

```
&OBST XB=0.2,0.3,0.2,0.3,0.05,0.047,SURF_ID='STEEL'/  
&OBST XB=0.197,0.303,0.197,0.2,0.047,0.07,SURF_ID='STEEL' /  
&OBST XB=0.197,0.2,0.197,0.303,0.047,0.07,SURF_ID='STEEL'/  
&OBST XB=0.3,0.303,0.197,0.303,0.047,0.07,SURF_ID='STEEL'/  
&OBST XB=0.197,0.303,0.3,0.303,0.047,0.07,SURF_ID='STEEL'/
```

```
&SPEC ID='WATER VAPOR' /
```

```
&SURF ID = 'PINE',MATL_ID= 'PINE','STEEL', MATL_ID(1,1) = 'PINE',MATL_ID(1,2)  
= 'MOISTURE', MATL_MASS_FRACTION(1,:) = 0.965,0.035, EXTERNAL_FLUX= 50.,  
COLOR = 'WHITE',BACKING = 'INSULATED',THICKNESS=  
0.0188,0.0007,CELL_SIZE_FACTOR=0.5,STRETCH_FACTOR=1,BURN_AWAY = .TRUE./
```

```
&SURF ID = 'PINE2',MATL_ID= 'PINE','STEEL',MATL_ID(1,1) = 'PINE',MATL_ID(1,2)  
= 'MOISTURE', MATL_MASS_FRACTION(1,:) = 0.965,0.035, EXTERNAL_FLUX= 50.,  
COLOR = 'WHITE',BACKING = 'INSULATED', THICKNESS=  
0.0188,0.0007,CELL_SIZE_FACTOR=0.5,STRETCH_FACTOR=1,BURN_AWAY = .TRUE./
```

```
&REAC ID = 'PINE_FUEL',C = 3.4,H = 6.2,O = 2.5, CO_YIELD = 0.007, SOOT_YIELD =  
0.006,HEAT_OF_COMBUSTION = 11210., IDEAL=.FALSE./HEAT_OF_COMBUSTION =  
11210
```

```
&RADI RADIATION=.TRUE. /
```

```
&MATL ID='PINE', CONDUCTIVITY_RAMP='k_PINE',SPECIFIC_HEAT_RAMP='c_PINE',  
DENSITY=423., Emissivity= 1.0, N_REACTIONS=1,  
SPEC_ID='PINE_FUEL',NU_SPEC=0.874,MATL_ID = 'CHAR',NU_MATL = 0.126,
```

HEAT_OF_REACTION=131, E=70.34E3, N_S=0.348, A=2.66E3/ NU_SPEC=0.874
original

&RAMP ID='c_PINE', T= 20., F=1.1 /
&RAMP ID='c_PINE', T=60., F=1.23 /
&RAMP ID='c_PINE', T=225., F=1.7 /

&RAMP ID='k_PINE', T= 20., F=0.168 /
&RAMP ID='k_PINE', T=225., F=0.2 /

&MATL ID = 'MOISTURE', EMISSIVITY = 1.0, DENSITY = 1000., CONDUCTIVITY = 0.6,
SPECIFIC_HEAT = 4.19, N_REACTIONS = 1, A = 4.5E6, E = 56.6E3, N_S = 0.34,
SPEC_ID = 'WATER VAPOR', NU_SPEC = 1.0, HEAT_OF_REACTION= 2260. /

&MATL ID = 'CHAR', EMISSIVITY = 1.0, DENSITY = 110.,
CONDUCTIVITY_RAMP='k_char', SPECIFIC_HEAT_RAMP='c_char'/

&RAMP ID='c_char', T= 20., F=0.724 /Rahul new
&RAMP ID='c_char', T=120., F=1.097 /

&RAMP ID='k_char', T= 20., F=0.069 /Rahul new
&RAMP ID='k_char', T=120., F=0.102 /

&SURF ID= 'STEEL', MATL_ID = 'STEEL', COLOR = 'RED', BACKING =
'EXPOSED', THICKNESS= 0.003 /

&MATL ID = 'STEEL', EMISSIVITY = 0.9, DENSITY = 7850., SPECIFIC_HEAT_RAMP =
'c_steel', CONDUCTIVITY_RAMP = 'k_steel'/

&RAMP ID='c_steel', T= 20., F=0.45 /
&RAMP ID='c_steel', T=377., F=0.60 /
&RAMP ID='c_steel', T=677., F=0.85 /

&RAMP ID='k_steel', T= 20., F=48. /
&RAMP ID='k_steel', T=677., F=30. /

&VENT MB='XMIN', SURF_ID='OPEN'/
&VENT MB='XMAX', SURF_ID='OPEN'/
&VENT MB='YMIN', SURF_ID='OPEN'/
&VENT MB='YMAX', SURF_ID='OPEN'/
&VENT MB='ZMAX', SURF_ID='OPEN'/
&VENT MB='ZMIN', SURF_ID='OPEN'/

&SLCF PBX=0.25, QUANTITY='TEMPERATURE'/
&SLCF PBY=0.25, QUANTITY='TEMPERATURE'/

&BNDF QUANTITY='WALL TEMPERATURE'/
&BNDF QUANTITY='NET HEAT FLUX'/
&BNDF QUANTITY='RADIATIVE HEAT FLUX'/

&DEVC ID= 'Temperature1', XYZ=0.25,0.25,0.07, QUANTITY= 'WALL
TEMPERATURE', IOR=3/

```

&DEVC      ID= 'Temperature2', XYZ=0.22,0.22,0.07, QUANTITY= 'WALL
TEMPERATURE',IOR=3/
&DEVC      ID= 'Temperature3', XYZ=0.25,0.22,0.07, QUANTITY= 'WALL
TEMPERATURE',IOR=3/

&DEVC      ID= 'Inside Temperature1', XYZ=0.25,0.25,0.07375, QUANTITY= 'INSIDE
WALL TEMPERATURE',IOR=3/
&DEVC      ID= 'Inside Temperature2', XYZ=0.25,0.25,0.0725, QUANTITY= 'INSIDE
WALL TEMPERATURE',IOR=3/
&DEVC      ID= 'Inside Temperature3', XYZ=0.25,0.25,0.07125, QUANTITY= 'INSIDE
WALL TEMPERATURE',IOR=3/
&DEVC      ID= 'Inside Temperature4', XYZ=0.25,0.25,0.07, QUANTITY= 'INSIDE WALL
TEMPERATURE',IOR=3/
&DEVC      ID= 'Inside Temperature5', XYZ=0.25,0.25,0.06875, QUANTITY= 'INSIDE
WALL TEMPERATURE',IOR=3/
&DEVC      ID= 'Inside Temperature6', XYZ=0.25,0.25,0.0675, QUANTITY= 'INSIDE
WALL TEMPERATURE',IOR=3/
&DEVC      ID= 'Inside Temperature7', XYZ=0.25,0.25,0.06625, QUANTITY= 'INSIDE
WALL TEMPERATURE',IOR=3/
&DEVC      ID= 'Inside Temperature8', XYZ=0.25,0.25,0.065, QUANTITY= 'INSIDE
WALL TEMPERATURE',IOR=3/
&DEVC      ID= 'Inside Temperature9', XYZ=0.25,0.25,0.06375, QUANTITY= 'INSIDE
WALL TEMPERATURE',IOR=3/
&DEVC      ID= 'Inside Temperature10', XYZ=0.25,0.25,0.0625, QUANTITY= 'INSIDE
WALL TEMPERATURE',IOR=3/

&DEVC ID= 'RADIATIVE HEAT', XYZ=0.25,0.25,0.07,
QUANTITY='RADIATIVE_FLUX',IOR=3/
&DEVC ID= 'CONVECTIVE HEAT', XYZ=0.25,0.25,0.07,
QUANTITY='CONVECTIVE_FLUX',IOR=3/
&DEVC      ID= 'Thickness', XYZ=0.25,0.25,0.07, QUANTITY='WALL
THICKNESS',IOR=3 /

&MISC TMPA=20,RESTART=.TRUE./

&TAIL/

```

E.2 FDS input file for Cone Calorimeter simulation of PMMA with in-house input data

```

&CHID='PMMA', TITLE='Cone calorimeter'/ for 50kW/m2, with 20k/min heating rate data

&MESH IJK=20,20,200 , XB = 0.15,0.25,0.15,0.25,0,1/
&MESH IJK=20,20,200 , XB = 0.25,0.35,0.15,0.25,0,1/
&MESH IJK=20,20,200 , XB = 0.15,0.25,0.25,0.35,0,1/
&MESH IJK=20,20,200 , XB = 0.25,0.35,0.25,0.35,0,1/

&TIME T_END=1500, WALL_INCREMENT=1., DT=0.01/
&DUMP DT_HRR = 1.0, DT_DEVC = 1.0, DT_RESTART=5. /

```

&OBST XB=0.215,0.285,0.215,0.285,0.05,0.075 ,SURF_ID = 'PMMA SHEET'/
&OBST XB=0.2,0.215,0.2,0.3,0.05,0.075 ,SURF_ID = 'PMMA SHEET2'/
&OBST XB=0.285,0.3,0.2,0.3,0.05,0.075 ,SURF_ID = 'PMMA SHEET2'/

&OBST XB=0.2,0.3,0.2,0.215,0.05,0.075 ,SURF_ID = 'PMMA SHEET2'/
&OBST XB=0.2,0.3,0.285,0.3,0.05,0.075 ,SURF_ID = 'PMMA SHEET2'/

&OBST XB=0.2,0.3,0.2,0.3,0.05,0.047,SURF_ID='STEEL'/
&OBST XB=0.197,0.303,0.197,0.2,0.047,0.075,SURF_ID='STEEL' /
&OBST XB=0.197,0.2,0.197,0.303,0.047,0.075,SURF_ID='STEEL'/
&OBST XB=0.3,0.303,0.197,0.303,0.047,0.075,SURF_ID='STEEL'/
&OBST XB=0.197,0.303,0.3,0.303,0.047,0.075,SURF_ID='STEEL'/

&SURF ID = 'PMMA SHEET',MATL_ID= 'PMMA','STEEL',EXTERNAL_FLUX =
50., COLOR = 'BLACK',BACKING = 'INSULATED',THICKNESS=
0.025,0.0007,CELL_SIZE_FACTOR=0.5,STRETCH_FACTOR=1,BURN_AWAY = .TRUE./

&SURF ID = 'PMMA SHEET2',MATL_ID= 'PMMA','STEEL',EXTERNAL_FLUX= 50.,
COLOR = 'BLACK',BACKING = 'INSULATED',THICKNESS=
0.025,0.0007,CELL_SIZE_FACTOR=0.5,STRETCH_FACTOR=1,BURN_AWAY = .TRUE./

&REAC ID = 'PMMA_FUEL',C = 5.,H = 8.,O = 2., CO_YIELD = 0.007, SOOT_YIELD =
0.014, HEAT_OF_COMBUSTION=21295., IDEAL=.FALSE. /

&RADI RADIATION=.TRUE. /

&MATL ID='PMMA', ABSORPTION_COEFFICIENT=2700.,
CONDUCTIVITY_RAMP='k_pmma',SPECIFIC_HEAT_RAMP='c_pmma', DENSITY=1210.,
Emissivity= 0.85, N_REACTIONS=1,
SPEC_ID='PMMA_FUEL',NU_SPEC=1.,HEAT_OF_REACTION=1830, E=188.5E3,
N_S=1.35,A=1.64E13/

&RAMP ID='c_pmma', T= 20., F=1.47 /
&RAMP ID='c_pmma', T=100., F=1.47 /

&RAMP ID='k_pmma', T= 20., F=0.1945 /
&RAMP ID='k_pmma', T=100., F=0.1945 /

&SURF ID= 'STEEL', MATL_ID = 'STEEL',COLOR = 'RED',BACKING =
'EXPOSED',THICKNESS= 0.003 /

&MATL ID = 'STEEL', EMISSIVITY = 0.9, DENSITY = 7850., SPECIFIC_HEAT_RAMP =
'c_steel', CONDUCTIVITY_RAMP = 'k_steel'/

&RAMP ID='c_steel', T= 20., F=0.45 /
&RAMP ID='c_steel', T=377., F=0.60 /
&RAMP ID='c_steel', T=677., F=0.85 /
&RAMP ID='k_steel', T= 20., F=48. /
&RAMP ID='k_steel', T=677., F=30. /

```
&VENT MB='XMIN',SURF_ID='OPEN'/
&VENT MB='XMAX',SURF_ID='OPEN'/
&VENT MB='YMIN',SURF_ID='OPEN'/
&VENT MB='YMAX',SURF_ID='OPEN'/
&VENT MB='ZMAX',SURF_ID='OPEN'/
&VENT MB='ZMIN',SURF_ID='OPEN'/
```

```
&SLCF PBX=0.25, QUANTITY='TEMPERATURE'/
&SLCF PBY=0.25, QUANTITY='TEMPERATURE'/
```

```
&BNDF QUANTITY='WALL TEMPERATURE'/
&BNDF QUANTITY='NET HEAT FLUX'/
&BNDF QUANTITY='RADIATIVE HEAT FLUX'/
```

```
&DEVC ID= 'Temperature', XYZ=0.255,0.255,0.075, QUANTITY= 'WALL
TEMPERATURE',IOR=3/
&DEVC ID= 'Inside Temperature1', XYZ=0.255,0.255,0.07375, QUANTITY= 'INSIDE
WALL TEMPERATURE',IOR=3/
&DEVC ID= 'Inside Temperature2', XYZ=0.255,0.255,0.0725, QUANTITY= 'INSIDE
WALL TEMPERATURE',IOR=3/
&DEVC ID= 'Inside Temperature3', XYZ=0.255,0.255,0.07125, QUANTITY= 'INSIDE
WALL TEMPERATURE',IOR=3/
&DEVC ID= 'Inside Temperature4', XYZ=0.255,0.255,0.07, QUANTITY= 'INSIDE
WALL TEMPERATURE',IOR=3/
&DEVC ID= 'Inside Temperature5', XYZ=0.255,0.255,0.06875, QUANTITY= 'INSIDE
WALL TEMPERATURE',IOR=3/
&DEVC ID= 'Inside Temperature6', XYZ=0.255,0.255,0.0675, QUANTITY= 'INSIDE
WALL TEMPERATURE',IOR=3/
&DEVC ID= 'Inside Temperature7', XYZ=0.255,0.255,0.06625, QUANTITY= 'INSIDE
WALL TEMPERATURE',IOR=3/
&DEVC ID= 'Inside Temperature8', XYZ=0.255,0.255,0.065, QUANTITY= 'INSIDE
WALL TEMPERATURE',IOR=3/
&DEVC ID= 'Inside Temperature9', XYZ=0.255,0.255,0.06375, QUANTITY= 'INSIDE
WALL TEMPERATURE',IOR=3/
&DEVC ID= 'Inside Temperature10', XYZ=0.255,0.255,0.0625, QUANTITY= 'INSIDE
WALL TEMPERATURE',IOR=3/
```

```
&DEVC ID= 'RADIATIVE HEAT', XYZ=0.255,0.255,0.075,
QUANTITY='RADIATIVE_FLUX',IOR=3/
&DEVC ID= 'CONVECTIVE HEAT', XYZ=0.255,0.255,0.075,
QUANTITY='CONVECTIVE_FLUX',IOR=3/
&DEVC ID= 'Thickness', XYZ=0.255,0.255,0.075, QUANTITY='WALL
THICKNESS',IOR=3 /
```

```
&MISC TMPA=20,RESTART=.TRUE./
```

```
&TAIL/
```